

國立臺灣大學獸醫專業學院獸醫學研究所



博士論文

Graduate Institute of Veterinary Medicine
School of Veterinary Medicine
National Taiwan University
Doctoral Dissertation

口蹄疫病毒 3A 蛋白致內質網改造之機制

與病毒空殼蛋白應用

Mechanism of Foot-and-Mouth Disease Virus 3A Induced-ER
Remodeling and Diagnostic Application of Virus-Like Particles

李恆瑋

Heng-Wei Lee

指導教授：鄭益謙 博士

Advisor: Ivan-Chen Cheng, Ph.D.

中華民國 111 年 11 月

November, 2022

國立臺灣大學獸醫專業學院獸醫學研究所
博士學位論文學術倫理聲明書

本人已完全瞭解本所學術倫理之定義與行為規範，特別是針對抄襲之規範。本人保證，提交學位口試論文的所有內容是由本人撰寫。本人也保證，論文中所引用之他人著作，皆按規定引用。如有涉及違反著作權法、本所學術倫理行為規範、以及其他相關法規，願擔負相關法律責任。

Declaration of Academic Integrity for Students of Graduate Institute of Veterinary
Medicine, National Taiwan University

I have read and understood the Institute's policy on academic integrity in general and plagiarism in particular. I undertake that all the material presented for examination is my own work and has not been written for me, in whole or in part, by any other person. I also undertake that any quotation or paraphrase from the work of another person has been duly referenced in the work which I present for examination. I also acknowledge that I shall bear all consequences resulting from any disciplinary and legal action taken in accordance with Copyright Act, the Institute's policy on academic integrity, and other relevant laws.

立書人 Student Name : 李恆璋
(親筆簽章 Signature)
學號 Student I.D. no. : d06629010
日期 Date : 2022 / 10 / 31 (YYYY/MM/DD)

國立臺灣大學博士學位論文
口試委員會審定書

口蹄疫病毒 3A 蛋白致內質網改造之機制

與病毒空殼蛋白應用

Mechanism of Foot-and-Mouth Disease Virus 3A Induced-ER
Remodeling and Diagnostic Application of Virus-Like Particles

本論文係李恆璋君 (d06629010) 在國立臺灣大學獸醫學系、所完成之博士學位論文，於民國 111 年 10 月 21 日承下列考試委員審查通過及口試及格，特此證明

口試委員：

鄭益濤

(簽名)

張東慶 (指導教授)

蔣沛云

楊平政

王冠廷

系主任、所長

張若嘉 (簽名)

致謝



首先，我想要感謝剛接觸研究時遇到的三位貴人，鄭益謙老師、林有良博士和曾建仁學長。前兩位前輩在我大學徬徨時引領我進入了實驗室，曾學長則讓我見識到研究的自由與絢麗。另外，我還要感謝我在中研院當研究助理時遇到的前老闆徐尚德博士，他對於研究的挑戰精神影響了我，讓我相信想要獲得巨大的成果，就要相信自己勇於嘗試、不要給自己設限。這也是我會選擇回台大就讀博士班的原因之一，因為我相信自己可以是解開「O/TAW/97 無法感染牛」原因的人。雖然最終以失敗告終，但能提出 3A-induced ER remodeling 相關機制，我自己還是挺滿意的。

另外，感謝四位委員：楊平政博士、王宜萱博士、張惠雯老師和蔡沛學老師。每位都提出實實在在的建議並指出我的不足，不只讓我把這本博士論文修改更好，也讓我在未來的實驗設計上可以更加完善。此外，謝謝實驗室的賴修涓學長以及學弟們（劉玠澧和馬邵毅）在這段時間各方面的支持。


I want to thank Midgley et al., Gladue et al., and Gonzalez-Magaldi et al. Although, perhaps, some of you disagreed with, even scorned, my study and hypothesis, I still showed high reverence towards all of you. Because of your publication, I could step further. Thanks to the Journals that were willing to accept my manuscripts, including Viruses, International Journal of Molecular Sciences, and Veterinary Microbiology. In the future, I will devote myself to virological study, then do more advanced research in this field.

中文摘要



多數正股 RNA 病毒入侵細胞後會將宿主胞器進行改造，目的是為了保護病毒 RNA 與集中資源，營造出對病毒最優化的複製環境。其中包括冠狀病毒、登革熱病毒、腸病毒和口蹄疫病毒。然而，至今人們對於病毒改造胞器的機制多半不甚了解。腸病毒與口蹄疫病毒皆屬於 *Picornaviridae* 家族，且有相對大量的研究基礎，值得口蹄疫病毒研究借鏡。已知腸病毒 3A 蛋白可與 COPI 因子 GBF1 作用，可能與改造 Golgi 或 ERGIC (ER-to-Golgi intermediate compartment) 相關，改造的胞器稱為 replication organelles (ROs)。但文獻指出口蹄疫病毒增殖需要的是 COPII 因子而非 COPI，且改造胞器推測為內質網。因此，本研究主題之一是深度探究口蹄疫病毒 3A 蛋白與 COPII 機制，企圖建立一個假說說明口蹄疫病毒是如何將宿主的內質網進行改造。

對應 GBF1 於 COPI 機制所扮演的角色，我們大膽假設並證實口蹄疫病毒 3A 蛋白可與 COPII 因子 Sec12 以及 Sar1 作用。證明的方法為 Co-immunoprecipitation assay 和 Colocalization test。另外，使細胞表現不同長度的 3A 蛋白並接合螢光蛋白 GFP (Green fluorescent protein) 或 APEX 2 後，以螢光顯微鏡或穿透式電子顯微鏡發現 3A 的第 42 至 92 氨基酸 (3A 全長 153 氨基酸) 就足以將內質網改造，雖然改造功能弱於全長 3A。其中「42-59」與「76-92」氨基酸同與 Sar1 的 pocket (第 198 氨基酸附近) 作用。總結，我們的假說為 3A 與 Sar1 以及內質網上的 Sec12 作用，藉此加速 Sec12 活化 Sar1。兩個 active Sar1 同時與 3A 上的 42-59 及 72-92 氨基酸區域結合，3A 貼在內質網膜上藉由這方式將膜外凹成 vesicle。該 vesicle 推測為口蹄疫病毒 RO 的前身。此機制不需要 COPII 因子內外 coat 蛋白參與，顯然與 COPII 傳統機制迥異。雖然，這 model 仍需要更精確的其他實驗佐證，但根據我們的實驗結果以及各方的文獻資料，我們認為這 model 是可能性最高、最完美的詮釋。



除了研究口蹄疫病毒非結構蛋白 3A 外，我們企圖建立一個無病毒參與的血清檢測試劑，以取代只能於負壓實驗室操作的血清中和試驗 (Serum Neutralization test, SNT)。實際構想為以病毒空殼蛋白 (Virus-Like Particles, VLPs) 為抗原、單源抗體 (Monoclonal Antibodies, MAbs) 為 capture antibody 和 tracer，建構 blocking ELISA (bELISA)。口蹄疫病毒中 O 血清型別影響全球最為廣泛，包括台灣。其病毒表面上已知有 5 個中和抗原決定位，當中只有 site 1 為 linear epitope，其它則需要經過蛋白折疊甚至需多個蛋白互相擠壓折疊才能構成。可想而知，常規做法以合成 peptide 去鑑定單源抗體的結合位並不可行。另外，製備中和決定位突變之病毒在台灣又不恰當。所以，為了從已製備的單源抗體庫存中篩選出 site 2 MAb，我們建立了一套以 VLP 為基準的鑑定平臺。構想為表現 wild-type 與 site 2 突變的兩種 VLPs，篩選出可與正常 VLP 作用但無法與 site 2 mutated VLP 作用的 MAb。VLP 製備方法參考 Polacek 等人的論文：表現病毒的 P1 蛋白與少量的 3C 酵素，P1 經過 3C 切割後自行組裝成 VLP。總之，藉此方法成功篩選出 10 個 site 2 MAbs。

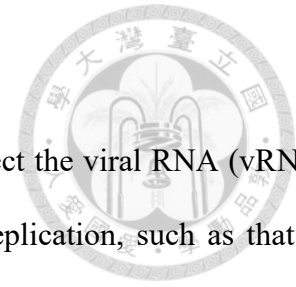
接下來，以同樣方式鑑定出 S11B MAb 辨識 site 3。由於血清中抗體除了 5 種中和抗體外，還有不具備中和能力的抗體。為了能反映出血清的中和能力，我們原先希望偵測血清中各 site 的抗體成分。實際作法為以 VLP 為抗原，搭配不同 site MAb 為 tracer (包括 site 1、site 2 和 site 3)，結果以 site 3 MAb 為 tracer 所得的值與 SN titer 有最好的相關性 ($R^2 = 0.8071$, $n=63$)。但同時我們也注意到抗體所佔據體積幾乎涵蓋整個病毒基本重複結構 (protomer)，代表抗體之間難免有 steric effect，這同時意謂著 site 3 MAb 所測得 (阻擋掉) 的抗體不只有 site 3 抗體。以 MAb 為 tracer 是不可能精確測得該類抗體的濃度。另一方面，由於 VLP 容易崩解，我們同時也採用了未切割過的 P1 蛋白為抗原建構檢測系統。雖然，P1 無法呈現 site 3，其抗原完整性比 VLP 差，但最終 P1-based bELISA 搭配 site 1 Q10E MAb 為 tracer 仍有不錯

的 SN titer 相關性 ($R^2 = 0.7680, n=63$) 。

總之，本論文分成兩大主題。其一，研究口蹄疫病毒非結構蛋白 3A 如何改造細胞胞器，其機制牽涉到兩個未被發現的作用關係 (3A-Sar1 和 3A-Sec12) 。我們相信這機制在口蹄疫病毒 RO 形成機制中是最為關鍵的環節。另一主題著重在結構蛋白、VLP 和抗體。我們建立了一套以 VLP 為基準的 MAbs 鑑定平臺，以及以 VLP 或 P1 為抗原的 bELISA 檢測系統。希望能 在產業和應用端做出貢獻。

關鍵字：口蹄疫病毒、3A 蛋白、COPII 機制、病毒空殼蛋白、單源抗體、阻斷型 ELISA

Abstract



Most positive-stranded RNA viruses modify host organelles to protect the viral RNA (vRNA) and concentrate resources. The modified environment optimizes viral replication, such as that of coronavirus, dengue virus, enterovirus, and foot-and-mouth disease virus (FMDV). However, the mechanism of a virus reorganizing cellular endomembranes is barely understood. Enterovirus and FMDV both belong to the *Picornaviridae* family; therefore, the relatively large body of research on enterovirus can provide a reference for FMDV. Enteroviral 3A protein can interact with the COPI factor GBF1, which is possibly associated with modifying the Golgi and ERGIC (ER-to-Golgi intermediate compartment) into replication organelles (ROs). However, previous research indicates that FMDV replication depends on the COPII factor instead of COPI, and it should be the ER (endoplasmic reticulum) that is modified. Therefore, one of our goals was to profoundly investigate the FMDV 3A protein and the COPII pathway to build a model to explain how FMDV remodels the ER into ROs.

As the counterpart of GBF1 in the COPI pathway, we hypothesized that FMDV 3A interacted with the COPII factors Sec12 and Sar1, which was further proved by co-immunoprecipitation assay and colocalization test in 3A expressing cells. In addition, the region of aa 42–92 for 3A (full length: 153 aa), despite showing relatively low performance compared to its full length, is sufficient for modifying the ER into vesicle-like structures, according to fluorescence microscopy and transmission electron microscopy images of cells expressing truncated 3A fusing to GFP (green fluorescent protein) and APEX2, respectively. Furthermore, the regions of aa 42–59 and aa 76–92 can bind to the pocket on Sar1 (around aa 198). In short, we hypothesize that FMDV 3A enhances Sar1 activation by co-interacting with Sar1 and Sec12. Two active Sar1 interact with aa 42–59 and aa 76–92 of 3A, whereby 3A can directly curve the ER membrane into protrusive vesicle-like structures. These vesicles might be the precursors of FMDV RO. This mechanism is independent of COPII inner and outer coat proteins and distinct from the traditional COPII pathway. Although it still requires further

experiments to prove, we think the model we raised is the most reasonable and ideal interpretation for our data and previous references.

In addition to studying the FMDV non-structural protein 3A, we aimed to develop a diagnostic tool for seroconversion of FMDV to replace the serum neutralization test (SNT), which can only be conducted in a negative pressure laboratory. The format of blocking ELISA was designed with FMD virus-like particles (VLPs) as diagnostic antigens and monoclonal antibodies (MAbs) as capture antibodies and tracers. There are five neutralization sites in serotype O, which is prevalent worldwide, including in Taiwan. Only site 1 is a linear epitope; others are conformational structures that demand protein folding and mutual interaction between subunits. Synthetic peptides are thus unsuitable for mapping and screening most neutralizing antibodies. In addition, the generation of site-mutated artificial FMDV is not allowed in Taiwan. Therefore, we established a platform based on VLP to screen out site MAbs from a well-prepared MAb pool. Based on the study by Polacek and colleagues, we expressed viral P1 protein (or site 2 mutated P1) with a relatively low amount of 3C protease within the cells. Processed P1 (or mutated P1) self-assembled into VLPs (or site 2 mutated VLPs (mVLPs)). Ten site 2 MAbs were screened for mutations that abrogated or inhibited the binding.

Next, the site 3 MAb, S11B, was characterized by the same strategy as that of the site 2 MAb. Given that those serum antibodies are composed of five neutralizing antibodies and “non-neutralizing” antibodies, our first goal was to detect each neutralizing antibody by indicating MAbs. Therefore, bELISAs based on VLP paired with the site 1, site 2, and site 3 MAbs were performed. The PI value from VLPs paired with S11B MAb showed the highest correlation to SN titer ($R^2 = 0.8071$, $n=63$). On the other hand, we found that the site 3 MAb as a tracer would detect (block) not only site 3 antibodies. Because of the large bulk of antibodies compared to repeating unit protomers of virions, it was almost impossible to detect specific antibodies by bELISA with MAb. Although the antigenicity of P1, which failed to present site 3, is not an authentic representation of virions compared to VLPs, it can avoid the problem of dissociation from VLPs. Hence, unprocessed P1 was also used

as an antigen for bELISA, and it demonstrated a good performance ($R^2 = 0.7680$, $n=63$) when paired with the site 1 MAb Q10E.

In summary, this thesis is divided into two parts. One is to study how FMDV non-structure 3A protein modifies the organelles. The modification is involved two undiscovered interactions (3A-Sar1 and 3A-Sec12). We believe the mechanism we raised is most critical in RO formation. The other topic is about structure protein, VLP, and antibodies. We established a platform based on VLP to characterize MAb's binding sites and a detection system based on VLP or P1 for evaluating vaccinated animal serum, hoping we can contribute to industrial and practical areas.

Keywords: Foot-and-Mouth Disease Virus, 3A protein, COPII pathway, Virus-Like Particles,
Monoclonal antibodies, blocking ELISA

目錄 Contents

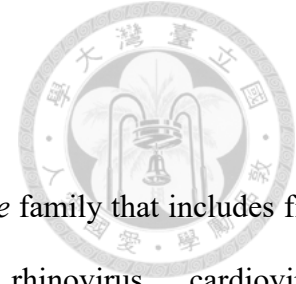


致謝		I
中文摘要		II
Abstract		V
Chapter I	General introduction	1
	1.1 Foot-and-mouth disease virus	2
	1.2 COPI/COPII pathway	8
	1.3 Replication organelles	13
	1.4 Motor protein complex: dynein/dynactin	18
	1.5 Neutralization sites	21
	1.6 Virus-like particle	24
	1.7 Summary	25
Chapter II	Foot-and-Mouth Disease Virus 3A Hijacks Sar1 and Sec12 for ER Remodeling in a COPII-Independent Manner	44
	<i>Viruses 2022</i>	
Chapter III	Dynamic Character of Foot-and-Mouth Disease Virus 3A vesicles	76
	<i>Unpublished</i>	
Chapter IV	Neutralizing monoclonal antibodies against porcine foot-and-mouth disease virus mapped to antigenic site 2 by utilizing novel mutagenic virus-like particles to detect the antigenic change	91
	<i>Veterinary Microbiology 2018</i>	
Chapter V	The Use of Distinctive Monoclonal Antibodies in FMD VLP- and P1-Based Blocking ELISA for the Seromonitoring of Vaccinated Swine	100
	<i>International Journal of Molecular Sciences 2022</i>	
Chapter VI	General discussion	112
	6.1 Mechanism of Foot-and-Mouth Disease Virus 3A Induced-ER Remodeling	
	6.2 Diagnostic Application of Virus-Like Particles	
	6.3 Conclusion and Future Works	

Chapter I

General Introduction

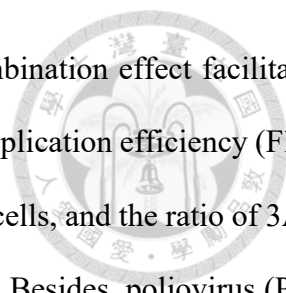




1.1 Foot-and-mouth disease virus

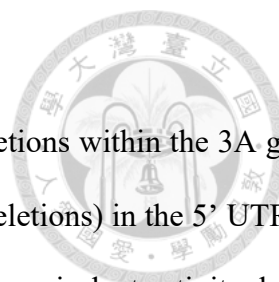
1.1.1 Brief review of Foot-and-Mouth disease virus

Foot-and-mouth disease virus (FMDV) belongs to the *Picornaviridae* family that includes five genera: enterovirus (Poliovirus, Coxsackievirus, and EV71), rhinovirus, cardiovirus (encephalomyocarditis virus), hepatovirus, and aphthovirus (FMDV) (Flint et al., 2015). Like other picornaviruses, FMDV contains a single positive-stranded viral RNA (vRNA) encapsidated in a ~30 nm diameter icosahedral structure (Fry et al., 2005). The structure comprises twelve copies of pentamers, and a pentamer consists of five protomers; a protomer is formed from four structural proteins, VP1, VP2, VP3, and VP4 (Fry et al., 2005). After viral entry and vRNA release, vRNA recruits host translation factors on the “Internal Ribosome Entry Site” (IRES) in the 5’ un-translation region (5’ UTR), followed by the translation of the single open reading frame (ORF) (Mason et al., 2003). The translation mechanism was termed IRES-dependent, distinct from cap-dependent translation for most host proteins (Lamphear et al., 1995). The polyprotein encoded from ORF would be initially divided into L protease (L^{pro}), P1-2A, and P2-P3 due to co-translational processing in *cis* of L^{pro} and self-cleavage activity of 2A (Mason et al., 2003). Next, P1-2A and P2-P3 would be processed by 3C protease ($3C^{pro}$) and divided into structure proteins (VP0, VP3, and VP1) and non-structure proteins (2A, 2B, 2C, 3A, 3B, 3C, and 3D polymerase) (Mason et al., 2003). VP0 would be divided into VP4 and VP2 after the assembly of a virion (Mason et al., 2003a). Therefore, one strategy for virus-like particle (VLP) production is co-expression of P1 and $3C^{pro}$ so that processed P1 would self-assemble into VLP (Gullberg et al., 2013; Polacek et al., 2013). In addition, intermediate precursor proteins, 3AB and 3CD as examples, harbor other activities distinct from mature proteins. Although it is still uncertain for FMDV, these intermediate proteins of enterovirus reportedly participate in RNA amplification (Flint et al., 2015; Ilnytska et al., 2013). For example, enteroviral 3AB proteins are located at the membrane surface by a membrane-bound activity of the 3A portion; simultaneously, the 3B portion would be poly-uridylylated and serve as primer binding to the poly-A



tail of vRNA and 3D polymerase (Jackson and Belsham, 2021). The combination effect facilitates vRNA duplication on the membrane of replication organelles, increasing replication efficiency (Flint et al., 2015). In fact, 3A is less abundant than 3AB in enterovirus-infected cells, and the ratio of 3AB and 3A is also essential for optimal viral replication (Ilnytska et al., 2013). Besides, poliovirus (PV) 3CD protease is the major proteinase for viral P1 processing instead of 3C^{pro} (Ypma-Wong et al., 1988). Although 3CD shows no RNA polymerase activity, it still binds to the 5'UTR as an irreplaceable replication factor (Gamarnik and Andino, 1998) and is essential for the uridylation of 3B (Paul et al., 2000).

FMDV is a highly contagious agent with worldwide distribution. The susceptible host ranges almost cloven-hoofed animals, including swine, cattle, sheep, goats, antelope, and deer. Seven serotypes (A, O, C, Asia 1, SAT1, SAT2, and SAT3) show no cross-reaction with each other; multiple subtypes and variants also challenge vaccination policy (Ma et al., 2011). Upon infection, animals suffer from acute, systemic vesicular disease preferentially in the mouth and feet. Other clinical signs include fever, viremia, and myocarditis (in piglet). Besides, a persistent asymptomatic infection could occur in ruminants (Longjam et al., 2011). In addition to a strict international trade barrier, the outbreak of FMD would lead to substantial economic losses. In 1997, a severe outbreak in Taiwan lasted for at least 16 years. The epidemic was caused by a porcophilic strain O/TAW/97 (O/97) (Dunn, 1997). After stamping out and blanket vaccination, the O/Penghu/12 was the last porcophilic strain isolated in Taiwan in 2012. Except for this strain, another virus strain called O/TAW/99 (O/99) was isolated in Kimen in 1999. In alignment with the sequences, O/99 belonged to the PanAsia toptotype distinguished from the Cathay toptotype for O/97 (Knowles et al., 2005; Mason et al., 2003b). Although few clinical events happened sporadically in Kimen, a distance from the main island of Taiwan, Taiwan's main island was finally certified as an FMDV-free zone without vaccination by OIE in 2020 (OIE., 2021).

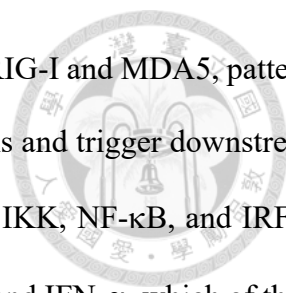


1.1.2 The porcophilic strain O/TAW/97

The O/97 strain is avirulent to cattle presumably because of gene deletions within the 3A gene (30 nucleotide deletions) and the pseudoknot (PK) region (43 nucleotide deletions) in the 5' UTR. It had been widely accepted that the ten amino acid loss of 3A results in cattle-avirulent activity, but it was debatable (Beard and Mason, 2000; Ma et al., 2014; Pacheco et al., 2013; Stenfeldt et al., 2018). The O/HKN/21/70 virus strain isolated in 1970 also contains amino acid 93-102 deletion in 3A, just like O/97, while it is highly virulent to cattle and swine (Knowles et al., 2001). When the partial replacement included the 3A gene from O/97, the chimeric virus significantly restricted the replication in bovine kidney cells and did not lead to a local lesion on the bovine tongue; however, the cattle inoculated with chimeric virus finally developed into a systemic disease (Beard and Mason, 2000). Conversely, if the replacement ranged almost all O/97, including the PK region, it showed no local and systemic disease in cattle (Beard and Mason, 2000). Zhu and colleagues further proved that PK region deletion contributed to lower cattle virulence (Zhu et al., 2019). Although virus shedding was detected in two of five infected cattle for the PK partial deletion virus, the clinical signs are relatively mild compared to wild-type virus infection (Zhu et al., 2019). These data indicated that, except for 3A gene deletion, the PK region should be concerned for the atypic host range of O/97. Nonetheless, the underlying reason and mechanism are still an enigma. To answer this, first, we should clearly illustrate the biological function of the PK region and 3A protein and the effect of the deletions.

1.1.3 The interplays between type I interferon pathway and FMDV

Research indicates that, after viral entry, viruses must defend against host antiviral activity, especially the type I IFN pathway (Randall and Goodbourn, 2008). No exception was FMDV. The following demonstrates the IFN pathway and examples of how FMDV counter-attacks antiviral activity. For RNA viral replication, it was inevitable to produce long double-stranded RNA (dsRNA)



that should not exist in normal cells (Randall and Goodbourn, 2008). The RIG-I and MDA5, pattern-recognition receptors (PRRs) from host cells, recognize these viral dsRNAs and trigger downstream signaling. The signaling factors include VISA, TRAF3, TRAF6, NEMO, IKK, NF- κ B, and IRF-3, finally activating the IFN promoter on chromosomes for producing IFN- β and IFN- α , which of them are type I interferons (Li et al., 2021; Randall and Goodbourn, 2008). The IFN- β (and IFN- α) are secreted and activate IFN- α/β receptors (IFNAR1/IFNAR2 heterodimer) on the cell surface nearby. Activated receptors phosphorylate STAT1 and STAT2, thereby inducing STAT1-STAT2 heterodimerization. The heterodimer interacts with karyopherin 1 (KPNA1), an importin, followed by nuclear translocation (Randall and Goodbourn, 2008). The complex, together with IRF9, binds to an inducible stimulatory response element (ISRE) on chromosomes to produce various antiviral proteins, such as PKR (protein kinase R), 2'5' OAS (2'5'-oligoadenylate synthetase), and RNase L (Flint et al., 2015; Randall and Goodbourn, 2008). In short, the type I interferon pathway includes three phases: induction (dsRNA recognition to IFN production), transduction (IFN receptor activation to antiviral protein production), and antiviral protein response (Randall and Goodbourn, 2008) (Fig. 1).

Despite the potent antiviral activity, viruses still take over the cells due to viral counter-attacking. It can be a ubiquitous inhibition for host protein synthesis or a specific pathway blockage (Li et al., 2021; Ma et al., 2018; Peng et al., 2020; Rodriguez Pulido and Saiz, 2017). For example, 3C^{pro} would cleave eIF4G and eIF4A to suppress most protein translation, including antiviral protein synthesis (Belsham et al., 2000). L^{pro} can remove eIF4G's N-terminus, essential for cap-dependent translation but not IRES-dependent translation, thereby specifically inhibiting host protein expression (Guan and Belsham, 2017; Kirchweiger et al., 1994). For pathway blockage, L^{pro} degrades the p65 subunit of NF- κ B (de Los Santos et al., 2007) and deubiquitinates RIG-I, TBK, TRAF3, and TRAF6 (Wang et al., 2011a). Viral 3C^{pro} degrades NEMO and KPNA1 with protease activity (Du et al., 2014; Wang et al., 2012) while degrading PKR in a lysosomal manner (Li et al., 2017). VP3 interacts with VISA

and inhibits its expression (Li et al., 2016b). Viral 3A protein will be discussed later (see 1.1.4).

In fact, the interferon pathway is much more complicated and mediated by positive and negative feedback. Interferon promotes PKR production in an inactive form (Flint et al., 2015). PKR is activated by detecting dsRNA (Flint et al., 2015), catalyzed by stress granule marker G3BP1 (Yang et al., 2020). Active PKR further phosphorylates eIF2 α and IKK (Flint et al., 2015; Garcia et al., 2007). Phosphorylated eIF2 α cannot support protein translation, thereby inhibiting viral protein synthesis (Flint et al., 2015). Phosphorylated IKK would transduce the signal by degradation of I κ B to relieve NF- κ B (Randall and Goodbourn, 2008), which create a sort of positive feedback for the type I interferon pathway. G3BP1 reportedly would upregulate RIG-I and MDA-5 (Li et al., 2021), so G3BP1 also enhances the interferon pathway in many ways. Because 3C and L protease could break down G3BP1, it was another strategy for the virus to inhibit anti-viral activity (Visser et al., 2019; Ye et al., 2018). Oppositely, there is negative feedback. Interferon promotes ISG15, which binds to RIG-I and LRRC25 (Du et al., 2018). LRRC25 interacts with autophagic receptor p62. Therefore, ISG15 regulated the amounts of RIG-I by autophagic degradation as the complicated complex, RIG-I: ISG15: LRRC25: p62 (Du et al., 2018) (Fig. 1). More complicated, NF- κ B signaling stabilizes LRRC25, whereas LRRC25 inhibits the signaling by autophagic degradation of NF- κ B (Feng et al., 2017). Therefore, when the virus promotes the function of LRRC25, it enhances negative feedback and inhibits the host response.

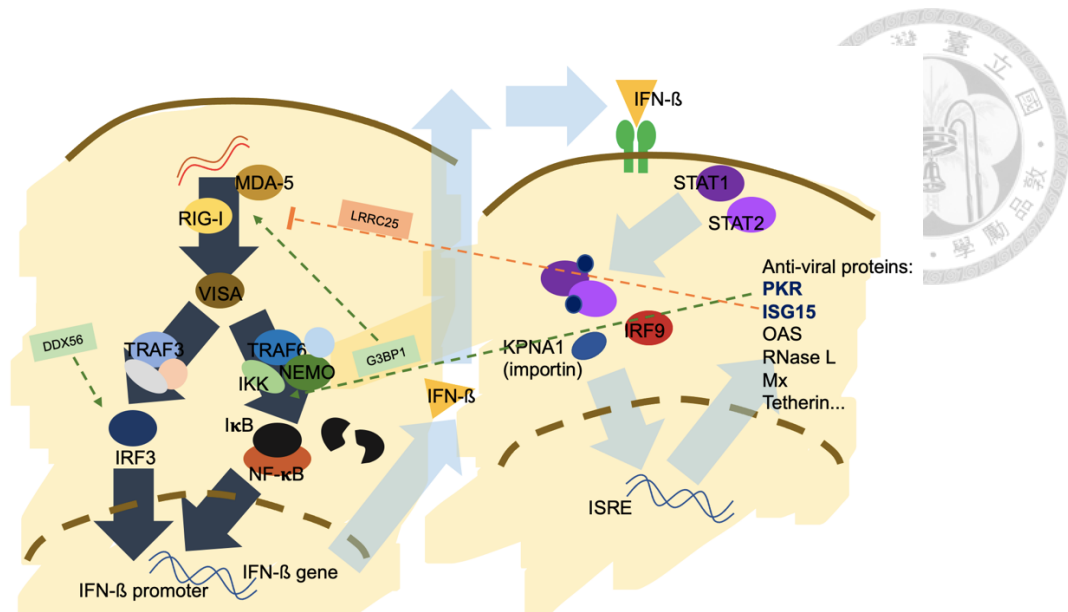
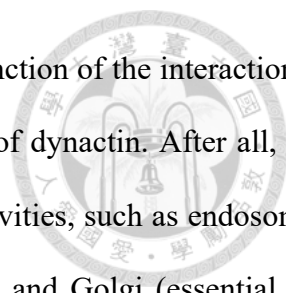


Figure 1. The schematic diagram for type I interferon pathway.

1.1.4 The current knowledge of FMDV 3A protein

FMDV 3A consists of 153 amino acids, much longer than those in other picornaviruses, divided into N-terminus, hydrophobic region (HR), and C-terminus. Based on the colocalization test and membrane fractionation assay, FMDV 3A has been proved attached on the ER membrane (Gonzalez-Magaldi et al., 2014; Moffat et al., 2005). The N-terminus of 3A harbors two alpha-helix turns responsible for dimerization essential for viral replication (Gonzalez-Magaldi et al., 2012). Because of the understanding of O/TAW/97, we know that the C-terminus of 3A is highly associated with virulence and host range (Ma et al., 2014). Besides, numerous host factors were proved as 3A interaction partners, including DCTN3, LRRC25, DDX56, RHA (RNA helicase A), G3BP1, and RNA sensors (RIG-I, MDA-5, and VISA) (Fu et al., 2019; Gladue et al., 2014; Lawrence and Rieder, 2009; Li et al., 2016a; Yang et al., 2020). DCTN3 (dynactin subunit 3) is a dynein/dynactin complex subunit. According to Gladue et al.'s study, the A89P mutation of 3A would abrogate the interaction leading to less virulence in cattle (Gladue et al., 2014). Moreover, they claimed 3A of O/TAW/97 with P89 failed to interact with DCTN3 from cattle. Overexpression of DCTN3 decreased viral yield, as did overexpression of other subunits (GFP-p150^{Glued} and GFP-dynamitin), which led to disruption



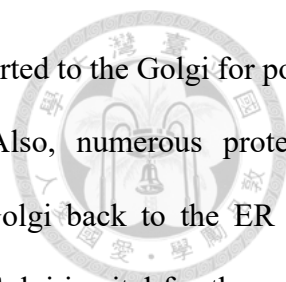
of dynactin arrangement (Gladue et al., 2014). However, the biological function of the interaction is still unknown: the interaction aims at utilizing or inhibiting the function of dynactin. After all, the dynein/dynactin motor protein complex is involved in several cellular activities, such as endosomal trafficking (essential for viral entry) and the trafficking between the ER and Golgi (essential for interferon production). It is a complex issue to be discussed.

The RNA sensors (RIG-I, MDA-5, and VISA) were bound to the N-terminus (aa 1-51) of 3A, resulting in disruption and down-regulation of the interferon pathway (Li et al., 2016a). Besides, 3A would enhance LRRC25 expression and degrade G3BP1 in an autophagic manner (Yang et al., 2020). According to the co-immunoprecipitation assay, there are interactions between 3A and G3BP1, 3A and LRRC25, and LRRC25 and G3BP1 (Yang et al., 2020). As mentioned above, LRRC25 degrades RIG-I by autophagy (Du et al., 2018); therefore, we presume G3BP1 would be tethered to the autophagy degrading complex by 3A. In addition, FMDV 3A also interacts with DDX56 (one of the RNA helicases), inhibiting the phosphorylation of IRF-3 (Fu et al., 2019). In summary, FMDV 3A counter-attacks the type-I interferon pathway by degrading G3BP1 and RIG-I and inhibiting the phosphorylation of IRF-3 through DDX56.

Although the role of IFN antagonism for 3A is relatively straightforward, the other 3A functions remain largely unknown, such as the role of host specificity. The O1CaΔ3A recombinant and wild-type viruses showed no differences in antiviral cytokines at the primary infection site (dorsal nasopharynx) for cattle, also suggesting that 3A association for cattle virulence was not due to host response (Stenfeldt et al., 2018). Many questions required answers, such as a biological function of interaction with DCTN3, the mechanism for LRRC25 upregulation, and the role in replication organelles.

1.2 The COPI/COPII pathway

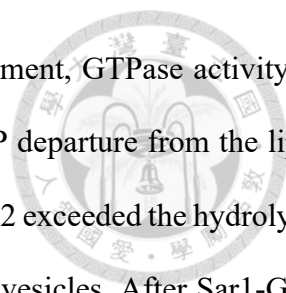
1.2.1 Introduction of COPI/COPII pathway



In some cases, newly synthesized proteins in the ER would be transported to the Golgi for post-translation modification, secretion, and exerting of their function. Also, numerous proteins participating in the trafficking demand retrograde transport from the Golgi back to the ER for recycling. Therefore, regulating protein trafficking between the ER and Golgi is vital for the cells; thanks to several cytologists, we know the COPI/COPII pathway governs the trafficking and have a deep understanding of its mechanisms (Szul and Sztul, 2011). In mammals, not yeasts, COPII vesicles carrying cargo proteins would be generated only from the ER, while COPI vesicles came from the ER-to-Golgi intermediate (ERGIC) and Golgi. In other words, the COPII pathway takes control of the ER to ERGIC transport, while the ERGIC to Golgi and retrograde movement are responsible by the COPI pathway (Appenzeller-Herzog and Hauri, 2006).

In detail, COPI factor GBF1 would be recruited to the ERGIC or Golgi because of PI4P lipids with its HDS1 domain (Meissner et al., 2018), followed by the recruitment of Arf1-GDP (Kirchhausen, 2000). After the exchange of GDP to GTP by GBF1, the N-terminus of Arf1 inserts into the membrane, further recruiting the COPI coat protein complex to bend the membrane into vesicles. Meanwhile, cargo proteins would be loaded into vesicles by interacting with the COPI complex (Kirchhausen, 2000).

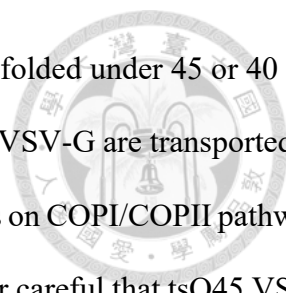
The COPII-mediated transport shows a similar mechanism. Sec12 integrating into the ER membrane would recruit Sar1-GDP for GTP exchange. The conformational change happens to Sar1 with the N-terminus attaching to ER membrane (Gurkan et al., 2006; Huang et al., 2001; McMahon et al., 2012) (some suggest the N-terminus of Sar1 inserts into the membrane (Cruz and Buchkovich, 2017; Fromme et al., 2008; Zanetti et al., 2011)). Sar1 activation is followed by recruitment of COPII inner coat proteins, Sec23 and Sec24. Sec23 recruits outer coat proteins Sec31 and Sec13 for membrane curvature (Zanetti et al., 2011). In most cases, cargo proteins or receptors interact with Sec24 for cargo loading (Zanetti et al., 2011). However, glycolipid glycosyltransferases (GGTs) interact directly with Sar1. In detail, the (R/K)X(R/K) motif on GGTs binds the A-site pocket on Sar1



around N94, N126, and D198 (Quintero et al., 2010). After Sec31 recruitment, GTPase activity of Sar1 would also be catalyzed by Sec23 and Sec31, followed by Sar1-GDP departure from the lipid (Long et al., 2010; Zanetti et al., 2011). Only if the Sar1 loading rate by Sec12 exceeded the hydrolysis rate by Sec23 and Sec31 would Sar1-GTP polymerize to sculpt a neck of vesicles. After Sar1-GTP turns into Sar1-GDP, the necks are constricted due to Sar1 departure to complete vesicle fission (Long et al., 2010). Therefore, the Sar1 GTP cycle is essential for COPII vesicle formation, and hydrolysis rate regulation determines the vesicles' size. For example, the two isotypes of Sar1 in mammals generate different sizes of COPII vesicles. Sar1b possesses weaker GTPase activity resulting in a larger size, while vice versa for Sar1a (Zanetti et al., 2011). In addition, the TANGO1 can connect to Sec12 and cargo protein procollagen I (Yuan et al., 2018). The increasing involvement of Sec12 in cargo packages induces a consequence akin to slowing the GTP hydrolysis, thereby delaying neck constriction. It leads to giant COPII vesicle formation than those without TANGO1 (Yuan et al., 2018). Besides these, Sec31 phosphorylation, Sec24 O-linked N-acetylglucosamine, and Sec23 ubiquitination would also affect the size of COPII vesicles (Peotter et al., 2019). On the other hand, when the dynamic GTP cycle was blocked, such as constitutive Sar1-GTP (H79G mutation) or Sar1-GDP (T39N mutation) over-expression, COPII vesicles failed to be generated, resulting in secretory blockage (Long et al., 2010). A polymerization-defective mutant of Sar1 (156-QTTG-159 to AAAA mutation) failed to generate the neck of the vesicles, thereby inhibiting the COPII pathway (Long et al., 2010).

1.2.2 A standard tool for monitoring COPI/COPII pathway

Like most plasma membrane proteins, vesicular stomatitis virus glycoprotein (VSV-G) undergoes the trafficking from the ER to Golgi for glycosylation, finally destining to the plasma membrane. To monitor the trafficking, a temperature-sensitive mutant of VSV-G protein (tsO45 VSV-G) fused with fluorescent protein was a theoretical model (Appenzeller-Herzog and Hauri, 2006;



Moffat et al., 2005; Moffat et al., 2007). Specifically, tsO45 VSV-G is misfolded under 45 or 40 °C, retaining within the ER lumen. When shifting to 32 °C, the refolded tsO45 VSV-G are transported to the Golgi and the plasma membrane. This system was widely used in studies on COPI/COPII pathway (Appenzeller-Herzog and Hauri, 2006). However, we should be skeptical or careful that tsO45 VSV-G transport represents the condition of the COPII pathway. For instance, although the mutation of Sar1 on 156-QTTG-159 blocks procollagen transport from the ER to the Golgi, the tsO45 VSV-G is still transported to the plasma membrane (Long et al., 2010). Moreover, some claimed that Sec13 depletion would not affect the transport of tsO45 VSV-G and that Sec13 might be dispensable for COPII vesicles for packaging small cargo (Townley et al., 2008; Zanetti et al., 2011).

1.2.3 The viral examples utilizing COPI/COPII pathway

The essential COPI/COPII pathway for cellular function has been reviewed above; it is also crucial in some viruses. A simple example is viral plasma membrane proteins that require glycosylation, such as VSV-G, influenza virus HA, and coronavirus S proteins (Springer et al., 2014; Ujike and Taguchi, 2015). Besides, Ebola virus Matrix protein VP40 and Coronavirus M (membrane) protein also require COPII machinery for protein trafficking (Ujike and Taguchi, 2015; Yamayoshi et al., 2008). Rotaviral NSP4 facilitates capsid protein VP7 trimerization, which demands COPI machinery (Martinez et al., 2019). More specifically, NSP4 exits the ER in COPII vesicle, trafficking together with VP7 (Crawford et al., 2019). Generally speaking, the COPII pathway, as well as COPI, is also involved in virion maturation.

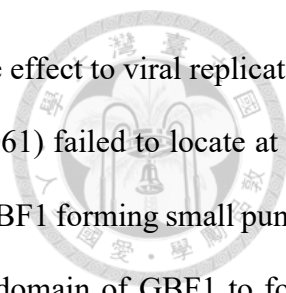
Enterovirus is also highly associated with COPI factors. The viral 3A proteins from coxsackievirus B3 (CVB3) and poliovirus (PV), but not human rhinovirus (HRV), would directly interact with COPI factor GBF1 to inhibit Arf1 activation (Wessels et al., 2006a; Wessels et al., 2006b). The interaction involves the N terminus of 3A and the N-terminal part of GBF1 (aa 2-62) (Viktorova et al., 2019; Wessels et al., 2006b). Several studies suggest that GEF (GTP exchange

factor) activity of GBF1 is required for viral replication because either knockdown of GBF1 or expression of GEF functional defective GBF1 would inhibit PV and CVB3 replication (Belov et al., 2008; Lanke et al., 2009; Viktorova et al., 2019). Now, the only known GBF1's function should be to activate Arf1 by GEF activity.

1.2.4 The roles and intricate relationships of 3A, GBF1, and Arf1

It is still presumable that GBF1 facilitates viral replication based on unrevealed function. It is because the over-expression of constitutively active Arf1 (Q71L mutation) could not rescue polioviral replication in the presence of GBF1 inhibitor (Belov et al., 2008), and knockdown of Arf1 would not reduce CVB3 replication (Lanke et al., 2009). These findings presumably indicate that Arf1 activation by GBF1 is not essential for the virus. Nonetheless the supposition was disagreed by the same scientific group around Belov afterward; they found that Arf1 knockdown would increase the sensitivity to GBF1 inhibition, showing the importance of Arf1 (Moghimi et al., 2020). Besides, double knockdowns of Arf1 and Arf3 would inhibit EV71 (Wang et al., 2014).

Because Arf1 activation can facilitate PI4KB recruitment (Godi et al., 1999), some believe PV 3A interacts with GBF1 for Arf1 activation, then recruiting PI4KB to RO. However, this hypothesis was challenged by several studies (Jackson and Belsham, 2021). A serine insertion after residue 14 for PV 3A and residue 15 for CVB3 3A (namely 3A-2 and 3A-ins 16S, respectively) would abrogate the binding toward GBF1 (Jackson and Belsham, 2021). The virus harboring this mutated 3A is viable and still sensitive to the GBF1 inhibitor (Brefeldin A (BFA)), and overexpression of GBF1 can rescue the mutants from BFA inhibition. Because of these, parts of experts claim the 3A: GBF1 interaction is dispensable for viral replication (Jackson and Belsham, 2021), although the virus needs GBF1. Oppositely, although 3A-2 mutants are viable, they show a delayed and reduced replication level (Belov et al., 2008; Viktorova et al., 2019). In addition, it is still possible that the insertion weakens, but not wholly removes, the ability to bind GBF1 (Jackson and Belsham, 2021). These results point



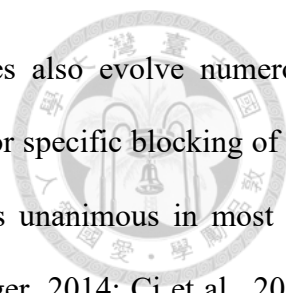
out that the interaction of enteroviral 3A and GBF1 should contribute some effect to viral replication but is not vital. Without the C terminal domain, GBF1 truncation (aa 1-1061) failed to locate at the Golgi, whereas co-expression with PV 3A protein could lead to truncated GBF1 forming small puncta. Similarly, 3A-2 that fails to interact with GBF1 requires the C-terminal domain of GBF1 to form puncta. In short, except N-terminus of GBF1 that interacts with 3A, the C-terminus also exerts an unknown function for PV replication (Viktorova et al., 2019). Enteroviral 3A would indirectly (Greninger et al., 2012) or directly (Dorobantu et al., 2014) recruit PI4KB that phosphorylates PI (phosphatidylinositol) into PI4P. PI4P favors GBF1's binding. In my opinion, 3A might recruit GBF1 in a circumvent manner with PI4P. Moreover, GBF1 requires its C-terminal domain to locate at the Golgi membrane, supposedly also leading 3A (3AB) into the right place for viral replication. Collectively, enteroviral 3A binds to GBF1 (Rhinovirus now belongs to *Rhinovirus* genera, not *Enterovirus*), which binds to PI4P and activates Arf1. Active Arf1 recruits PI4KB that phosphorylates PI into PI4P. In addition, enteroviral 3A hijacks ACBD3 to recruit PI4KB (see 1.3.2, Fig. 2). Supposedly, the intricate interacting inter-network would compensate for the function in different loss-of-function assays, thereby leading to an unclear and controversial mechanism.

Because of some similarity in the binding region on GBF1, it was once hypothesized that viral 3A protein mimics the function of Rab1B that facilitates COPI vesicle budding (Greninger, 2015). The fact that enterovirus would hijack autophagosomes to release infectious vesicles (Chen et al., 2015) might explain why 3A mimics the function of Rab1B, but everything still lacks evidence.

1.3 Replication organelles

1.3.1 Brief introduction of endomembrane modification by the viruses

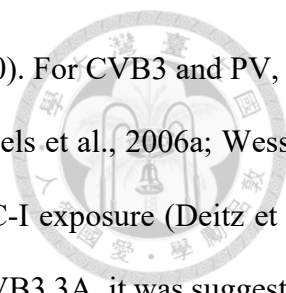
Even though viruses penetrate the cells, cells harbor several strategies to attack the virus, including the type I interferon pathway (Randall and Goodbourn, 2008). Host RNA sensors in the cytoplasm detect viral RNA (vRNA), triggering a sequential signaling cascade and finally producing



antiviral proteins (Randall and Goodbourn, 2008). For survival, viruses also evolve numerous abilities for counter-attacking the host defense (Ma et al., 2018). Except for specific blocking of the signaling, protection of viral RNA in a specific compartment or area is unanimous in most (+) stranded RNA viruses (Belov et al., 2012; Chatel-Chaix and Bartenschlager, 2014; Ci et al., 2020; Cortese et al., 2020; den Boon and Ahlquist, 2010). That is, they modify host organelles into replication sites to avoid vRNA from detection by RNA sensors and degradation by RNase (Egger et al., 1996). The modified architectures could also gather the resources, and the lipid environment could offer a platform for recruiting essential factors for vRNA duplication (van der Schaar et al., 2016). Despite a similar final goal, different viruses target different host organelles. For example, the brome mosaic virus modifies mitochondria into invaginated compartments (den Boon and Ahlquist, 2010). Coronaviruses modify the ER into double-membrane vesicles with a pore (Cortese et al., 2020; Wolff et al., 2020). Hepatitis C virus generates protrusion-type vesicles from the ER (Chatel-Chaix and Bartenschlager, 2014), while Zika and Dengue virus reorganize the ER into invagination-type compartments by viral NS1 proteins (Ci et al., 2020). The Golgi (or ERGIC) would be remodeled by enteroviruses (van der Schaar et al., 2016), while encephalomyocarditis virus (EMCV) and FMDV might target the ER (Dorobantu et al., 2016; Monaghan et al., 2004). Despite numerous studies, the mechanism for how these viruses reshape the endomembrane into replication sites remains largely unknown, especially for FMDV.

1.3.2 The mechanism and studies for enteroviral replication organelles

In the *Picornaviridae* family (including FMDV and enteroviruses), the modified compartment terms replication organelles (ROs) (Greninger, 2015). Enteroviruses, including poliovirus (PV), coxsackievirus B3 (CVB3), and enterovirus 71 (EV71), show some differences from FMDV (Berryman et al., 2016; Midgley et al., 2013; Moffat et al., 2005; Monaghan et al., 2004). Still, enterovirus is a valuable reference for FMDV due to abundant and deep research. Most believe the



mechanism starts from viral 3A proteins (Greninger, 2015; Hsu et al., 2010). For CVB3 and PV, 3A would block Arf1 activation by interacting with COPI factor GBF1 (Wessels et al., 2006a; Wessels et al., 2006b). It further detrimentally affects cytokine secretion and MHC-I exposure (Deitz et al., 2000; Dodd et al., 2001). Although Arf1 was pulled down together with CVB3 3A, it was suggestive of an indirect interaction through GBF1. That is because 3A would not be coprecipitated with constitutive Arf1-GTP (Q71L mutation) that showed little connection toward GBF1 (Wessels et al., 2006b). Besides the association with COPI factors, PV 3A also interacts with ACBD3 (acyl-CoA-binding protein domain 3) that recruits PI4KB (Greninger et al., 2012). PI4KB phosphorylates PI (phosphatidylinositol) lipid into PI4P to attract several viral and host factors, including 3D polymerase, 3C protease, and OSBP (oxysterol-binding protein) (Hsu et al., 2010; Shengjuler et al., 2017; van der Schaar et al., 2016). Therefore, viral RNA duplication mainly occurs on the surface of ROs (Hsu et al., 2010), and OSBP exchanges PI4P for cholesterol from the ER (van der Schaar et al., 2016). Cholesterol accumulation increases lipid fluid, which might be one reason for RO formation (Ilnytska et al., 2013). This change also impacts the processing of 3CD polymerase (Ilnytska et al., 2013). Reportedly, PI4KB also facilitates CVB3 3AB processing (Melia et al., 2017). It is noteworthy that GBF1's HSD1 domain contains PIP membrane binding site (Viktorova et al., 2019), presumably leading to a positive feedback loop for replication complex formation: 3A-ACBD3-PI4KB-PI4P-GBF1-3A. The mechanism for cholesterol accumulation is far more intricate. Viral 2BC increases cholesterol (or low-density lipoprotein) uptake by clathrin-mediated endocytosis, and PI4KB prevents cholesterol from cycling back to the plasma membrane by directly interacting with Rab11, a marker of recycling endosomes (Ilnytska et al., 2013). In fact, the whole picture of the enteroviral RO mechanism is incomplete and debatable. For instance, EV71 3A showed less connection with GBF1 and ACBD3 (Greninger et al., 2012), but EV71 reportedly requires GBF1 and Arf1 (Wang et al., 2014). Interestingly, knockdown of single Arf1 would not inhibit EV71, as shown for other enteroviruses; however, double knockdowns of Arf1 and Arf3 significantly inhibit the virus (Wang

et al., 2014). In 2020, the report even pointed out that at the end of the virus cycle, enteroviral ROs gather not only Arf1 but also Arf3, Arf4, Arf5, and Arf6 (Moghimi et al., 2020). They even claimed Arf1 activation directly supports the development of ROs because Arf1 (or Arf6) knockdown would increase sensitivity to GBF1 inhibition (Moghimi et al., 2020). This view is different from that in the past. Here, we summarize the simplified “putative” mechanism of enteroviral RO formation in Figure 2.

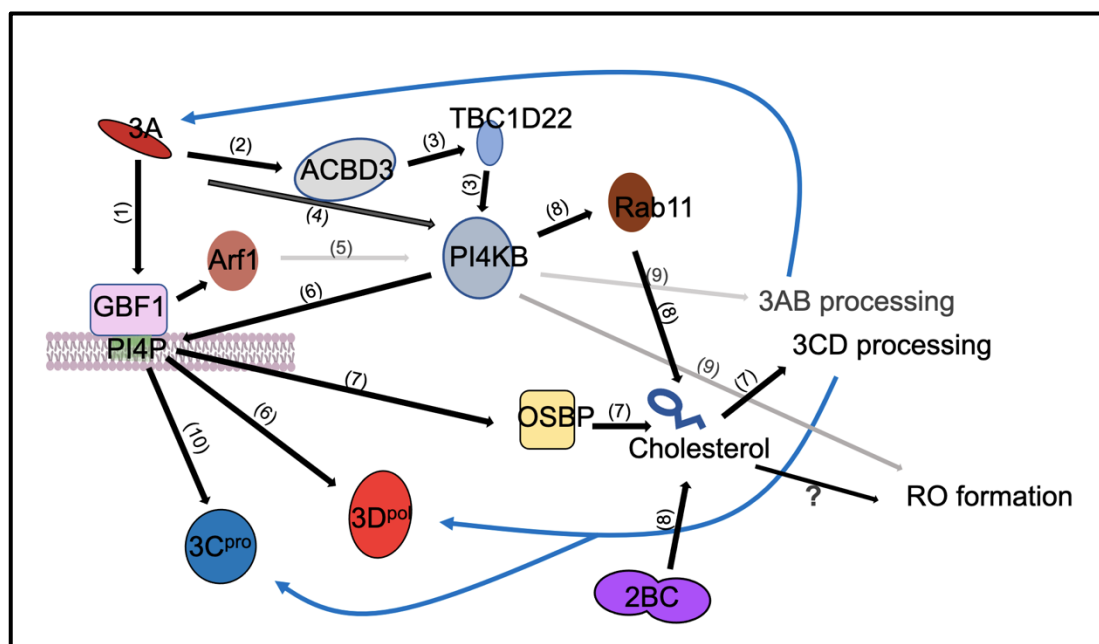
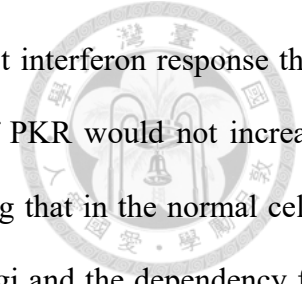


Figure 2. The schematic for a putative mechanism of enteroviral RO formation. The references include as below. (1) (Wessels et al., 2006b); (2) (Greninger et al., 2012); (3) (Greninger et al., 2013); (4) (Dorobantu et al., 2014); (5) (Godi et al., 1999); (6) (Hsu et al., 2010); (7) (Arita et al., 2013); (8) (Illynska et al., 2013); (9) (Melia et al., 2017); (10) (Shengjuler et al., 2017).

The study for the CVB3 3A-H57Y mutant questioned the role of RO. The mutant could survive in the presence of PI4KB inhibitor, though showing a delayed growth curve and severely delayed RO formation (Melia et al., 2017). They suggested that counter-attacking for the anti-viral response was so powerful that RO’s protection for vRNA was dispensable. Therefore, the mutant without RO’s

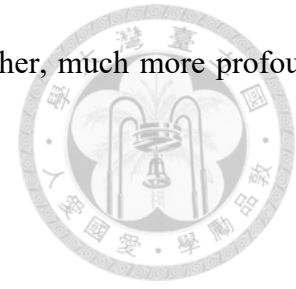


protection in the presence of PI4KB inhibitor did not elicit a more robust interferon response than that without the inhibitor (Melia et al., 2017). Likewise, knockdown of PKR would not increase mutant viral replication under the inhibitor (Melia et al., 2017), indicating that in the normal cells, RO barely protected vRNA. They further implied that reshaping the Golgi and the dependency for PI4KB aimed to subtly change the structure and the angle of 3AB on the membrane, increasing 3AB processing (Melia et al., 2017). The H57Y mutation on 3A could dispense with the need in that situation for 3AB processing, thereby resistant to PI4KB inhibitor (Melia et al., 2017). Reliable data supported their supposition. However, RO's role in recruiting replication factors and controlling the variation of concentration between 3AB and "3A and 3B" should not be underestimated for optimal replication.

1.3.3 Recent understanding of FMDV ROs

As mentioned above, FMDV shows different characteristics distinct from enterovirus (EV). (1) FMDV is resistant to GBF1 inhibitors (Midgley et al., 2013; O'Donnell et al., 2001). (2) FMDV 2BC, not 3A, blocks the secretory pathway in the TsO45 VSV G model (Moffat et al., 2005; Moffat et al., 2007). (3) FMDV RO seems as homologous vesicles, not as heterologous tubules for enteroviral RO. (Belov et al., 2012; Monaghan et al., 2004) (4) PI4K and PI4P are not required for FMDV (Berryman et al., 2016; Loundras et al., 2016). (5) The C-terminus of FMDV 3A is much longer than that of other picornaviruses, and the topology is much like EV 3AB instead of EV 3A (Fujita et al., 2007; Gonzalez-Magaldi et al., 2014). Now, we know FMDV utilizes the COPII pathway, instead of COPI, for viral replication (Midgley et al., 2013). In addition, when FMDV ROs appear at the early stage, it shows normal Golgi appearance and fragmented rER (Monaghan et al., 2004). These facts strongly suggest that FMDV modifies the ER into RO. EMCV is also proved to modify the ER, while it still requires PI4KA and PI4P (Dorobantu et al., 2015). Therefore, the mechanism for FMDV RO should be different from other picornaviruses. Alternatively, the key reaction for picornaviral membrane

modification remains unnoticed. To answer the question, we needed further, much more profound research.

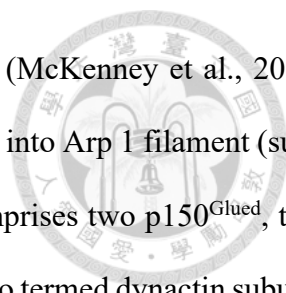


1.4 Motor protein complex: dynein/dynactin

1.4.1 Fundamental knowledge of dynein/dynactin

Cytosol's high viscosity and crisscrossing cytoskeletal filaments result in large objects being macroscopically immobile by free diffusion in the cytosol, such as vesicles and viruses (Greber and Way, 2006). It is known that the trafficking inside the cells is regulated by motor proteins, including dynein, kinesin, and myosin, which viruses would also hijack (Greber and Way, 2006). For example, the vaccinia virus (~300 nm) diffuses at speeds of 2 $\mu\text{m/hr}$ in the cytoplasm, whereas adenoviruses (~ 100 nm) could move at speeds of 1-3 $\mu\text{m/s}$ based on motor proteins (Greber and Way, 2006). The three motor proteins showed different characteristics. Dynein drives minus-end-directed transport along microtubules, such as the movement for endosomes from plasma membrane toward the Golgi and the movement for COPII vesicles from the ER toward Golgi. Kinesin carries out positive-end-directed transport on microtubules, and myosin drives the transport on actin (Greber and Way, 2006). This section below discusses dynein.

Dynein (dynein-1) consists of a motor domain for mechanical motion and a tail domain for cargo binding, regulation, and homodimerization. Dimerization is essential for dynein exerting its function (Carter et al., 2016), just like feet walking on microtubules. In detail, the motor domain consists of a ring of six AAA+ (ATPase Associated with various Activities) ATPase domains, in which ATP drives conformational change (Carter et al., 2016). The catalytic cycle makes the dynein step on the microtubules. The tail contains a light-intermediate chain (LIC), intermediate chain (IC), light chains (LCs, including LC7, LC8, and Tctex), and heavy chain (HC); it connects to its co-factor, dynactin (Carter et al., 2016). Although dynein plays a pivotal role in the movement, dynactin is also essential for processive motility. In the absence of dynactin, mammalian dynein could only show a short back-



forth movement on microtubules, presumably in thermo-driven diffusion (McKenney et al., 2014; Splinter et al., 2012). Dynactin, composed of several subunits, could divide into Arp 1 filament (such as p62 and Arp1) and the shoulder (Carter et al., 2016). The shoulder comprises two p150^{Glued}, two p24, and four dynamitin (p50) (Carter et al., 2016). The p24 (or p22) was also termed dynactin subunit 3 (DCTN3) (Schroer, 2004; Urnavicius et al., 2015). Overexpression of p150^{Glued} or dynamitin would be a common strategy for studying the effect on the loss function of dynein (Dodding and Way, 2011; Gladue et al., 2014).

1.4.2 The adaptors of dynein/dynactin complex

As mentioned above, the dynein/dynactin complex is necessary for processive movement. However, the affinity for these two complexes is extremely low (Splinter et al., 2012). For transporting vesicles, it also lacks a connection to the motor complex. Therefore, it requires another factor to exert normal biological function: adaptors. For example, Bicaudal D2 (BICD2) as an adaptor can stabilize the dynein-dynactin complex by co-interacting with dynein and dynactin; meanwhile, it interacts with Rab6 to drive the Rab6-vesicles moving from the Golgi (McKenney et al., 2014; Splinter et al., 2012). Other dynein/dynactin-associated adaptors include hSpindly, Rab11-FIP3, Hook3, and Hook1 (Dwivedi et al., 2019). They target different vesicles for movement. Although some think dynactin directly connects to Sec23 of COPII vesicle with p150^{Glued} (Fromme et al., 2008), it is more believable that there are other dynein adaptors not yet discovered for COPII vesicles.

1.4.3 Other functions for dynein

In addition to vesicular transport, dynein also participates in the organization of mitotic spindles (Tanenbaum et al., 2013). In more detail, dimeric dynein can bind two anti-parallel microtubule bundles simultaneously with two motor domains. Without the need for dynactin, dynein causes the sliding of microtubules during mitosis (Tanenbaum et al., 2013). Besides, dynein also mediates the

position of the nucleus. In detail, forward nuclear movement (toward the leading edge) depends on the force generated by dynein/dynactin complex, while myosin controls rearward movement (Zhu et al., 2017). Moreover, dynein-2 possibly assembles with polymeric intraflagellar transport trains that are essential for cilia biogenesis and would be transported by kinesin-II (Toropova et al., 2019).

1.4.4 Examples of viruses interplaying with dynein/dynactin

After endocytosis, most viruses within endosomes utilize retrograde transport driven by dynein/dynactin to arrive at their desired destinations, such as the nucleus, the ER, and the Golgi. In contrast to hitchhiking the endosomes, some viruses choose to interact with dynein directly. For instance, when the adenovirus is exposed to low pH in the endosome, the hexon capsid subunit is exposed and directly binds to the dynein IC and LIC1 (Dodding and Way, 2011). The partially disassembled adenovirus further moves towards the nucleus by dynein. After binding to the nuclear pore complex, the capsid binds kinesin-1, tearing the virion apart and viral DNA transporting into the nucleus (Flint et al., 2015). For herpesvirus virus 1, an inner tegument component directly interacts with dynein as well (Dodding and Way, 2011). Besides viral entry, dynein is also essential for glycosylation of viral proteins, such as influenza virus hemagglutinin (HA). After all, it takes charge of COPII vesicle movement (Flint et al., 2015). Some viruses, such as herpesvirus, assemble their virion within the nucleus; therefore, viral structure proteins are transported into the nucleus, requiring motor protein (Flint et al., 2015).

Viruses utilize the host trafficking system in life cycles by interacting with motor protein subunits, as mentioned above. However, some interactions remain unknown for their purpose. For example, DCTN3 interacts with FMDV 3A protein, reportedly essential for FMDV replication in cattle (Gladue et al., 2014). However, the biological function of 3A-DCTN3 has not been investigated. Besides, the interaction between rabies phosphoprotein (P) and LC8 is another enigma (Raux et al., 2000). The interaction might not be associated with virus transcription and dynein-mediated transport

but is involved in the nuclear import of P protein (Moseley et al., 2007).

In brief, dynein is essential not only for cells but also for most viruses in several aspects, and much research about this field is in need.



1.5 Neutralization sites

Endocytosis is a major route for FMDV to invade the cells, initiated by attaching to cellular receptors, such as integrins ($\alpha v\beta 6$, $\alpha v\beta 3$, $\alpha v\beta 8$, and $\alpha v\beta 1$), heparan sulfate, and JMJD6 (Lawrence et al., 2016; Wang et al., 2015). Integrins bind to the RGD motif on the GH-loop (VP1-145 to 147) of VP1, and heparan sulfate binds to VP3 near VP2 (Wang et al., 2015). The binding site for JMJD6 was presumed to cross VP1-95 and VP3-70 (Lawrence et al., 2016). Theoretically, neutralization antibodies block viruses from these receptors, as it literally means neutralizing the virions. To identify neutralizing antibody binding sites (neutralization sites), virologists performed an escape mutant assay that cultured FMDV in a low concentration of neutralizing monoclonal antibody (MAb). The selective pressure and viral polymerase's error-prone nature would let the virus evolve into mutants that escape MAb's binding. In other words, the mutation is the critical residue for neutralizing sites. Five neutralization sites were identified in serotype O virus, as shown in Table 1 and Figure 3.

Table 1. The critical residues of neutralization sites in serotype O viruses

	Site 1	Site 2	Site 3	Site 4	Site 5
Subunit protein	VP1	VP2	VP1	VP3	VP1
Critical residues	144, 148, 150, 208	70, 71, 72, 73, 75, 77, 131, 191	43, 44	56, 58	149
References	(Kitson et al., 1990; McCahon et al., 1989; Xie et al., 1987)	(Asfor et al., 2014; Kitson et al., 1990; McCahon et al., 1989; Xie et al., 1987)	(Crowther et al., 1993; Kitson et al., 1990; McCahon et al., 1989; Xie et al., 1987)	(Barnett et al., 1998; Kitson et al., 1990; McCahon et al., 1989)	(Aktas and Samuel, 2000)

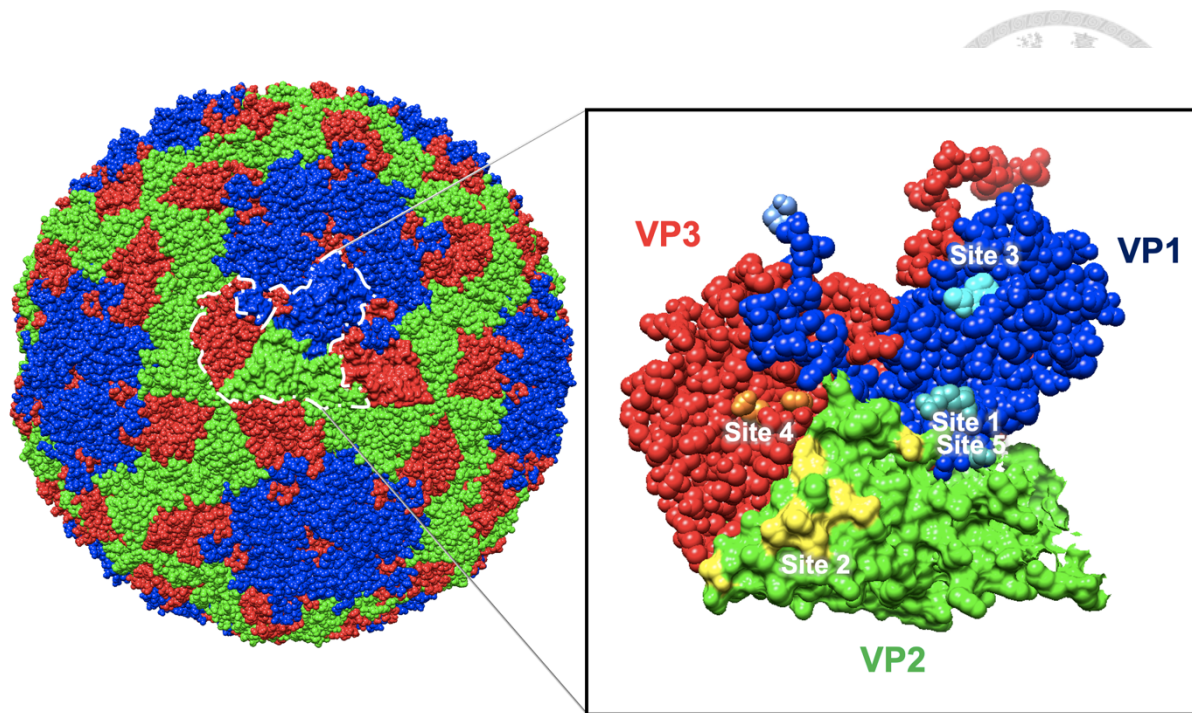
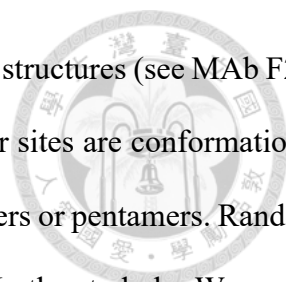


Figure 3. The simulation of virion and protomer for O1M-S093Y strain (PDB: 5DDJ) with indicated neutralizing sites. Sites 1 and 5 are located on the GH-loop (dusty blue) of VP1 and site 3 (cyan) on VP1 near the five-fold axis. Site 2 (yellow) situates at VP2; site 4 (orange) is at VP3.

Because of the location near the RGD motif, site 1 was presumed as the most crucial epitope in the past. However, in 2012, it was proved that site 2 was the most immunodominant epitope (Mahapatra et al., 2012). The conclusion came from the neutralization tests with escape mutants for indicated sites. For example, site 1 antibodies within the serum could not neutralize site 1 escape mutant; therefore, the serum's neutralization ability (neutralizing titer) would decrease compared to wild-type virus. The reduction could be considered as the contribution by the indicated site of antibodies when neutralizing the wild-type virus. As a result, most antibodies were directed to site 2 in most vaccinated animals, followed by site 1 antibodies, while antibodies against sites 3, 4, and 5 showed minor contributions to neutralization activity (Mahapatra et al., 2012).

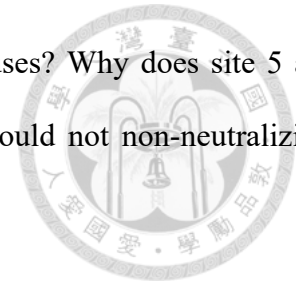
Except for escape mutant assay, other strategies remain for identifying and characterizing neutralizing MAbs, such as the synthetic peptide approach. Indirect ELISA with synthetic peptides ranging from the GH-loop can identify most site 1 MAbs (Cheng et al., 2006; Yang et al., 2014).



However, parts of site 1 MABs still seem to recognize conformational site 1 structures (see MAB F21-48 in the study by Yang et al.) (Yang et al., 2014). Most importantly, other sites are conformational epitopes and can only be presented in high-order structures, such as protomers or pentamers. Random peptide phage display is another tool for mapping antibody binding sites. In the study by Wang and colleagues, a neutralizing MAB against Asia 1 serotype virus failed to recognize linear VP1 in a Western blot. However, it was proved to bind GH-loop on VP1 (VP1-144 to 149) by phage display and reverse genetic system (Wang et al., 2011b). Possibly, phage-displaying random peptides, though non-identical to viral sequence, could mimic a conformational epitope on a viral protein in some cases. The reverse genetic system is another widely-used mapping method, directly generating site mutated virus and examining MAB's neutralizing ability toward it (Asfor et al., 2014; Wang et al., 2011b). However, the infectious clone is highly restrictive and regulated due to biosafety concerns, especially in Taiwan. Finally, given advanced biophysics, resolving the atomic structure of immuno-complex is the straight, flawless way for mapping neutralizing antibody (nanobody, or scFv) binding sites (Dong et al., 2021; Zheng et al., 2019). Of course, it is a difficult task and high tech demands.

Different serotypes showed slightly different critical residues in different nomenclature. For example, the neutralization site on the VP1 GH-loop for serotype C is site A. Site 5 for serotype Asia 1 situates at VP3-218 instead of VP1-149 (Grazioli et al., 2013). Still, three parts should be unanimous in importance: the GH-loop of VP1, the BC-loop of VP2, and VP3 near VP3-58. The classification of neutralization sites can help us understand the event of “blocking viruses,” whereas some neutralizing antibodies are not fit, and the critical residues give limited information. For example, the mutation on VP3-59 could escape the presumed site 4 antibody's binding (Yang et al., 2014). Some neutralizing MABs bind to the region across more than one site (Barnett et al., 1998). Reportedly, the binding toward virion would possibly trigger premature uncoating and dissociating of the virus (Dong et al., 2021). Because the antibody (or nanobody) inhibited the virus, it would still be classified into neutralizing antibodies. Therefore, the mechanism for neutralizing antibodies remains some questions

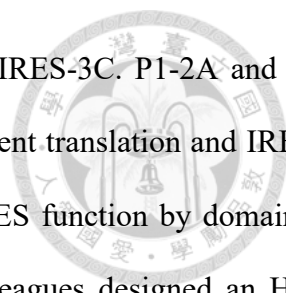
to be answered. In other words, why could site 3 antibodies inhibit viruses? Why does site 5 are conformational epitope? Considering the large antibody volume, why could not non-neutralizing antibodies block the virus?



1.6 Virus-like particles

As introduced above, the P1-2A polyprotein would be processed by 3C protease (3C^{pro}) into VP0, VP3, VP1, and 2A (Fry et al., 2005). Immediately after synthesis, P1 (or P1-2A) itself folds into an unprocessed protomer, while, only after cleavage by 3C^{pro}, processed protomers in five self-assemble into a pentamer (Fry et al., 2005). The twelve pentamers assemble a whole virion; in the meantime, VP0 would be cleaved into VP4 and VP2 (Fry et al., 2005). There are two general ways for VLP production. One is the production and purification of individual subunit proteins, including VP0, VP3, and VP1, widely adopted in the *E. coli* expression system (Guo et al., 2013; Lee et al., 2009). Researchers usually fused SUMO fusion protein to the subunit for increasing solubility, avoiding inclusion bodies. After purification and removal of SUMO, subunits self-assemble into VLPs (Guo et al., 2013; Lee et al., 2009).

The other strategy is the co-expression of P1 and 3C^{pro} within the cells. The cassette P1-2A-3C gene is a popular scheme that utilizes the self-cleavage activity of 2A (Abrams et al., 1995). Given the cistronic genetic display, the strategy could apply to baculovirus, mammalian cells, and even plant expression systems (Gullberg et al., 2013; Mohana Subramanian et al., 2012; Pan et al., 2008). However, P1-2A and 3C proteins would be synthesized in equal amounts in this scheme. 3C^{pro} degrades several host factors, including eIF4G and eIF4A that are essential for host translation (Belsham et al., 2000). Therefore, 3C^{pro} is cytotoxic and limiting the production of VLP. To deal with this, scientists mediate or alter the processing activity of 3C^{pro} by mutation, such as C142S and L127P (Gullberg et al., 2013; Puckette et al., 2017). Downregulation of the 3C production is another strategy, including utilizing mutated IRES and HIV frameshift (Gullberg et al., 2013; Porta et al., 2013). In



detail, Gullberg and colleagues rearranged the FMDV gene into P1-2A-IRES-3C. P1-2A and 3C proteins are governed by two different translation systems, 5' cap-dependent translation and IRES-dependent translation (Gullberg et al., 2013). Next, they mutilate the IRES function by domain 2 mutation to decrease 3C production. On the other hand, Porta and colleagues designed an HIV frameshift gene that links to P1-2A and 3C genes (Porta et al., 2013). Because the frameshift sequence frameshifts every 20 times, 3C translation, as an in-frame gene, is reduced to approximately 5% of P1-2A. However, the cistronic genetic display also means a lack of flexibility; it is hard to find an excellent balance between processing and cytotoxicity. The co-transfection strategy circumvents the problem; in Polacek et al. study, they co-transfect P1 plasmids with relatively small amounts of 3C plasmids to avoid excess 3C that inhibits total protein production (Polacek et al., 2013).

Although antigenicity for VLP is almost authentic to that for virion and FMDV replication can be dispensable, the un-stability of VLP is a significant problem for application. Some researchers progress by mutations to enforce the links between structure proteins (Deepak et al., 2019; Ganji et al., 2018). In short, more researchers are advancing the production and application of VLP.

1.7 Summary

FMD virion attaches to host receptors inducing endocytosis. The endosomes containing the viruses move toward MTOC by dynein motor protein. After fusing with lysosomes, the acidic environment triggers the viruses to be uncoated, further releasing the viral genome. The (+) stranded viral RNA directly recruits host translation factors for expressing viral polyproteins. The polyproteins were then divided and processed into several structure proteins and non-structure proteins due to viral L protease, 2A, and 3C protease. The non-structure protein 3D polymerase synthesizes (-) stranded RNA from positive one and vice versa. In the meantime, the virus somehow modifies host organelles into replication organelles to optimize the replication. The structure proteins, including VP0, VP3, and VP1, encapsulate (+) viral RNA along with 3B. VP0 is then cleaved into VP4 and VP2, making

the complex more compact. After cell lysis, the mature viruses would be released and infect the next acceptable cells (Fig. 4). However, the virus cycle might be more complicated; recent studies show some exceptions, such as micropinocytosis for viral entry and exosomes for viral release (Han et al., 2016; Zhang et al., 2019).

Although the virus cycle should basically be described above, it still needs to be discovered. For instance, how a virus remodels host organelles is an enigma. We believe 3A protein is the critical factor, so we intend to understand the function of 3A deeply. On the other hand, antibodies can prevent a virus from contacting host receptors, but that only means some. We tend to detect neutralizing antibodies from vaccinated animals to evaluate protectivity. Considering the virion's conformational and highly folding structure, we choose virus-like particles for our study and for developing our detection system, blocking ELISA.

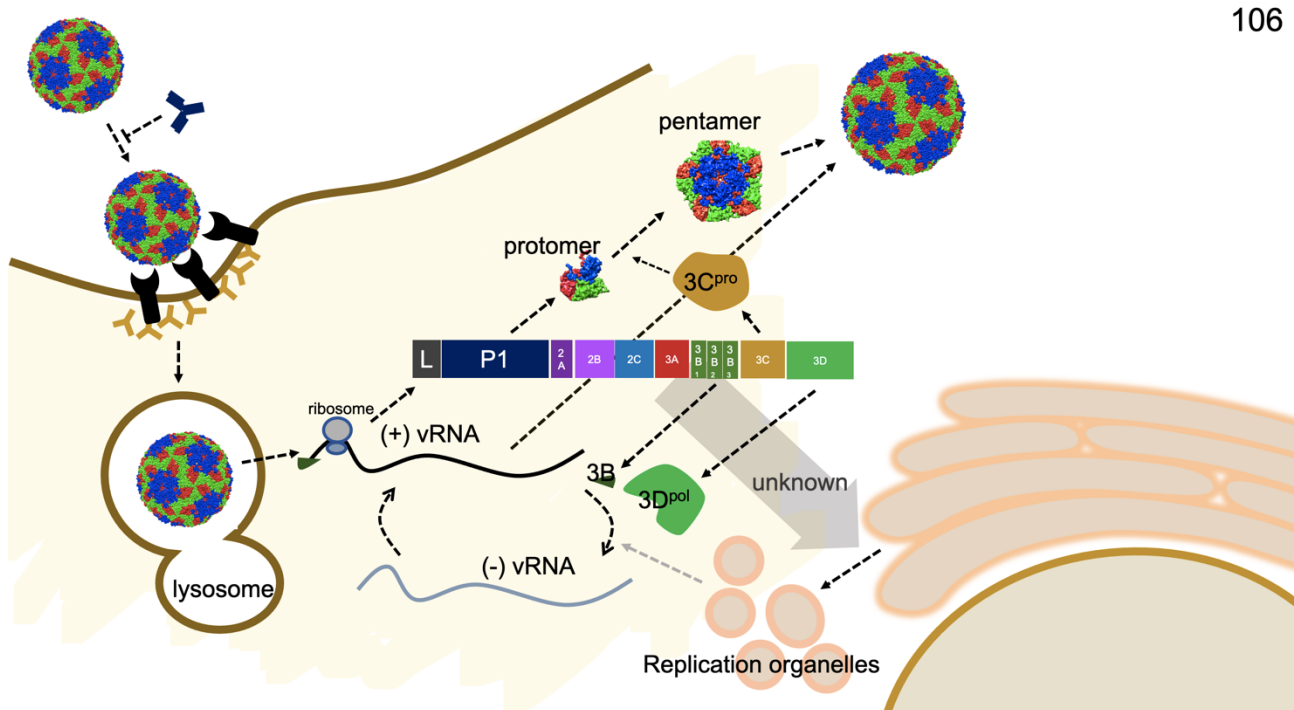
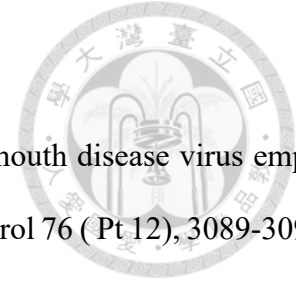
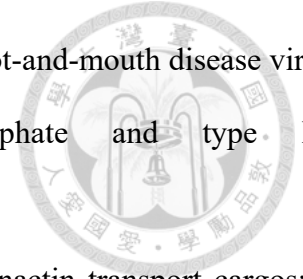


Figure 4. FMDV life cycle within the cells.

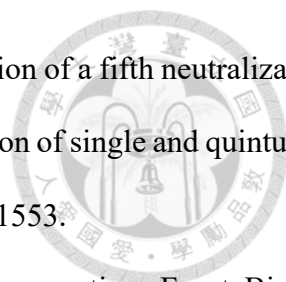


References

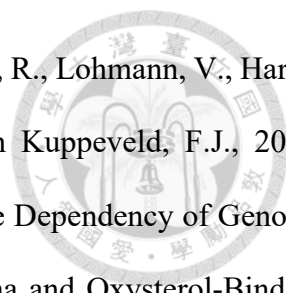
- Abrams, C.C., King, A.M., Belsham, G.J., 1995. Assembly of foot-and-mouth disease virus empty capsids synthesized by a vaccinia virus expression system. *J Gen Virol* 76 (Pt 12), 3089-3098.
- Aktas, S., Samuel, A.R., 2000. Identification of antigenic epitopes on the foot and mouth disease virus isolate O1/Manisa/Turkey/69 using monoclonal antibodies. *Rev Sci Tech* 19, 744-753.
- Appenzeller-Herzog, C., Hauri, H.P., 2006. The ER-Golgi intermediate compartment (ERGIC): in search of its identity and function. *J Cell Sci* 119, 2173-2183.
- Arita, M., Kojima, H., Nagano, T., Okabe, T., Wakita, T., Shimizu, H., 2013. Oxysterol-binding protein family I is the target of minor enviroxime-like compounds. *J Virol* 87, 4252-4260.
- Asfor, A.S., Upadhyaya, S., Knowles, N.J., King, D.P., Paton, D.J., Mahapatra, M., 2014. Novel antibody binding determinants on the capsid surface of serotype O foot-and-mouth disease virus. *J Gen Virol* 95, 1104-1116.
- Barnett, P.V., Samuel, A.R., Pullen, L., Ansell, D., Butcher, R.N., Parkhouse, R.M., 1998. Monoclonal antibodies, against O1 serotype foot-and-mouth disease virus, from a natural bovine host, recognize similar antigenic features to those defined by the mouse. *J Gen Virol* 79 (Pt 7), 1687-1697.
- Beard, C.W., Mason, P.W., 2000. Genetic determinants of altered virulence of Taiwanese foot-and-mouth disease virus. *J Virol* 74, 987-991.
- Belov, G.A., Feng, Q., Nikovics, K., Jackson, C.L., Ehrenfeld, E., 2008. A critical role of a cellular membrane traffic protein in poliovirus RNA replication. *PLoS Pathog* 4, e1000216.
- Belov, G.A., Nair, V., Hansen, B.T., Hoyt, F.H., Fischer, E.R., Ehrenfeld, E., 2012. Complex dynamic development of poliovirus membranous replication complexes. *J Virol* 86, 302-312.
- Belsham, G.J., McInerney, G.M., Ross-Smith, N., 2000. Foot-and-mouth disease virus 3C protease induces cleavage of translation initiation factors eIF4A and eIF4G within infected cells. *J Virol* 74, 272-280.



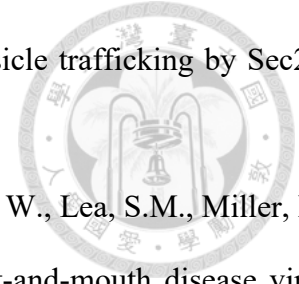
- Berryman, S., Moffat, K., Harak, C., Lohmann, V., Jackson, T., 2016. Foot-and-mouth disease virus replicates independently of phosphatidylinositol 4-phosphate and type III phosphatidylinositol 4-kinases. *J Gen Virol* 97, 1841-1852.
- Carter, A.P., Diamant, A.G., Urnavicius, L., 2016. How dynein and dynactin transport cargos: a structural perspective. *Curr Opin Struct Biol* 37, 62-70.
- Chatel-Chaix, L., Bartenschlager, R., 2014. Dengue virus- and hepatitis C virus-induced replication and assembly compartments: the enemy inside--caught in the web. *J Virol* 88, 5907-5911.
- Chen, Y.H., Du, W., Hagemeijer, M.C., Takvorian, P.M., Pau, C., Cali, A., Brantner, C.A., Stempinski, E.S., Connelly, P.S., Ma, H.C., Jiang, P., Wimmer, E., Altan-Bonnet, G., Altan-Bonnet, N., 2015. Phosphatidylserine vesicles enable efficient en bloc transmission of enteroviruses. *Cell* 160, 619-630.
- Cheng, I.C., Liang, S.M., Tu, W.J., Chen, C.M., Lai, S.Y., Cheng, Y.C., Lee, F., Huang, T.S., Jong, M.H., 2006. Study on the porcineophilic foot-and-mouth disease virus I. production and characterization of monoclonal antibodies against VP1. *J Vet Med Sci* 68, 859-864.
- Ci, Y., Liu, Z.Y., Zhang, N.N., Niu, Y., Yang, Y., Xu, C., Yang, W., Qin, C.F., Shi, L., 2020. Zika NS1-induced ER remodeling is essential for viral replication. *J Cell Biol* 219.
- Cortese, M., Lee, J.Y., Cerikan, B., Neufeldt, C.J., Oorschot, V.M.J., Kohrer, S., Hennies, J., Schieber, N.L., Ronchi, P., Mizzon, G., Romero-Brey, I., Santarella-Mellwig, R., Schorb, M., Boermel, M., Mocaer, K., Beckwith, M.S., Templin, R.M., Gross, V., Pape, C., Tischer, C., Frankish, J., Horvat, N.K., Laketa, V., Stanifer, M., Boulant, S., Ruggieri, A., Chatel-Chaix, L., Schwab, Y., Bartenschlager, R., 2020. Integrative Imaging Reveals SARS-CoV-2-Induced Reshaping of Subcellular Morphologies. *Cell Host Microbe* 28, 853-866 e855.
- Crawford, S.E., Criglar, J.M., Liu, Z., Broughman, J.R., Estes, M.K., 2019. COPII Vesicle Transport Is Required for Rotavirus NSP4 Interaction with the Autophagy Protein LC3 II and Trafficking to Viroplasms. *J Virol* 94.



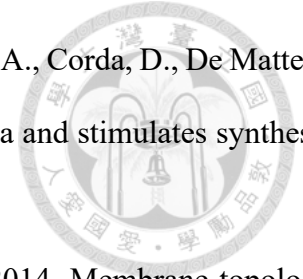
- Crowther, J.R., Farias, S., Carpenter, W.C., Samuel, A.R., 1993. Identification of a fifth neutralizable site on type O foot-and-mouth disease virus following characterization of single and quintuple monoclonal antibody escape mutants. *J Gen Virol* 74 (Pt 8), 1547-1553.
- Cruz, L., Buchkovich, N.J., 2017. Rerouting the traffic from a virus perspective. *Front Biosci (Landmark Ed)* 22, 1845-1866.
- de Los Santos, T., Diaz-San Segundo, F., Grubman, M.J., 2007. Degradation of nuclear factor kappa B during foot-and-mouth disease virus infection. *J Virol* 81, 12803-12815.
- Deepak, P.R., Saravanan, P., Biswal, J.K., Basagoudanavar, S.H., Dechamma, H.J., Umapathi, V., Sreenivasa, B.P., Tamilselvan, R.P., Krishnaswamy, N., Zaffer, I., Sanyal, A., 2019. Generation of acid resistant virus like particles of vaccine strains of foot-and-mouth disease virus (FMDV). *Biologicals* 60, 28-35.
- Deitz, S.B., Dodd, D.A., Cooper, S., Parham, P., Kirkegaard, K., 2000. MHC I-dependent antigen presentation is inhibited by poliovirus protein 3A. *Proc Natl Acad Sci U S A* 97, 13790-13795.
- den Boon, J.A., Ahlquist, P., 2010. Organelle-like membrane compartmentalization of positive-strand RNA virus replication factories. *Annu Rev Microbiol* 64, 241-256.
- Dodd, D.A., Giddings, T.H., Jr., Kirkegaard, K., 2001. Poliovirus 3A protein limits interleukin-6 (IL-6), IL-8, and beta interferon secretion during viral infection. *J Virol* 75, 8158-8165.
- Dodding, M.P., Way, M., 2011. Coupling viruses to dynein and kinesin-1. *EMBO J* 30, 3527-3539.
- Dong, H., Liu, P., Bai, M., Wang, K., Feng, R., Zhu, D., Sun, Y., Mu, S., Li, H., Harmsen, M., Sun, S., Wang, X., Guo, H., 2021. Structural and molecular basis for foot-and-mouth disease virus neutralization by two potent protective antibodies. *Protein Cell*.
- Dorobantu, C.M., Albuлесcu, L., Harak, C., Feng, Q., van Kampen, M., Strating, J.R., Gorbalenya, A.E., Lohmann, V., van der Schaar, H.M., van Kuppeveld, F.J., 2015. Modulation of the Host Lipid Landscape to Promote RNA Virus Replication: The Picornavirus Encephalomyocarditis Virus Converges on the Pathway Used by Hepatitis C Virus. *PLoS Pathog* 11, e1005185.



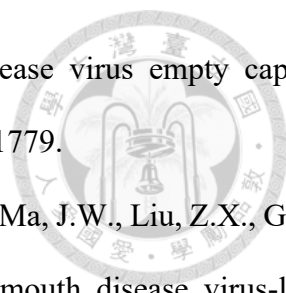
- Dorobantu, C.M., Albulescu, L., Lyoo, H., van Kampen, M., De Francesco, R., Lohmann, V., Harak, C., van der Schaar, H.M., Strating, J.R., Gorbalenya, A.E., van Kuppeveld, F.J., 2016. Mutations in Encephalomyocarditis Virus 3A Protein Uncouple the Dependency of Genome Replication on Host Factors Phosphatidylinositol 4-Kinase IIIalpha and Oxysterol-Binding Protein. *mSphere* 1.
- Dorobantu, C.M., van der Schaar, H.M., Ford, L.A., Strating, J.R., Ulferts, R., Fang, Y., Belov, G., van Kuppeveld, F.J., 2014. Recruitment of PI4KIIIbeta to coxsackievirus B3 replication organelles is independent of ACBD3, GBF1, and Arf1. *J Virol* 88, 2725-2736.
- Du, Y., Bi, J., Liu, J., Liu, X., Wu, X., Jiang, P., Yoo, D., Zhang, Y., Wu, J., Wan, R., Zhao, X., Guo, L., Sun, W., Cong, X., Chen, L., Wang, J., 2014. 3Cpro of foot-and-mouth disease virus antagonizes the interferon signaling pathway by blocking STAT1/STAT2 nuclear translocation. *J Virol* 88, 4908-4920.
- Du, Y., Duan, T., Feng, Y., Liu, Q., Lin, M., Cui, J., Wang, R.F., 2018. LRRC25 inhibits type I IFN signaling by targeting ISG15-associated RIG-I for autophagic degradation. *EMBO J* 37, 351-366.
- Dwivedi, D., Chawla, P., Sharma, M., 2019. Incorporating Motility in the Motor: Role of the Hook Protein Family in Regulating Dynein Motility. *Biochemistry* 58, 1026-1031.
- Egger, D., Pasamontes, L., Bolten, R., Boyko, V., Bienz, K., 1996. Reversible dissociation of the poliovirus replication complex: functions and interactions of its components in viral RNA synthesis. *J Virol* 70, 8675-8683.
- Feng, Y., Duan, T., Du, Y., Jin, S., Wang, M., Cui, J., Wang, R.F., 2017. LRRC25 Functions as an Inhibitor of NF-kappaB Signaling Pathway by Promoting p65/RelA for Autophagic Degradation. *Sci Rep* 7, 13448.
- Flint, S.J., Racaniello, V.R., Rall, G.F., Skalka, A.M., Enquist, L.W., 2015. Principles of virology, 4th edition. Edition. ASM Press, Washington, DC, volumes p.

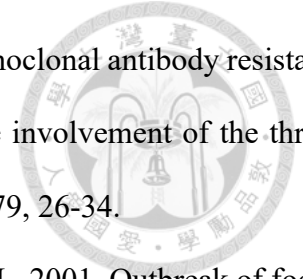


- Fromme, J.C., Orci, L., Schekman, R., 2008. Coordination of COPII vesicle trafficking by Sec23. *Trends Cell Biol* 18, 330-336.
- Fry, E.E., Newman, J.W.I., Curry, S., Najjam, S., Jackson, T., Blakemore, W., Lea, S.M., Miller, L., Burman, A., King, A.M.Q., Stuart, D.I., 2005. Structure of Foot-and-mouth disease virus serotype A10 61 alone and complexed with oligosaccharide receptor: receptor conservation in the face of antigenic variation. *J Gen Virol* 86, 1909-1920.
- Fu, S.Z., Yang, W.P., Ru, Y., Zhang, K.S., Wang, Y., Liu, X.T., Li, D., Zheng, H.X., 2019. DDX56 cooperates with FMDV 3A to enhance FMDV replication by inhibiting the phosphorylation of IRF3. *Cell Signal* 64, 109393.
- Fujita, K., Krishnakumar, S.S., Franco, D., Paul, A.V., London, E., Wimmer, E., 2007. Membrane topography of the hydrophobic anchor sequence of poliovirus 3A and 3AB proteins and the functional effect of 3A/3AB membrane association upon RNA replication. *Biochemistry* 46, 5185-5199.
- Gamarnik, A.V., Andino, R., 1998. Switch from translation to RNA replication in a positive-stranded RNA virus. *Genes Dev* 12, 2293-2304.
- Ganji, V.K., Biswal, J.K., Lalzampuia, H., Basagoudanavar, S.H., Saravanan, P., Tamil Selvan, R.P., Umapathi, V., Reddy, G.R., Sanyal, A., Dechamma, H.J., 2018. Mutation in the VP2 gene of P1-2A capsid protein increases the thermostability of virus-like particles of foot-and-mouth disease virus serotype O. *Appl Microbiol Biotechnol* 102, 8883-8893.
- Garcia, M.A., Meurs, E.F., Esteban, M., 2007. The dsRNA protein kinase PKR: virus and cell control. *Biochimie* 89, 799-811.
- Gladue, D.P., O'Donnell, V., Baker-Bransetter, R., Pacheco, J.M., Holinka, L.G., Arzt, J., Pauszek, S., Fernandez-Sainz, I., Fletcher, P., Brocchi, E., Lu, Z., Rodriguez, L.L., Borca, M.V., 2014. Interaction of foot-and-mouth disease virus nonstructural protein 3A with host protein DCTN3 is important for viral virulence in cattle. *J Virol* 88, 2737-2747.

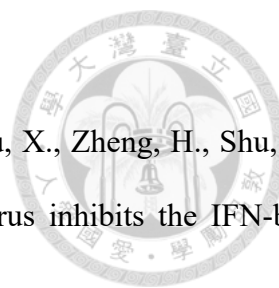


- Godi, A., Pertile, P., Meyers, R., Marra, P., Di Tullio, G., Iurisci, C., Luini, A., Corda, D., De Matteis, M.A., 1999. ARF mediates recruitment of PtdIns-4-OH kinase-beta and stimulates synthesis of PtdIns(4,5)P2 on the Golgi complex. *Nat Cell Biol* 1, 280-287.
- Gonzalez-Magaldi, M., Martin-Acebes, M.A., Kremer, L., Sobrino, F., 2014. Membrane topology and cellular dynamics of foot-and-mouth disease virus 3A protein. *PLoS One* 9, e106685.
- Gonzalez-Magaldi, M., Postigo, R., de la Torre, B.G., Vieira, Y.A., Rodriguez-Pulido, M., Lopez-Vinas, E., Gomez-Puertas, P., Andreu, D., Kremer, L., Rosas, M.F., Sobrino, F., 2012. Mutations that hamper dimerization of foot-and-mouth disease virus 3A protein are detrimental for infectivity. *J Virol* 86, 11013-11023.
- Grazioli, S., Fallacara, F., Brocchi, E., 2013. Mapping of antigenic sites of foot-and-mouth disease virus serotype Asia 1 and relationships with sites described in other serotypes. *J Gen Virol* 94, 559-569.
- Greber, U.F., Way, M., 2006. A superhighway to virus infection. *Cell* 124, 741-754.
- Greninger, A.L., 2015. Picornavirus-Host Interactions to Construct Viral Secretory Membranes. *Molecular Basis of Viral Infection* 129, 189-212.
- Greninger, A.L., Knudsen, G.M., Betegon, M., Burlingame, A.L., Derisi, J.L., 2012. The 3A protein from multiple picornaviruses utilizes the golgi adaptor protein ACBD3 to recruit PI4KIIIbeta. *J Virol* 86, 3605-3616.
- Greninger, A.L., Knudsen, G.M., Betegon, M., Burlingame, A.L., DeRisi, J.L., 2013. ACBD3 interaction with TBC1 domain 22 protein is differentially affected by enteroviral and kobuviral 3A protein binding. *mBio* 4, e00098-00013.
- Guan, S.H., Belsham, G.J., 2017. Separation of foot-and-mouth disease virus leader protein activities; identification of mutants that retain efficient self-processing activity but poorly induce eIF4G cleavage. *J Gen Virol* 98, 671-680.
- Gullberg, M., Muszynski, B., Organtini, L.J., Ashley, R.E., Hafenstein, S.L., Belsham, G.J., Polacek,

- 
- C., 2013. Assembly and characterization of foot-and-mouth disease virus empty capsid particles expressed within mammalian cells. *J Gen Virol* 94, 1769-1779.
- Guo, H.C., Sun, S.Q., Jin, Y., Yang, S.L., Wei, Y.Q., Sun, D.H., Yin, S.H., Ma, J.W., Liu, Z.X., Guo, J.H., Luo, J.X., Yin, H., Liu, X.T., Liu, D.X., 2013. Foot-and-mouth disease virus-like particles produced by a SUMO fusion protein system in *Escherichia coli* induce potent protective immune responses in guinea pigs, swine and cattle. *Vet Res* 44, 48.
- Gurkan, C., Stagg, S.M., Lapointe, P., Balch, W.E., 2006. The COPII cage: unifying principles of vesicle coat assembly. *Nat Rev Mol Cell Biol* 7, 727-738.
- Hsu, N.Y., Ilnytska, O., Belov, G., Santiana, M., Chen, Y.H., Takvorian, P.M., Pau, C., van der Schaar, H., Kaushik-Basu, N., Balla, T., Cameron, C.E., Ehrenfeld, E., van Kuppeveld, F.J., Altan-Bonnet, N., 2010. Viral reorganization of the secretory pathway generates distinct organelles for RNA replication. *Cell* 141, 799-811.
- Huang, M., Weissman, J.T., Beraud-Dufour, S., Luan, P., Wang, C., Chen, W., Aridor, M., Wilson, I.A., Balch, W.E., 2001. Crystal structure of Sar1-GDP at 1.7 Å resolution and the role of the NH2 terminus in ER export. *J Cell Biol* 155, 937-948.
- Ilnytska, O., Santiana, M., Hsu, N.Y., Du, W.L., Chen, Y.H., Viktorova, E.G., Belov, G., Brinker, A., Storch, J., Moore, C., Dixon, J.L., Altan-Bonnet, N., 2013. Enteroviruses harness the cellular endocytic machinery to remodel the host cell cholesterol landscape for effective viral replication. *Cell Host Microbe* 14, 281-293.
- Jackson, T., Belsham, G.J., 2021. Picornaviruses: A View from 3A. *Viruses* 13.
- Kirchhausen, T., 2000. Three ways to make a vesicle. *Nat Rev Mol Cell Biol* 1, 187-198.
- Kirchweger, R., Ziegler, E., Lamphear, B.J., Waters, D., Liebig, H.D., Sommergruber, W., Sobrino, F., Hohenadl, C., Blaas, D., Rhoads, R.E., et al., 1994. Foot-and-mouth disease virus leader proteinase: purification of the Lb form and determination of its cleavage site on eIF-4 gamma. *J Virol* 68, 5677-5684.



- Kitson, J.D., McCahon, D., Belsham, G.J., 1990. Sequence analysis of monoclonal antibody resistant mutants of type O foot and mouth disease virus: evidence for the involvement of the three surface exposed capsid proteins in four antigenic sites. *Virology* 179, 26-34.
- Knowles, N.J., Samuel, A.R., Davies, P.R., Kitching, R.P., Donaldson, A.I., 2001. Outbreak of foot-and-mouth disease virus serotype O in the UK caused by a pandemic strain. *Vet Rec* 148, 258-259.
- Lamphear, B.J., Kirchweger, R., Skern, T., Rhoads, R.E., 1995. Mapping of functional domains in eukaryotic protein synthesis initiation factor 4G (eIF4G) with picornaviral proteases. Implications for cap-dependent and cap-independent translational initiation. *J Biol Chem* 270, 21975-21983.
- Lanke, K.H., van der Schaar, H.M., Belov, G.A., Feng, Q., Duijsings, D., Jackson, C.L., Ehrenfeld, E., van Kuppeveld, F.J., 2009. GBF1, a guanine nucleotide exchange factor for Arf, is crucial for coxsackievirus B3 RNA replication. *J Virol* 83, 11940-11949.
- Lawrence, P., Rai, D., Conderino, J.S., Uddowla, S., Rieder, E., 2016. Role of Jumonji C-domain containing protein 6 (JMJD6) in infectivity of foot-and-mouth disease virus. *Virology* 492, 38-52.
- Lawrence, P., Rieder, E., 2009. Identification of RNA helicase A as a new host factor in the replication cycle of foot-and-mouth disease virus. *J Virol* 83, 11356-11366.
- Lee, C.D., Yan, Y.P., Liang, S.M., Wang, T.F., 2009. Production of FMDV virus-like particles by a SUMO fusion protein approach in *Escherichia coli*. *J Biomed Sci* 16, 69.
- Li, C., Zhu, Z., Du, X., Cao, W., Yang, F., Zhang, X., Feng, H., Li, D., Zhang, K., Liu, X., Zheng, H., 2017. Foot-and-mouth disease virus induces lysosomal degradation of host protein kinase PKR by 3C proteinase to facilitate virus replication. *Virology* 509, 222-231.
- Li, D., Lei, C., Xu, Z., Yang, F., Liu, H., Zhu, Z., Li, S., Liu, X., Shu, H., Zheng, H., 2016a. Foot-and-mouth disease virus non-structural protein 3A inhibits the interferon-beta signaling



pathway. *Sci Rep* 6, 21888.

Li, D., Yang, W., Yang, F., Liu, H., Zhu, Z., Lian, K., Lei, C., Li, S., Liu, X., Zheng, H., Shu, H., 2016b. The VP3 structural protein of foot-and-mouth disease virus inhibits the IFN-beta signaling pathway. *FASEB J* 30, 1757-1766.

Li, K., Wang, C., Yang, F., Cao, W., Zhu, Z., Zheng, H., 2021. Virus-Host Interactions in Foot-and-Mouth Disease Virus Infection. *Front Immunol* 12, 571509.

Long, K.R., Yamamoto, Y., Baker, A.L., Watkins, S.C., Coyne, C.B., Conway, J.F., Aridor, M., 2010. Sar1 assembly regulates membrane constriction and ER export. *J Cell Biol* 190, 115-128.

Longjam, N., Deb, R., Sarmah, A.K., Tayo, T., Awachat, V.B., Saxena, V.K., 2011. A Brief Review on Diagnosis of Foot-and-Mouth Disease of Livestock: Conventional to Molecular Tools. *Vet Med Int* 2011, 905768.

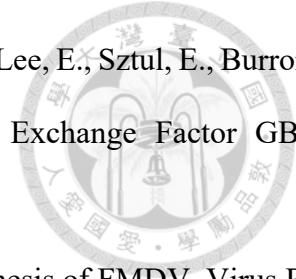
Loundras, E.A., Herod, M.R., Harris, M., Stonehouse, N.J., 2016. Foot-and-mouth disease virus genome replication is unaffected by inhibition of type III phosphatidylinositol-4-kinases. *J Gen Virol* 97, 2221-2230.

Ma, L.N., Zhang, J., Chen, H.T., Zhou, J.H., Ding, Y.Z., Liu, Y.S., 2011. An overview on ELISA techniques for FMD. *Virol J* 8, 419.

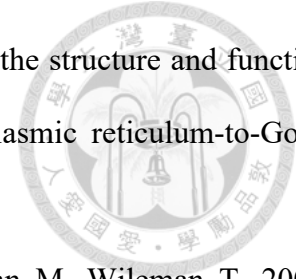
Ma, X., Li, P., Bai, X., Sun, P., Bao, H., Lu, Z., Cao, Y., Li, D., Chen, Y., Qiao, Z., Liu, Z., 2014. Sequences outside that of residues 93-102 of 3A protein can contribute to the ability of foot-and-mouth disease virus (FMDV) to replicate in bovine-derived cells. *Virus Res* 191, 161-171.

Ma, X.X., Ma, L.N., Chang, Q.Y., Ma, P., Li, L.J., Wang, Y.Y., Ma, Z.R., Cao, X., 2018. Type I Interferon Induced and Antagonized by Foot-and-Mouth Disease Virus. *Front Microbiol* 9, 1862.

Mahapatra, M., Hamblin, P., Paton, D.J., 2012. Foot-and-mouth disease virus epitope dominance in the antibody response of vaccinated animals. *J Gen Virol* 93, 488-493.



- Martinez, J.L., Arnoldi, F., Schraner, E.M., Eichwald, C., Silva-Ayala, D., Lee, E., Sztul, E., Burrone, O.R., Lopez, S., Arias, C.F., 2019. The Guanine Nucleotide Exchange Factor GBF1 Participates in Rotavirus Replication. *J Virol* 93.
- Mason, P.W., Grubman, M.J., Baxt, B., 2003. Molecular basis of pathogenesis of FMDV. *Virus Res* 91, 9-32.
- McCahon, D., Crowther, J.R., Belsham, G.J., Kitson, J.D., Duchesne, M., Have, P., Melen, R.H., Morgan, D.O., De Simone, F., 1989. Evidence for at least four antigenic sites on type O foot-and-mouth disease virus involved in neutralization; identification by single and multiple site monoclonal antibody-resistant mutants. *J Gen Virol* 70 (Pt 3), 639-645.
- McKenney, R.J., Huynh, W., Tanenbaum, M.E., Bhabha, G., Vale, R.D., 2014. Activation of cytoplasmic dynein motility by dynactin-cargo adapter complexes. *Science* 345, 337-341.
- McMahon, C., Studer, S.M., Clendinen, C., Dann, G.P., Jeffrey, P.D., Hughson, F.M., 2012. The structure of Sec12 implicates potassium ion coordination in Sar1 activation. *J Biol Chem* 287, 43599-43606.
- Meissner, J.M., Bhatt, J.M., Lee, E., Styers, M.L., Ivanova, A.A., Kahn, R.A., Sztul, E., 2018. The ARF guanine nucleotide exchange factor GBF1 is targeted to Golgi membranes through a PIP-binding domain. *J Cell Sci* 131.
- Melia, C.E., van der Schaar, H.M., Lyoo, H., Limpens, R., Feng, Q., Wahedi, M., Overheul, G.J., van Rij, R.P., Snijder, E.J., Koster, A.J., Barcena, M., van Kuppeveld, F.J.M., 2017. Escaping Host Factor PI4KB Inhibition: Enterovirus Genomic RNA Replication in the Absence of Replication Organelles. *Cell Rep* 21, 587-599.
- Midgley, R., Moffat, K., Berryman, S., Hawes, P., Simpson, J., Fullen, D., Stephens, D.J., Burman, A., Jackson, T., 2013. A role for endoplasmic reticulum exit sites in foot-and-mouth disease virus infection. *J Gen Virol* 94, 2636-2646.
- Moffat, K., Howell, G., Knox, C., Belsham, G.J., Monaghan, P., Ryan, M.D., Wileman, T., 2005.



Effects of foot-and-mouth disease virus nonstructural proteins on the structure and function of the early secretory pathway: 2BC but not 3A blocks endoplasmic reticulum-to-Golgi transport. *J Virol* 79, 4382-4395.

Moffat, K., Knox, C., Howell, G., Clark, S.J., Yang, H., Belsham, G.J., Ryan, M., Wileman, T., 2007.

Inhibition of the secretory pathway by foot-and-mouth disease virus 2BC protein is reproduced by coexpression of 2B with 2C, and the site of inhibition is determined by the subcellular location of 2C. *J Virol* 81, 1129-1139.

Moghimi, S., Viktorova, E., Zimina, A., Szul, T., Sztul, E., Belov, G.A., 2020. Enterovirus Infection

Induces Massive Recruitment of All Isoforms of Small Cellular Arf GTPases to the Replication Organelles. *J Virol* 95.

Mohana Subramanian, B., Madhanmohan, M., Sriraman, R., Chandrasekhar Reddy, R.V., Yuvaraj,

S., Manikumar, K., Rajalakshmi, S., Nagendrakumar, S.B., Rana, S.K., Srinivasan, V.A., 2012. Development of foot-and-mouth disease virus (FMDV) serotype O virus-like-particles (VLPs) vaccine and evaluation of its potency. *Antiviral Res* 96, 288-295.

Monaghan, P., Cook, H., Jackson, T., Ryan, M., Wileman, T., 2004. The ultrastructure of the

developing replication site in foot-and-mouth disease virus-infected BHK-38 cells. *J Gen Virol* 85, 933-946.

Moseley, G.W., Roth, D.M., DeJesus, M.A., Leyton, D.L., Filmer, R.P., Pouton, C.W., Jans, D.A.,

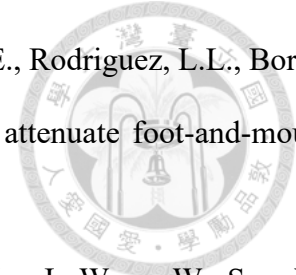
2007. Dynein light chain association sequences can facilitate nuclear protein import. *Mol Biol Cell* 18, 3204-3213.

O'Donnell, V.K., Pacheco, J.M., Henry, T.M., Mason, P.W., 2001. Subcellular distribution of the

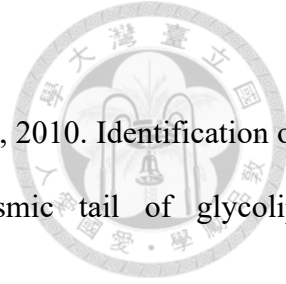
foot-and-mouth disease virus 3A protein in cells infected with viruses encoding wild-type and bovine-attenuated forms of 3A. *Virology* 287, 151-162.

OIE. 2021. Foot and mouth disease: Official Disease Status (OIE).

Pacheco, J.M., Gladue, D.P., Holinka, L.G., Arzt, J., Bishop, E., Smoliga, G., Pauszek, S.J., Bracht,

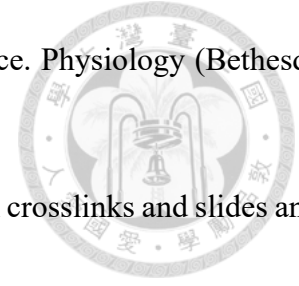


- A.J., O'Donnell, V., Fernandez-Sainz, I., Fletcher, P., Piccone, M.E., Rodriguez, L.L., Borca, M.V., 2013. A partial deletion in non-structural protein 3A can attenuate foot-and-mouth disease virus in cattle. *Virology* 446, 260-267.
- Pan, L., Zhang, Y., Wang, Y., Wang, B., Wang, W., Fang, Y., Jiang, S., Lv, J., Wang, W., Sun, Y., Xie, Q., 2008. Foliar extracts from transgenic tomato plants expressing the structural polyprotein, P1-2A, and protease, 3C, from foot-and-mouth disease virus elicit a protective response in guinea pigs. *Vet Immunol Immunopathol* 121, 83-90.
- Paul, A.V., Rieder, E., Kim, D.W., van Boom, J.H., Wimmer, E., 2000. Identification of an RNA hairpin in poliovirus RNA that serves as the primary template in the in vitro uridylylation of VPg. *J Virol* 74, 10359-10370.
- Peng, J., Yi, J., Yang, W., Ren, J., Wen, Y., Zheng, H., Li, D., 2020. Advances in Foot-and-Mouth Disease Virus Proteins Regulating Host Innate Immunity. *Front Microbiol* 11, 2046.
- Peotter, J., Kasberg, W., Pustova, I., Audhya, A., 2019. COPII-mediated trafficking at the ER/ERGIC interface. *Traffic* 20, 491-503.
- Polacek, C., Gullberg, M., Li, J., Belsham, G.J., 2013. Low levels of foot-and-mouth disease virus 3C protease expression are required to achieve optimal capsid protein expression and processing in mammalian cells. *J Gen Virol* 94, 1249-1258.
- Porta, C., Xu, X., Loureiro, S., Paramasivam, S., Ren, J., Al-Khalil, T., Burman, A., Jackson, T., Belsham, G.J., Curry, S., Lomonossoff, G.P., Parida, S., Paton, D., Li, Y., Wilsden, G., Ferris, N., Owens, R., Kotecha, A., Fry, E., Stuart, D.I., Charleston, B., Jones, I.M., 2013. Efficient production of foot-and-mouth disease virus empty capsids in insect cells following down regulation of 3C protease activity. *J Virol Methods* 187, 406-412.
- Puckette, M., Clark, B.A., Smith, J.D., Turecek, T., Martel, E., Gabbert, L., Pisano, M., Hurtle, W., Pacheco, J.M., Barrera, J., Neilan, J.G., Rasmussen, M., 2017. Foot-and-Mouth Disease (FMD) Virus 3C Protease Mutant L127P: Implications for FMD Vaccine Development. *J*

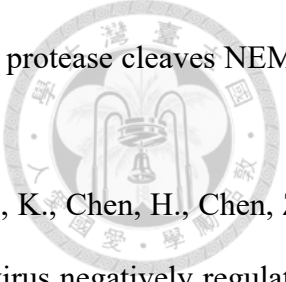


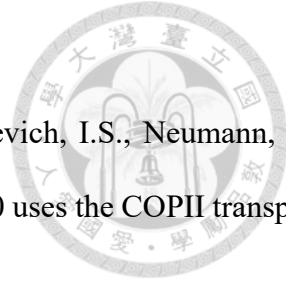
Virology 91.

- Quintero, C.A., Giraud, C.G., Villarreal, M., Montich, G., Maccioni, H.J., 2010. Identification of a site in Sar1 involved in the interaction with the cytoplasmic tail of glycolipid glycosyltransferases. *J Biol Chem* 285, 30340-30346.
- Randall, R.E., Goodbourn, S., 2008. Interferons and viruses: an interplay between induction, signalling, antiviral responses and virus countermeasures. *J Gen Virol* 89, 1-47.
- Raux, H., Flamand, A., Blondel, D., 2000. Interaction of the rabies virus P protein with the LC8 dynein light chain. *J Virol* 74, 10212-10216.
- Rodriguez Pulido, M., Saiz, M., 2017. Molecular Mechanisms of Foot-and-Mouth Disease Virus Targeting the Host Antiviral Response. *Front Cell Infect Microbiol* 7, 252.
- Schroer, T.A., 2004. Dynactin. *Annu Rev Cell Dev Biol* 20, 759-779.
- Shengjuler, D., Chan, Y.M., Sun, S., Moustafa, I.M., Li, Z.L., Gohara, D.W., Buck, M., Cremer, P.S., Boehr, D.D., Cameron, C.E., 2017. The RNA-Binding Site of Poliovirus 3C Protein Doubles as a Phosphoinositide-Binding Domain. *Structure* 25, 1875-1886 e1877.
- Splinter, D., Razafsky, D.S., Schlager, M.A., Serra-Marques, A., Grigoriev, I., Demmers, J., Keijzer, N., Jiang, K., Poser, I., Hyman, A.A., Hoogenraad, C.C., King, S.J., Akhmanova, A., 2012. BICD2, dynactin, and LIS1 cooperate in regulating dynein recruitment to cellular structures. *Mol Biol Cell* 23, 4226-4241.
- Springer, S., Malkus, P., Borchert, B., Wellbrock, U., Duden, R., Schekman, R., 2014. Regulated oligomerization induces uptake of a membrane protein into COPII vesicles independent of its cytosolic tail. *Traffic* 15, 531-545.
- Stenfeldt, C., Arzt, J., Pacheco, J.M., Gladue, D.P., Smoliga, G.R., Silva, E.B., Rodriguez, L.L., Borca, M.V., 2018. A partial deletion within foot-and-mouth disease virus non-structural protein 3A causes clinical attenuation in cattle but does not prevent subclinical infection. *Virology* 516, 115-126.



- Szul, T., Sztul, E., 2011. COPII and COPI traffic at the ER-Golgi interface. *Physiology (Bethesda)* 26, 348-364.
- Tanenbaum, M.E., Vale, R.D., McKenney, R.J., 2013. Cytoplasmic dynein crosslinks and slides anti-parallel microtubules using its two motor domains. *Elife* 2, e00943.
- Toropova, K., Zalyte, R., Mukhopadhyay, A.G., Mladenov, M., Carter, A.P., Roberts, A.J., 2019. Structure of the dynein-2 complex and its assembly with intraflagellar transport trains. *Nat Struct Mol Biol* 26, 823-829.
- Townley, A.K., Feng, Y., Schmidt, K., Carter, D.A., Porter, R., Verkade, P., Stephens, D.J., 2008. Efficient coupling of Sec23-Sec24 to Sec13-Sec31 drives COPII-dependent collagen secretion and is essential for normal craniofacial development. *J Cell Sci* 121, 3025-3034.
- Ujike, M., Taguchi, F., 2015. Incorporation of spike and membrane glycoproteins into coronavirus virions. *Viruses* 7, 1700-1725.
- Urnavicius, L., Zhang, K., Diamant, A.G., Motz, C., Schlager, M.A., Yu, M., Patel, N.A., Robinson, C.V., Carter, A.P., 2015. The structure of the dynactin complex and its interaction with dynein. *Science* 347, 1441-1446.
- van der Schaar, H.M., Dorobantu, C.M., Albulescu, L., Strating, J., van Kuppeveld, F.J.M., 2016. Fat(al) attraction: Picornaviruses Usurp Lipid Transfer at Membrane Contact Sites to Create Replication Organelles. *Trends Microbiol* 24, 535-546.
- Viktorova, E.G., Gabaglio, S., Meissner, J.M., Lee, E., Moghimi, S., Sztul, E., Belov, G.A., 2019. A Redundant Mechanism of Recruitment Underlies the Remarkable Plasticity of the Requirement of Poliovirus Replication for the Cellular ArfGEF GBF1. *J Virol* 93.
- Visser, L.J., Medina, G.N., Rabouw, H.H., de Groot, R.J., Langereis, M.A., de Los Santos, T., van Kuppeveld, F.J.M., 2019. Foot-and-Mouth Disease Virus Leader Protease Cleaves G3BP1 and G3BP2 and Inhibits Stress Granule Formation. *J Virol* 93.
- Wang, D., Fang, L., Li, K., Zhong, H., Fan, J., Ouyang, C., Zhang, H., Duan, E., Luo, R., Zhang, Z.,

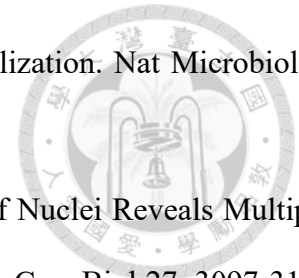
- 
- Liu, X., Chen, H., Xiao, S., 2012. Foot-and-mouth disease virus 3C protease cleaves NEMO to impair innate immune signaling. *J Virol* 86, 9311-9322.
- Wang, D., Fang, L., Li, P., Sun, L., Fan, J., Zhang, Q., Luo, R., Liu, X., Li, K., Chen, H., Chen, Z., Xiao, S., 2011a. The leader proteinase of foot-and-mouth disease virus negatively regulates the type I interferon pathway by acting as a viral deubiquitinase. *J Virol* 85, 3758-3766.
- Wang, G., Wang, Y., Shang, Y., Zhang, Z., Liu, X., 2015. How foot-and-mouth disease virus receptor mediates foot-and-mouth disease virus infection. *Virology* 531, 1-9.
- Wang, H., Zhao, L., Li, W., Zhou, G., Yu, L., 2011b. Identification of a conformational epitope on the VP1 G-H Loop of type Asia1 foot-and-mouth disease virus defined by a protective monoclonal antibody. *Vet Microbiol* 148, 189-199.
- Wang, J., Du, J., Jin, Q., 2014. Class I ADP-ribosylation factors are involved in enterovirus 71 replication. *PLoS One* 9, e99768.
- Wessels, E., Duijsings, D., Lanke, K.H., van Dooren, S.H., Jackson, C.L., Melchers, W.J., van Kuppeveld, F.J., 2006a. Effects of picornavirus 3A Proteins on Protein Transport and GBF1-dependent COP-I recruitment. *J Virol* 80, 11852-11860.
- Wessels, E., Duijsings, D., Niu, T.K., Neumann, S., Oorschot, V.M., de Lange, F., Lanke, K.H., Klumperman, J., Henke, A., Jackson, C.L., Melchers, W.J., van Kuppeveld, F.J., 2006b. A viral protein that blocks Arf1-mediated COP-I assembly by inhibiting the guanine nucleotide exchange factor GBF1. *Dev Cell* 11, 191-201.
- Wolff, G., Limpens, R., Zevenhoven-Dobbe, J.C., Laugks, U., Zheng, S., de Jong, A.W.M., Koning, R.I., Agard, D.A., Grunewald, K., Koster, A.J., Snijder, E.J., Barcena, M., 2020. A molecular pore spans the double membrane of the coronavirus replication organelle. *Science* 369, 1395-1398.
- Xie, Q.C., McCahon, D., Crowther, J.R., Belsham, G.J., McCullough, K.C., 1987. Neutralization of foot-and-mouth disease virus can be mediated through any of at least three separate antigenic



sites. *J Gen Virol* 68 (Pt 6), 1637-1647.

- Yamayoshi, S., Noda, T., Ebihara, H., Goto, H., Morikawa, Y., Lukashevich, I.S., Neumann, G., Feldmann, H., Kawaoka, Y., 2008. Ebola virus matrix protein VP40 uses the COPII transport system for its intracellular transport. *Cell Host Microbe* 3, 168-177.
- Yang, M., Xu, W., Goolia, M., Zhang, Z., 2014. Characterization of monoclonal antibodies against foot-and-mouth disease virus serotype O and application in identification of antigenic variation in relation to vaccine strain selection. *Virology* 11, 136.
- Yang, W., Li, D., Ru, Y., Bai, J., Ren, J., Zhang, J., Li, L., Liu, X., Zheng, H., 2020. Foot-and-Mouth Disease Virus 3A Protein Causes Upregulation of Autophagy-Related Protein LRRC25 To Inhibit the G3BP1-Mediated RIG-Like Helicase-Signaling Pathway. *J Virol* 94.
- Ye, X., Pan, T., Wang, D., Fang, L., Ma, J., Zhu, X., Shi, Y., Zhang, K., Zheng, H., Chen, H., Li, K., Xiao, S., 2018. Foot-and-Mouth Disease Virus Counteracts on Internal Ribosome Entry Site Suppression by G3BP1 and Inhibits G3BP1-Mediated Stress Granule Assembly via Post-Translational Mechanisms. *Front Immunol* 9, 1142.
- Ypma-Wong, M.F., Dewalt, P.G., Johnson, V.H., Lamb, J.G., Semler, B.L., 1988. Protein 3CD is the major poliovirus proteinase responsible for cleavage of the P1 capsid precursor. *Virology* 166, 265-270.
- Yuan, L., Kenny, S.J., Hemmati, J., Xu, K., Schekman, R., 2018. TANGO1 and SEC12 are copackaged with procollagen I to facilitate the generation of large COPII carriers. *Proc Natl Acad Sci U S A* 115, E12255-E12264.
- Zanetti, G., Pahuja, K.B., Studer, S., Shim, S., Schekman, R., 2011. COPII and the regulation of protein sorting in mammals. *Nat Cell Biol* 14, 20-28.
- Zheng, Q., Zhu, R., Xu, L., He, M., Yan, X., Liu, D., Yin, Z., Wu, Y., Li, Y., Yang, L., Hou, W., Li, S., Li, Z., Chen, Z., Li, Z., Yu, H., Gu, Y., Zhang, J., Baker, T.S., Zhou, Z.H., Graham, B.S., Cheng, T., Li, S., Xia, N., 2019. Atomic structures of enterovirus D68 in complex with two

monoclonal antibodies define distinct mechanisms of viral neutralization. *Nat Microbiol* 4, 124-133.



Zhu, R., Antoku, S., Gundersen, G.G., 2017. Centrifugal Displacement of Nuclei Reveals Multiple LINC Complex Mechanisms for Homeostatic Nuclear Positioning. *Curr Biol* 27, 3097-3110 e3095.

Zhu, Z., Yang, F., Cao, W., Liu, H., Zhang, K., Tian, H., Dang, W., He, J., Guo, J., Liu, X., Zheng, H., 2019. The Pseudoknot Region of the 5' Untranslated Region Is a Determinant of Viral Tropism and Virulence of Foot-and-Mouth Disease Virus. *J Virol* 93.

Chapter II



Foot-and-Mouth Disease Virus 3A Hijacks Sar1 and Sec12 for ER Remodeling in a COPII-Independent Manner

Reprint from Viruses, Vol. 14, Author(s): Heng-Wei Lee, Yi-Fan Jiang, Hui-Wen Chang, Ivan-Chen Cheng, Title of article: Foot-and-Mouth Disease Virus 3A Hijacks Sar1 and Sec12 for ER Remodeling in a COPII-Independent Manner, open access (2022) of MDPI.

Foot-and-Mouth Disease Virus 3A Hijacks Sar1 and Sec12 for ER Remodeling in a COPII-Independent Manner

Heng-Wei Lee ¹, Yi-Fan Jiang ^{1,2} , Hui-Wen Chang ^{1,2}  and Ivan-Chen Cheng ^{1,*}

- ¹ School of Veterinary Medicine, National Taiwan University, Taipei 106, Taiwan; d06629010@ntu.edu.tw (H.-W.L.); yfjiang@ntu.edu.tw (Y.-F.J.); huiwenchang@ntu.edu.tw (H.-W.C.)
- ² Graduate Institute of Molecular and Comparative Pathobiology, School of Veterinary Medicine, National Taiwan University, Taipei 106, Taiwan
- * Correspondence: ivancheng@ntu.edu.tw

Abstract: Positive-stranded RNA viruses modify host organelles to form replication organelles (ROs) for their own replication. The enteroviral 3A protein has been demonstrated to be highly associated with the COPI pathway, in which factors operate on the ER-to-Golgi intermediate and the Golgi. However, Sar1, a COPII factor exerting coordinated action at endoplasmic reticulum (ER) exit sites rather than COPI factors, is required for the replication of foot-and-mouth disease virus (FMDV). Therefore, further understanding regarding FMDV 3A could be key to explaining the differences and to understanding FMDV's RO formation. In this study, FMDV 3A was confirmed as a peripheral membrane protein capable of modifying the ER into vesicle-like structures, which were neither COPII vesicles nor autophagosomes. When the C-terminus of 3A was truncated, it was located at the ER without vesicular modification. This change was revealed using mGFP and APEX2 fusion constructs, and observed by fluorescence microscopy and electron tomography, respectively. For the other 3A truncation, the minimal region for modification was aa 42–92. Furthermore, we found that the remodeling was related to two COPII factors, Sar1 and Sec12; both interacted with 3A, but their binding domains on 3A were different. Finally, we hypothesized that the N-terminus of 3A would interact with Sar1, as its C-terminus simultaneously interacted with Sec12, which could possibly enhance Sar1 activation. On the ER membrane, active Sar1 interacted with regions of aa 42–59 and aa 76–92 from 3A for vesicle formation. This mechanism was distinct from the traditional COPII pathway and could be critical for FMDV RO formation.

Keywords: foot-and-mouth disease virus 3A protein; COPII factors; ER remodeling



Citation: Lee, H.-W.; Jiang, Y.-F.; Chang, H.-W.; Cheng, I.-C. Foot-and-Mouth Disease Virus 3A Hijacks Sar1 and Sec12 for ER Remodeling in a COPII-Independent Manner. *Viruses* **2022**, *14*, 839. <https://doi.org/10.3390/v14040839>

Academic Editors: Chao-Nan Lin and Peck Toung Ooi

Received: 8 March 2022

Accepted: 16 April 2022

Published: 18 April 2022

Publisher's Note: MDPI stays neutral with regard to jurisdictional claims in published maps and institutional affiliations.



Copyright: © 2022 by the authors. Licensee MDPI, Basel, Switzerland. This article is an open access article distributed under the terms and conditions of the Creative Commons Attribution (CC BY) license (<https://creativecommons.org/licenses/by/4.0/>).

1. Introduction

All positive-stranded RNA viruses, including enterovirus and foot-and-mouth disease virus (FMDV) (family *Picornaviridae*), modify the host organelle to achieve their own replication. The modified organelles are termed “replication organelles” (ROs) [1,2]. It has been postulated that ROs could serve as platforms for recruiting key components for viral replication, concentrating resources in favor of the virion package [3,4], and shielding the viral RNA from RNases and RNA sensors [5]. Much is known about the mechanism of RO formation for enteroviruses (including poliovirus (PV), coxsackie B virus (CBV), and rhinovirus). For example, the PV 3A protein has been observed to “hijack” COPI factor GBF1, resulting in the inhibition of Arf1 activation [6] and secretory blockage [7]. However, the biological function should be verified. In a recent study, it was suggested that Arf1 activation directly supported RO formation [8]. In addition, 3A accumulation required 3A–GBF1 interaction [9]. However, PV 3A also interacted with ACDB3, further recruiting PI4KB for phosphorylating phosphoinositol (PI) lipids into PI4P [10,11], which might attract viral 3D polymerase [11], 3C protease [12], and host protein OSBP [13]. OSBP further exchanged PI4P for cholesterol from the endoplasmic reticulum (ER). The cholesterol accumulation

mediated the processing of the viral precursor protein [13] and could be one of the factors in RO formation. Collectively, the viral 3A (or 3AB) protein could represent an RO marker protein that is highly associated with enteroviral RO development [13,14]. However, this has not been proven in FMDV. Numerous differences between FMDV and enterovirus exist: (1) FMDV has been shown to be resistant to GBF1 inhibitors [15,16] and highly associated with the COPII pathway, rather than COPI [16]. (2) The combination of FMDV 2B and 2C, instead of 3A, can block the secretory pathway in the TsO45 VSV G protein trafficking model [17,18]. (3) According to the results of the transmission electron microscopy (TEM) from Monaghan et al., FMDV RO is homologous and gathers beside the nucleus, while enteroviral RO appears as heterologous vesicles or tubules [2,19]. (4) FMDV does not require PI4K or PI4P [20,21]. (5) The C-terminus of FMDV 3A is longer than the C-termini of other picornaviruses and has an unknown biological function. Therefore, more efforts are required to understand FMDV RO formation, especially for FMDV 3A.

The FMD viral genome consists of a single open reading frame (ORF) that is translated into a polyprotein, which is then cleaved into structural proteins (VP0, VP3, and VP1) and nonstructural proteins (L^{Pro}, 2A, 2B, 2C, 3A, 3B, 3C^{Pro}, and 3D polymerase) [22]. Among these, 3A appears to be a peripheral membrane protein located on the ER with its N-terminus and C-terminus exposed to the cytoplasm [23]. The N-terminus contains two α -helices responsible for homodimerization and are essential for viral replication [24], while the C-terminus of 3A has been associated with host tropism [25,26]. However, the detailed mechanism and the biological function of 3A remain largely unknown. Currently, FMDV 3A is only known to be a multifunctional protein that participates in countering antiviral activity via the upregulation of LRRC25 and the autophagic degradation of RNA sensors [27]. In addition to LRRC25, G3BP1, and RNA sensors, the other 3A-associated interaction partners include DDX56, DCTN3 (dynactin subunit 3), vimentin, and RNA helicase A [28–31]. Despite intense study, many questions remain, such as the mechanism of LRRC25's upregulation, the biological function of 3A–DCTN3 interactions, and the role of 3A in RO formation.

Protein trafficking from the ER to the ER-to-Golgi intermediate compartment (ERGIC) is mediated by the COPII pathway [32]. To generate COPII vesicles from the ER, Sar1 is recruited and activated by Sec12—a guanidine exchange factor—at the ER exit site (ERES). In other words, Sec12 exchanges the GDP of Sar1–GDP (inactive form) for GTP, inducing a conformational change in Sar1, with the N-terminus attaching to the ER membrane. Active Sar1 recruits the COPII inner coat proteins Sec23 and Sec24, as well as the outer coat proteins Sec13 and Sec31, to bend the membrane into vesicle-like structures [33]. Meanwhile, most cargo proteins and cargo receptors can interact with Sec24 to be loaded into the forming vesicles. To form a neck of vesicles, active Sar1 polymerizes. After Sar1 hydrolysis, vesicle scission is complete and the COPII vesicles are released from the ER toward the ERGIC [33]. The opposite direction of transport and the trafficking from the ERGIC to the Golgi are, instead, mediated by the COPI pathway. Therefore, the COPI/COPII machinery is crucial for protein secretion and vital for cells [32]. It was found that the machinery was also utilized by enterovirus and FMDV [8,16].

In our studies, the topology of 3A was first examined using homemade monoclonal antibodies (MAbs). Next, we proved that FMDV 3A expression alone could modify the ER into a specific vesicle-like structure. With the help of the APEX system, the detailed structure was examined under TEM. Moreover, without the N- or C-terminus of 3A, the ER remodeling was lost and the 3A was consequently retained at the ER. With the preservation of the regions near the hydrophobic region (HR), namely, aa 42–58 and aa 77–92, the truncated 3A was sufficient for reshaping the ER. The modification was associated with two unpublished host partners, Sar1 and Sec12, both of which are COPII factors. The depletion of Sar1 (or Sec12) and the expression of dominant-negative mutants hampered the remodeling. Furthermore, this is the first study to examine the features of 3A-induced vesicles from the web-like structure of the ER and to reveal the mechanism of

their formation. These findings may serve to further the investigation of FMDV and other picornaviral ROs in the future.

2. Materials and Methods

2.1. Cells and Reagents

PK-15 cells and A549 cells were maintained in Dulbecco's modified Eagle medium (DMEM) with 10% FBS. Rapamycin (Sigma, R0395) and digitonin (Sigma, D141) were purchased. The commercial antibodies used in this study included anti-FLAG mouse antibody (Sigma, F1804), anti-FLAG rabbit antibody (Sigma, F7425), anti- β -actin (Cell Signaling Technology, #3700), anti-GFP (Invitrogen, MA5-15256), anti-calreticulin (LSBio, LS-B9387), anti-LC3B (Cell Signaling Technology, #2775), anti-Sec23A (Novus Biologicals, NBP2-34842), anti-Sec31A (Abcam, ab86600), anti-giantin (Sigma, SAB2100948), anti-Sec12 (LSBio, LS-C29886), and anti-Sar1 (Novus Biologicals, NBP2-20261).

2.2. Plasmids

2.2.1. 3A-Associated Constructs

The primers used in this study can be found in Supplementary Table S1. To construct the expression plasmids pcDNA-3A(O99) and pcDNA-3A(O97), the 3A genes for O/TAW/97 (GenBank No. AY593835.1) and O/TAW/99 (GenBank No. AJ539136.1) were amplified (Phusion™ High-Fidelity DNA Polymerase, Thermo Scientific) from the O/TAW/97 cDNA pool and synthesized correspondingly. The 3A genes were subcloned into pcDNA-3.1(+) using the *Hind*III and *Xho*I sites with C-terminal His tag fusion; the endogenous *Nhe*I site within O/97 3A was further removed by site-direct mutagenesis without changing the amino acid sequence (GENEART site-directed mutagenesis system, Invitrogen, Carlsbad, CA, USA). The mGFP genes were inserted into pcDNA-3.1(+) with *Nhe*I/*Xho*I sites, in which a *Hind*III site was inserted between the mGFP gene and *Xho*I site, thereby generating pcDNA-mGFP. The 3A genes from pcDNA-3A(O99) and pcDNA-3A(O97) were individually subcloned into pcDNA-mGFP by *Hind*III/*Xho*I, thereby generating pcDNA-mGFP-3A(O99) and pcDNA-mGFP-3A(O97).

The d1D-2A-eGFP (d1A: deleted 1D gene; the last 33 nt of VP1 gene from O/TAW/97) cassette flanked by *Nhe*I-*Bam*HI and *Hind*III-*Xho*I was inserted into pcDNA-3.1(+) using the *Nhe*I and *Xho*I restriction enzymes, thereby generating the pcDNA-2A-eGFP vector. Next, various truncations of 3A genes were inserted between *Hind*III/*Xho*I (or *Hind*III/*Xba*I) sites. For the 3A-eGFP_{2A} constructs, the genes and restriction sites from pcDNA-2A-eGFP were rearranged. The d1D2A gene was subcloned into pcDNA-3.1(+) with *Nhe*I/*Xho*I sites, adding a *Bam*HI site to the 5' end of the d1D2A gene. Next, the eGFP gene was inserted into the plasmid using *Nhe*I/*Bam*HI, and a *Hind*III site was added to the 5' end of the eGFP gene. The variant truncated 3A genes were further inserted using *Nhe*I/*Hind*III.

The synthesized APEX2 gene, following the study by Lam et al. [34], was purchased and inserted into pcDNA-3.1(+) using *Nhe*I and *Xho*I. The indicated truncated or full-length 3A genes were inserted using *Xho*I and *Xba*I. For the GST fusion plasmids, the GFP genes in the variant mGFP- version and -eGFP_{2A} versions were replaced with GST genes using the *Nhe*I/*Hind*III and *Hind*III/*Xho*I enzymes, respectively.

2.2.2. Host-Factor Plasmids

The Sar1a and Sec12 cDNA clones from swine and cattle were purchased from Origene (sSar1: NM_001031786; cSar1: XM_005226384; sSec12: XM_003125297; cSec12: NM_001076875). They were inserted into pcDNA-3.1(+) with a FLAG tag at the N-terminus. The sSar1 mutant constructs, including H79G, T39N, and QTTG (156-QTTG-159 to AAAA), were generated using the GENEART site-directed mutagenesis system (Invitrogen) with the indicated primers, while D198 was replaced with alanine using standard PCR with the primers BamHI-sSar1-F and XhoI-msSar1-D198A-R. The mutation of I41A for sSec12 was also performed with a GENEART site-directed mutagenesis system (Invitrogen).

2.2.3. Others

The mCherry gene, flanked by the peptide sequences of calreticulin and the KDEL motif, was inserted into pcDNA-3.1(+) using *NheI* and *HindIII* to generate pcDNA-mCherry-ER. The plasmid for expressing mCherry-LC3B was a gift from David Rubinsztein (Addgene plasmid # 40827). The 2B and 2C genes were amplified from the O/TAW/97 cDNA pool and then subcloned into pcDNA-3.1(+) for pcDNA-2B and pcDNA-2C. These two plasmids were further inserted into mGFP genes using *NheI* and *KpnI*, thereby generating pcDNA-mGFP-2B and pcDNA-mGFP-2C.

2.3. Monoclonal Antibody Preparation

BALB/c mice were immunized using purified SUMO-3ABC (O/97) and GST-3ABC (O/99), which were expressed from *E. coli*. Immunized spleen cells were fused with SP2/O-Ag14 myeloma cells. After 1–2 weeks, hybridoma supernatants were screened by IFA with 3A(O99), 3A(O97), and FMDV acetone-fixed cell plates. After at least two limited dilutions, the positive clones were further characterized. QA2, PA1, and T10E were selected for this study. Their isotypes all belonged to IgG2a/κ. The purified monoclonal antibodies were obtained according to the method used in a previous study [35]. The hybridoma was inoculated intraperitoneally into BALB/c for ascetic fluid and purified using Protein G (GE Healthcare). The purified antibodies were further conjugated with the fluorescent dye Dylight488 (Abcam, ab201799), according to the manufacturer's instructions.

2.4. Western Blotting

Equal volumes of cell lysates or eluates from co-immunoprecipitation (co-IP) were mixed with a sample loading buffer (Bionovas, FA0020) and incubated at 95 °C for 5 min. The samples were separated by 13.5% SDS-PAGE, transferred to a nitrocellulose membrane (PALL, 79548), and blocked using 5% (*w/v*) skim milk in PBST at room temperature (RT) for 30 min. The proteins on the membranes were detected using the indicated antibodies, with overnight incubation at 4 °C, and the corresponding horseradish peroxidase (HRP)-conjugated secondary antibodies were used with incubation at RT for 1 h. Given that bands were masked by the light and the heavy chains of antibodies used in the co-IP step, secondary antibodies against native antibodies (Abcam, ab131366, which could not recognize mouse IgG1) or specific mouse native antibodies (Abcam, ab131368) were used for the elution samples.

2.5. Immunofluorescence Assay and Confocal Live-Cell Imaging

PK-15 or A549 cells, grown on a confocal μ-dish (ibidi, IB-81156), were transfected with the indicated plasmids for 24 h. For standard IFA protocols, cells were fixed using 4% paraformaldehyde in PBS for 15 min at 37 °C and further permeabilized using 0.5% TX-100 for 5 min at RT. For the examination of the 3A protein topology, fixed cells were permeabilized using 50 μg ml⁻¹ of digitonin for 5 min at RT. After being washed with PBS three times, the samples were incubated with primary antibodies for 2 h at 37 °C, followed by incubation with appropriate secondary antibodies for 1 h at 37 °C. When double-labeling was performed, both antibodies were added together. The nucleus was stained with Hoechst stain (Invitrogen, H3569) at a 1:10,000 dilution for 15 min at 37 °C. All the imaging was performed under an Olympus IX-83 microscope connected to a CMOS (Complementary Metal Oxide Semiconductor) color camera. Live cells were maintained on the microscope stage at 37 °C.

2.6. Autophagy Induction

PK-15 cells in 24-well plates were transfected for 21 h. After washing with PBS, the medium was replaced with fresh DMEM, DMEM with 100 nM rapamycin, or starvation medium (20 mM HEPES, pH 7.4, 140 mM NaCl, 1 mM CaCl₂, 1 mM MgCl₂, 5 mM glucose, 1% BSA) for 3 h. The cells were collected in 50 μL of RIPA buffer (Bio Basic, RB4478); 5 μL

of cell lysates were analyzed in a 6M urea 13.5% SDS gel, followed by Western blotting to detect LC3BI and LC3BII.

2.7. Transmission Electron Microscopy and Electron Tomography

PK-15 cells were seeded on an Aclar film (Electron Microscopy Science) in 6-well plates. After transfection for the indicated plasmids containing the APEX2 fusion protein gene for 24 h, the cells were rinsed using PBS, followed by 2% glutaraldehyde fixation in 0.1 M phosphate buffer (PB, pH 7.3) for 1 h on ice. After five washes with PBS, 20 mM glycine in PBS was added for 5 min to quench the free aldehyde groups. After another five washes, the cells were incubated with diaminobenzidine (DAB) solution with H₂O₂ (5 min for APEX2-3A, 15 min for APEX2-NHR, 30 min for APEX2-N2HRC, and 30 min for APEX2-N2HRC1). The cells were further rinsed in 0.1M PB (2 min × 5 times) and immersed in 2% osmium tetroxide in 0.1 M PB for 30 min. The cells were then rinsed in distilled water (2 min × 5 times) before overnight staining in a 2% aqueous solution of uranyl acetate. The cells in the monolayer were further subjected to a standard protocol of dehydration and embedding (Spurr's medium) for TEM imaging. The specimen blocks were checked and trimmed under a stereomicroscope and ultra-thin sections (70 nm) were obtained from the area with positive signals (dark cells). The sections were observed using a transmission electron microscope (TEM, FEI Tecnai G2 TF20 Super TWIN) operating at 120 kV. For electron tomography, serial sections (200 nm) through the APEX2-positive cells were obtained [36]. Double-tilt electron tomography was performed with the TEM (FEI Tecnai G2 TF20), operating at 200 kV. The structures of the organelles were depicted using the Amira/Avizo software.

2.8. Recombinant Vaccinia Expression System

The protocol followed that of a previous study [37]. HTK⁻ cells were seeded in 6-well plates for 1 day, followed by vTF7-3 infection for the production of T7 polymerase within cells for 1 h. The indicated plasmids, containing a T7 promoter, were transfected to the cells by using TurboFect (Thermo Scientific, Carlsbad, CA, USA). After 20–24 h, the cells were ruptured by three freeze–thaw cycles in 500 µL of PBS with a protease inhibitor (Millipore, 539134). Finally, the cell debris was removed by 10,000 × g centrifugation for 20 min.

2.9. Immunoprecipitation Assay

For each sample, 1 µg of anti-FLAG antibody (Sigma, F1804) or PA1 MAb was incubated with 10 µL of Protein G Mag Sepharose (GE Healthcare) in 500 µL of binding buffer (50 mM Tris, pH 7.5, 150 mM NaCl) with slow end-over-end mixing for 1 h at RT. Cell lysates that came from the vTF7-3 expression system or transfected PK-15 cells were applied for the co-immunoprecipitation assay. For the vTF7-3 expression system, a 200 µL sample was incubated with anti-FLAG antibody–magnetic beads overnight after the removal of the binding buffer. For the transfected PK-15 cells, which were harvested using 200 µL of RIPA buffer in each well of 6-well plates, 180 µL samples were applied. After mixing overnight at 4 °C, the magnetic beads were washed with PBS or RIPA three times. After replacement with a clean Eppendorf tube, the bead was washed with PBS again. Finally, the sample was eluted with 20 µL of 2% SDS and analyzed by Western blotting.

2.10. Knockdown Assay

A549 cells were seeded in a 6-well plate and then transfected with the indicated plasmids expressing shRNA, including pLAS2w.Ppuro (empty vector), Sar1-1 (target: CCAGTTCCTAGGACTCTACAA), Sar1-2 (target: CGTGAGATATTTGGGCTTTAT), Sec12-0 (target: GCTGGCCTAAAGATGCAATAA), and Sec12-4 (target: GTGTGCTTCAACCAC-GATAAT). The plasmids were purchased from the National RNAi Core Facility in Taiwan. After 24 h post-transfection, the cells were selected using 1 µg ml⁻¹ puromycin for 3–4 days and maintained in DMEM with 0.5 µg ml⁻¹ puromycin for more than 2 weeks. For siRNA transfection, cells were seeded in a 24-well plate 1 day before siRNA transfection, in accor-

dance with the manufacturer's instructions for Lipofectamine MessengerMAX Reagent (Thermo Scientific, LMRNA). The target sequence for non-target and Sar1 siRNA was as follows: non-target (UUCUCCGAACGUGUCACGU) and Sar1 (CCAGUUCCUAGGACU-CUACAA), which were purchased from Biotools. To increase the knockdown efficiency, A549 cells were transfected repeatedly after 24 h of siRNA transfection. At 6 h after the last siRNA transfection, pcDNA-mGFP-N2HRC1 was transfected into the cells.

3. Results

3.1. Membrane Topology of Peripheral FMDV 3A Protein

Unlike the other picornaviruses, FMDV 3A is a peripheral membrane protein located on the ER [23,38]. However, it was useful to confirm this with another method. To probe further, we first produced three powerful anti-FMDV 3A MAb, namely QA2, PA1, and T10E, against the O/TAW/97 (O/99) and O/TAW/97 (O/97) strains. The O/97 strain was a porcophilic strain with ten amino acid deletions (aa 93–102) in the 3A protein, while the 3A of O/99 was relatively conserved with respect to another strain (Figure S1). Using variant monomeric GFP (mGFP) fused-3A truncated proteins (Figure 1a), the binding sites for these antibodies were determined by Western blotting (Figure 1b). QA2 MAb recognized the N-terminus of 3A (aa 1–41) for the O/99 and O/97 virus strains. PA1 and T10E could only interact with the C-terminus of 3A for O/99 and O/97 individually (Figure 1c), which is a highly diverse region between these two virus strains (Figure S1). Under digitonin treatment, the antibody could penetrate through the plasma membrane but not the ER or other organelles. For verification, calreticulin, a marker protein located within the ER lumen, was detected using a Triton X-100 treatment but not a digitonin treatment (Figure 1d). However, three anti-3A MABs could detect 3A in all the conditions (Figure 1e), indicating that 3A was a peripheral membrane protein with both the N- and C-termini exposed to the cytoplasm.

3.2. FMDV 3A Protein Modified ER into Punctae

Based on co-localization testing, O'Donnell et al. had suggested that FMDV-induced 3A-containing vesicles may have originated from the ER [15], and Gonzalez-Magaldi et al. had further confirmed a connection between the FMDV 3A protein and the ER [23]. In our study, we found that the FMDV 3A immunofluorescence signal showed no co-localization with the ER marker protein calreticulin in 3A-transfected PK-15 cells (Figure S2a), despite the 3A punctae displaying a web-like pattern. To identify the ER structure in live cells without alteration by fixation, we constructed mCherry-ER, in which mCherry was fused with the peptide signal of calreticulin and the KDEL motif (referring to the study by Roderick et al. [39]). A similar strategy was used in several previous studies [40–42]; afterwards, the cells were examined by immunofluorescence assays (IFAs) (Figure S2b). After the co-expression of mCherry-ER and mGFP-3A, mGFP-3A punctae appeared at the site where the ER fragmented (Figure 2a). As shown in the right panel of Figure 2a, the ER structure was disrupted in the area (white arrow) displaced by mGFP-3A punctae, which were linked in a web-like pattern. In the early expression (3 h post-transfection), mGFP-3A showed a web-like structure, but it was only partially co-localized with mCherry-ER (Figure S2c). Therefore, we considered that 3A punctae had been derived from the ER (Figure S2d). Approximately 60% of the mGFP-3A-positive cells showed a punctate pattern, while the others appeared as a diffuse type (Figure S2e). If the C-terminus of 3A had been truncated, they showed a clean reticular pattern and were highly co-localized with mCherry-ER (Figure 2b). These results support the concept that 3A molecules were located at the ER, and, by exerting an unknown function that required the C-terminus, 3A modified the ER into punctae. To determine the region essential for puncta formation, 3A was truncated into several parts. Considering that GFP interfered with the structure of the truncated 3A, the truncated 3A was fused to the C-terminus of mGFP (or 2_A eGFP) or the N-terminus of eGFP $_{2A}$ (2A: FMDV 2A peptide, 19 aa) (Figure 2c and Figure S2f). As a result, N2HRC1 spanning the region of aa 42–92 was sufficient for puncta formation (Figure 2c).

However, it appeared as a web-like structure with a low expression level (approximately 28% of that for the transfected cells) (Figure 2d). This result suggested that the ability was dampened but not entirely abrogated by deleting the N1 and C2 regions.

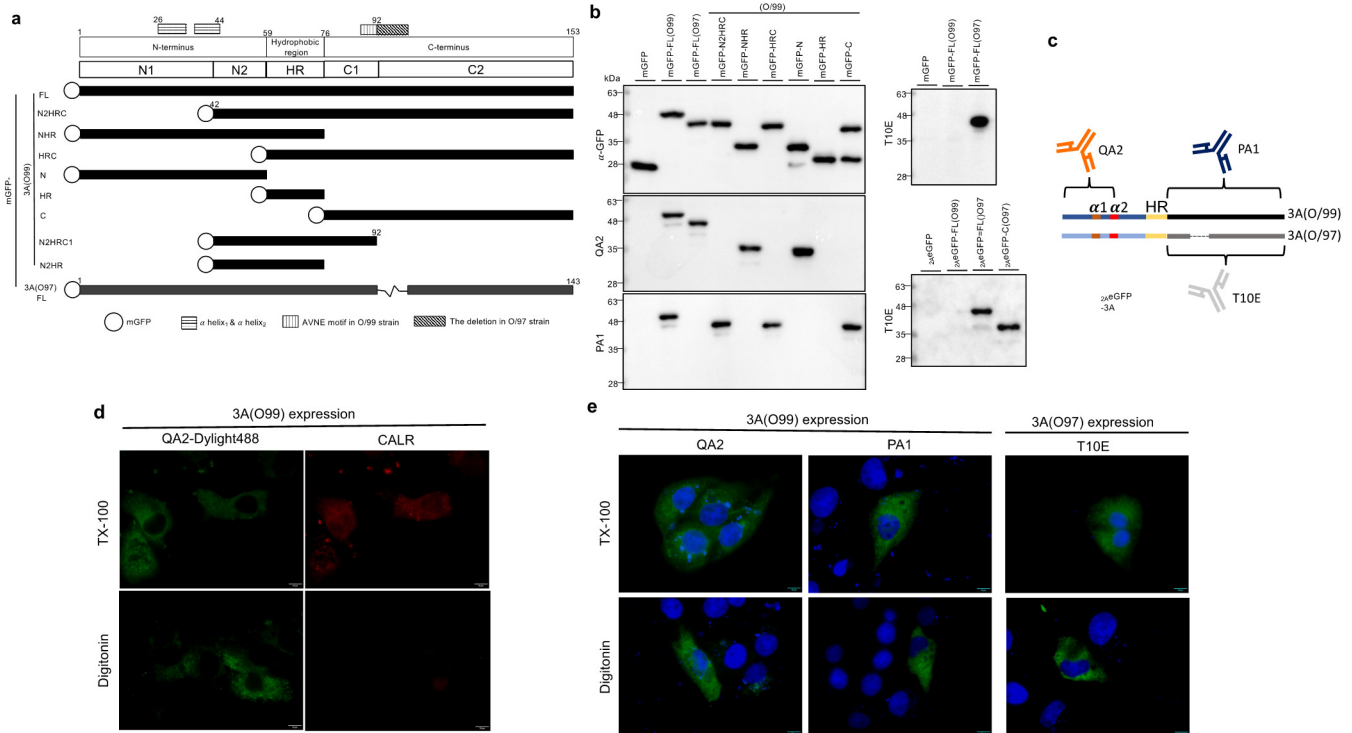


Figure 1. (a) Diagram representing the different truncations of O/99 3A or O/97 3A fused with monomeric GFP (mGFP). We set the alpha-helix2 region and the deletion region in O/97 as the turning points to separate the N- and C-termini into N1/N2 and C1/C2. All the truncation forms here used the O/99 normal virus strain as a template, including the aa 1–41 deletion (mGFP-N2HRC), aa 1–41 and aa 93–153 deletion (mGFP-N2HRC1), N-terminus deletion (mGFP-HRC), C-terminus deletion (mGFP-NHR), hydrophobic region (mGFP-HR), C-terminus (mGFP-C), and N-terminus (mGFP-N). (b) The constructs, expressed in PK-15 cells, were used to examine homemade anti-3A MAbs by Western blotting. QA2 could not recognize N2HRC, indicating the binding site located at the region within aa 1–41 of 3A, while PA1 recognized the C-terminus of 3A from O/99. The binding site for T10E should be the C-terminus of O/97 3A. (2AeGFP: eGFP fused with FMDV 2A peptide in N-terminus.) (c) The schematic of the MAb binding sites on 3A protein. (d) PK15 cells were transfected for expressing 3A from O/99 or O/97. After fixation, the cells were permeabilized using Triton X-100 or digitonin. Anti-calreticulin rabbit antibodies were used to stain the cells in the control group, followed by anti-rabbit secondary antibodies (red) and MAb QA2 conjugated to Dylight 488 (green) for dual labelling. (e) For the examination of the topology of 3A, the cells were stained with the indicated MAb (QA2, PA1, or T10E), followed by anti-mouse secondary antibodies. The nucleus was stained using Hoechst stain.

In addition to 3A, the viral membrane proteins 2B and 2C were also examined. Consistent with previous studies [17,43], mGFP-2B would generally be located at the ER without obvious ER damage (Figure S2g, left), as compared to mGFP-3A. mGFP-2C also showed co-localization with mCherry-ER and no ER fragmentation at a moderate expression level (Figure S2g, right).

3.3. The 3A Punctae Were Distinct from Traditional COPII Vesicles or Autophagosomes

It has been reported that FMDV induced autophagy in favor of viral replication [44] and 3A expression upregulated LRRC25, an autophagy-related protein [27]. In addition, FMDV was postulated to initiate viral replication at the sites associated with the ER exit site

(ERES), which was responsible for COPII vesicle formation [16]. Therefore, we aimed to exclude the possibility that 3A punctae were COPII vesicles or autophagosomes. According to IFA, 3A punctae from 3A (O99) were not co-localized with the COPII inner and outer coat proteins Sec23A and Sec31A (Figure 3a). Meanwhile, most cells for 3A expression led to Sec31A dispersion and downregulation (Figure 3a and Figure S3), which agreed with previous findings where FMDV infection had led to the dispersal and downregulation of Sec31 [16]. However, upon the activation of autophagy, LC3B-I was converted into LC3B-II and this became evident as punctae (Figure 3b,c; see starvation condition). Based on the LC3B-II/LC3B-I ratio detected by immunoblotting, the 3A protein mildly induced autophagy, as compared to empty vector transfection (Figure 3b,c). As they were not co-localized with mCherry-LC3B (Figure 3c), it was clear that mGFP-3A punctae were not autophagosomes. These results indicate that 3A punctae were specific structures and distinct from COPII vesicles and autophagosomes.

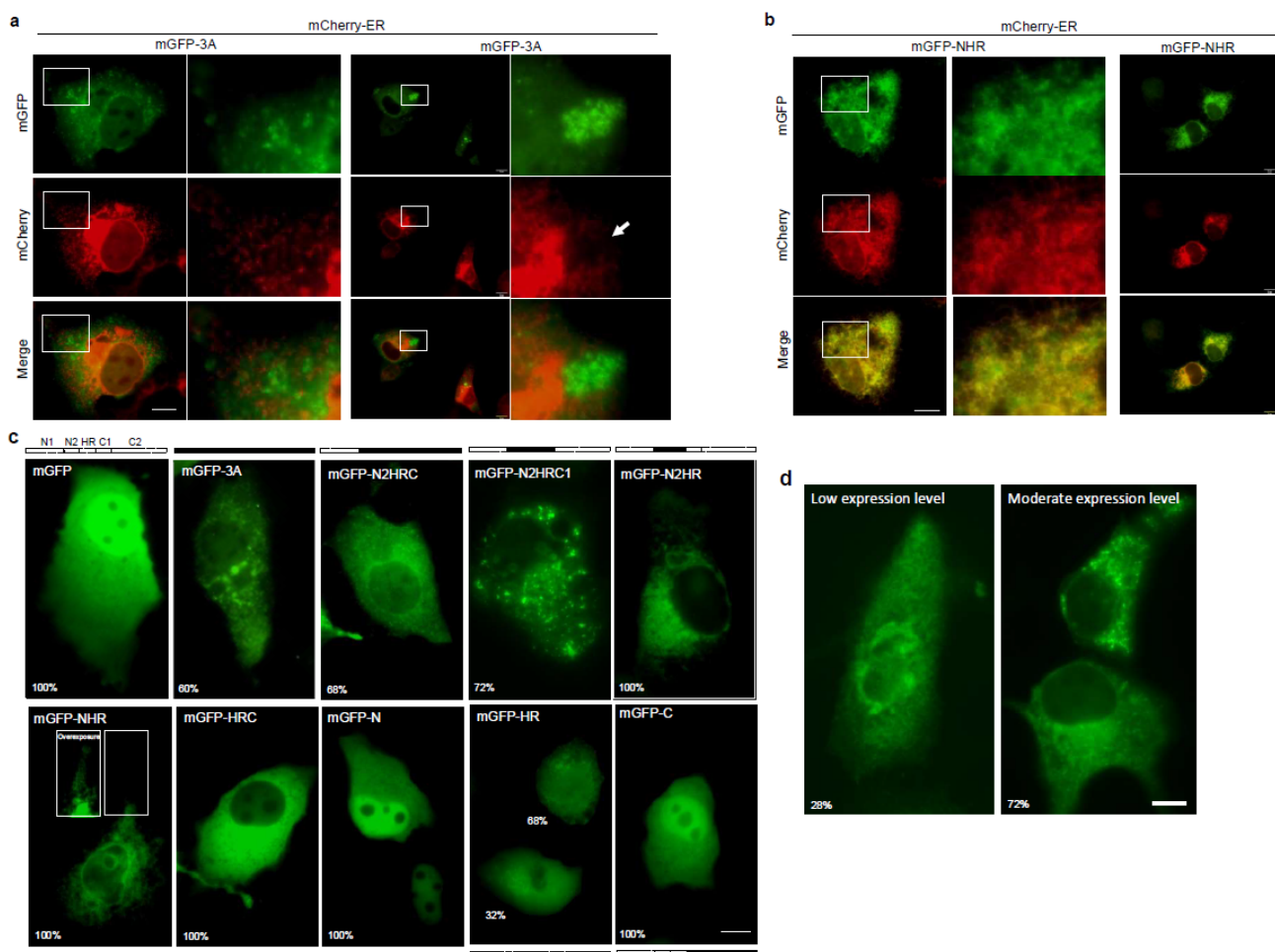


Figure 2. (a,b) Images obtained in PK-15 live with mCherry-ER and mGFP-3A (or mGFP-NHR) co-expressed. The white arrow indicates the area of ER fragmentation. (c) Images of the variant truncation of 3A, in which the N-terminus was fused to mGFP. The mGFP diffused within the cytoplasm and nucleus. More than half of the cells expressing mGFP-3A, mGFP-N2HRC, and mGFP-N2HRC1 (60%, 68%, and 72%, respectively) showed multiple punctae in the population. In addition, mGFP-N2HR and mGFP-NHR showed reticular patterns, while only 68% of the mGFP-HR-expressing cells were reticular and the others appeared to be diffuse-type. The mGFP-HRC protein distributed diffusely in the cytoplasm, and mGFP-N and mGFP-C in the cytoplasm and nucleus. (d) N2HRC1 expression in PK-15 cells showing reticular and punctae patterns at low (with longer exposure time) and moderate expression levels. Scale bar, 10 μ m.

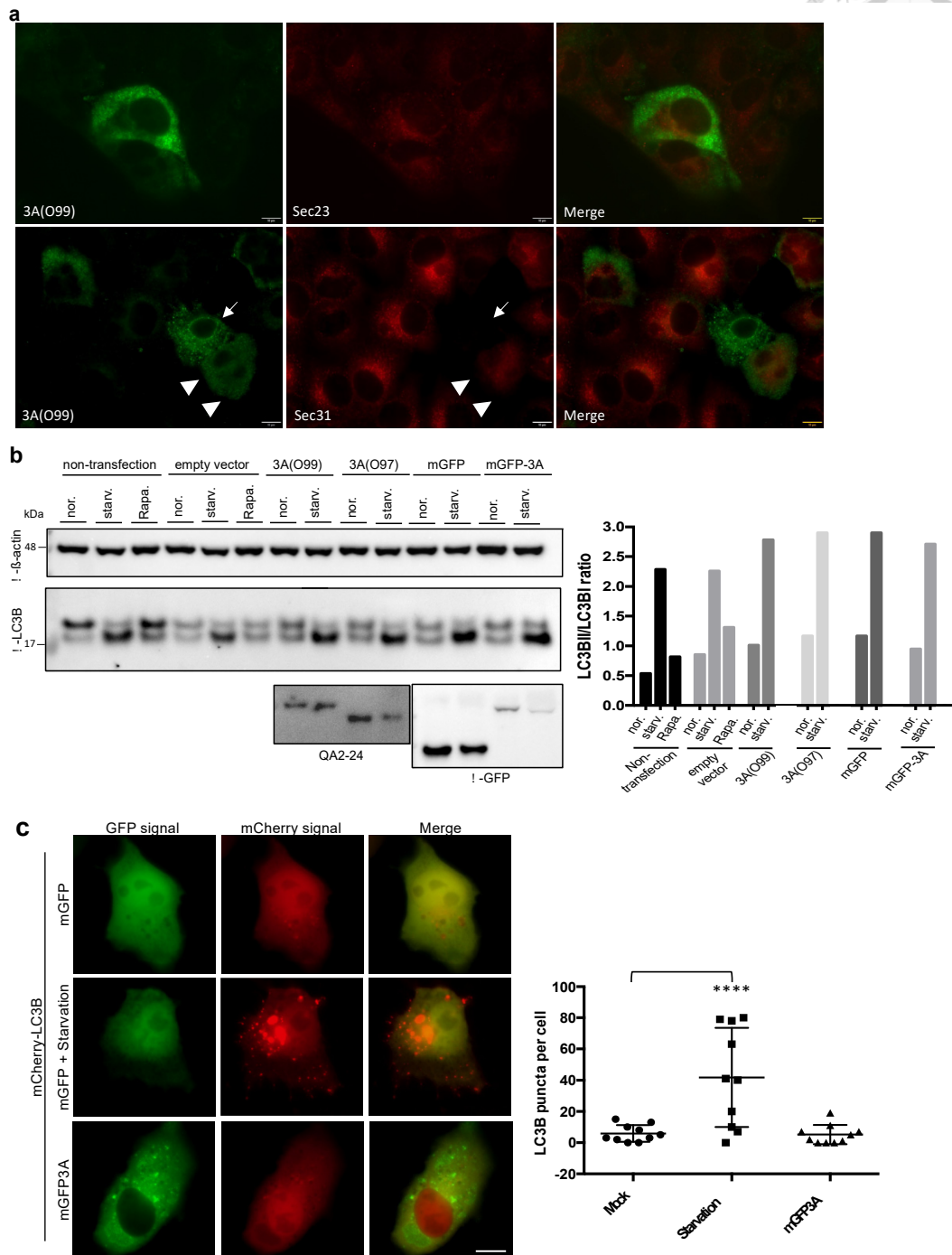


Figure 3. (a) PK-15 cells expressing 3A (O99) were stained with specific anti-Sec23A or Sec31A rabbit antibodies, followed by anti-rabbit antibodies conjugated with Alexa Flour 594. Finally, the 3A (O99) protein was further identified using QA2-Dylight488. The white arrow indicates the cell expressing 3A showing downregulation of Sec31, while white arrowheads indicate those showing Sec31 dispersion. (b) PK-15 cells were transfected using an empty vector (pcDNA-3.1(+)), pcDNA-mGFP, pcDNA-3A, or pcDNA-mGFP-3A for 21 h. The cells were further incubated in either normal, 100 nM rapamycin, or starvation condition medium for 3 h. The LC3B proteins from these cell lysates were analyzed by Western blotting and quantified using the ImageJ software. (c) PK-15 cells co-expressing mCherry-LC3B with mGFP or mGFP-3A. The cells expressing mGFP in starvation condition medium for 3 h were regarded as a positive control for autophagy activation and showed much more LC3B punctae than did the non-treated cells, but there was no significant increase in mGFP-3A overexpression. Scale bar, 10 μ m. **** $p < 0.0001$.

3.4. The Ultrastructure of the 3A Vesicle-like Structure as Observed Using Transmission Electron Microscopy

To gain better insight into the ultrastructure of the 3A punctae, we used electron microscopy and the APEX system, in which the APEX2 fusion protein could be directly stained using diaminobenzidine (DAB) directly. First, the patterns of APEX2-3A and APEX2-NHR were similar to those of the mGFP fusion constructs in IFA (Figure S4a). The APEX2-NHR clearly illustrated the ER structure under electron tomography (Figure 4a, Video S1). For the full length of 3A, as expected, the ER was disrupted into vesicle-like structures surrounded by APEX2-3A (Figure 4b; Video S2). The diameter of these structures was heterologous and approximately 80.15 ± 26.54 nm ($n = 83$). Similarly, these modified structures were also found in cells expressing APEX2-N2HRC (Figure S4b) and APEX2-N2HRC1 (Figure 4c). Moreover, in APEX2-N2HRC1-expressing cells, we also observed dark reaction products with segmented ER membranes (Figure 4c, white arrowheads), which were presumably in their state prior to reshaping. All the evidence pointed to 3A curving the ER membrane into vesicle-like structures and N2HRC1 preserving that ability.

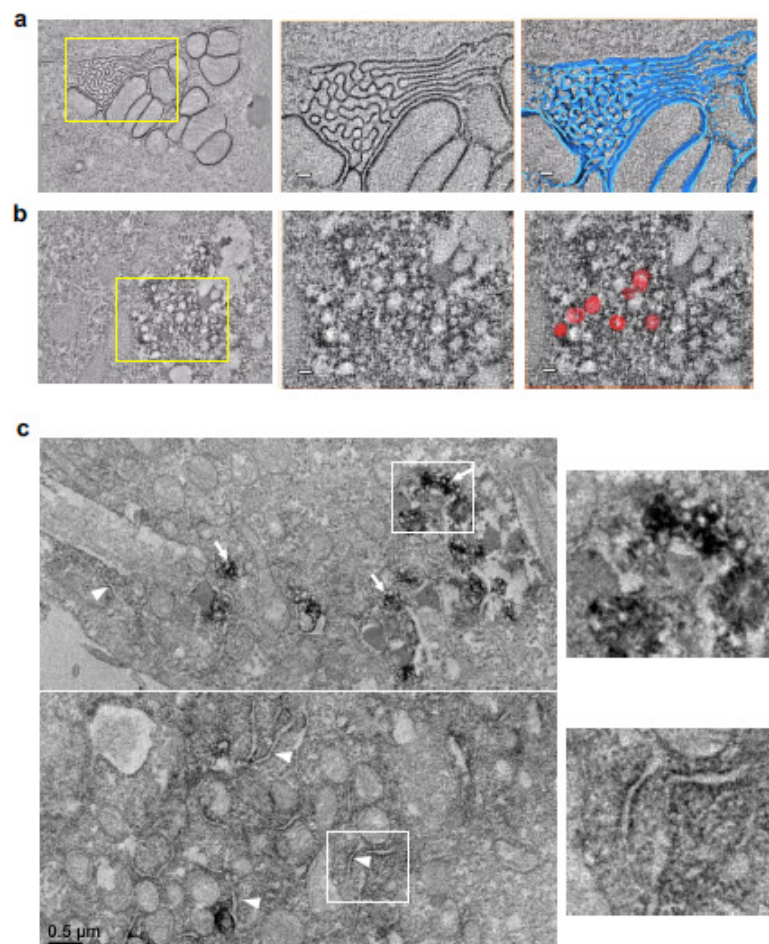


Figure 4. Electron tomography images of (a) APEX2-NHR and (b) APEX2-3A. The serial section was obtained from PK-15 cells expressing APEX2-NHR or APEX2-3A (full-length of 3A). The ER structures with DAB reaction products for APEX2-NHR (blue) were illustrated in the Amira/Avizo software, while eight vesicle-like structures with APEX2-3A were manually illustrated (red) as representative examples. (c) TEM images of APEX2-N2HRC1. White arrows indicate vesicle-like structures with APEX2-N2HRC1. In addition, segmented ER was found and marked by a DAB reaction (white arrowheads).

3.5. COPII Factors, Sar1 and Sec12, Were Found to Be Novel 3A Interaction Partners

Given that polioviral and coxsackieviral 3A interacts with the COPI factor GBF1 [6,45] and that FMDV has been highly associated with the COPII pathway [16], we tested whether 3A would interact with the COPII factors Sar1 and Sec12. After the co-expression of 3A and Sar1 (or Sec12) in a recombinant vaccinia (vTF7-3) transient expression system, the interactions were examined by anti-FLAG co-immunoprecipitation (co-IP). As shown in Figure 5a,b, 3A from both the O/99 and O/97 virus strains was co-immunoprecipitated with recombinant Sar1 and Sec12 from swine and cattle. Therefore, these two novel interactions were probably independent of the host species and the virus strains. In addition, the reciprocal co-IP by PA1 MAb was tested (Figure 5c). Furthermore, in PK-15 cells co-expressing 3A with sSar1 (Sar1 from swine) or sSec12 (Sec12 from swine), co-localization was detected in double immunofluorescence using anti-FLAG rabbit antibody and QA2 MAb (Figure 5d).

Next, we mapped the binding sites on 3A for these two interactions. For Sec12, truncated 3A fragments with an N-terminal fusion of mGFP- or a C-terminal fusion of -eGFP_{2A} were co-expressed with sSec12 in PK-15 cells. After sSec12 was pulled down, mGFP-HR and C-eGFP_{2A} were detected, indicating that the binding site for Sec12 on 3A ranged from HR to the C-terminus (Figure 5e). Further truncation of the C-terminus narrowed this down to the C2 region, aa 93–153 (Figure 5e,g). For the Sar1–3A interaction, truncated GST-3A or 3A-GST was co-expressed with sSar1 in the vTF7-3 expression system due to its sufficient production level for sSar1. The results show that all three fragments, including the N-terminus, HR, and C-terminus, were associated with Sar1 (Figure 5f). More precisely, the region between the N1 and HR regions showed a high affinity for Sar1, while the N2 and C1 regions adjoining HR also interacted with Sar1 (Figure 5f,g).

3.6. Knockdown of Sar1 or Sec12 Inhibited Formation of 3A Punctae

Due to the strong association of Sar1 and Sec12, we reasoned that these two interactions could be responsible for the formation of 3A punctae. To verify our conclusion, a knockdown assay was performed. Considering the well-reviewed papers for knockdown in human species and the high abundance of the Sar1 protein in PK-15 cells, the human pulmonary cell line A549 was chosen for the knockdown assay. Furthermore, we chose mGFP-N2HRC1, as the weaker reshaping ability of N2HRC1 would be easier to manipulate and observe. It is well known that 3A is a multifunctional protein; the truncation of 3A and removal of its other abilities would help us to evaluate the impact on the depletion of Sar1 and Sec12 for puncta formation.

First, Sec12 and Sar1 were knocked down in A549 cells with shRNA or siRNA individually (Figure S5a). As expected, puncta formation was inhibited in the Sec12 shRNA-A549 cell line (A0 cells) (Figure 6a). The re-expression of sSec12 restored the vesicular pattern, but not that of the Sec12 guanine nucleotide exchange factor-deficient mutant I41A (a mutation referred to previously [46]) (Figure 6a and Figure S5b). These findings indicate that Sar1 activation may be essential for ER remodeling. Similarly, after Sar1 siRNA treatment, the number of punctae decreased in comparison to that after non-target siRNA treatment, while the re-expression of sSar1 could restore puncta formation (Figure 6b and Figure S5c). It is well known that the COPII coat proteins Sec23 and Sec31 catalyze Sar1 GTPase activity, leading to the release of Sar1. Only when the Sar1 activation rate exceeds coat-induced hydrolysis does Sar1 polymerize to form a constricted neck, further exerting vesicle fission dependent on Sar1 hydrolysis. In short, the GTP cycle of Sar1 was essential for COPII vesicle formation [47]. Therefore, constitutive Sar1-GTP (H79G), constitutive Sar1-GDP (T39N), or defective organization Sar1 (156-QTTG-159 to AAAA) mutants could all block the COPII pathway. In our studies, during the co-expression of msSar1-T39N or msSar1-QTTG (m: mutated) with mGFP-N2HRC1, the formation of 3A punctae was significantly inhibited (Figure 6c). Nonetheless, msSar1-H79G did not disrupt puncta formation; instead, it enhanced it (Figure 6c). In addition, co-IP confirmed that all the mutated Sar1 showed a preserved interaction with 3A (Figure S5d).

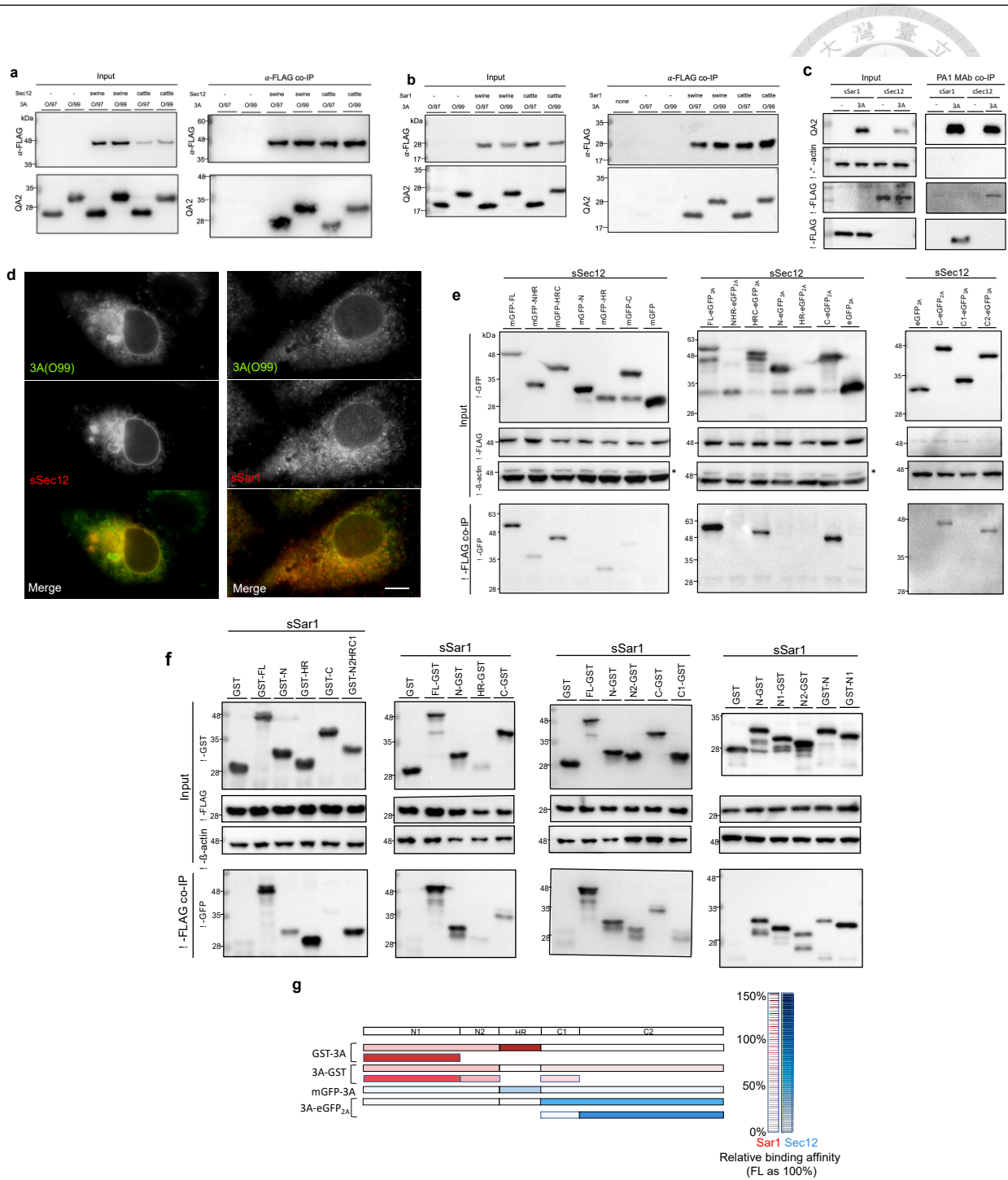


Figure 5. The examination of interactions between 3A and Sec12 or Sar1. (a) In the vTF7-3 expression system, HTK cell lysates for the co-expression of 3A from O/97 or O/99 and Sec12 from swine or cattle were applied to anti-FLAG co-immunoprecipitation assays: empty vector, pcDNA 3.1(+), none: non-transfection. (b) The examination for Sar1 was performed using the same procedure. (c) Reciprocal co-immunoprecipitation was performed with anti-3A MAb PA1. (d) PK-15 cells co-expressing 3A (O99) with sSec12 or sSar1. The cells were double-labeled for 3A and recombinant COPII factors using MAb QA2 and anti-FLAG rabbit antibodies, followed by anti-mouse and anti-rabbit secondary antibodies conjugated with Alexa Fluor 647 (green) and Alexa Fluor 594 (red), correspondingly. Scale bar, 10 μm. (e) PK-15 cells co-expressing sSec12 with variant truncation GFP version for anti-FLAG co-immunoprecipitation. *: residual signal for Sec12. (f) Co-expression of sSar1 with the truncated GST variants in the vTF7-3 system was applied for co-IP. (g) The diagram represents the relative binding affinity of each part of Sar1 or Sec12. The protein level of full-length 3A from the elution was regarded as 100%. Due to a relatively low expression level, HR-GST for Sar1 was excluded.

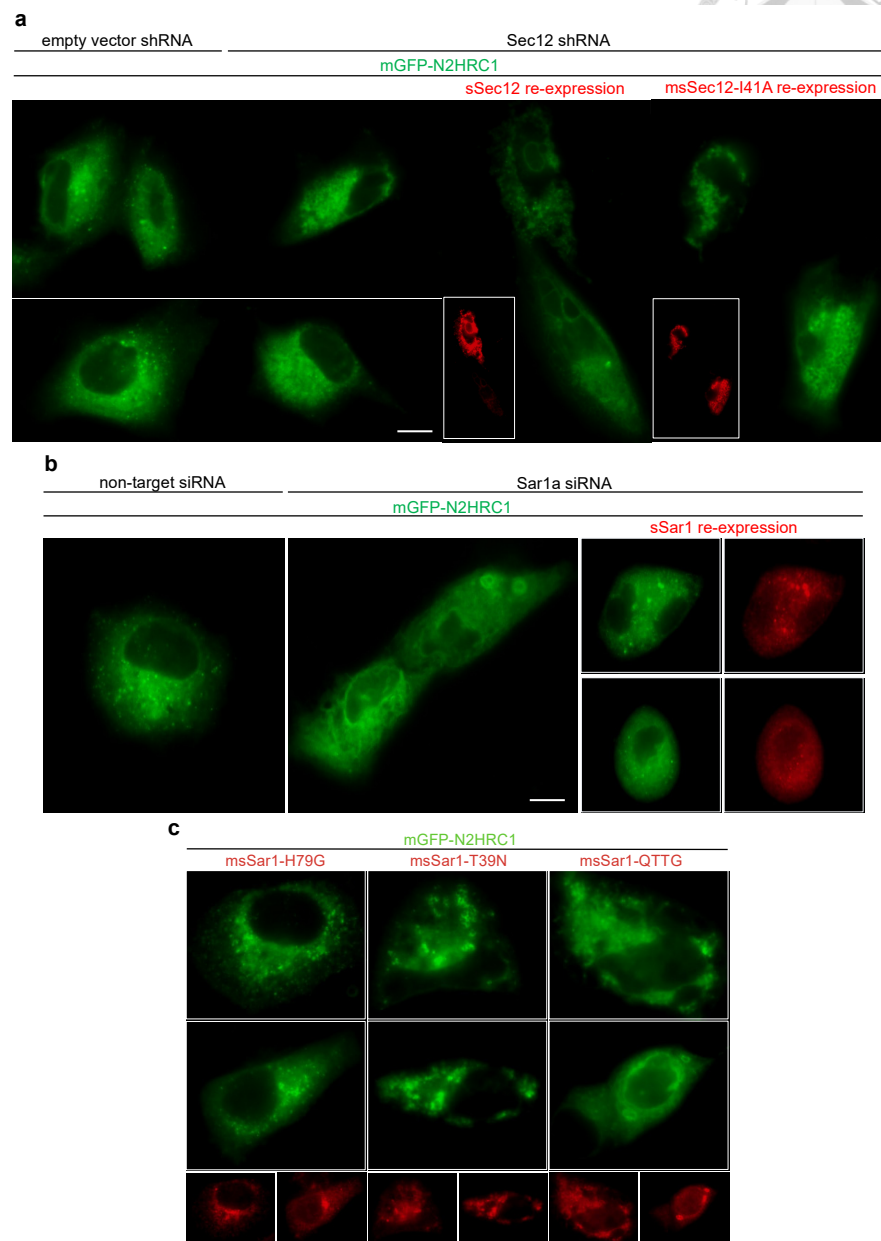


Figure 6. The fluorescence patterns of mGFP-N2HRC1 in A549 cells were examined under different conditions. (a) mGFP-N2HRC1 was expressed in A549 cells, constitutively expressing control shRNA or Sec12 shRNA. It showed a reticular pattern with punctae for pLAS2w.Ppuro (empty vector) cell lines, while the punctae significantly decreased in the Sec12 shRNA cell line (A0 cells). For the re-expression assay, the A0 cells were co-expressed with mGFP-N2HRC1 and sSec12 (wild type or I41A). The sSec12 proteins were identified using an anti-FLAG mouse antibody (red). (b) A549 cells were treated with siRNA (non-target; targeting Sar1), followed by mGFP-N2HRC1 expression. For the re-expression assay, sSar1 and mGFP-N2HRC1 were co-expressed after Sar1 knockdown and IFA identified recombinant Sar1, as above. Scale bar, 10 μ m. (c) A549 cells were co-transfected for mGFP-N2HRC1 and dominant-negative msSar1 (mutated sSar1), which was labeled with anti-FLAG antibodies (red).

3.7. The Model of Active Sar1–3A Intercalating Complex for ER Remodeling

Based on our mapping analysis, we presumed that FMDV 3A might enhance Sar1 activation by tethering Sar1 to Sec12 with the N-terminus and C-terminus individually. After Sar1 activation, 3A intercalated with two active Sar1s to curve the ER membrane with the N2 and C1 regions (Figure 7). Therefore, mGFP-N2HRC1 preserved the ability for

membrane curvature. In addition, 3A expression resulted in Golgi disassembly (Figure S6), as also reported by O'Donnell [15], since the blockade of the COPII pathway resulted in Golgi disruption due to failure in the transportation of PDIA3 [48]. In combination with the 3A-induced Sec31 dispersal (Figure S3), FMDV 3A should hijack Sar1 and disrupt the function of COPII machinery.

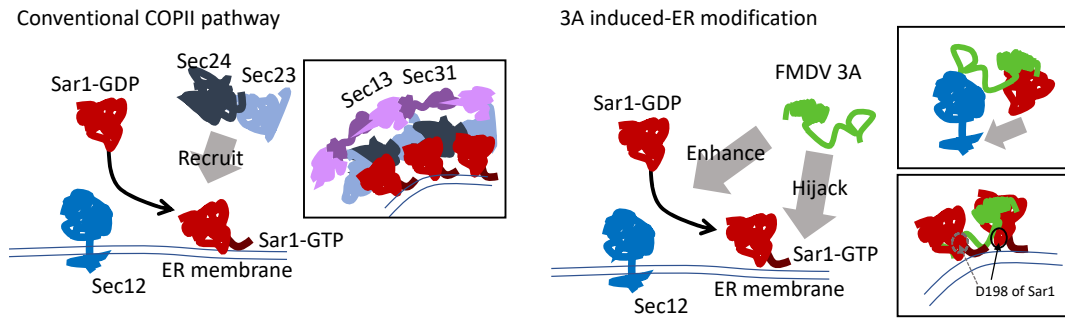


Figure 7. In the conventional COPII pathway, after activation by Sec12, Sar1 attaches to the ER membrane with the N-terminus, further recruiting the inner coat proteins Sec23 and Sec24. Sec24 recruits the COPII outer coat proteins Sec31 and Sec13 to bend the membrane into a vesicle-like structure. In FMDV 3A-expressing cells, we hypothesized that FMDV 3A modifies the ER into a vesicle-like structure, including Sar1 activation/enhancement and 3A—a Sar1–GTP intercalating complex. That is, 3A enhances Sar1 activation. Next, 3A intercalates into two active Sar1s to bend the membrane into vesicle-like structures.

It has been reported that glycolipid glycosyltransferases (GGTs) directly interacted with Sar1 for transportation from the ER to the Golgi [49]. More precisely, the (R/K)X(R/K) motif at the GGT's cytoplasmic tail bound to the pocket around D198, N126, and N94 at Sar1. The D198A mutation of Sar1 abrogated the interaction for GGTs, resulting in the accumulation of GGTs at the ER [49,50]. However, the D198A mutation should not affect most of the protein trafficking from the ER to the Golgi. Surprisingly, we found that msSar1-D198A led to the inhibition of puncta formation (Figure 8a). Most importantly, the D198A mutation significantly decreased the ability to bind to the N2 and C1 domains of 3A (Figure 8b). The D198 residue, the last amino acid of Sar1, was positioned near the membrane, which fit our model.

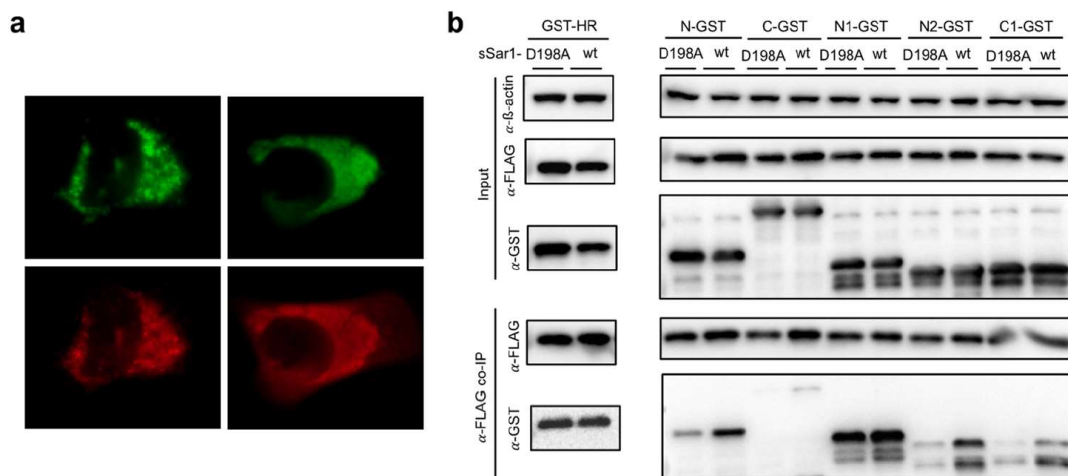


Figure 8. (a) msSar1-D198A (red) and mGFP-N2HRC1 (green) were co-expressed in A549 cells, followed by IFA for identifying recombinant Sar1 with anti-FLAG antibody. (b) The variant of truncated 3A fused with GST was co-expressed with wild-type sSar1 or the D198A mutation of Sar1. After anti-FLAG co-IP, fragments of 3A were examined by anti-GST antibodies. *: the nonspecific band.

4. Discussion

Several advanced studies have revealed that viruses can modify host organelles to serve as replication sites or provide viral RNP transport [1,51–54]. How viruses modify a host endomembrane has been a focus of research in the field, especially in the case of positive single-stranded RNA viruses. Notable studies on enteroviral replication organelles (ROs) have been conducted. Although some components, such as ACBD3, PI4K, OSBP, and cholesterol, have proved essential for enteroviral ROs, the actual causes of RO formation are not yet fully understood [3,13,55]. Currently, the viral 3A protein is thought to be a key component and one of the initiators. However, FMDV 3A is unique compared to proteins from other picornaviruses [23].

In a study by Gonzalez-Magaldi et al., they utilized a co-localization test, a fluorescence recovery after photobleaching (FRAP) analysis, a fluorescence loss in photobleaching (FLIP) analysis, and a membrane-bounded fraction analysis to support the idea that 3A was a peripheral ER membrane protein [23]. In this study, we have demonstrated new evidence showing that FMDV 3A is a peripheral membrane protein by using digitonin and monoclonal antibodies. Moreover, FMDV 3A modified the ER into vesicle-like structures, as determined by fluorescent live microscopy and electron tomography with the APEX system. Following up on a study reporting that FMDV was associated with the COPII pathway [16], we found that two COPII factors, Sar1 and Sec12, interacted with FMDV 3A based on a co-IP and co-localization test, and these two interactions were associated with 3A-induced ER remodeling, as shown by knockdown and re-expression assays. Finally, we built a model to explain how FMDV 3A modified the ER.

In our hypothesized model, 3A tethered Sar1 to Sec12 for activation via the N-terminus and C2 region. Due to the failure of the active Sar1 pull-down assay, this assumption should be validated by future research. However, Sar1 activation is necessary for remodeling, as functionally deficient Sec12 (I41A-msSec12) would be unable to restore 3A puncta formation in Sec12-depleted cells. After attaching to the ER membrane, two active Sar1s interacted with the 3A protein in the N2 and C1 regions, causing membrane curvature—instead of recruiting Sec23 and Sec24. Therefore, mGFP-N2HRC1 preserved the ability for ER remodeling. Constitutively active Sar1 (msSar1-H79G) enhanced 3A puncta formation, while constitutively inactive (T39N) and polymerization-deficient (156-QTTG-159 to AAAA) Sar1 inhibited that formation. In addition, 3A expression disrupted the COPII pathway, inducing Sec31 dispersal and Golgi disorganization. Most importantly, the D198A mutation of Sar1 inhibited the interaction with the N2 and C1 regions of 3A, thereby inhibiting puncta formation. The D198A mutation did not inhibit Sar1 activation or most protein trafficking that is dependent on COPII vesicles [50]. As the position of D198 for active Sar1 is located near the membrane, the amino acid fits the positions of the N2 and C1 regions of 3A that adjoin the hydrophobic region. Although this study was not focused on examining the specific membrane-remodeling processes, future experiments using cell-free techniques [46,56] and giant unilamellar vesicles (GUVs) are warranted to highlight our proposed model [57].

The results of the knockdown assay also indicated that 3A puncta formation required Sar1 and Sec12, although we had numerous difficulties. For example, an attempt to use PK-15 cells in an shRNA strategy was unsuccessful, possibly due to the narrow window between lethal doses of puromycin and the efficient knockdown condition for Sar1 and Sec12. Moreover, we were unable to find available antibodies against endogenous Sec12 from PK-15 cells in Western blotting. Therefore, A549 cells were selected for this experiment. In addition, the shRNA Sar1 A549 cell lines did not survive the puromycin selection; therefore, the siRNA strategy was adopted as an alternative for the Sar1 knockdown assay.

Due to the biosecurity issues in Taiwan, our studies were restricted by virus-free regulations, so our hypothesis could be in question. However, a study by Midgley et al. presented reliable experiments for FMDV infection [16]. They showed that the knockdown of Sar1 significantly inhibited FMDV infection in IBRS2 cells. The T39N mutation of Sar1 inhibited FMDV infection in IBRS2 cells, while the H79G mutation did not. FMDV infection led to the dispersal of outer coat protein Sec31 labeling in HeLa cells. These results

agree with our model's prediction that FMDV 3A utilized and required active Sar1 for ER remodeling, resulting in interference with the COPII pathway. The ER remodeling should be the initiation of RO formation, which is essential for viral replication.

The ER is commonly utilized and modified by viruses such as hepatitis C virus, influenza virus, Zika virus, and reovirus [40,51,58,59]. Zika virus provides a simple but straightforward example of how a virus modifies the ER. Zika NS1 proteins, located within the ER lumen, homodimerize to induce ER invagination, which is probably similar in dengue virus [59]. However, most other viruses may be more complicated. For example, reovirus-induced ER modification has required both σ NS and μ NS proteins [40]. For poliovirus (an enterovirus), the formation of the modified structure mimicking the RO required the co-expression of 3A and 2BC [60]. We also considered that the mechanism of RO formation could have been associated with 2B and 2C and required further exploration.

Overall, to our knowledge, this study is the first to demonstrate that the FMDV 3A protein modified the ER into vesicle-like structures. The modification was synchronized by two unrecognized interactions, 3A–Sec12 and 3A–Sar1. In combination with other indirect evidence, we presumed that 3A enhanced Sar1 activation and further interacted with two active Sar1 proteins such that the membrane was bent into vesicle-like structures, which may be the first and most important step in RO formation during FMDV infection.

Supplementary Materials: The following supporting information can be downloaded at: <https://www.mdpi.com/article/10.3390/v14040839/s1>, Figure S1: Alignment of the amino acid sequence of 3A among O1Campos, O/TAW/99, and O/TAW/97 virus strains; Figure S2: The fluorescent images for 3A, calreticulin, mCherry-ER, truncated 3A fused with GFP, mGFP-2B, and mGFP-2C; Figure S3: The transfected cells co-stained with anti-3A and anti-Sec31A antibodies; Figure S4: The immunofluorescent images of APEX2-3A and APEX2-NHR and the ultrastructure of APEX2-N2HRC; Figure S5: Supporting information for knockdown and re-expression assay and a co-immunoprecipitation assay of 3A and mutated Sar1s (or mutated Sec12); Figure S6: FMDV 3A expression resulted in the dispersal of the Golgi, shown by IFA; Table S1: A list of cloning primers; Video S1: Electron tomogram of APEX2-NHR in PK-15 cells; Video S2: Electron tomogram of APEX2-3A in PK-15 cells.

Author Contributions: I.-C.C. and H.-W.L. conceived the project. Y.-F.J. conducted the experiments for TEM, and the other experiments were designed and performed by H.-W.L.; H.-W.L. and Y.-F.J. wrote the manuscript; H.-W.C. and I.-C.C. revised the manuscript. All authors have read and agreed to the published version of the manuscript.

Funding: This research was funded by the Ministry of Science and Technology, Taiwan (108-2313-B-002-019, 109-2313-B-002-014, and 109-2320-B-002-038-MY3), the Biological Electron Microscopy Core Facility, Academia Sinica, Taiwan (AS-CFII-108-119), and the Academia Sinica Cryo-EM facility, Taiwan (AS-CFII-108-110).

Institutional Review Board Statement: The animal study protocol was approved by the Institutional Animal Care and Use Committee protocols at National Taiwan University (approval number: NTU107-EL-00203) for studies involving animals.

Informed Consent Statement: Not applicable.

Data Availability Statement: The data presented in this study are available on request from the corresponding author.

Acknowledgments: The authors are pleased to acknowledge Chung-An Tan for help in editing the manuscript and Chi-Yu Fu for providing technical support on the Amira/Avizo software.

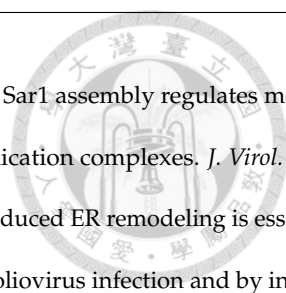
Conflicts of Interest: The authors declare no conflict of interest.

References

1. Belov, G.A.; van Kuppeveld, F.J. (+)RNA viruses rewire cellular pathways to build replication organelles. *Curr. Opin. Virol.* **2012**, *2*, 740–747. [[CrossRef](#)] [[PubMed](#)]
2. Monaghan, P.; Cook, H.; Jackson, T.; Ryan, M.; Wileman, T. The ultrastructure of the developing replication site in foot-and-mouth disease virus-infected BHK-38 cells. *J. Gen. Virol.* **2004**, *85 Pt 4*, 933–946. [[CrossRef](#)] [[PubMed](#)]

3. van der Schaar, H.M.; Dorobantu, C.M.; Albuлесcu, L.; Strating, J.; van Kuppeveld, F.J.M. Fat(al) attraction: Picornaviruses Usurp Lipid Transfer at Membrane Contact Sites to Create Replication Organelles. *Trends Microbiol.* **2016**, *24*, 535–546. [[CrossRef](#)]
4. Greninger, A.L. Picornavirus-Host Interactions to Construct Viral Secretory Membranes. *Mol. Basis Viral Infect.* **2015**, *129*, 189–212.
5. Egger, D.; Pasamontes, L.; Bolten, R.; Boyko, V.; Bienz, K. Reversible dissociation of the poliovirus replication complex: Functions and interactions of its components in viral RNA synthesis. *J. Virol.* **1996**, *70*, 8675–8683. [[CrossRef](#)]
6. Wessels, E.; Duijsings, D.; Niu, T.K.; Neumann, S.; Oorschot, V.M.; de Lange, F.; Lanke, K.H.; Klumperman, J.; Henke, A.; Jackson, C.L.; et al. A viral protein that blocks Arf1-mediated COP-I assembly by inhibiting the guanine nucleotide exchange factor GBF1. *Dev. Cell* **2006**, *11*, 191–201. [[CrossRef](#)]
7. Wessels, E.; Duijsings, D.; Notebaart, R.A.; Melchers, W.J.; van Kuppeveld, F.J. A proline-rich region in the coxsackievirus 3A protein is required for the protein to inhibit endoplasmic reticulum-to-golgi transport. *J. Virol.* **2005**, *79*, 5163–5173. [[CrossRef](#)]
8. Moghimi, S.; Viktorova, E.; Zimina, A.; Szul, T.; Sztul, E.; Belov, G.A. Enterovirus Infection Induces Massive Recruitment of All Isoforms of Small Cellular Arf GTPases to the Replication Organelles. *J. Virol.* **2020**, *95*, e01629-20. [[CrossRef](#)]
9. Viktorova, E.G.; Gabaglio, S.; Meissner, J.M.; Lee, E.; Moghimi, S.; Sztul, E.; Belov, G.A. A Redundant Mechanism of Recruitment Underlies the Remarkable Plasticity of the Requirement of Poliovirus Replication for the Cellular ArfGEF GBF1. *J. Virol.* **2019**, *93*, e00856-19. [[CrossRef](#)]
10. Greninger, A.L.; Knudsen, G.M.; Betegon, M.; Burlingame, A.L.; Derisi, J.L. The 3A protein from multiple picornaviruses utilizes the golgi adaptor protein ACBD3 to recruit PI4KIIIbeta. *J. Virol.* **2012**, *86*, 3605–3616. [[CrossRef](#)]
11. Hsu, N.Y.; Ilytska, O.; Belov, G.; Santiana, M.; Chen, Y.H.; Takvorian, P.M.; Pau, C.; van der Schaar, H.; Kaushik-Basu, N.; Balla, T.; et al. Viral reorganization of the secretory pathway generates distinct organelles for RNA replication. *Cell* **2010**, *141*, 799–811. [[CrossRef](#)] [[PubMed](#)]
12. Shengjuler, D.; Chan, Y.M.; Sun, S.; Moustafa, I.M.; Li, Z.L.; Gohara, D.W.; Buck, M.; Cremer, P.S.; Boehr, D.D.; Cameron, C.E. The RNA-Binding Site of Poliovirus 3C Protein Doubles as a Phosphoinositide-Binding Domain. *Structure* **2017**, *25*, 1875–1886.e7. [[CrossRef](#)] [[PubMed](#)]
13. Ilytska, O.; Santiana, M.; Hsu, N.Y.; Du, W.L.; Chen, Y.H.; Viktorova, E.G.; Belov, G.; Brinker, A.; Storch, J.; Moore, C.; et al. Enteroviruses harness the cellular endocytic machinery to remodel the host cell cholesterol landscape for effective viral replication. *Cell Host Microbe* **2013**, *14*, 281–293. [[CrossRef](#)] [[PubMed](#)]
14. Chen, Y.H.; Du, W.; Hagemeyer, M.C.; Takvorian, P.M.; Pau, C.; Cali, A.; Brantner, C.A.; Stempinski, E.S.; Connelly, P.S.; Ma, H.C.; et al. Phosphatidylserine vesicles enable efficient en bloc transmission of enteroviruses. *Cell* **2015**, *160*, 619–630. [[CrossRef](#)]
15. O'Donnell, V.K.; Pacheco, J.M.; Henry, T.M.; Mason, P.W. Subcellular distribution of the foot-and-mouth disease virus 3A protein in cells infected with viruses encoding wild-type and bovine-attenuated forms of 3A. *Virology* **2001**, *287*, 151–162. [[CrossRef](#)]
16. Midgley, R.; Moffat, K.; Berryman, S.; Hawes, P.; Simpson, J.; Fullen, D.; Stephens, D.J.; Burman, A.; Jackson, T. A role for endoplasmic reticulum exit sites in foot-and-mouth disease virus infection. *J. Gen. Virol.* **2013**, *94 Pt 12*, 2636–2646. [[CrossRef](#)]
17. Moffat, K.; Howell, G.; Knox, C.; Belsham, G.J.; Monaghan, P.; Ryan, M.D.; Wileman, T. Effects of foot-and-mouth disease virus nonstructural proteins on the structure and function of the early secretory pathway: 2BC but not 3A blocks endoplasmic reticulum-to-Golgi transport. *J. Virol.* **2005**, *79*, 4382–4395. [[CrossRef](#)]
18. Moffat, K.; Knox, C.; Howell, G.; Clark, S.J.; Yang, H.; Belsham, G.J.; Ryan, M.; Wileman, T. Inhibition of the secretory pathway by foot-and-mouth disease virus 2BC protein is reproduced by coexpression of 2B with 2C, and the site of inhibition is determined by the subcellular location of 2C. *J. Virol.* **2007**, *81*, 1129–1139. [[CrossRef](#)]
19. Belov, G.A.; Nair, V.; Hansen, B.T.; Hoyt, F.H.; Fischer, E.R.; Ehrenfeld, E. Complex dynamic development of poliovirus membranous replication complexes. *J. Virol.* **2012**, *86*, 302–312. [[CrossRef](#)]
20. Berryman, S.; Moffat, K.; Harak, C.; Lohmann, V.; Jackson, T. Foot-and-mouth disease virus replicates independently of phosphatidylinositol 4-phosphate and type III phosphatidylinositol 4-kinases. *J. Gen. Virol.* **2016**, *97*, 1841–1852. [[CrossRef](#)]
21. Loundras, E.A.; Herod, M.R.; Harris, M.; Stonehouse, N.J. Foot-and-mouth disease virus genome replication is unaffected by inhibition of type III phosphatidylinositol-4-kinases. *J. Gen. Virol.* **2016**, *97*, 2221–2230. [[CrossRef](#)] [[PubMed](#)]
22. Seki, F.; Ono, N.; Yamaguchi, R.; Yanagi, Y. Efficient isolation of wild strains of canine distemper virus in Vero cells expressing canine SLAM (CD150) and their adaptability to marmoset B95a cells. *J. Virol.* **2003**, *77*, 9943–9950. [[CrossRef](#)] [[PubMed](#)]
23. Gonzalez-Magaldi, M.; Martin-Acebes, M.A.; Kremer, L.; Sobrino, F. Membrane topology and cellular dynamics of foot-and-mouth disease virus 3A protein. *PLoS ONE* **2014**, *9*, e106685. [[CrossRef](#)] [[PubMed](#)]
24. Gonzalez-Magaldi, M.; Postigo, R.; de la Torre, B.G.; Vieira, Y.A.; Rodriguez-Pulido, M.; Lopez-Vinas, E.; Gomez-Puertas, P.; Andreu, D.; Kremer, L.; Rosas, M.F.; et al. Mutations that hamper dimerization of foot-and-mouth disease virus 3A protein are detrimental for infectivity. *J. Virol.* **2012**, *86*, 11013–11023. [[CrossRef](#)] [[PubMed](#)]
25. Beard, C.W.; Mason, P.W. Genetic determinants of altered virulence of Taiwanese foot-and-mouth disease virus. *J. Virol.* **2000**, *74*, 987–991. [[CrossRef](#)] [[PubMed](#)]
26. Pacheco, J.M.; Gladue, D.P.; Holinka, L.G.; Arzt, J.; Bishop, E.; Smoliga, G.; Pauszek, S.J.; Bracht, A.J.; O'Donnell, V.; Fernandez-Sainz, I.; et al. A partial deletion in non-structural protein 3A can attenuate foot-and-mouth disease virus in cattle. *Virology* **2013**, *446*, 260–267. [[CrossRef](#)]
27. Yang, W.; Li, D.; Ru, Y.; Bai, J.; Ren, J.; Zhang, J.; Li, L.; Liu, X.; Zheng, H. Foot-and-Mouth Disease Virus 3A Protein Causes Upregulation of Autophagy-Related Protein LRRC25 To Inhibit the G3BP1-Mediated RIG-Like Helicase-Signaling Pathway. *J. Virol.* **2020**, *94*, e02086-19. [[CrossRef](#)]

28. Fu, S.Z.; Yang, W.P.; Ru, Y.; Zhang, K.S.; Wang, Y.; Liu, X.T.; Li, D.; Zheng, H.X. DDX56 cooperates with FMDV 3A to enhance FMDV replication by inhibiting the phosphorylation of IRF3. *Cell Signal.* **2019**, *64*, 109393. [CrossRef]
29. Lawrence, P.; Rieder, E. Identification of RNA helicase A as a new host factor in the replication cycle of foot-and-mouth disease virus. *J. Virol.* **2009**, *83*, 11356–11366. [CrossRef]
30. Ma, X.; Ling, Y.; Li, P.; Sun, P.; Cao, Y.; Bai, X.; Li, K.; Fu, Y.; Zhang, J.; Li, D.; et al. Cellular Vimentin Interacts with Foot-and-Mouth Disease Virus Nonstructural Protein 3A and Negatively Modulates Viral Replication. *J. Virol.* **2020**, *94*, e00273–20. [CrossRef]
31. Gladue, D.P.; O'Donnell, V.; Baker-Bransetter, R.; Pacheco, J.M.; Holinka, L.G.; Arzt, J.; Pauszek, S.; Fernandez-Sainz, I.; Fletcher, P.; Brocchi, E.; et al. Interaction of foot-and-mouth disease virus nonstructural protein 3A with host protein DCTN3 is important for viral virulence in cattle. *J. Virol.* **2014**, *88*, 2737–2747. [CrossRef] [PubMed]
32. Zanetti, G.; Pahuja, K.B.; Studer, S.; Shim, S.; Schekman, R. COPII and the regulation of protein sorting in mammals. *Nat. Cell Biol.* **2011**, *14*, 20–28. [CrossRef] [PubMed]
33. Gurkan, C.; Stagg, S.M.; Lapointe, P.; Balch, W.E. The COPII cage: Unifying principles of vesicle coat assembly. *Nat. Rev. Mol. Cell Biol.* **2006**, *7*, 727–738. [CrossRef] [PubMed]
34. Lam, S.S.; Martell, J.D.; Kamer, K.J.; Deerinck, T.J.; Ellisman, M.H.; Mootha, V.K.; Ting, A.Y. Directed evolution of APEX2 for electron microscopy and proximity labeling. *Nat. Methods* **2015**, *12*, 51–54. [CrossRef]
35. Lee, H.W.; Deng, M.C.; Pan, C.H.; Chang, H.W.; Cheng, I.C. Neutralizing monoclonal antibodies against porcine foot-and-mouth disease virus mapped to antigenic site 2 by utilizing novel mutagenic virus-like particles to detect the antigenic change. *Vet. Microbiol.* **2018**, *222*, 124–131. [CrossRef] [PubMed]
36. Jiang, Y.F.; Lin, H.L.; Fu, C.Y. 3D Mitochondrial Ultrastructure of Drosophila Indirect Flight Muscle Revealed by Serial-section Electron Tomography. *J. Vis. Exp.* **2017**, *130*, 56567. [CrossRef]
37. Fuerst, T.R.; Niles, E.G.; Studier, F.W.; Moss, B. Eukaryotic transient-expression system based on recombinant vaccinia virus that synthesizes bacteriophage T7 RNA polymerase. *Proc. Natl. Acad. Sci. USA* **1986**, *83*, 8122–8126. [CrossRef]
38. Choe, S.S.; Kirkegaard, K. Intracellular topology and epitope shielding of poliovirus 3A protein. *J. Virol.* **2004**, *78*, 5973–5982. [CrossRef]
39. Roderick, H.L.; Campbell, A.K.; Llewellyn, D.H. Nuclear localisation of calreticulin in vivo is enhanced by its interaction with glucocorticoid receptors. *FEBS Lett.* **1997**, *405*, 181–185. [CrossRef]
40. Tenorio, R.; Fernandez de Castro, I.; Knowlton, J.J.; Zamora, P.F.; Lee, C.H.; Mainou, B.A.; Dermody, T.S.; Risco, C. Reovirus sigmaNS and muNS Proteins Remodel the Endoplasmic Reticulum to Build Replication Neo-Organelles. *mBio* **2018**, *9*, e01253–18. [CrossRef]
41. Morosky, S.; Lennemann, N.J.; Coyne, C.B. BPIFB6 Regulates Secretory Pathway Trafficking and Enterovirus Replication. *J. Virol.* **2016**, *90*, 5098–5107. [CrossRef] [PubMed]
42. Delorme-Axford, E.; Morosky, S.; Bomberger, J.; Stolz, D.B.; Jackson, W.T.; Coyne, C.B. BPIFB3 regulates autophagy and coxsackievirus B replication through a noncanonical pathway independent of the core initiation machinery. *mBio* **2014**, *5*, e02147. [CrossRef] [PubMed]
43. Ao, D.; Guo, H.C.; Sun, S.Q.; Sun, D.H.; Fung, T.S.; Wei, Y.Q.; Han, S.C.; Yao, X.P.; Cao, S.Z.; Liu, D.X.; et al. Viroporin Activity of the Foot-and-Mouth Disease Virus Non-Structural 2B Protein. *PLoS ONE* **2015**, *10*, e0125828. [CrossRef] [PubMed]
44. Ranjitha, H.B.; Ammanathan, V.; Guleria, N.; Hosamani, M.; Sreenivasa, B.P.; Dhanesh, V.V.; Santhoshkumar, R.; Sagar, B.K.C.; Mishra, B.P.; Singh, R.K.; et al. Foot-and-mouth disease virus induces PERK-mediated autophagy to suppress the antiviral interferon response. *J. Cell Sci.* **2020**, *134*, 240622. [CrossRef]
45. Wessels, E.; Duijsings, D.; Lanke, K.H.; Melchers, W.J.; Jackson, C.L.; van Kuppeveld, F.J. Molecular determinants of the interaction between coxsackievirus protein 3A and guanine nucleotide exchange factor GBF1. *J. Virol.* **2007**, *81*, 5238–5245. [CrossRef]
46. Yuan, L.; Kenny, S.J.; Hemmati, J.; Xu, K.; Schekman, R. TANGO1 and SEC12 are copackaged with procollagen I to facilitate the generation of large COPII carriers. *Proc. Natl. Acad. Sci. USA* **2018**, *115*, E12255–E12264. [CrossRef]
47. Aridor, M. COPII gets in shape: Lessons derived from morphological aspects of early secretion. *Traffic* **2018**, *19*, 823–839. [CrossRef]
48. Petrosyan, A.; Cheng, P.W.; Clemens, D.L.; Casey, C.A. Downregulation of the small GTPase SAR1A: A key event underlying alcohol-induced Golgi fragmentation in hepatocytes. *Sci. Rep.* **2015**, *5*, 17127. [CrossRef]
49. Giraud, C.G.; Maccioni, H.J. Endoplasmic reticulum export of glycosyltransferases depends on interaction of a cytoplasmic dibasic motif with Sar1. *Mol. Biol. Cell* **2003**, *14*, 3753–3766. [CrossRef]
50. Quintero, C.A.; Giraud, C.G.; Villarreal, M.; Montich, G.; Maccioni, H.J. Identification of a site in Sar1 involved in the interaction with the cytoplasmic tail of glycolipid glycosyltransferases. *J. Biol. Chem.* **2010**, *285*, 30340–30346. [CrossRef]
51. de Castro Martin, I.F.; Fournier, G.; Sachse, M.; Pizarro-Cerda, J.; Risco, C.; Naffakh, N. Influenza virus genome reaches the plasma membrane via a modified endoplasmic reticulum and Rab11-dependent vesicles. *Nat. Commun.* **2017**, *8*, 1396. [CrossRef] [PubMed]
52. Strating, J.R.; van Kuppeveld, F.J. Viral rewiring of cellular lipid metabolism to create membranous replication compartments. *Curr. Opin. Cell Biol.* **2017**, *47*, 24–33. [CrossRef] [PubMed]
53. Shulla, A.; Randall, G. (+) RNA virus replication compartments: A safe home for (most) viral replication. *Curr. Opin. Microbiol.* **2016**, *32*, 82–88. [CrossRef] [PubMed]
54. Fernandez de Castro, I.; Tenorio, R.; Ortega-Gonzalez, P.; Knowlton, J.J.; Zamora, P.F.; Lee, C.H.; Fernandez, J.J.; Dermody, T.S.; Risco, C. A modified lysosomal organelle mediates nonlytic egress of reovirus. *J. Cell Biol.* **2020**, *219*, e201910131. [CrossRef]
55. Belov, G.A.; Sztul, E. Rewiring of cellular membrane homeostasis by picornaviruses. *J. Virol.* **2014**, *88*, 9478–9489. [CrossRef]
56. Melville, D.; Gorur, A.; Schekman, R. Fatty-acid binding protein 5 modulates the SAR1 GTPase cycle and enhances budding of large COPII cargoes. *Mol. Biol. Cell* **2019**, *30*, 387–399. [CrossRef]

- 
57. Long, K.R.; Yamamoto, Y.; Baker, A.L.; Watkins, S.C.; Coyne, C.B.; Conway, J.F.; Aridor, M. Sar1 assembly regulates membrane constriction and ER export. *J. Cell Biol.* **2010**, *190*, 115–128. [[CrossRef](#)]
58. Wolk, B.; Buchele, B.; Moradpour, D.; Rice, C.M. A dynamic view of hepatitis C virus replication complexes. *J. Virol.* **2008**, *82*, 10519–10531. [[CrossRef](#)]
59. Ci, Y.; Liu, Z.Y.; Zhang, N.N.; Niu, Y.; Yang, Y.; Xu, C.; Yang, W.; Qin, C.F.; Shi, L. Zika NS1-induced ER remodeling is essential for viral replication. *J. Cell Biol.* **2020**, *219*, e201903062. [[CrossRef](#)]
60. Suhy, D.A.; Giddings, T.H., Jr.; Kirkegaard, K. Remodeling the endoplasmic reticulum by poliovirus infection and by individual viral proteins: An autophagy-like origin for virus-induced vesicles. *J. Virol.* **2000**, *74*, 8953–8965. [[CrossRef](#)]



Supplementary Information

Foot-and-mouth disease virus 3A hijacks Sar1 and Sec12 for ER remodeling in a COPII-independent manner

Heng-Wei Lee¹, Yi-Fan Jiang^{1,2}, Hui-Wen Chang^{1,2}, Ivan-Chen Cheng^{1* *}

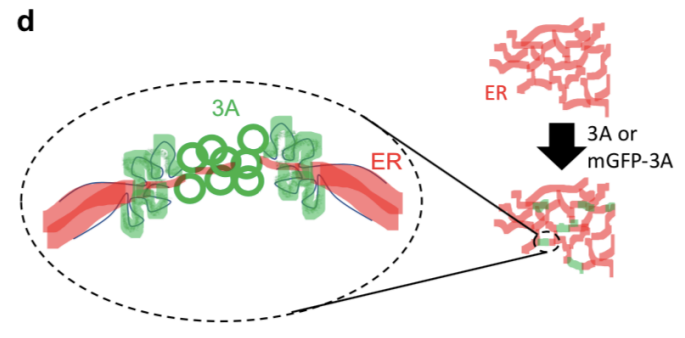
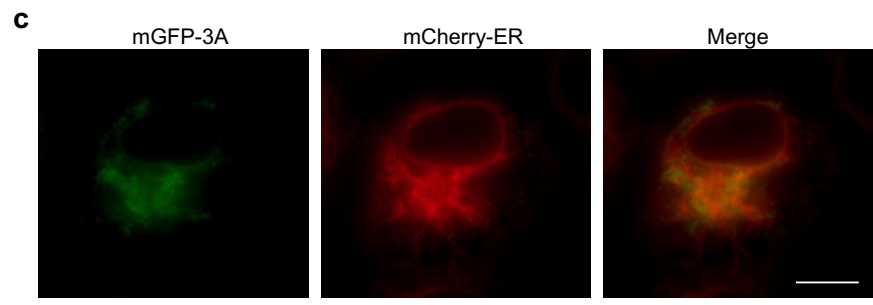
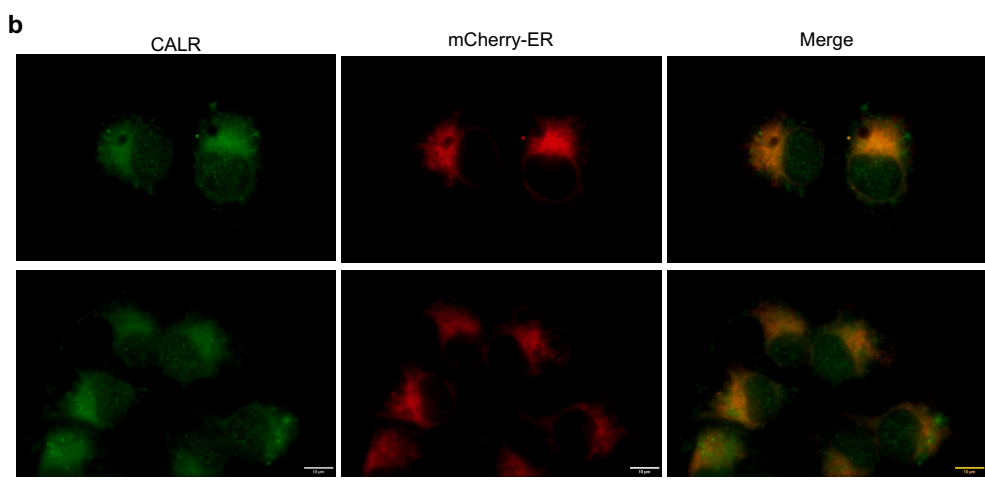
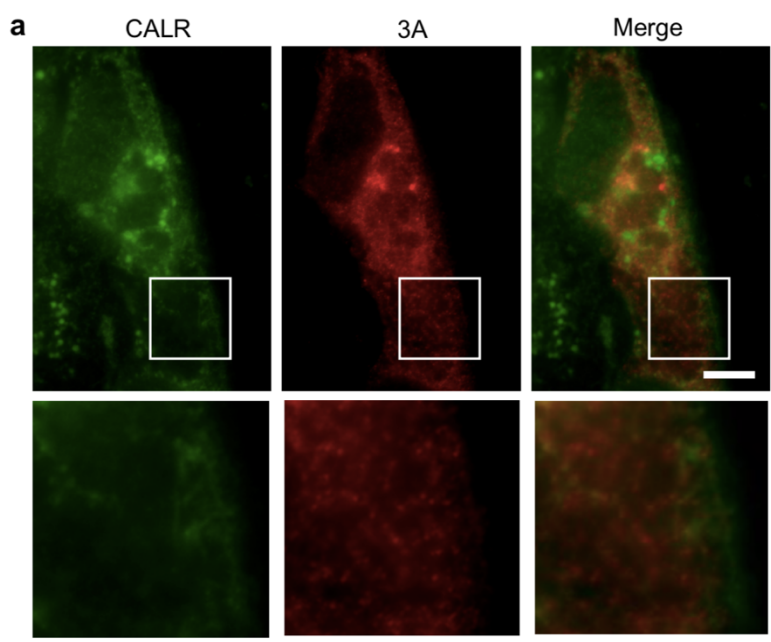
¹ *School of Veterinary Medicine, National Taiwan University, Taipei, 106, Taiwan*

² *Graduate Institute of Molecular and Comparative Pathobiology, School of Veterinary Medicine, National Taiwan University, Taipei, 106, Taiwan*

Correspondence: ivancheng@ntu.edu.tw (I.-C.C)

Supplementary Figures S1-S6

Supplementary Table S1



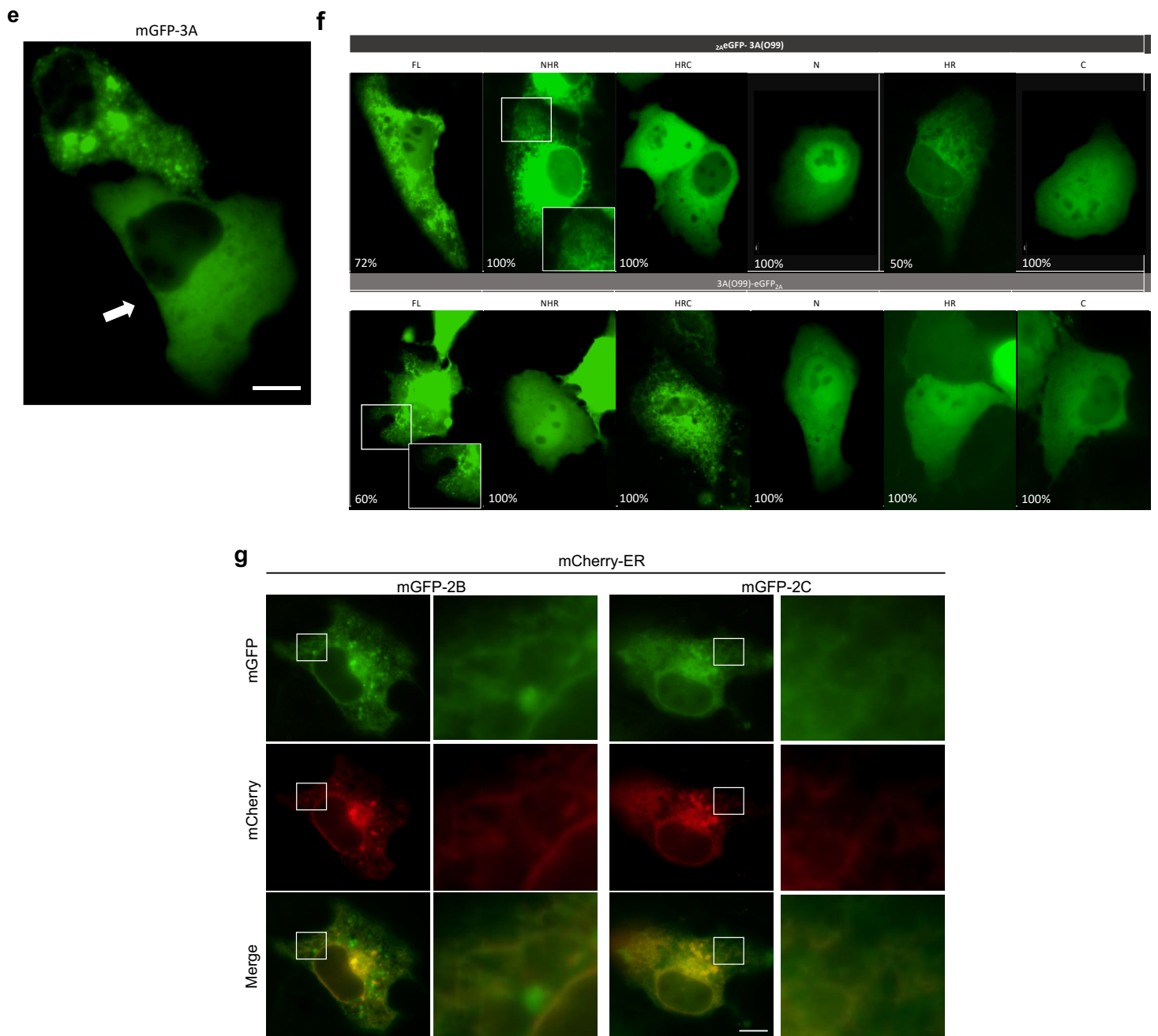


Figure S2. (a) Double immunofluorescence to 3A (red) and calreticulin (green) revealed with QA2 MAb and anti-calreticulin (CALR) rabbit antibody, followed by appropriate secondary antibodies (Alexa 594 conjugated anti-mouse antibody and FITC conjugated anti-rabbit antibody). (b) PK-15 cells expressing mCherry-ER were fixed and stained with anti-CALR rabbit antibody, followed by anti-rabbit antibody coupled with FITC. (c) After 3 hr post-transfection, PK-15 cells co-expressing mGFP-3A and mCherry-ER were examined by fluorescence microscopy. (d) The diagram depicts the modification of ER by 3A and the limitation of fluorescence microscopy. (e) PK-15 cells expressing mGFP-3A showed two different groups, diffuse-type (white arrow) and cells with multiple punctae. (f) The images from variant truncated 3A fused to eGFP. The N- or C-terminal eGFP was also fused to the 2A peptide of FMDV, which exhibited self-cleavage activity. It was originally designed for a cistronic co-expression system; however, we found that, if other protein genes that served 2A as linkage were added, the cleavage was not complete (data not shown).

Therefore, these plasmids were not used for further construction. However, mGFP-3A and $_{2A}eGFP$ -3A truncated versions showed identical results; we thought 2A peptide would not interfere with the localization of 3A. Similar to mGFP-3A, 72% and 60% of $_{2A}eGFP$ -3A and 3A- eGFP $_{2A}$ showed punctate patterns, respectively, while the others were diffuse-type. In addition, $_{2A}eGFP$ -NHR and HRC- eGFP $_{2A}$ both showed clear reticular patterns. Only 50% of $_{2A}eGFP$ -HR expressing cells appeared as reticular pattern; the others were diffuse. The other truncations distributed diffusely in the cytoplasm and nucleus. **(g)** PK-15 cells co-expressing mCherry-ER with mGFP-2B or mGFP-2C were examined for colocalization test. Scale bar, 10 μ m.

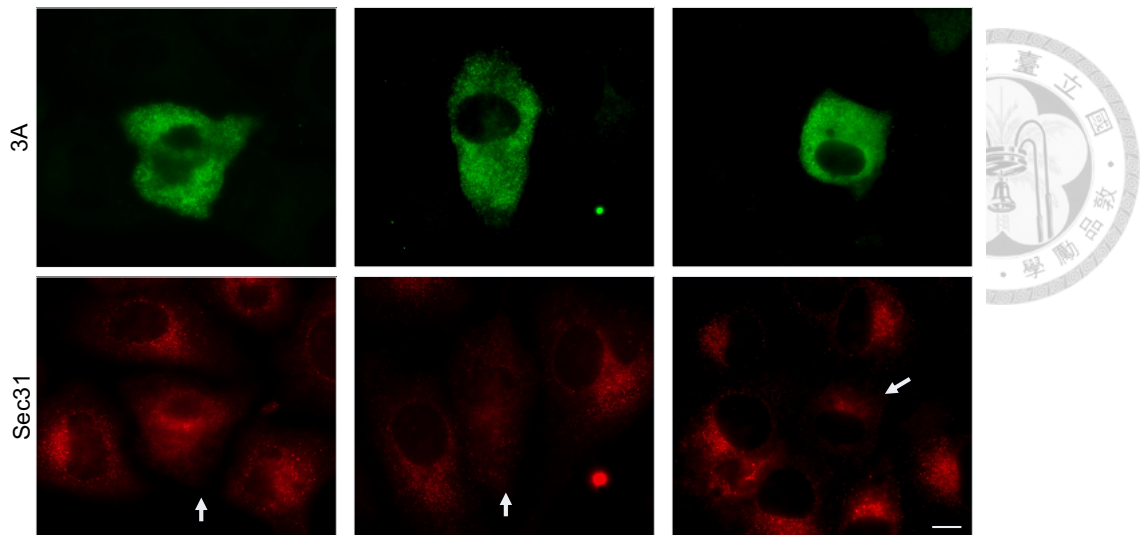


Figure S3. The transfected cells were stained with anti-Sec31A rabbit antibodies, followed by anti-rabbit secondary antibodies (red). Finally, 3A was identified with QA2-Dylight488 (green). The Sec31A signal in 3A-expressing cells (white arrows) was dispersed within the cytoplasm compared to non-transfected cells. Scale bar, 10 μm .

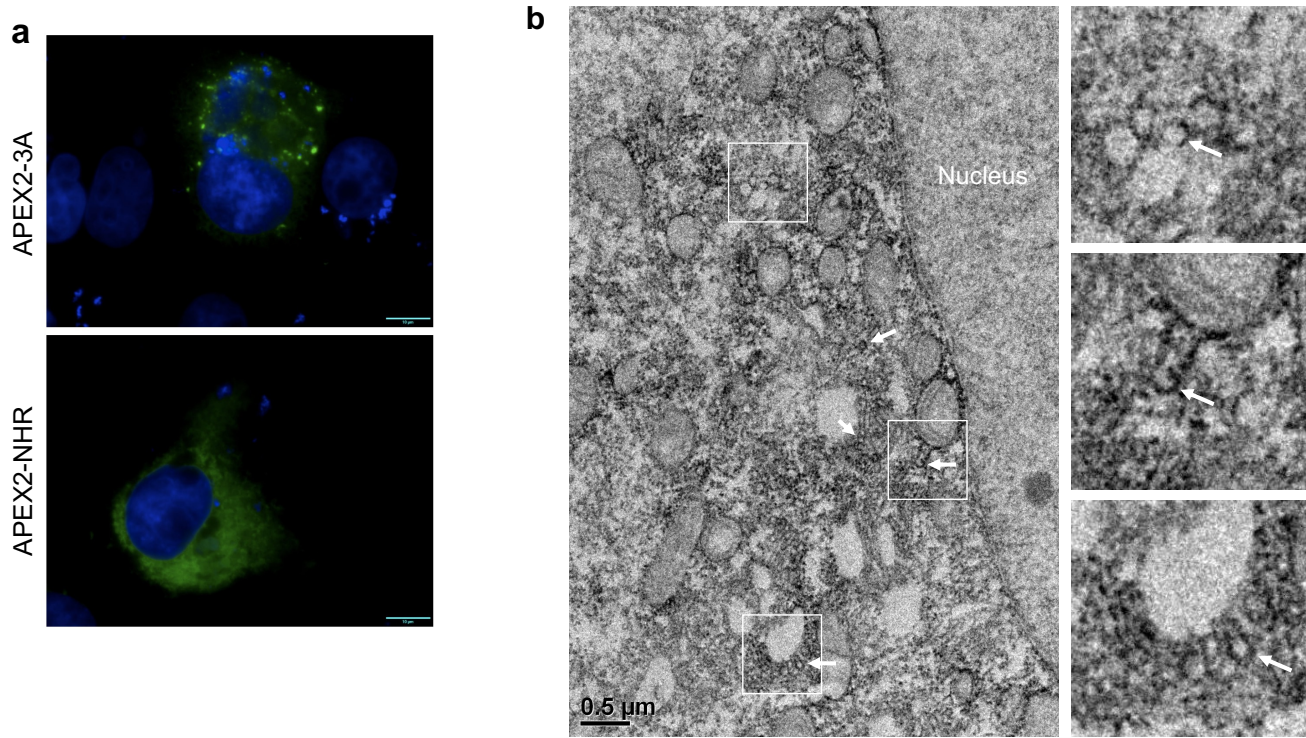


Figure S4. (a) The patterns of APEX2-3A and APEX2-NHR were examined under IFA by QA2 MAb. (b) The PK-15 cells' ultrastructure for expression of APEX2-N2HRC in TEM. The white arrows indicate modified structures around DAB reaction products.

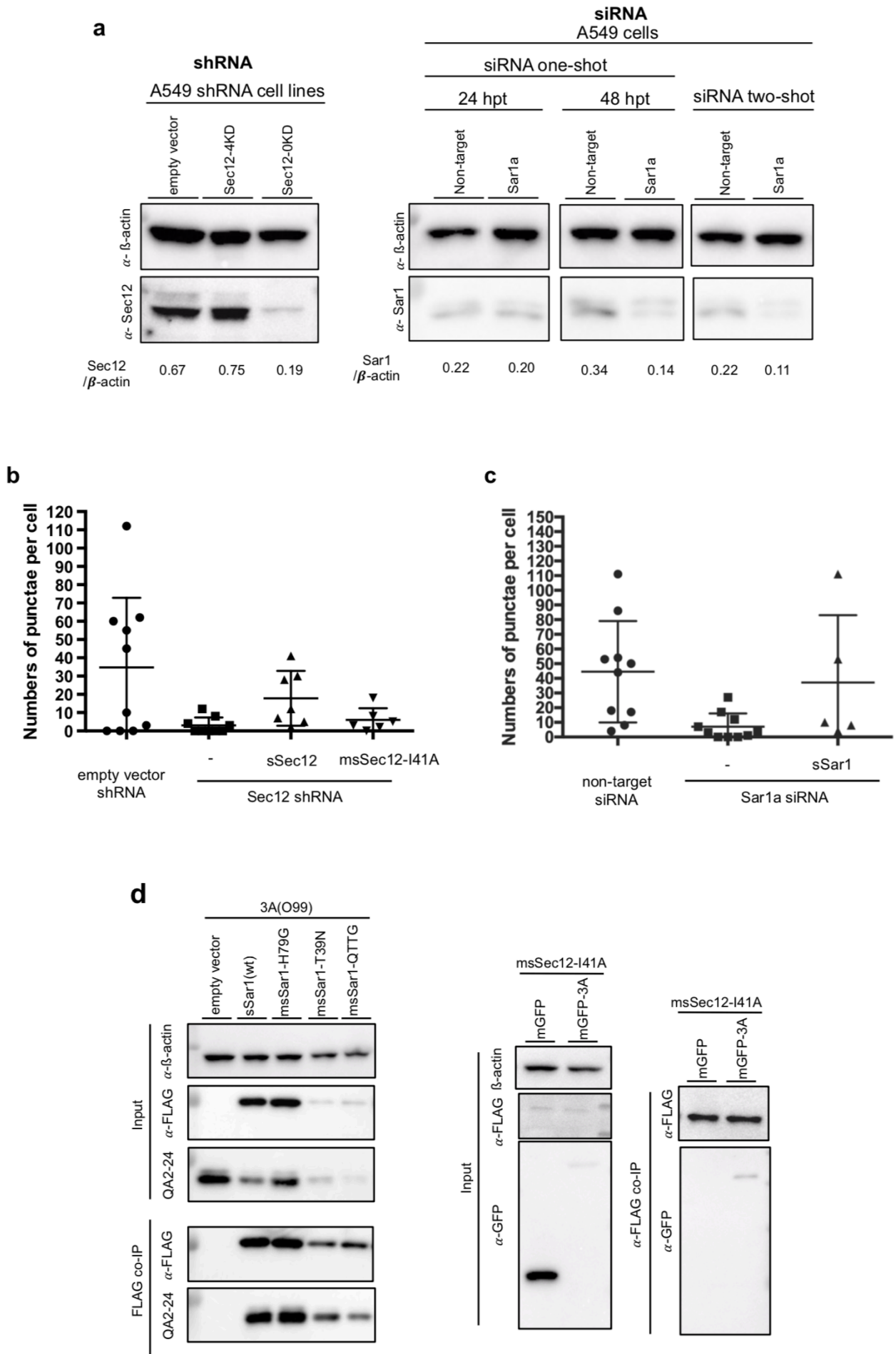


Figure S5. (a) For Sec12 knockdown, A549 cells were transfected with pLAS2w.Ppuro (empty vector), Sec12-4 (target sequence: GTGTGCTTCAACCACGATAAT) or Sec12-0 (target sequence: GCTGGCCTAAAGATGCAATAA), followed by puromycin selection for more than 2 weeks. The cell lysates were examined by western blotting. The Sec12 knockdown cell line was successfully established for Sec12-0 and named A0 cells. For Sar1 knockdown, due to failure to establish the shRNA cell line, siRNA (target sequence: CCAGTTCCTAGGACTCTACAA) was chosen as an alternative. After siRNA transfection for 24 hr or 48 hr, cell lysates were examined by western blotting. To elevate knockdown efficiency, we performed double transfection at a 24 hr interval. Cells were harvested at the next 24 hours (after the last transfection of siRNA), which was adopted for the following experiments. The band intensities for indicated proteins were quantified in ImageJ software and standardized by β -actin. (b, c) The numbers of punctae were quantified in different condition for knockdown and re-expression assay. (d) HTK cell lysates, co-expressing 3A and wild-type (or mutants) of sSar1, were applied to co-immunoprecipitation assay. All mutants of sSar1 preserved the ability to interact with 3A. Empty vector: pcDNA-3.1(+). Similarly, in PK-15 cell lysates, the I41A mutation of Sec12 would not abrogate the interaction with 3A, as proved by mGFP-3A.

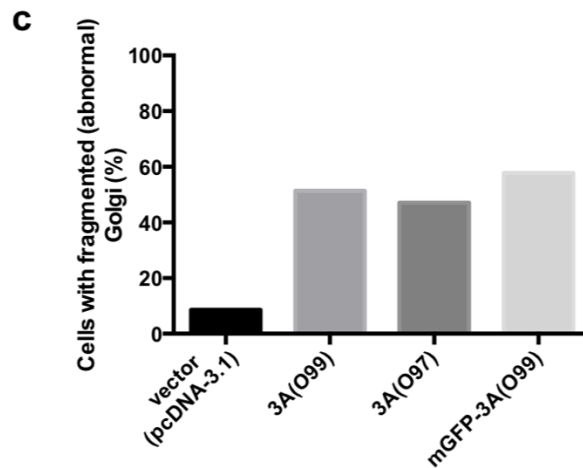
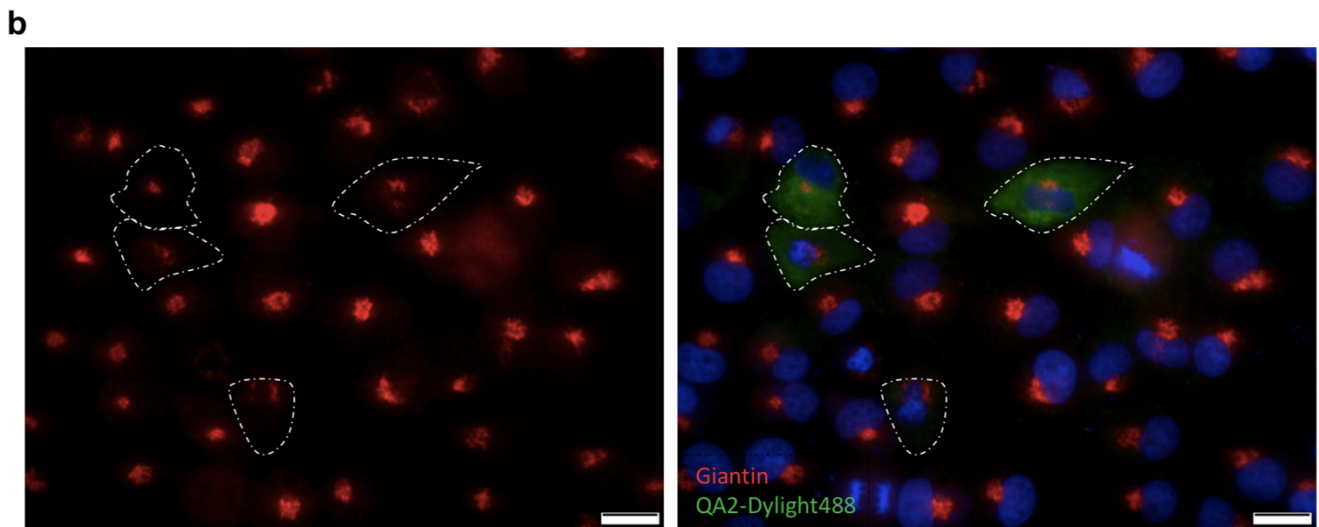
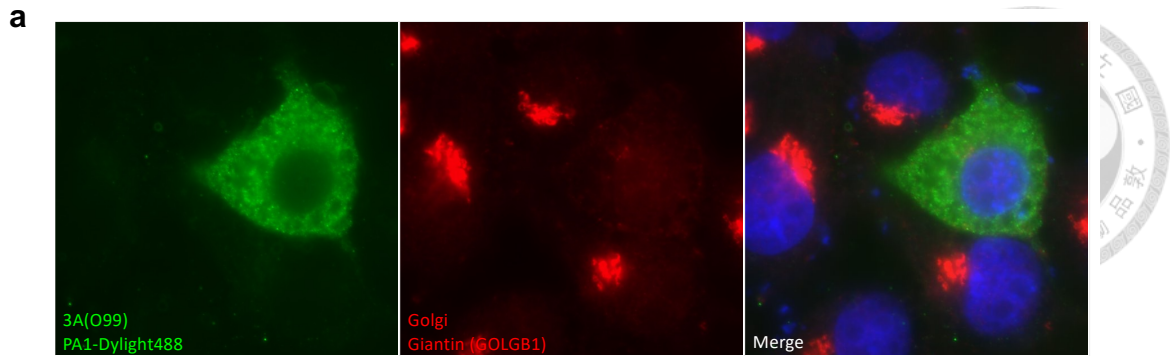
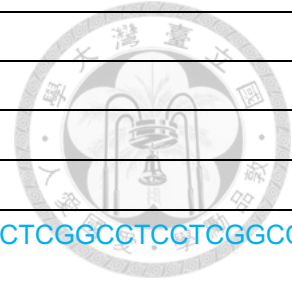


Figure S6. FMDV 3A expression resulted in the dispersal of the Golgi, shown by IFA. (a, b) The fixed PK-15 expressing 3A(O99) were subsequently incubated for anti-giantin rabbit antibodies, anti-rabbit antibodies-Alexa Fluor 594, and PA1-Dylight488 or QA2-Dylight488. Chromosomes were stained with Hoechst 33258. (c) PK-15 cells were transfected for 3A(O99), 3A(O97), and mGFP-3A(O99). Golgi integrity was examined in about 100 cells for each group, with mitotic cells excluded.

Supplementary Table S1. A list of cloning primers

Primer name	Sequence (5' to 3')
(mGFP-, eGFP- or GST-) HindIII-3A-XhoI (or XbaI)	
HindIII-3A(O99)-F	AAAAAGCTTGCCACCATGGCCATCTCAATTCCTTCCCAAAGG
XhoI-3A(O99)His-R	AACTCGAGTCAATGATGGTGGTGGTGGTGGTTCAGCTTGTGGTTGTTCTTC
HindIII-3A(O97)-F	AAAAAGCTTGCCACCATGGCCATTTCAATCCCTTCCCAGAAG
XhoI-3A(O97)His-R	AACTCGAGTCAATGATGGTGGTGGTGGTGGTTCAGCTCGCGGTTGTTC
XhoI-3A(O99)-R	AACTCGAGTCAATTCAGCTTGTGGTTGTTCTTC
HindIII-3A(O97)C-F	AAAAAGCTTGCCACCATGGCCCGCCAAGCGCGCAAG
XbaI-3A(O99)N-R	AATCTAGATTAGTTTTCTTCAGGCGC
HindIII-3A(O99)HR-F	AAAAAGCTTATGGCCTTTGAGATAGTTGCCCTGTG
XhoI-3A(O99)HR-R	AAACTCGAGTCAGATCATGATCACTATGTTTGCC
HindIII-3A(O99)C-F	AAAAAGCTTATGGCCCGCGAGACTCGCAAG
HindIII-3A(O99)a2-F	AAAAAGCTTGCCACCATGGCCATCCAGCAGACCTCATTG
XbaI-3A(O99)a1-R	TTTCTAGATTAGAGAGGCCGGAGCTCC
(APEX2) XhoI-3A-XbaI	
XhoI-3A(O99)-F	AACTCGAGATGGCCATCTCAATTCCTTCCCAAAGG
XbaI-3A(O99)-R	AATCTAGATTATTCAGCTTGTGGTTGTTCTTC
XbaI-3A(O99)HR-R	AATCTAGATTAGATCATGATCACTATGTTTGCC
XhoI-3A(O99)a2-F	AACTCGAGATGGCCATCCAGCAGACCTCATTG
XbaI-3A(O99)tC1-R	AATCTAGATTACTCGTTCATGATCATCC
NheI-3A-HindIII (-GFP or -GST)	
NheI-3A(O97)-F	AAAGCTAGCATGATTTCAATCCCTTCCCAGAAG
HindIII-3A(O97)-R	AAAAAGCTTTTCAGCTCGCGGTTGTTC
NheI-3A(O99)-F	AAAGCTAGCATGGCCATCTCAATTCCTTCCCAAAGG
HindIII-3A(O99)-R	AAAAAGCTTTTCAGCTTGTGGTTGTTCTTC
HindIII-3A(O99)N-R	AAAAAGCTTGTTTTCTTCAGGCGC
NheI-3A(O99)HR-F	AAAGCTAGCATGGCCTTTGAGATAGTTGCCCTGTG
HindIII-3A(O99)HR-R	AAAAAGCTTGATCATGATCACTATGTTTGCC
NheI-3A(O99)C-F	AAAGCTAGCATGGCCCGCGAGACTCGCAAG
HindIII-3A(O99)tC1-R	AAAAAGCTTCTCGTTCATGATCATCC
NheI-3A(O99)tC2-F	AAAGCTAGCATGGCCTACATTGAGAAGGCAAGCATC
HindIII-3A(O99)a1-R	AAAAAGCTTGAGAGGCCGGAGCTCC
NheI-3A(O99)a2-F	AAAGCTAGCATGGCCATCCAGCAGACCTCATTG
Vectors or others	
NheI-GFP-F	AAAGCTAGCATGGGCAGCAAGGGCGAGG
XhoI-HindIII-GFP-R	AACTCGAGTCAAAGCTTCTTGACAGCTCGTCCATG
NheI-BamHI-d1D-F	AAAGCTAGCGCCACCATGGGATCCACAAGCAGAGGATTGTGG
NheI-BamHI-d1D2A-F	AAAGCTAGCATGCTCGAGCACAAGCAGAGGATTGTGG
XhoI-d1D2A-R	TTTCTCGAGGGGCCAGGGTTGG



NheI-HindIII-GFP-F	AAAGCTAGCATGAAGCTTATGAGCAAGGGCGAGG
BamHI-GFP-R	AAAGGATCCCTTGTACAGCTCGTCCATG
NheI-GST-F	AAAGCTAGCATGGCCTCCCCTATACTAGGTTATTG
BamHI-HindIII-GST-R	AAGGATCCCTTAAGCTTTTTTGGAGGATGGTCCG
HindIII-GST-F	AAAAGCTTATGGCCTCCCCTATACTAGGTTATTG
XhoI-GST-R	AACTCGAGTTATTTTGGAGGATGGTCCG
NheI-CALR-mCherry-F	AAAGCTAGCATGGCCCTGCTATCCGTGCCGCTGCTGCTCGGCCCTCCGGCCTGGC CGTCGCCGAGATGGTGAGCAAGGGC
HindIII-KDEL-mCherry-R	AAAAGCTTTTACAGCTCGTCCCTTCTGTACAGCTCGTCC
BamHI-sSar1-F	TTGGATCCATGCTTTTCATCTTTGAGTGGATCTAC
2B or 2C	
NheI-FLAG-2B-F	AAAGCTAGCATGGATTACAAGGATGACGACGATAAGGGTACCCCTTCTTCTTCTCC GAC
EcoRI-stop-BamHI-2B-R	AAAGAATTCCTTAGGATCCCTGCTTTTCTGCTCTCTCG
NheI-FLAG-Kpnl-2C-F	AAAGCTAGCATGGATTACAAGGATGACGACGATAAGGGTACCCCTCAAAGCACGTGA CATCAAC
EcoRI-stop-BamHI-2C-R	AAAGAATTCCTTAGGATCCCTGTTTAAATATCAGGTGGCTCG
Mutagenesis	
O973A-dNheI-F	GGAGACGAGTGGCGCCAGCGCTGTCGGTTTC
O973A-dNheI-R	GAAACCGACAGCGCTGGCGCCACTCGTCTCC
msSar1-H79G-F	TTTGATCTCGGTGGGGGTGAGCAAGCACGTCCG
msSar1-H79G-R	CGACGTGCTTGCTCACCCCCACCGAGATCAAA
msSar1-T39N-F	ACAATGCAGGCAAAAACACTCTTTTACACAT
msSar1-T39N-R	ATGTGTAAGAGAGTGTTTTGCCTGCATTGT
msSar1-QTTG-F	TTTGGGCTTTATGGAGCCGCCGAGCAAAAGGGGAATGTGACC
msSar1-QTTG-R	GGTCACATTCCTTCTTGCTGCGGGGGCTCCATAAAGCCCAA
XhoI-msSar1-D198A-R	AACTCGAGTCAGGCAATATACTGGGAGAGCCAGC
sSec12-I41A-F	GCTGCCAAGACCGGTGCAAAGAACGGCGTGCAC
sSec12-I41A-R	GTGCACGCCGTTCTTTGCACCGGTCTTGGCAGC
m3A-49,50-F	CAGACCTCATTTGTGGCCCGCTTTTAAGCGCCT
m3A-49,50-R	AGGCGCTTAAAAGCGGCGGCACAAATGAGGTCTG
m3A-53,54-F	GTGAAGCGCGCTTTTGGCCCGCTGAAGGAAAATT
m3A-53,54-R	AAGTTTTCTTCAGGGCGGCAAAAGCGCGCTTAC
m3A-54,56-F	AAGCGCGCTTTAAGGCCCTGGCGGAAAATTGAGAT
m3A-54,56-R	ATCTCAAAGTTTTCCGCCAGGGCCTTAAAAGCGCGCTT
m3A-80,81,82-F	CATGATCCGCGAGACTGCCGCCGACAGCAGATGGTGGATG
m3A-80,81,82-R	CATCCACCATCTGCTGTGCGGGCGGAGTCTCGCGGATCATG
m3A-125,126,127-F	CACCACTGTTGGTTTTGCCGCCGCAACTCTCCCGGGACAC
m3A-125,126,127-R	GTGTCCCGGGAGAGTTGCGGGCGGCGAAACCAACAGTGGTG

Green: restriction site; Red: start codon or stop codon; Blue: tag or additional signal peptide; Yellow: mutation site

Chapter III



Dynamic Character of Foot-and-Mouth Disease

Virus 3A Vesicles

(Unpublished)

Dynamic Character of Foot-and-Mouth Disease Virus 3A Vesicles

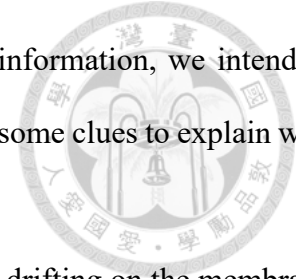


Abstract

DCTN3, a subunit of the motor protein complex, was found to interact with Foot-and-mouth disease virus (FMDV) 3A protein by Gladue and colleagues in 2014. However, the biological function has not been revealed, whether it aims to disrupt or utilize motor protein complexes. Our previous study proved that FMDV 3A would utilize COPII factors to modify the ER into vesicle-like structures. Therefore, it is tempting to investigate the state of motion for 3A vesicles. This study examined the interaction between 3A and DCTN3 in different virus strains and host species. We also found the dynamic movement of 3A, moving along microtubules. Nonetheless, we cannot further show the link between DCTN3 interaction and the dynamic character of 3A puncta and cannot tell whether dynein exerts the 3A movement. It demands a clear model for dynein function and a much more detailed examination. In short, we showed an interesting character of 3A puncta, a “dynamic movement”; however, the mechanism still requires further investigation.

1. Introduction

Several viruses utilize host trafficking for invading and releasing the virions, such that adenovirus moves toward the nucleus after penetration of the plasma membrane by binding dynein intermediate chain (IC) and light-intermediate chain 1 (LIC1) (Dodding and Way, 2011). However, it is elusive for some interactions between viral proteins and motor protein subunits. For instance, foot-and-mouth disease virus (FMDV) 3A protein was found to interact with DCTN3 from cattle, while the biological function remains enigmatic. The A89P mutation on 3A abrogates the interaction, and recombinant viruses harboring the mutation displayed a delayed disease for cattle. When the virus was reisolated from the experimentally infected cattle, the 89 aa of 3A was mutated back to alanine or leucine (Gladue et al., 2014). Coincidentally, the 89 amino acid position is proline in porciphilic

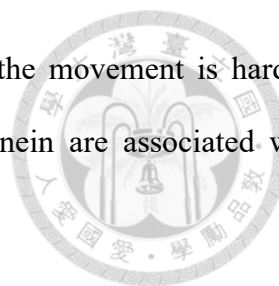


strain O/TAW/97 that hardly infects cattle (Dunn, 1997). Based on the information, we intend to study the biological function of the 3A-DCTN3 interaction, hoping to find some clues to explain why 3A of O/TAW/97 played an important role in host specificity.

FMDV 3A was a peripheral membrane protein on the ER, reportedly drifting on the membrane (Gonzalez-Magaldi et al., 2014). In our previous study, FMDV 3A protein modifies the ER into vesicle-like structures by interacting with COPII factors, Sar1 and Sec12. The specialized vesicles were neither COPII vesicles nor autophagosomes (Lee et al., 2022). We strongly suggested it was a premature structure of replication organelles. Under electron microscopy, in early infection (1.5-2 hours post-infection), FMDV ROs and fragmented rough endoplasmic reticulum (rER) accumulate in the perinuclear region. The intact apparatuses of the Golgi appear around the edge of that area. (Monaghan et al., 2004). All cytoplasmic organelles gathering beside the nucleus trigger our interest in whether FMDV RO would move, just like Hepatitis C virus replication complex (RC) compartment using NS5A-GFP as a marker (Wolk et al., 2008).

The vesicle trafficking within the cytoplasm depends on motor protein complexes, including dynein, kinesin, and myosin (Greber and Way, 2006). Dynein and kinesin drive on the microtubules in opposite directions. Dynein is responsible for minus end-directed transport, namely direction toward the microtubule organization center (MTOC), such as the transport from the ER toward the Golgi. Kinesin drives the vesicle for positive end-directed transport (Greber and Way, 2006). Generally speaking, dynein requires dynactin and adaptors for vesicular trafficking. For example, Bicaudal D2 (BICD2) as an adaptor binds dynactin and dynein for stabilization; meanwhile, connecting to Rab6 to pull Rab6-vesicles from the Golgi (Splinter et al., 2012). To our knowledge, the adaptors for COPII vesicles have not yet been revealed. Much research is demanded. Whether FMDV 3A proteins could play a role as RO adaptors might be worth considering.

Here, we first examine the interaction between FMDV 3A and DCTN3 in different virus strains and host species and reveal the dynamic character of mGFP-3A puncta. The movement depends on



microtubules, given that Nocodazole inhibits the movement. However, the movement is hard to record and quantify. We cannot claim that DCTN3 interaction and dynein are associated with movement. It requires further, more detailed examination.

2. Materials & Methods

2.1. Cells and reagents

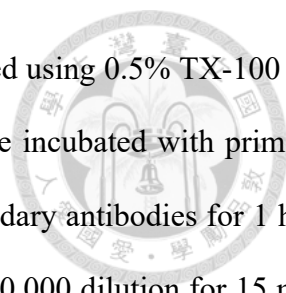
PK-15, human TK⁻ 143 (HTK⁻), Vero, BHK-21, A549, HEK293 cells were maintained in Dulbecco's modified Eagle medium (DMEM) with 10% FBS. Nocodazole (Sigma, M1404), HPI-4 (Sigma, H4541), and ML-7 (Sigma, I2774) were purchased. QA2-24 MAb against 3A was produced and characterized in a previous study (Lee et al., 2022). Commercial antibodies used in this study included anti-FLAG mouse antibody (Sigma, F1804), anti- β -actin (Cell Signaling Technology, #3700), anti-GFP (Invitrogen, MA5-15256), and anti-microtubule (Sigma, T6199). MT tracker (Invitrogen, T34077) and Alexa Fluor 594 Phalloidin (Invitrogen, A12381) were also used to visualize microtubule and actin in live cells.

2.2. Plasmids

The DCTN3 cDNA clones from swine and cattle were purchased from Origene (sDCTN3: XM_003130656; cDCTN3: NM_001075660). Both DCTN3 genes were inserted into pcDNA-3.1(+) with a FLAG tag at the C terminus. The 3A-associated constructs were generated in a previous study (Lee et al., 2022).

2.3. Immunofluorescence assay and confocal live microscopy

The protocol followed that of a previous study (Lee et al., 2022). PK-15 cells on a confocal μ -dish (ibidi, IB-81156) were transfected with the indicated plasmids for 24 h. Cells were fixed using



4% paraformaldehyde in PBS for 15 min at 37 °C and further permeabilized using 0.5% TX-100 for 5 min at RT. After being washed with PBS three times, the samples were incubated with primary antibodies for 2 h at 37 °C, followed by incubation with appropriate secondary antibodies for 1 h at 37 °C. The nucleus was stained with Hoechst (Invitrogen, H3569) at a 1:10,000 dilution for 15 min at 37 °C. All the imaging was performed under an Olympus IX-83 microscope connected to a CMOS (Complementary Metal Oxide Semiconductor) color camera at 37 °C for live cells.

2.4. Recombinant vaccinia expression system

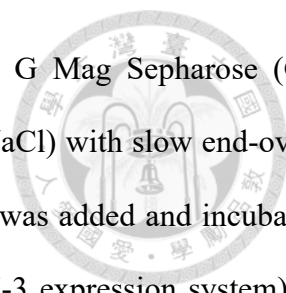
The protocol followed that of previous studies (Fuerst et al., 1986; Lee et al., 2022). HTK⁻ cells in 6-well plates were infected by vTF7-3 recombinant vaccinia virus for 1 h and transfected with plasmids containing T7 promoter using TurboFect (Thermo Scientific, R0531). After 20-24 h, cells were ruptured by freeze-thaw cycles 3 times in 500 µl PBS with protease inhibitor (Millipore, 539134). Finally, the cell debris was removed by 10,000 g centrifugation for 20 min.

2.5. Western blotting

The protocol followed that of a previous study (Lee et al., 2022). The samples were separated by 13.5% SDS-PAGE, transferred to a nitrocellulose membrane (PALL, 79548), and blocked using 5% (w/v) skim milk in PBST at room temperature (RT) for 30 min. The proteins on the membranes were detected using the indicated antibodies, with overnight incubation at 4 °C, and the corresponding horseradish peroxidase (HRP)- conjugated secondary antibodies (Abcam, ab131366; Abcam, ab131368) were used with incubation at RT for 1 h.

2.6. Co-immunoprecipitation Assay

The protocol followed that of a previous study (Lee et al., 2022). For each sample, 1 µg of anti-



FLAG antibody (Sigma, F1804) was incubated with 10 μ L of Protein G Mag Sepharose (GE Healthcare) in 500 μ L of binding buffer (50 mM Tris, pH 7.5, 150 mM NaCl) with slow end-over-end mixing for 1 h at RT. After removal of the binding buffer, a sample was added and incubated overnight at 4°C. The magnetic beads were washed with PBS (for vTF7-3 expression system) or RIPA (for PK-15 cells expression) three times. After replacing in with a clean Eppendorf tube, the bead was washed with PBS again. Finally, the sample was eluted with 20 μ L of 2% SDS and analyzed by Western blotting.

2.7. Cell viability

The procedure followed the manufacturer's instructions (Roche, No. 11465007001). PK-15 cells were grown in 96-well plates. For testing Nocodazole, cells were incubated in a 100 μ l medium with indicated drug concentration at 4°C for 2 h. For testing HPI-4 and ML-7, cells were incubated for 24 h. After incubation in the different conditions, the cells were added 10 μ l of MTT (3-(4,5-dimethyl-2-thiazolyl)-2,5-diphenyl tetrazolium bromide) for 4 h at 37°C. The solubilization solution (10% SDS, 10 mM HCl) was added and incubated overnight. The OD values at 550 nm and 690 nm were recorded. The cell viability was calculated with the following formula.

$$\text{Cell viability (\%)} = \frac{[A_{550} - A_{690}] \text{ of indicated condition}}{[A_{550} - A_{690}] \text{ of nontreatment}}$$

2.8. Nocodazole treatment

PK-15 cells on a confocal μ -dish (ibidi, IB-81156) were transfected with pcDNA-mGFP-3A(O99) for 1 day. Before Nocodazole treatment, cells were examined under fluorescent microscopy at 37 °C with the cells' position were recorded. After incubation with 50 μ M Nocodazole at 4°C for 1 h, the exact cells were examined at 37°C again. The mock group was incubated at 4 °C without other treatment and examined as mentioned above.



3. Results

3.1. The 3A-DCTN3 interactions were confirmed, showing differences between virus strains and species.

FMDV 3A from the O1C strain was proved to interact with cattle DCTN3 (cDCTN3) by two-yeast hybridization, mammalian two-hybrid systems, and colocalization test in FMDV infected cells (Gladue et al., 2014). To confirm the interaction, we co-express 3A from O/99 virus strain (O/99 3A) and DCTN3 from swine (sDCTN3) in PK-15 cells for the colocalization test (Fig. 1A). Furthermore, the two targets were expressed in vTF7-3 expression system for anti-FLAG co-immunoprecipitation. After pulling down recombinant DCTN3, O/99 3A showing in the elution proves the interaction. This interaction was independent of host species (cattle or swine) and virus strains (O/97 or O/99). The results of O/97 3A binding cDCTN3 contradict those from yeast-two hybridization by Gladue and colleagues (Gladue et al., 2014).

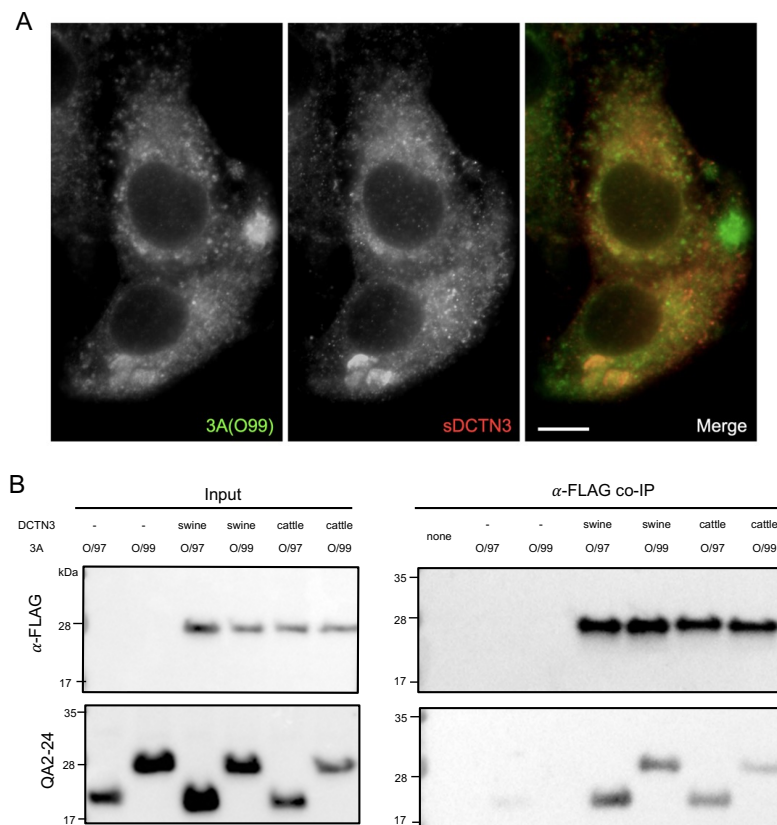


Figure 1. The interaction between 3A and DCTN3 in different virus strains and host species.

(A) PK-15 cells were co-transfected for 3A(O99) and sDCTN3 (s: swine). Double immunostaining was performed by anti-3A MAb (QA2) and rabbit anti-DCTN3 antibodies, followed by secondary antibodies. Bar: 10 μ m. (B) 3A and DCTN3 were co-expressed in the vTF7-3 expression system, and cell lysates were applied to anti-FLAG co-immunoprecipitation.

3.2. The HR and C regions of 3A bound to DCTN3.

For mapping out the binding sites on 3A for DCTN3, PK-15 cells co-expressed sDCTN3 with various truncated 3A fused with mGFP on N-terminus or eGFP_{2A} (2A: FMDV 2A peptide, 18 aa) on C-terminus. The results from the anti-FLAG pulldown assay showed that the regions of 3A contacting DCTN3 range from HR (hydrophobic region) to the C terminus. The GFP-C showed less association with sDCTN3 than C-eGFP_{2A}, possibly because GFP fusion protein interfered with the nearby structure of the C region. Collectively, the central contact site on 3A should locate at the C terminus

(aa 77-153) near HR (aa 59-76). The supposition accords that amino aa 89 of 3A is critical for DCTN3 interaction (Gladue et al., 2014). Moreover, our results indicated that the hydrophobic region (HR) also contributes to the interaction.

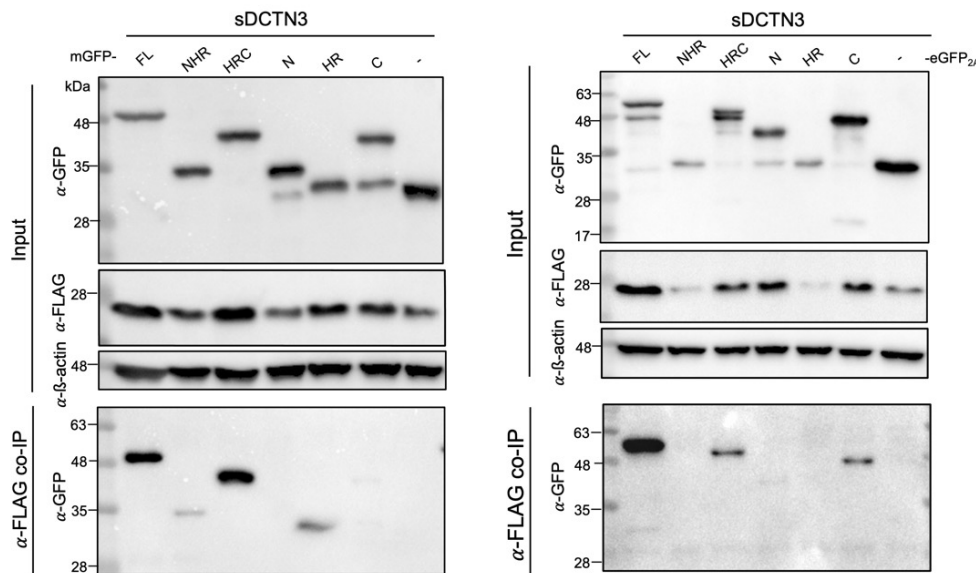
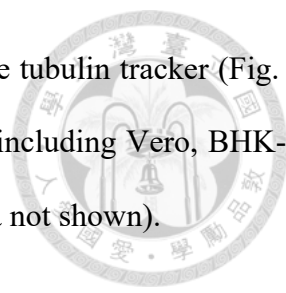


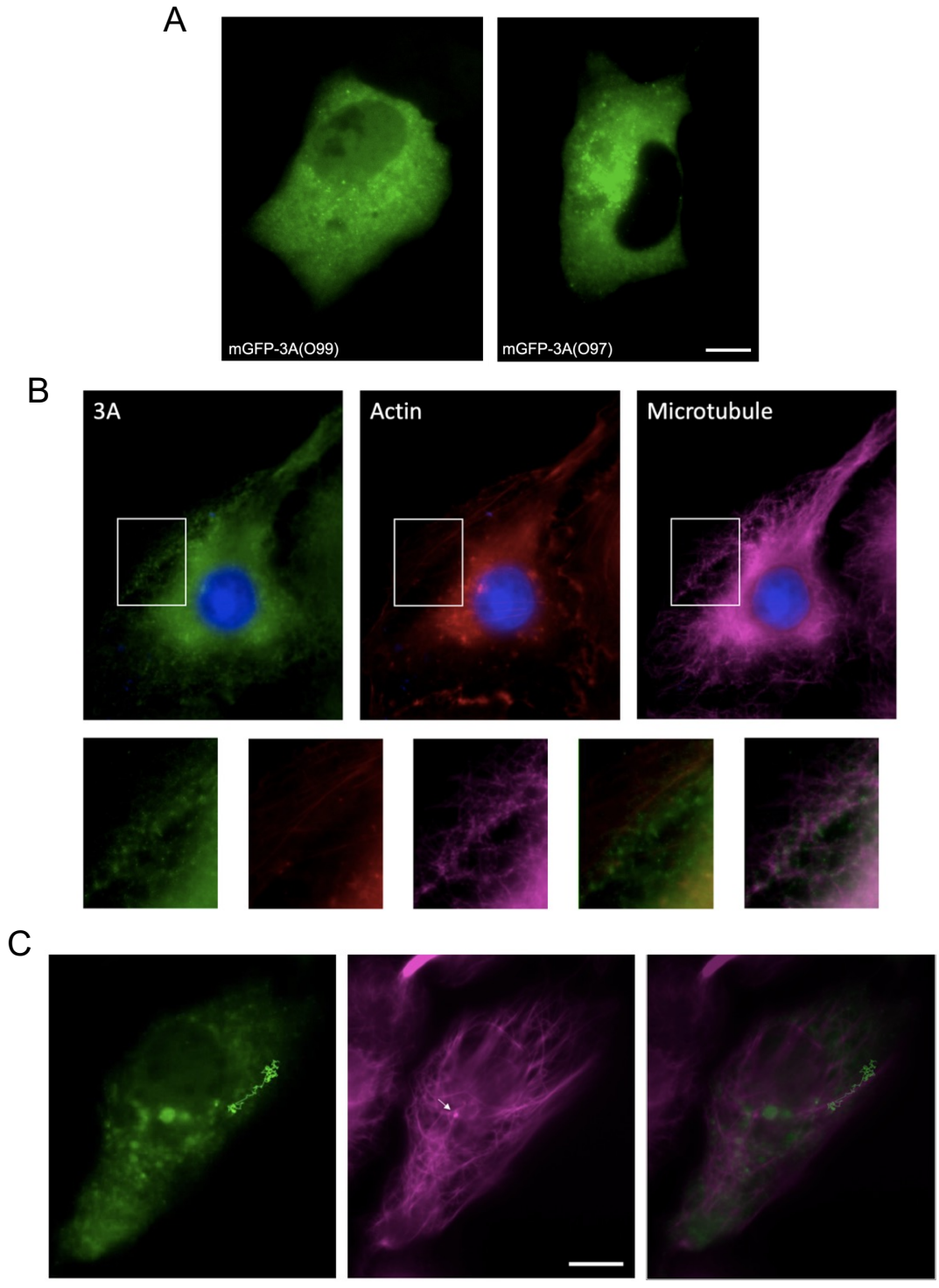
Figure 2. Examining binding domains on 3A by anti-FLAG co-immunoprecipitation and variant 3A truncation. Truncated 3A with N-terminal fusion protein, mGFP, were co-expressed with sDCTN3 in PK-15 cells. The cell lysates were applied to anti-FLAG co-IP assay. Truncated 3A with C-terminal fusion, eGFP_{2A}, were performed in the same procedure.

3.3. Highly dynamic 3A puncta moved along microtubules.

Given the association with DCTN3, it was tempting to see whether 3A within the cells could move. Therefore, PK-15 cells expressing mGFP-3A were examined under live fluorescent microscopy. Although about 30-40% of cells showed diffuse type, as in our previous study (Lee et al., 2022), we focused on the others showing reticular patterns with puncta (Fig. 3A). Most larger puncta were static. In contrast, the tiny puncta were highly dynamic (Video 1). In triple staining, 3A puncta were much more associated with microtubule than actin in fixed 3A-expressing cells (Fig. 3B).



In live cells, mGFP-3A puncta moved along microtubule, identified by the tubulin tracker (Fig. 3C and Video 2). The dynamic puncta would also appear in other line cells, including Vero, BHK-21, HEK293, and A549 cells, although most puncta would be more static (data not shown).



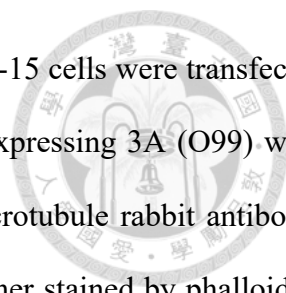


Figure 3. The dynamic FMDV 3A puncta on the microtubules. (A) PK-15 cells were transfected for mGFP-3A(O99) (left) and mGFP-3A(O97) (right). (B) PK-15 cells expressing 3A (O99) were fixed, followed by triple staining. Microtubules were stained by anti-microtubule rabbit antibody, followed by anti-mouse conjugated with Alexa Flour 647. Actin was further stained by phalloidin-Alexa Flour 594. Finally, 3A was identified QA2-Dylight 488. (C) The tracking line of 3A puncta in live PK-15 cell expressing mGFP-3A. The cellular microtubule structure was visualized with Tubulin Tracker™ Deep Red (Docetaxel-Deep Red). Bars: 10 μ m.

3.4. The dynamic character was inhibited in Nocodazole treatment.

Further, 50 μ M Nocodazole was used to depolarize microtubules for 1 hr at 4°C. As expected, there was no difference for dynamic 3A puncta before and after 4°C incubation without Nocodazole (Fig. 4D; Video 3). For the group with Nocodazole, mGFP puncta significantly became static (Fig. 4D; Video 4) and formed large aggregations (Fig. 4D; Video 5); both were typical evidence for microtubule-dependent movement. Next, we presumed that dynein/dynactin drives the dynamic 3A puncta. However, after the treatment of the dynein inhibitor (100 μ M HPI-4, even overnight), there was no significant blockage of 3A puncta movement (data not shown). It was the same for the myosin inhibitor (7.5 μ M ML-7 overnight) (data not shown).

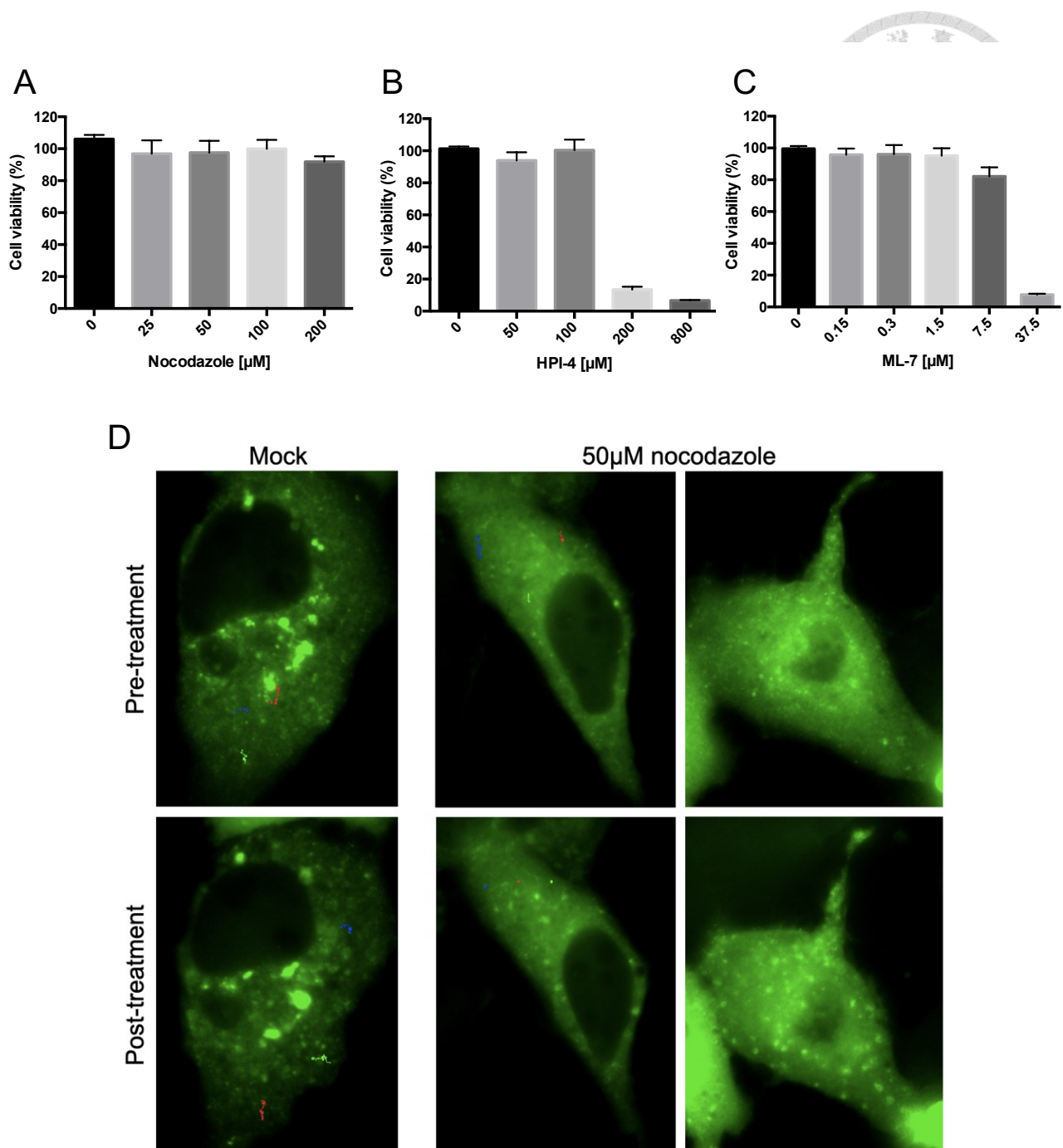
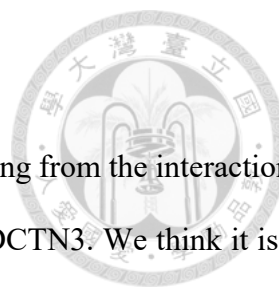


Figure 4. Nocodazole inhibition assay. (A, B, C) MTT assay was performed for microtubule depolymerizer (Nocodazole), dynein inhibitor (HPI-4), and myosin inhibitor (ML-7). (D) PK-15 cells expressing mGFP-3A were examined before 50 μM Nocodazole treatment and after treatment. The mock group was incubated at 1 hr at 4°C as treatment groups. Red, green, and blue lines represent the tracking lines for three mGFP-3A puncta within around 10 seconds.



4. Discussion

Our initial attempt is to answer the host specificity of O/TAW/97, starting from the interaction of 3A and DCTN3. According to the reference, O/97 3A cannot bind cattle DCTN3. We think it is the crucial point if O/97 3A can interact with swine DCTN3. However, although we confirmed the interaction between FMDV 3A and DCTN3, we unexpectedly found that O/97 3A could bind DCTN3 from cattle in our anti-FLAG co-immunoprecipitation assay. Besides, regardless of whether O/99 or O/97, 3A disrupted the ER and formed dynamic puncta. The mechanism for the movement should depend on microtubule because puncta are situated at and moved on microtubule. Unfortunately, we cannot show further evidence to prove the association with dynein/dynactin.

To enforce and examine the DCTN3 interaction, we also tried the mammalian-two hybrid (M2H) system and proximal ligation assay (PLA). These two methods were conducted by commercial kits (Promega, CheckMate™; Sigma, Duolink™). However, in the M2H system, 3A fused with GAL4 or VP16 cannot transport into the nucleus even with nuclear localization sequence (NLS). Actually, mGFP alone would also transport into the nucleus, whereas, when fusing to 3A, it would be restricted on the ER failed to be translocated. In M2H, it can expect that no signal was detected even for examining the dimerization of FMDV 3A. For PLA, the signals were prone to be affected by the concentration of antibodies. Therefore, these two methods were not shown in this study.

In conclusion, we confirmed FMDV 3A-DCTN3 interaction and showed that 3A puncta were dynamic within the cells. The movement depends on microtubule. These characteristics exist in O/99, typical virus strain, and O/97. However, we cannot find the difference in interactions of DCTN3 and 3A between O/99 and O/97 strains, and we cannot explain the possible biological function of this interaction. It is a long way to go to understand the mechanism of cattle avirulence for O/97.

5. Supplementary data

Video 1: <https://www.youtube.com/watch?v=UQ95QJQuZ4o>;



Video 2: <https://www.youtube.com/watch?v=5YSqTpCpY7Q>;

Video 3: <https://www.youtube.com/watch?v=xG1jldXCroo>

Video 4: <https://www.youtube.com/watch?v=WwH3XJRnVDE>

Video 5: <https://www.youtube.com/watch?v=hrunQoufTUQ>

References

- Dodding, M.P., Way, M., 2011. Coupling viruses to dynein and kinesin-1. *EMBO J* 30, 3527-3539.
- Dunn, C.S., and A. I. Donaldson, 1997. Natural adaptation to pigs of a Taiwanese isolate of foot-and-mouth disease virus. *Vet. Rec* 141:174-175.
- Fuerst, T.R., Niles, E.G., Studier, F.W., Moss, B., 1986. Eukaryotic transient-expression system based on recombinant vaccinia virus that synthesizes bacteriophage T7 RNA polymerase. *Proc Natl Acad Sci U S A* 83, 8122-8126.
- Gladue, D.P., O'Donnell, V., Baker-Bransetter, R., Pacheco, J.M., Holinka, L.G., Arzt, J., Pauszek, S., Fernandez-Sainz, I., Fletcher, P., Brocchi, E., Lu, Z., Rodriguez, L.L., Borca, M.V., 2014. Interaction of foot-and-mouth disease virus nonstructural protein 3A with host protein DCTN3 is important for viral virulence in cattle. *J Virol* 88, 2737-2747.
- Gonzalez-Magaldi, M., Martin-Acebes, M.A., Kremer, L., Sobrino, F., 2014. Membrane topology and cellular dynamics of foot-and-mouth disease virus 3A protein. *PLoS One* 9, e106685.
- Greber, U.F., Way, M., 2006. A superhighway to virus infection. *Cell* 124, 741-754.
- Lee, H.W., Jiang, Y.F., Chang, H.W., Cheng, I.C., 2022. Foot-and-Mouth Disease Virus 3A Hijacks Sar1 and Sec12 for ER Remodeling in a COPII-Independent Manner. *Viruses* 14.
- Monaghan, P., Cook, H., Jackson, T., Ryan, M., Wileman, T., 2004. The ultrastructure of the developing replication site in foot-and-mouth disease virus-infected BHK-38 cells. *J Gen Virol* 85, 933-946.
- Splinter, D., Razafsky, D.S., Schlager, M.A., Serra-Marques, A., Grigoriev, I., Demmers, J., Keijzer,

N., Jiang, K., Poser, I., Hyman, A.A., Hoogenraad, C.C., King, S.J., Akhmanova, A., 2012. BICD2, dynactin, and LIS1 cooperate in regulating dynein recruitment to cellular structures. *Mol Biol Cell* 23, 4226-4241.

Wolk, B., Buchele, B., Moradpour, D., Rice, C.M., 2008. A dynamic view of hepatitis C virus replication complexes. *J Virol* 82, 10519-10531.

Chapter IV



Neutralizing monoclonal antibodies against porcineophilic foot-and-mouth disease virus mapped to antigenic site 2 by utilizing novel mutagenic virus-like particles to detect the antigenic change

Reprint from Veterinary Microbiology, Vol. 222, Author(s): Heng-Wei Lee, Ming-Chung Deng, Chu-Hsiang Pan, Hui-Wen Chang, Ivan-Chen Cheng, Title of article: Neutralizing monoclonal antibodies against porcineophilic foot-and-mouth disease virus mapped to antigenic site 2 by utilizing novel mutagenic virus-like particles to detect the antigenic change, open access (2018) of Elsevier.



Neutralizing monoclonal antibodies against porcine foot-and-mouth disease virus mapped to antigenic site 2 by utilizing novel mutagenic virus-like particles to detect the antigenic change

Heng-Wei Lee^a, Ming-Chung Deng^c, Chu-Hsiang Pan^c, Hui-Wen Chang^{a,b}, Ivan-Chen Cheng^{a,*}

^a School of Veterinary Medicine, National Taiwan University, Taipei, Taiwan, ROC

^b Graduate Institute of Molecular and Comparative Pathobiology, School of Veterinary Medicine, National Taiwan University, Taipei, Taiwan, ROC

^c Animal Health Research Institute, Council of Agriculture, Tamsui, New Taipei City, Taiwan, ROC

ARTICLE INFO

Keywords:

Foot-and-mouth disease virus
Neutralizing
Mutagenic
Monoclonal antibody
Virus-Like particle

ABSTRACT

In the case of serotype O foot-and-mouth disease virus (FMDV), antibodies against five neutralizing sites play a pivotal role in protection of animals, with site 1 being considered the most crucial. However, recent studies indicated that the antibodies of vaccinated farm animals are mainly against site 2 rather than site 1. In Taiwan, blanket vaccination had been implemented for more than fifteen years, in which the porcineophilic isolate O/Penghu/2012 showed significant amino acid alterations in site 2 compared to the early isolate O/TW/97. To study the antigenicity of site 2, MABs against site 2 are required. In this study, we generated site 2 mutated virus-like particles (mVLPs) with only VP2-S72N mutation, and successfully identified five site 2 MABs from a previously prepared O/TW/97 MAB panel by immunofluorescence assay (IFA) and ELISA based on the different reactivity to wild-type VLP and mVLP. In conclusion, the established model was proved as an effective method to reveal the epitope that a MAB recognizes. By applying this MAB panel and sequence alignment, we demonstrated that the O/Penghu/2012 isolate not only showed significant genetic difference in site 2 but also significant antigenic difference from the ancestral O/TW/97.

1. Introduction

Foot-and-Mouth disease virus (FMDV) causes highly contagious disease in cloven-hoofed animals. There are seven distinct serotypes (O, A, C, Asia 1, SAT1, SAT2 and SAT3) of FMDV without cross-protection between individual serotypes. Due to increased restrictions for international trade and carrier animals as a response to FMD invasion, the control of FMD is an important and difficult issue in agricultural industries (Grubman and Baxt, 2004; Jamal and Belsham, 2013; Mason et al., 2003). In 1997, a devastating outbreak caused by porcineophilic O/TW/97 hit Taiwan, resulting in losses of about 378 million US dollars (Yang et al., 1999). To combat FMDV, blanket vaccination, surveillance, and stamping-out policy have been implemented with success until 2012, in which O/Penghu/2012 was discovered as the last porcineophilic virus from this series of FMD cases.

FMDV belongs to the genus *Aphthovirus* within the *Picornaviridae* family, and consists of a single-stranded positive sense RNA genome (8.5kb) with only one open reading frame (ORF). When the genome is translated within the cell, a precursor protein called P1-2A would be synthesized, myristoylated, and folded into an unprocessed protomer

(Mateu et al., 1998), which is then processed into subunit proteins (VP0, VP3 and VP1) by 3C protease (3C^{pro}). Then, processed protomers would self-assemble into pentamers, which form a virion with a viral genome inside. In the meantime, VP0 is cleaved into VP2 and VP4 at this stage (Grubman and Baxt, 2004). From an immunological standpoint, five neutralizing sites (site 1–5) on the surface of serotype O FMDV have been identified (Aktas and Samuel, 2000; Barnett et al., 1998; Crowther et al., 1993; Kitson et al., 1990; McCahon et al., 1989; Xie et al., 1987). Historically, site 1 has been regarded as the most important epitope because it flanks RGD motif, which lies on VP1 and can bind to integrin receptors of host cells, triggering virus entry. However, recently findings suggest that site 2 on VP2, as opposed to site 1, may be the most immuno-dominant epitope for vaccinated animals (Mahapatra et al., 2012). Meanwhile, antibody titers of vaccinated animals are consistently lower as determined by routine virus neutralization test (VNT) with O/Penghu/2012 than with O/TW/97 (data not shown), and subsequently, a large nucleotide deviation on site 2 critical residues between these two isolates (GenBank No. AY593835.1[O/TW/97], GenBank No. KX377689.1[O/Penghu/2012]) was found. Therefore, the antigenic change of the porcineophilic FMDVs

* Corresponding author at: School of Veterinary Medicine, National Taiwan University Taipei, Taiwan No 1, Sec 4, Roosevelt Road, Taipei 10617, Taiwan, ROC.
E-mail address: ivancheng@ntu.edu.tw (I.-C. Cheng).

<https://doi.org/10.1016/j.vetmic.2018.06.002>

Received 11 March 2018; Received in revised form 16 April 2018; Accepted 4 June 2018
0378-1135/ © 2018 Elsevier B.V. All rights reserved.

on site 2 during the continuous vaccination became one of the aims to be investigated. To study the antigenic changes of site 2, specific monoclonal antibodies (MAbs) against site 2 are indispensable. Thus, the focus of this study is to screen site 2 MAbs from a panel of MAbs against O/TW/97.

Generally, there are three well-known methods for mapping binding sites of neutralizing MAbs for FMDV, which includes peptide-based approach, escape mutant assays, and site-directed mutagenesis in infectious clone followed by VNT (Cheng et al., 2006; Grazioli et al., 2013; Wang et al., 2011; Yang et al., 2014). The first method can only be applied on mapping linear epitope; whereas except for site 1, other sites are conformational epitopes, including site 2. The other two methods are unpredictable and time-consuming, and also involve bio-safety concern of handling the live virus. Based on these considerations, a modified method involving the expression of recombinant proteins by site-direct mutagenesis was used. However, an initial trial of MAb screening by expressing VP2 as the only antigen failed. This may be a result of improper folding of VP2 without neighboring subunits, or the binding sites of antibodies exceeding the surface of VP2. Thus, a novel platform, “site-direct mutagenesis based on virus-like particles (VLPs)”, was employed. Since VLPs are most similar to complete virions without the virulence of the live virus, using VLPs could be an optimal method for this research.

It is well known that site 2 consists of residues at positions 70–73, 75, 77 and 131 of VP2. In the study done by Asfor (Asfor et al., 2014), VP2-72 was chosen as a representative from seven well-known critical residues of site 2 to generate an artificially mutated virus (5M) in which the binding of site 2 MAbs (Asfor et al., 2014) may not occur. Furthermore, O/Penghu/2012 also had a mutation at this residue. Thus, the single VP2-S72N residue would be a good candidate to mutate on site 2 of VLPs to screen out site 2 MAbs based on their inability to bind with site 2-mutated VLPs (mVLPs).

In order to successfully synthesize a FMD VLP, several previously published expression systems were reviewed, such as the use of mammalian cells, recombinant baculovirus, *E. coli* expression systems, and transgenic plants (Abrams et al., 1995; Bhat et al., 2013; Lee et al., 2009; Pan et al., 2008; Polacek et al., 2013; Puckette et al., 2017). In general, most studies co-express P1-2A polyproteins and 3C^{pro} within the cells. After the nascent P1-2A is processed by 3C^{pro}, subunit proteins would self-assemble into VLPs. However, the final yield of VLPs is limited due to the cytotoxicity effect of 3C^{pro} on eIF4G and eIF4A1, which are both important translation factors of eukaryotic cells (Belsham et al., 2000). Therefore, this study chooses mammalian cells for co-transfecting small volumes of 3C plasmids relative to P1 plasmids or mP1 (mutated P1) plasmids in transient expression assays based on Polacek's (Polacek et al., 2013) method. The expressed product was examined by sucrose gradient centrifugation accompanied by ELISA and transmission electron microscopy (TEM).

With the results characterized by IFA and ELISA based on VLPs and mVLPs, five site 2 MAbs were identified. Finally, all twenty-six MAbs in the panel were used to analyze the antigenicity of virus isolate O/Penghu/2012. In addition to sequence alignment, the antigenic changes of site 2 were validated. These results showed that this MAb panel was a practical tool for examining antigenic evolution of the porcophilic FMDV under sustaining vaccination pressure in the field.

2. Materials and methods

2.1. Viruses and cells

FMDV serotype O, isolate O/TW/97 was propagated in a baby hamster kidney cell line BHK-21 and was used as the viral target in indirect immunofluorescence assay (IFA) and virus neutralization test (VNT). Another isolate, O/Penghu/2012, was also propagated in BHK-21 for IFA. Human TK⁻ 143 (HTK⁻) cells were used for transient-expression assays (Fuerst et al., 1986). Cell lines were all cultured in

Dulbecco's Modified Eagle Medium (DMEM, Sigma) containing 10% Hyclone fetal calf serum.

2.2. Monoclonal antibodies

MAbs were prepared in previous study (Cheng et al., 2006). In brief, hybridoma from the splenocytes of live O/TW/97 immunized BALB/c mice and SP2/0-Ag14 myeloma cells were screened by IFA with acetone-fixed BHK-21 plates inoculated with O/TW/97. Positive hybridoma was cloned at least three times by limiting dilution method. Twenty-six out of more than 300 previously obtained MAbs were included in this study. The hybridoma culture supernatant was collected for subsequent characterization. Isotypes were analyzed by commercial ELISA (Southern Biotech, Birmingham, AL, USA). The MAb Q10E-3 generated by the hybridoma was inoculated intraperitoneally into BALB/c mice for ascetic fluid. The ascetic fluid was then purified, quantified, and conjugated with horseradish peroxidase (Lighting-Link™ HRP Conjugation Kit, Innova Biosciences, Cambridge, UK) to produce an ELISA tracer, MAb Q10E-HRP.

2.3. Virus neutralization test (VNT)

VNT was performed according to OIE manual (Donaldson et al., 1996). In brief, two-fold serial dilutions of MAb (culture supernatant) were reacted with 100 TCID₅₀ of O/TW/97 virus. After incubation for 1 h at 37 °C, BHK-21 was added and cultured at 37 °C for 2 days. The plates were examined under microscope, and antibody titers were expressed as the reciprocal of the highest antibody dilution that neutralized the virus at the 50% end point.

2.4. Construction of recombinant plasmids and mutant plasmid

Viral RNA of FMDV O/TW/97, prepared in Animal Health Research Institute in Taiwan, was reverse transcribed into a cDNA pool with oligo (dT)₁₈ primer (RevertAid First Strand cDNA Synthesis Kit, Thermo Scientific). The VP2, P1, and 3C genes were amplified with high-fidelity DNA polymerase (Thermo Scientific) and primers as shown in Table 1. The amplicons were purified from agarose gel and ligated to pJET-1.2/blunt (Thermo Scientific) by blunt-end ligation to generate the plasmids pJET-VP2, pJET-P1 and pJET-3C respectively. After transformation and extraction, these plasmids were all digested with *Xho*I and *Xba*I, which existed within pJET-1.2/blunt. Purified genes were then inserted into separate pcDNA-3.1(+) (Invitrogen, Carlsbad, CA, USA) downstream of a T7 promoter, resulting in the plasmids pcDNA-VP2, pcDNA-P1, and pcDNA-3C. In order to make a point mutation on site 2 (VP2-S72N), pcDNA-P1 was manipulated by site-direct mutagenesis with specific overlapping primers (S72N-VP2-F' and S72N-VP2-R') shown in Table 1 to obtain the plasmid pcDNA-mP1 according to the manufacturer's instruction (GeneTailor Site-Directed Mutagenesis System, Invitrogen, Carlsbad, CA, USA).

2.5. Transient-expression assays

Transient-expression assays were performed according to previous studies (Fuerst et al., 1986; Polacek et al., 2013). HTK⁻ cells with 90% confluence in 96-well or 6-well plates were infected with vTF7-3, a recombinant vaccinia virus that could express T7 RNA polymerase. After 1 h virus adsorption at 37 °C, the infected cells were then transfected with the indicated amount of plasmid DNA by using TurboFect Reagent (Thermo Scientific). After 20 h post-transfection, the cells were fixed by ice-cold 80% acetone for IFA or ruptured by freeze-thaw cycles for cell lysates. For the preparation of VLPs and mVLPs, cells were co-transfected with 100 ng/well pcDNA-P1, or pcDNA-mP1, and 2.5 ng/well pcDNA-3C in 96-well plates; with 4000 ng/well pcDNA-P1 or pcDNA-mP1, and 100 ng/well pcDNA-3C in 6-well plates. HTK transfected with 200 ng/well VP2 plasmids only or P1 plasmids only in 96-

Table 1

Primers used for amplification and site-directed mutagenesis. Start and stop codons are underlined. Double underlines shows the codon for mutation, and the nucleotide that have been changed is in bold face.

Name	The sequence of oligonucleotide (5'-3')	Orientation
VP2-F'	T <u>ATG</u> GACAAGAAGACGGAAGAAAC	Sense
VP2-R'	<u>TC</u> ACTCTTTAGAGGGGAGCTC	Antisense
P1-F'	T <u>ATG</u> GGCGCCGGGCAATCCAG	Sense
P1-R'	<u>TC</u> ACTGTTTTGCGGGTGCCACAATC	Antisense
3C-F'	T <u>ATG</u> AGTGGTGCGCCACCGAC	Sense
3C-R'	<u>TT</u> CACTCGTGGTGTGGTTCAGGGTC	Antisense
S72N-VP2-F'	CCTGTTTGACTGGGTCACCA <u>AT</u> GACCCGTTTG	Sense
S72N-VP2-R'	TGGTGACCCAGTCAAACAGGTGGGTTTTGA	Antisense

well plates were prepared for IFA.

2.6. Indirect immunofluorescence assays (IFA)

HTK⁻ cells in 96-well plates, which expressed antigen by transient-expression assay or BHK-21 infected with O/TW/97 (or O/Penghu/2012), were fixed by 80% acetone for 1 h at 4 °C. After washing with phosphate buffered saline (PBS, Bionovas) three times, 100 µL/well of hybridoma culture supernatant was added for 2 h at 37 °C. After washing three times, FITC-conjugated goat anti-mouse Igs (ICN Cappel, Costa Mesa, CA, USA) with a 1: 1000 dilution was added and kept in the dark for 1 h at room temperature. After washing, plates were observed and recorded under an Olympus IX-83 microscope connected to a CMOS color camera.

2.7. Sucrose gradient centrifugation

HTK⁻ cells in 6-well plates was infected by vTF7-3 and then co-transfected with P1 (or mP1) and 3C plasmids, or transfected with P1 (or mP1) plasmids only. After incubation for 20 h, the medium was replaced with 0.5 ml PBS. Cells were ruptured by two freeze-thaw cycles and cleared of cell debris by centrifugation at 10,000 g for 20 min. These semi-purified cell lysates with 1.5 ml were loaded onto a 15–45% (w/v) sucrose gradient of 3.2 ml and centrifuged at 268,000 g for 2.5 h at 4 °C (Beckman, Optima™ MAX-E Ultracentrifuge). Each fraction with 250 µL was collected from the top sequentially and examined by MAb Q10E-based sandwich ELISA described as follows.

2.8. Transmission electron microscopy

Carbon coated formvar grids were dropped with 8 µL samples, which came from fractions showing the highest peak in MAb Q10E-based sandwich ELISA. After 5 min at room temperature, excess sample was removed by blotting with filter paper. After 6 repetitions, grids were floated on a drop of 1% phosphotungstic acid (pH 6–8) for 30 s. The excess stain was removed as mentioned above. Specimens were examined and recorded on a JOEL JEM-1400 transmission electron microscope operated at an acceleration voltage of 150 kV.

2.9. ELISAs

2.9.1. MAb Q10E-based sandwich ELISA

ELISA plates were coated with 400 ng/well purified ascetic MAb

Q10E-3 in carbonate-bicarbonate buffer (pH 9.6) at 37 °C for 1 h. After washing with PBST (PBS with 0.05% Tween-20, pH 7.3) and blocking with 0.5% skim milk powder in PBST, 1 µL sample from each fraction of sucrose gradient centrifugation were diluted by 50 µL blocking buffer and incubated at 37 °C for 1 h. After washing three times, horseradish peroxidase-conjugated Q10E-3 (Q10E-HRP) was added for 1 h, followed by TMB substrate (BD OptEIA™, San Diego, CA, USA). The reaction was stopped with 1 N HCl and measured at 450 nm by Sunrise™ Absorbance Reader (TECAN, Switzerland).

2.9.2. MAb Q10E-based direct ELISA

Samples of 1 µL/well from each fraction of sucrose gradient centrifugation were directly coated in an ELISA plate. After blocking and washing, Q10E-HRP was added in the plate. Finally, the reaction was stopped and measured as above.

2.9.3. Indirect ELISA

Semi-purified cell lysates of 1 µL/well were coated in an ELISA plate. After blocking and washing, 100 µL of hybridoma culture supernatant was added. After washing, horseradish peroxidase-conjugated goat anti-mouse antibodies (Jackson ImmunoResearch Laboratories, Inc., PA, USA) with a 1:2,000 dilution were added. Substrate and stop solutions were added as described above. After recording with the reader, the relative binding percentage (RBP) for each MAb was calculated based on the formula: $R = (O.D._{mVLP} / O.D._{Neg}) / (O.D._{VLP} / O.D._{Neg}) \times 100\%$. Negative control shown in the formula corresponds to the plate coated with the cell lysate transfected by pcDNA-3.1(+).

3. Results and discussion

3.1. Preliminary characterization of MABs

Twenty-six MABs were included for characterization in this study. In a previous study, MAB Q10E-3 was confirmed as a site 1 MAB (Cheng et al., 2006). Hence, Q10E-3 was regarded as the control in the following study. The results of neutralizing activities and Isotyping of all MABs were shown in Table 2 and Supplementary Table 1. Seventeen MABs (culture supernatant) had viral neutralizing activities (Table 2). In order to identify site 2 MABs from these neutralizing MABs other than MAB Q10E-3, the following studies were performed.

Table 2
Characterization of MAbs against FMDV O/TW/97.

	Group	MAb	VNT titer ^a	IFA ^b				ELISA ^c	
				VP2	P1	P1+3C (VLP)	mP1+3C (mVLP)	O/12	RBP (%)
Neutralizing MAbs	Control Site 1	Q10E-3	≥512	-	+	+	+	+	102.4
	Group I Site 2 MAb	O4A-1	16	-	+	+	-	-	7.2
		P11A-15	32	-	+	+	-	-	2.7
		O4D-1	16	-	+	+	-	-	-2.7
		Q4D-8	4	-	+	+	-	-	6
		S11E-9	16	-	+	+	-	-	3.3
	Group II Site 2 MAb	P3F-3	32	-	+	+	+	-	63.4
		P2B-1	64	-	+	+	+	-	51.5
		P3B-3	32	-	+	+	+	-	55
		T7C-3	64	-	+	+	+	-	35.2
		T4F-7	32	-	+	+	+	-	26.6
	Group III MAbs against "processed" P1	S11B-20	256	-	-	+	+	+	93.7
		N3C-3	8	-	-	+	+	+	95.1
		N10E-1	32	-	-	+	+	+	95.2
		S10F-1	64	-	-	+	+	+	94.8
I9B-2		16	-	-	+	+	-	94.4	
M10B-9		≥512	-	-	+	+	+	95.9	
Non-neutralizing MAbs	MAbs against "processed" P1	S8B-1	-	-	-	+	+	+	93.7
		R3C-10	-	-	-	+	+	+	96.3
		O2G-1	-	-	-	+	+	-	94.4
	Group IV ^d	P9E-1	-	-	+	+	+	+	90.7
		S3G-1	-	-	+	+	+	+	93.3
		O3G-2	-	-	+	+	+	+	98.1
		S9F-9	-	-	+	+	+	+	95.2
		S3D-1	-	-	+	+	+	+	93.3
		T4C-3	-	-	+	+	+	+	95.3

Samples tested here were all hybridoma culture supernatant.
^aEnd-point neutralizing dilution; - no neutralizing activity, < 3.
^bMAbs were tested by IFA with corresponding antigen; + positive; - negative.
^cRelative binding percentage by indirect ELISA.
^dBinding site not identified yet.

3.2. Identification of site 2 MAbs by mutated site 2 mVLP

VP2, P1, and 3C genes were cloned as pcDNA-VP2, pcDNA-P1, and pcDNA-3C individually. Their sequences were consistent with NCBI (GenBank No. AY593835.1), except for one mismatch on VP2-S1381 in

pcDNA-VP2 and pcDNA-P1.

In the initial phase, all twenty-six MAbs showed negative signals on cells transfected with pcDNA-VP2 by IFA (Table 2). It is unlikely that none of these MAbs are against VP2 or site 2, which is an immune-dominant epitope. This unexpected result might be due to the improper

Table 3
Antigenicity of P1 polyprotein with different ratio of 3C^{pro}.

3C/P1 plasmids ratio	Q10E-3	S11B-20	N3C-3	N10E-1	S10F-1	I9B-2	M10B-9	S8B-1	R3C-10	O2G-1
1	++	++	+	+	++	+	++	+	++	++
1/2	++	++	++	++	++	++	++	++	++	+++
1/4	++	++	++	++	++	+++	++	++	++	+++
1/20	+++	+++	+++	+++	+++	+++	+++	+++	+++	+++
1/40	+++	+++	+++	+++	+++	+++	+++	+++	+++	+++
1/200	+++	+++	+++	+++	+++	+++	+++	+++	+++	+++
1/400	+++	++	++	+++	++	+++	+++	++	+++	++
1/2000	+++	++	+	++	++	++	++	++	++	++
1/4000	+++	+	+	+	+	++	+	+	+	++
1/20000	+++	-	+	+	+	+	-	+	+	+
1/40000	+++	-	+	-	-	+	-	-	-	-
0	+++	-	-	-	-	-	-	-	-	-

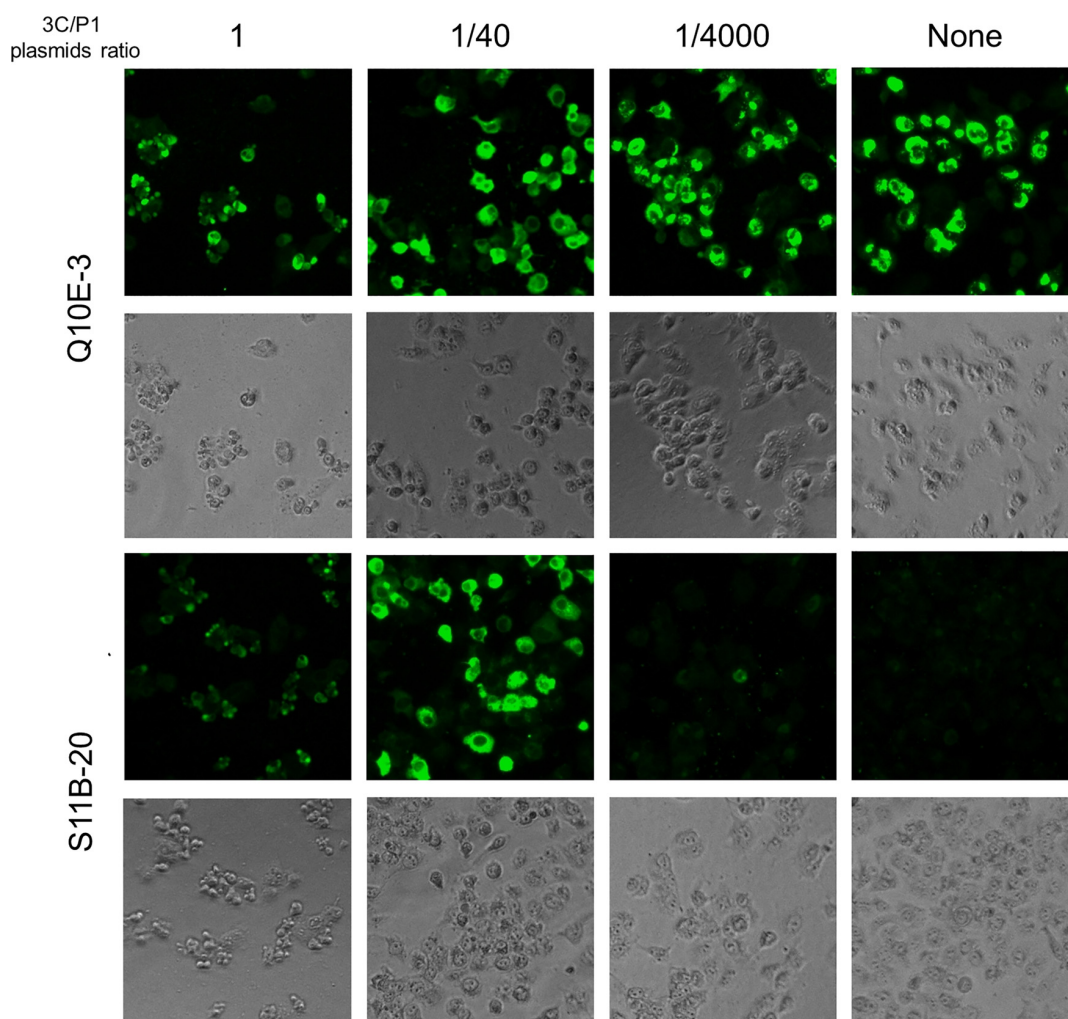


Fig. 1. Antigenicity of P1 polyprotein with different ratio of 3C^{pro}. To evaluate the appropriate dosage of pcDNA-3C, HTK⁻ cells were co-transfected with P1 plasmids and different levels of 3C plasmids and evaluated by Mab Q10E-3 and nine MAbs specific to processed P1. Mab Q10E-3, against linear form epitope, could recognize processed or unprocessed P1, indicating total expression proteins. S11B-20 could only recognize processed P1, and was regarded as the indicator for appropriate 3C activities.

folding of expressed VP2 or the binding sites of MAbs may span across the interface of more than one subunit protein. This result addressed the importance of expressing the target protein with natural conformation of both the complete virion and site 2 in the next step. Furthermore, it was found that seventeen out of twenty-six MAbs could recognize unprocessed protomers (P1), which are expressed by transfection with pcDNA-P1 only (Table 2). According to the study by Mateu, the folding

and organization of FMDV subunit proteins probably occur before they are cleaved from nascent P1 polyprotein, which could also be regarded as an unprocessed protomer and be recognized by some site 2 MAbs (Mateu et al., 1998). However, this study shows that nine MAbs (S11B-20, N3C-3, N10E-1, S10F-1, I9B-2, M10B-9, S8B-1, R3C-10 and O2G-1—Group III), including six neutralizing MAbs, could not recognize unprocessed protomers. This indicates that unprocessed

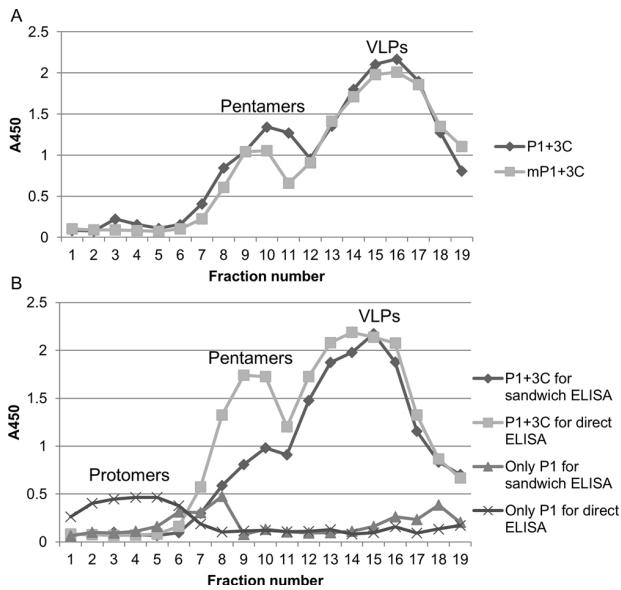


Fig. 2. Assembly of processed P1 (mP1) into VLP (mVLP). (A) Cell lysates from co-transfection with pcDNA-3C and pcDNA-P1 (or pcDNA-mP1) were loaded onto a 15–45% sucrose gradient. After ultra-high-speed centrifugation, 19 fractions were collected and analyzed by MAb Q10E-based sandwich ELISA. (B) Cell lysates from co-transfections or only transfection with pcDNA-P1 were also analyzed by MAb Q10E-based sandwich ELISA and MAb Q10E-based direct ELISA. VLP (75S), pentamer (12S), and protomer (5S) were indicated.

protomer could not present all neutralizing sites completely. Taken together, VLPs, instead of VP2 or unprocessed protomers, is optimal for site-direct mutagenesis in this study.

To synthesize VLPs, cells were co-transfected with pcDNA-P1 and pcDNA-3C. However, the dosage of 3C^{pro} in the expression system should be optimized first to avoid the known cytotoxic effect of 3C^{pro} that can reduce VLP production. Secondly, as the data already show, Group III MABs could not recognize unprocessed protomers, which could be the indicators of protomers processed by 3C^{pro} with functional activities in the expression system. This implies that only when unprocessed protomers are cleaved by 3C^{pro} and assemble to higher order structures such as pentamers, their antigenicity would be similar to virions and recognized by these indicators. Thus, in order to determine the optimal ratio of 3C^{pro} to P1, MAb Q10E-3, which can recognize the linear form of epitope site 1, was used as the indicator of P1 expression regardless of P1 being processed or not in the expression system.

Ultimately, the yield and antigenicity of P1 with different ratios of 3C^{pro} was examined using Q10E-3 and Group III MABs as indicators. As a result, the balance between cytotoxicity and processing was fine tuned to a pcDNA-3C/pcDNA-P1 ratio of about 1/40 (Table 3; Fig. 1).

To verify the assembly of VLP (or mVLP), cells co-transfected with an optimal ratio of pcDNA-P1 (or pcDNA-mP1) to pcDNA-3C were lysed and examined by sucrose gradient sedimentation followed by ELISA and TEM (Figs. 2 and 3). According to MAb Q10E-based sandwich ELISA, subunit proteins indeed self-assembled into higher-ordered pentamers and subsequent VLPs, and VP2-S72N mutation did not interfere with the assembly (Fig. 2A). In addition, no protomers were detected by MAb Q10E-based direct ELISA, which suggests the formed pentamers did not dissociate during purification (Fig. 2B). Finally, VLPs and mVLPs were shown as particles with about 25 nm by TEM (Fig. 3).

As described previously, VLP and mVLP were prepared in acetone-fixed cells or cell lysates. First, all twenty-six MABs showed positive signals for VLPs by IFA, indicating that these MABs recognized structural proteins, and the VLP had the authentic structure as that of the virion. It was demonstrated that none of the MABs recognized negative control, such as HTK⁻ cells or 3C^{pro}, by the same methods (data not shown). Next, according to the results of indirect ELISA, five neutralizing MABs' (Group I: O4A-1, P11A-15, O4D-1, Q4D-8 and S11E-9) relative binding percentages (RBPs) with mVLP were below 10% when compared with VLP (Table 2), which indicated that their affinities for antigens were apparently decreased by the mutation of VP2-S72N on mVLP. Therefore, these five MABs were identified as site 2 MABs conclusively. The other five neutralizing MABs (Group II: P3F-3, P2B-1, P3B-3, T7C-3 and T4F-7) showed 25–65% RBPs. It may indicate they are site 2 MABs, but VP2-S72N mutation could not fully abrogate the interaction with these five MABs, designated as Group II site 2 MABs (Table 2). The VP2-S72N mutation did not affect the binding affinity of the other sixteen MABs, including Q10E-3, Group III and IV MABs, whose RBPs were all above 90% (Table 2). Finally, the result of mVLP IFA was in accordance with that of ELISA. Group I MABs showed weak or no signal for mVLPs. The other twenty-one MABs all showed similar signals with both antigens (Fig. 4).

3.3. Identification of antigenic site 2 variation of O/TW/97 and O/Penghu/2012 by MAB panel

According to the amino acid sequence analysis for O/Penghu/2012, the critical residues of site 2 are mostly different from those of O/TW/97, with mutations at VP2-V70T, S72N, D73H and R77Q (Supplementary Fig. 1). In the previously discovered seven critical residues of site 2, O/Penghu/2012 has mutations at four residues.

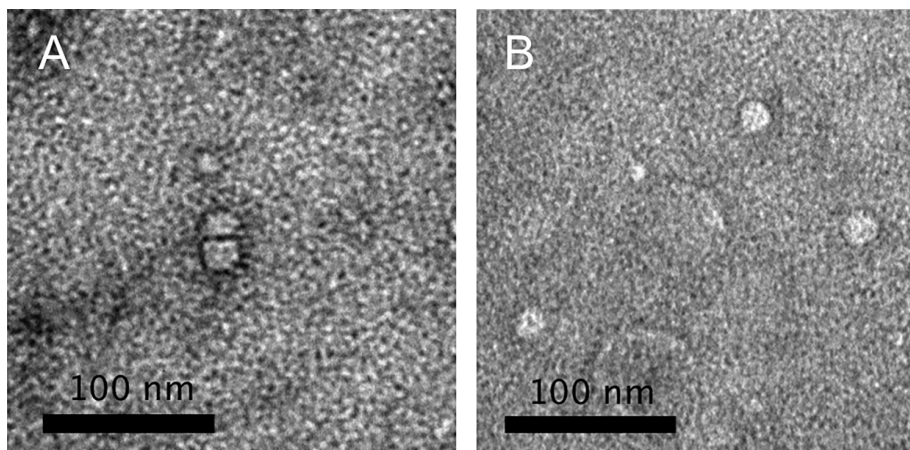


Fig. 3. Transmission electron micrograph showing virus like particles. (A) VLPs and (B) mVLPs with a diameter about 25 nm were observed by negative staining from the peak fraction of sucrose gradient centrifugation.

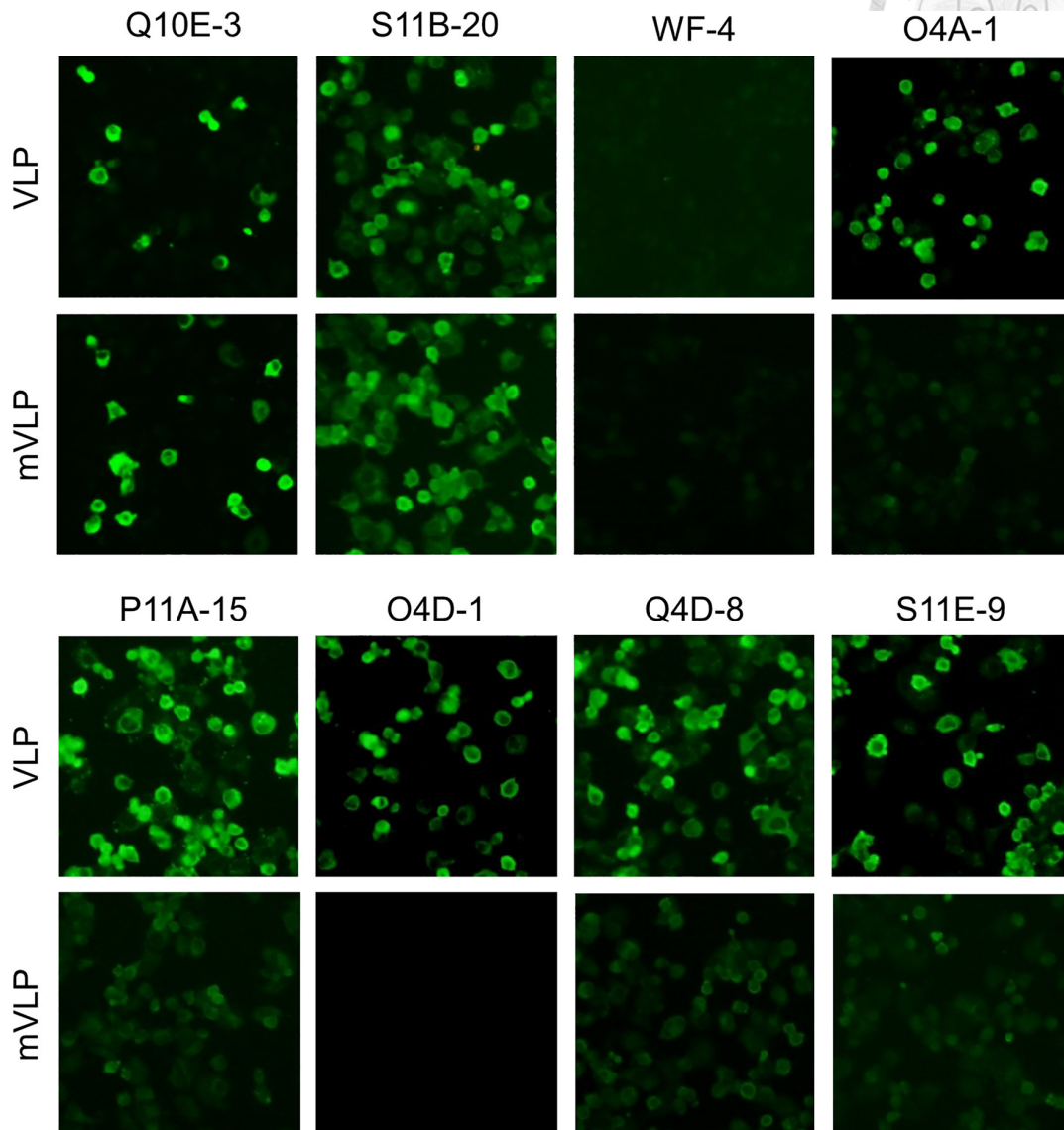


Fig. 4. Identification of site 2 MAb by mutant VLP by IFA. It is already known that MAbs Q10E-3 and S11B-20, as positive controls, are not affected by mutation of VP2-S72 N. The results of binding by these two MAbs indicated that VLP and mVLP were produced in an equal amount. WF-4 against NP of avian influenza virus was used as negative control. The other MAbs shown above were against site 2 and shown weak or no signals for mVLP.

However, the antigenic change of site 2 still needed to be investigated. The twenty-six characterized MAbs were then used for examining the antigenicity of O/Penghu/2012 via IFA. As expected, group I site 2 MAbs, whose RBPs with mVLP are below 10%, could not recognize O/Penghu/2012 in IFA, and five group II site 2 MAbs showing 25–65% RBPs with mVLP, could not either. Additionally, two MAbs in group III (the neutralizing I9B-2 and non-neutralizing O2G-1) had no reactivity with O/Penghu/2012 (Table 2; Fig. 5). Taken together, the antigenicity of site 2 has changed drastically from O/TW/97 to O/Penghu/2012.

Since site 2 antibodies of FMDV is among the most dominant in vaccinated animals (Mahapatra et al., 2012), we speculated that site 2 was put under strong selective pressure from vaccination measures in the field, resulting in the evolution of site 2. However, further research should be performed to validate this hypothesis; such as sequencing and comparing the virus isolates from the incidences between 1997 and 2012. Furthermore, the MAb panel should be used simultaneously to monitor the antigenic change.

4. Conclusion

This study establishes a platform for the identification of site 2 MAbs without using live FMDV. With the developed method, a panel of twenty-six MAbs against O/TW/97 was characterized, and five site 2 MAbs were identified. Subsequently, the MAb panel was tested to determine the antigenic change in site 2 from O/TW/97 to O/Penghu/2012. This mutagenic VLP platform can be applied to characterize other neutralizing MAbs in the future. This panel of MAbs against the primary FMDV isolate O/TW/97, showing great diversity, is helpful towards understanding the evolution of site 2 antigenicity under vaccine pressure in the field. As shown in this study, generating a MAb panel against the primary virus isolate during an outbreak and mapping the critical neutralizing MAbs by mutagenic VLP would be a valuable strategy for reference during disease control that utilizes the measure of vaccination, or in eradication programs that turn into longer campaigns.

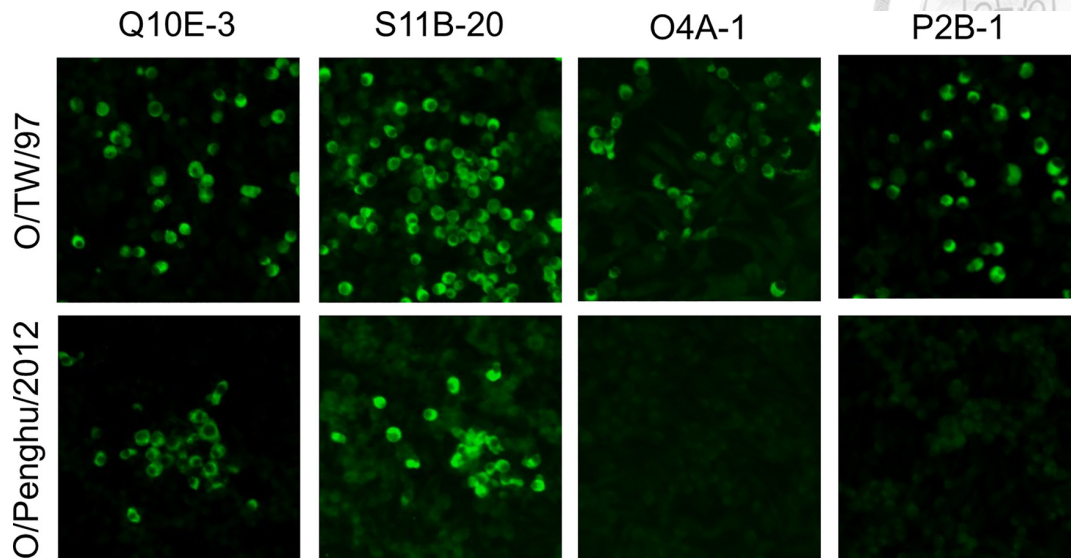


Fig. 5. Characterization of MAbs by O/TW/97 and O/Penghu/2012 by IFA. BHK-21 infected with virus isolate O/TW/97 and O/Penghu/2012 were fixed for IFA. Fourteen MAbs, such as MAbs Q10E-3 and S11B-20 shown above, could recognize both isolates. Twelve MAbs, such as MAbs O4A-1 and P2B-1, could not recognize O/Penghu/2012.

Acknowledgments

This work was supported by grants 104AS-10.1.2-BQ-B2 and 105AS-10.4.1-BQ-B1 of Bureau of Animal and Plant Health Inspection and Quarantine (Baphiq), Council of Agriculture, Taiwan, R.O.C. The authors are also pleased to acknowledge Chung-An Tan for help in editing the manuscript.

Appendix A. Supplementary data

Supplementary material related to this article can be found, in the online version, at doi:<https://doi.org/10.1016/j.vetmic.2018.06.002>.

References

- Abrams, C.C., King, A.M., Belsham, G.J., 1995. Assembly of foot-and-mouth disease virus empty capsids synthesized by a vaccinia virus expression system. *J. Gen. Virol.* 76 (Pt 12), 3089–3098.
- Aktas, S., Samuel, A.R., 2001. Identification of antigenic epitopes on the foot and mouth disease virus isolate O1/Manisa/Turkey/69 using monoclonal antibodies. *Rev. Sci. Tech.* 19, 744–753.
- Asfor, A.S., Upadhyaya, S., Knowles, N.J., King, D.P., Paton, D.J., Mahapatra, M., 2014. Novel antibody binding determinants on the capsid surface of serotype o foot-and-mouth disease virus. *J. Gen. Virol.* 95, 1104–1116.
- Barnett, P.V., Samuel, A.R., Pullen, L., Ansell, D., Butcher, R.N., Parkhouse, R.M., 1998. Monoclonal antibodies, against O1 serotype foot-and-mouth disease virus, from a natural bovine host, recognize similar antigenic features to those defined by the mouse. *J. Gen. Virol.* 79 (Pt 7), 1687–1697.
- Belsham, G.J., McInerney, G.M., Ross-Smith, N., 2000. Foot-and-mouth disease virus 3C protease induces cleavage of translation initiation factors eIF4A and eIF4G within infected cells. *J. Virol.* 74, 272–280.
- Bhat, S.A., Saravanan, P., Hosamani, M., Basagoudanavar, S.H., Sreenivasa, B.P., Tamilselvan, R.P., Venkataramanan, R., 2013. Novel immunogenic baculovirus expressed virus-like particles of foot-and-mouth disease (FMD) virus protect guinea pigs against challenge. *Res. Vet. Sci.* 95, 1217–1223.
- Cheng, I.C., Liang, S.M., Tu, W.J., Chen, C.M., Lai, S.Y., Cheng, Y.C., Lee, F., Huang, T.S., Jong, M.H., 2006. Study on the porcineophilic foot-and-mouth disease virus i. Production and characterization of monoclonal antibodies against VP1. *J. Vet. Med. Sci.* 68, 859–864.
- Crowther, J.R., Farias, S., Carpenter, W.C., Samuel, A.R., 1993. Identification of a fifth neutralizable site on type o foot-and-mouth disease virus following characterization of single and quintuple monoclonal antibody escape mutants. *J. Gen. Virol.* 74 (Pt 8), 1547–1553.
- Donaldson, A.I., JKitching, R.P., Barnett, P.V., 1996. Foot and mouth disease. In: *OIE Standards commission (Ed.), Manual of Standards for Diagnostic Tests and Vaccines*. Office International des Epizooties, Paris, France Capter 2.1.1.
- Fuerst, T.R., Niles, E.G., Studier, F.W., Moss, B., 1986. Eukaryotic transient-expression system based on recombinant vaccinia virus that synthesizes bacteriophage T7 RNA polymerase. *Proc. Natl. Acad. Sci. U. S. A.* 83, 8122–8126.
- Grazioli, S., Fallacara, F., Brocchi, E., 2013. Mapping of antigenic sites of foot-and-mouth disease virus serotype Asia 1 and relationships with sites described in other serotypes. *J. Gen. Virol.* 94, 559–569.
- Grubman, M.J., Baxt, B., 2004. Foot-and-mouth disease. *Clin. Microbiol. Rev.* 17, 465–493.
- Jamal, S.M., Belsham, G.J., 2013. Foot-and-mouth disease: past, present and future. *Vet. Res.* 44, 116.
- Kitson, J.D., McCahon, D., Belsham, G.J., 1990. Sequence analysis of monoclonal antibody resistant mutants of type o foot and mouth disease virus: evidence for the involvement of the three surface exposed capsid proteins in four antigenic sites. *Virology* 179, 26–34.
- Lee, C.D., Yan, Y.P., Liang, S.M., Wang, T.F., 2009. Production of FMDV virus-like particles by a SUMO fusion protein approach in *Escherichia coli*. *J. Biomed. Sci.* 16, 69.
- Mahapatra, M., Hamblin, P., Paton, D.J., 2012. Foot-and-mouth disease virus epitope dominance in the antibody response of vaccinated animals. *J. Gen. Virol.* 93, 488–493.
- Mason, P.W., Grubman, M.J., Baxt, B., 2003. Molecular basis of pathogenesis of FMDV. *Virus Res.* 91, 9–32.
- Mateu, M.G., Escarmis, C., Domingo, E., 1998. Mutational analysis of discontinuous epitopes of foot-and-mouth disease virus using an unprocessed capsid protomer precursor. *Virus Res.* 53, 27–37.
- McCahon, D., Crowther, J.R., Belsham, G.J., Kitson, J.D., Duchesne, M., Have, P., Meloen, R.H., Morgan, D.O., De Simone, F., 1989. Evidence for at least four antigenic sites on type O foot-and-mouth disease virus involved in neutralization; Identification by single and multiple site monoclonal antibody-resistant mutants. *J. Gen. Virol.* 70 (Pt 3), 639–645.
- Pan, L., Zhang, Y., Wang, Y., Wang, B., Wang, W., Fang, Y., Jiang, S., Lv, J., Wang, W., Sun, Y., Xie, Q., 2008. Foliar extracts from transgenic tomato plants expressing the structural polyprotein, P1-2A, and protease, 3C, from foot-and-mouth disease virus elicit a protective response in guinea pigs. *Vet. Immunol. Immunopathol.* 121, 83–90.
- Polacek, C., Gullberg, M., Li, J., Belsham, G.J., 2013. Low levels of foot-and-mouth disease virus 3C protease expression are required to achieve optimal capsid protein expression and processing in mammalian cells. *J. Gen. Virol.* 94, 1249–1258.
- Puckette, M., Clark, B.A., Smith, J.D., Turecek, T., Martel, E., Gabbert, L., Pisano, M., Hurtle, W., Pacheco, J.M., Barrera, J., Neilan, J.G., Rasmussen, M., 2017. Foot-and-mouth disease (FMD) virus 3C protease mutant L127P: implications for FMD vaccine development. *J. Virol.* 91.
- Wang, H., Zhao, L., Li, W., Zhou, G., Yu, L., 2011. Identification of a conformational epitope on the VP1 g-h loop of type Asia1 foot-and-mouth disease virus defined by a protective monoclonal antibody. *Vet. Microbiol.* 148, 189–199.
- Xie, Q.C., McCahon, D., Crowther, J.R., Belsham, G.J., McCullough, K.C., 1987. Neutralization of foot-and-mouth disease virus can be mediated through any of at least three separate antigenic sites. *J. Gen. Virol.* 68 (Pt 6), 1637–1647.
- Yang, P.C., Chu, R.M., Chung, W.B., Sung, H.T., 1999. Epidemiological characteristics and financial costs of the 1997 foot-and-mouth disease epidemic in Taiwan. *Vet. Rec.* 145, 731–734.
- Yang, M., Xu, W., Goolia, M., Zhang, Z., 2014. Characterization of monoclonal antibodies against foot-and-mouth disease virus serotype O and application in identification of antigenic variation in relation to vaccine strain selection. *Viol. J.* 11, 136.

Chapter V



The Use of Distinctive Monoclonal Antibodies in FMD VLP- and P1-Based Blocking ELISA for the Seromonitoring of Vaccinated Swine

Reprint from International Journal of Molecular Sciences, Vol. 23, Author(s): Heng-Wei Lee, Cheng-Yao Yang, Ming-Chang Lee, Shih-Ping Chen, Hui-Wen Chang, Ivan-Chen Cheng, Title of article: The Use of Distinctive Monoclonal Antibodies in FMD VLP- and P1-Based Blocking ELISA for the Seromonitoring of Vaccinated Swine, open access (2022) of MDPI.



Article

The Use of Distinctive Monoclonal Antibodies in FMD VLP- and P1-Based Blocking ELISA for the Seromonitoring of Vaccinated Swine

Heng-Wei Lee¹, Cheng-Yao Yang² , Ming-Chang Lee³, Shih-Ping Chen³, Hui-Wen Chang^{1,4} and Ivan-Chen Cheng^{1,*}

¹ School of Veterinary Medicine, National Taiwan University, Taipei 106, Taiwan;

d06629010@ntu.edu.tw (H.-W.L.); huiwenchang@ntu.edu.tw (H.-W.C.)

² Graduate Institute of Veterinary Pathobiology, National Chung Hsing University, Taichung 402, Taiwan; yangchengyao@nchu.edu.tw

³ Agricultural Technology Research Institute, Hsinchu 300, Taiwan; lee@mail.atri.org.tw (M.-C.L.); spchen@mail.atri.org.tw (S.-P.C.)

⁴ Graduate Institute of Molecular and Comparative Pathobiology, School of Veterinary Medicine, National Taiwan University, Taipei 106, Taiwan

* Correspondence: ivancheng@ntu.edu.tw

Abstract: The serum neutralization (SN) test has been regarded as the “gold standard” for seroconversion following foot-and-mouth disease virus (FMDV) vaccination, although a high-level biosafety laboratory is necessary. ELISA is one alternative, and its format is constantly being improved. For instance, standard polyclonal antisera have been replaced by monoclonal antibodies (MAbs) for catching and detecting antibodies, and inactive viruses have been replaced by virus-like particles (VLPs). To the best of current knowledge, however, no researchers have evaluated the performances of different MAbs as tracers. In previous studies, we successfully identified site 1 and site 2 MAbs Q10E and P11A. In this study, following the established screening platform, the VLPs of putative escape mutants from sites 1 to 5 were expressed and used to demonstrate that S11B is a site 3 MAb. Additionally, the vulnerability of VLPs prompted us to assess another diagnostic antigen: unprocessed polyprotein P1. Therefore, we established and evaluated the performance of blocking ELISA (bELISA) systems based on VLPs and P1, pairing them with Q10E, P11A, S11B, and the non-neutralizing TSG MAb as tracers. The results indicated that the VLP paired with S11B demonstrated the highest correlation with the SN titers ($R^2 = 0.8071$, $n = 63$). Excluding weakly positive serum samples (SN = 16–32, $n = 14$), the sensitivity and specificity were 95.65% and 96.15% ($\kappa = 0.92$), respectively. Additionally, the P1 pairing with Q10E also demonstrated a high correlation ($R^2 = 0.768$). We also discovered that these four antibodies had steric effects on one another to varying degrees, despite recognizing distinct antigenic sites. This finding indicated that MAbs as tracers could not accurately detect specific antibodies, possibly because MAbs are bulky compared to a protomeric unit. However, our results still provide convincing support for the application of two pairs of bELISA systems: VLP:S11B-HRP and P1:Q10E-HRP.

Keywords: foot-and-mouth disease virus; virus-like particles; blocking ELISA; monoclonal antibodies



Citation: Lee, H.-W.; Yang, C.-Y.; Lee, M.-C.; Chen, S.-P.; Chang, H.-W.; Cheng, I.-C. The Use of Distinctive Monoclonal Antibodies in FMD VLP- and P1-Based Blocking ELISA for the Seromonitoring of Vaccinated Swine. *Int. J. Mol. Sci.* **2022**, *23*, 8542. <https://doi.org/10.3390/ijms23158542>

Academic Editor: Menotti Ruvo

Received: 15 July 2022

Accepted: 29 July 2022

Published: 1 August 2022

Publisher's Note: MDPI stays neutral with regard to jurisdictional claims in published maps and institutional affiliations.



Copyright: © 2022 by the authors. Licensee MDPI, Basel, Switzerland. This article is an open access article distributed under the terms and conditions of the Creative Commons Attribution (CC BY) license (<https://creativecommons.org/licenses/by/4.0/>).

1. Introduction

Foot-and-mouth disease virus (FMDV) is highly contagious and affects all susceptible cloven-hoofed animals globally. In addition to the lack of cross-protection among the seven serotypes (O, A, C, Asia1, SAT1, SAT2, and SAT3), restrictions on the import of animal products are very strict, particularly those in FMDV-free countries. A facility with a high biosafety level is also required to handle live FMDV, which carries the potential risk of viral leakage. An effective countermeasure against FMDV outbreaks is blanket vaccination with selected strains followed by serum neutralization (SN) tests to determine the protective

antibody response [1,2]. However, both inactivated vaccine production and the SN test are highly restricted to high-level biosafety laboratories.

In 1997, a devastating FMDV outbreak resulted in tremendous economic loss in Taiwan. The virus strain, O/TW/97 (O/97), was characterized by porciphilic activity [3]. Following the guidelines of the OIE (Office International des Epizooties/World Organisation for Animal Health), mandatory vaccination with inactivated vaccines made using three strains—O 4174, O1 Campos, and O1 Manisa—was recommended by the World Reference Laboratory based on an evaluation of r_1 values greater than 0.3 [4] immediately following the outbreak. The FMDV strain O/98, a homologue of O/97, was produced and recognized as the vaccine strain later in Taiwan. After blanket vaccination and surveillance, O/Penghu/2012 was the last isolated virus from this series of FMD cases. In 1999, another virus strain was isolated in Kinmen, an archipelago far off the western coast of Taiwan. It was named O/TW/2/99 and classified as the PanAsia topotype, which is separate from Cathay O/TW/97 [5,6]. The FMD eradication campaign lasted until 2020, when Taiwan was recognized as an FMDV-free zone by the OIE.

FMDV is non-enveloped and consists of a single-stranded positive-sense RNA genome surrounded by a densely packed icosahedral protein shell. The shell comprises 60 copies of a protomer with four capsid proteins, VP1 to VP4, where VP4 is located on the inner side of the virion. FMDV targets host cell receptors, including integrins ($\alpha\beta 1$, $\alpha\beta 3$, $\alpha\beta 6$, and $\alpha\beta 8$), heparan sulfate, and JMJD6, for viral entry [7,8]. However, protective antibodies could effectively block the interaction between virions and receptors to neutralize the virus. Based on MAb escape mutant studies, five neutralizing sites have been described for serotype O. Site 1, located at the GH loop and carboxy terminus of VP1, includes VP1-144, 148, 150, and 208. The critical residues of site 2 are VP2-70, 71, 72, 73, 75, 77, 131, and 191. The residues in site 3 include VP1-43 and 44 at the BC loop of VP1 near the fivefold axis. Site 4 is located at VP3 (VP3-56 and 58), and site 5 at the GH loop of VP1 (VP1-149) [9–13]. Although these findings provide a basic understanding of neutralizing antibodies, the neutralizing sites differ among serotypes [14]. Additionally, with the exception of site 1, the neutralizing sites have conformational structures and cannot be presented by synthetic peptides [9]. Therefore, a platform based on virus-like particles (VLPs) established in a previous study was used to successfully identify more than six site 2 MAbs whose binding to VLPs could be abrogated or inhibited by VP2-S72N mutation on the VLPs [15]. The platform preserved the authentic antigenicity without using live or inactivated viruses. We presumed this could also apply to the screening and characterization of all neutralizing monoclonal antibodies.

The SN test is prescribed as a standard method for vaccine seromonitoring, even though it is laborious, expensive, and time-consuming, and it requires a high-level biosafety laboratory. In addition to the biological variability in SN tests, ELISA has been adopted by many laboratories to replace the SN test, and a more advanced format for ELISA has been developed [16]. In the beginning, the solid-phase competition ELISA (SPCE) format used polyclonal antisera as capture antibodies and tracers, with inactivated, purified viruses as antigens [17]. Later on, polyclonal antibodies were replaced by MAbs as the tracer and capture for large-scale serology [18], and VLPs replaced inactivated viruses, whose manufacture was limited to BSL3 laboratories [18,19]. A recombinant VP2 subunit protein from the Egyptian SAT2 isolate and a P1 capsid polyprotein of serotype O were also chosen as the diagnostic antigens [20,21]. The rP1-SPCE system paired guinea pig anti-serum as the tracer and demonstrated excellent agreement with in-house liquid-phase blocking ELISA [21]. In serotype O, the subunit protein could not represent the conformational neutralizing sites apart from the linear epitope (site 1), which was the only exception. Therefore, our study aimed to develop a blocking ELISA system based on VLPs or P1 combined with different tracer MAbs and evaluate the most suitable pairs.

2. Results

2.1. Identification of Binding Site for S11B Monoclonal Antibody

Previously, we determined that the Q10E MAb recognized site 1 based on a synthetic GH peptide on VP1 [22] and successfully proved the P11A MAb as the site 2 antibody using mutated VLP/VP2-S72N [15]. Meanwhile, the S11B MAb, a neutralizing antibody, was found not to recognize the unprocessed protomer P1. After processing and assembly, the capsid proteins formed a higher-order oligomer, possibly a pentamer, which could be bound to S11B [15]. To examine the binding of S11B at the neutralizing site, we expressed VLPs from putative escape mutants of O/TW/97, which included the VP1-L148R mutant for site 1, VP2-S72N and VP2-S131P mutants for site 2, VP1-P44L and VP1-K43A/P44A for site 3, VP3-D58K and VP3-H56A/D58A for site 4, and VP1-Q149H for site 5 (Figure 1A). As expected, the mutation at site 1 (VP1-L148R) almost abrogated the binding of the Q10E MAb (Figure 1B). The mutation of VP2-S72N inhibited the interaction between P11A and VLPs, while VP2-S131P had no significant impact (Figure 1C). Because the double mutations at site 3 (VP1-K43A/P44A) significantly inhibited the binding of S11B, we presumed that S11B was the site 3 MAb (Figure 1D). For normalizing the VLPs, the OD values of the indicated VLPs were adjusted using those from Q10E, except for the site 1 mutated VLP, and the same conclusion was reached (Figure S1A). The same was true when the values were adjusted using those from P11A, except for the site 2 mutated VLP (Figure S1B). In short, we produced and identified at least three neutralizing MABs: Q10E at site 1, P11A at site 2, and S11B at site 3, as indicated in Table 1.

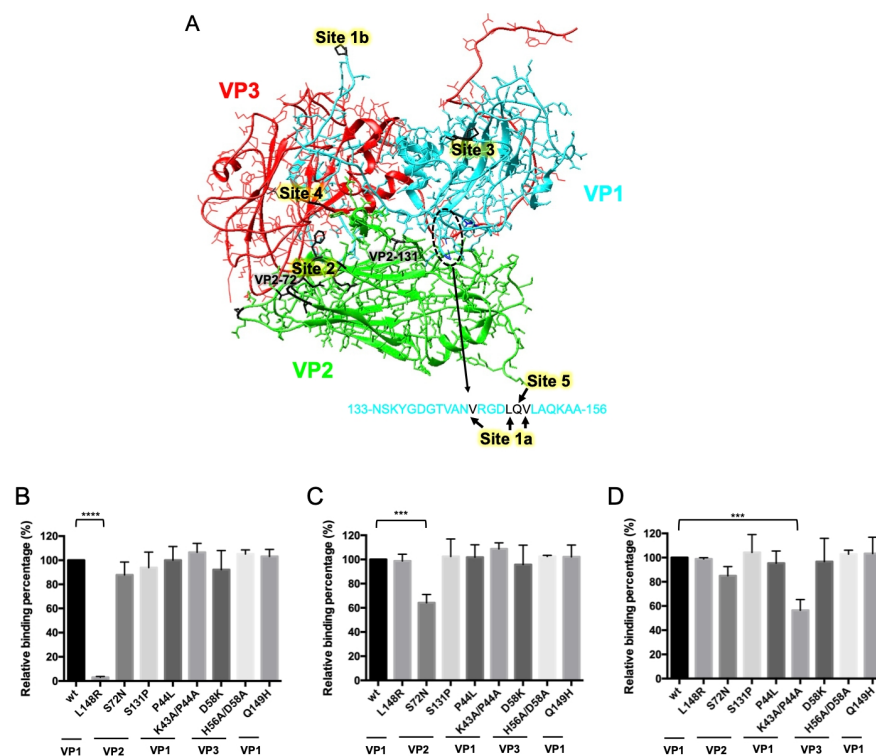


Figure 1. Schematic of neutralizing sites for serotype O and the relative binding percentages between MABs and mutated VLPs. (A) The critical residues of the neutralizing sites were illustrated on a protomer of O1M-S093Y (PDB 5ddj) using the UCSF Chimera software. (B–D) Sandwich ELISA was performed with the VLPs and mutated VLPs to determine the relative binding strength (compared with the wild type) of the MABs, including Q10E (B), P11A (C), and S11B (D). The relative binding percentages of the mutated VLPs were compared with those of the wild-type (100%) using ANOVA with Dunnett’s test. Each test was performed in triplicate. L148R—VP1-L148 mutated VLP; S72N and S131P—mutations of VLP2 in indicated amino acids; P44L and K43A/P44A—site 3 mutated VLPs; D58K and H56A/D58A—site 4 mutated VLPs; Q149H—site 5 mutated VLP. **** $p < 0.0001$, *** $p < 0.001$.

Table 1. Characterization of four anti-FMDV capsid monoclonal antibodies.

	Q10E	P11A	S11B	TSG
Isotype	IgG2a/κ	IgG3/κ	IgA/κ	IgG1/κ
Unprocessed protomer	+	+	−	+
Neutralizing activity	+	+	+	−
Binding site	Site 1 (VP1-148)	Site 2 (VP2-72)	Site 3 (VP1-43,44)	Unknown

2.2. Establishment of VLP- and GST-P1-Based bELISA

The three neutralizing MAb (Q10E, P11A, and S11B) and the non-neutralizing MAb TSG were applied as tracers in blocking ELISA paired with VLPs and P1. Excluding the S11B-HRP and P1 pair, seven pairs were tested using a small number ($n = 6$) of samples from FMDV vaccinated swine, including SN512, SN256-1, SN256-2, SN64, SN16-1, and SN16-2. Meanwhile, to assess the specificity, negative sera ($n = 12$) against FMDV were also tested, including sera from five specific pathogen-free (SPF) pigs; sera against pseudorabies (PR), classic swine fever (CSF), and swine vesicular disease (SVD); in addition to three negative sera from imported pigs. The PI values of the positive samples were above 40% in the VLP pairs with Q10E-HRP, TSG-HRP, or S11B-HRP. The negative samples had values under 20% (Figure 2). The combination of the VLP and S11B-HRP performed particularly well; the PI values were 80–95% for the positive antisera and lower than 16% for the negative sera (Figure 2).

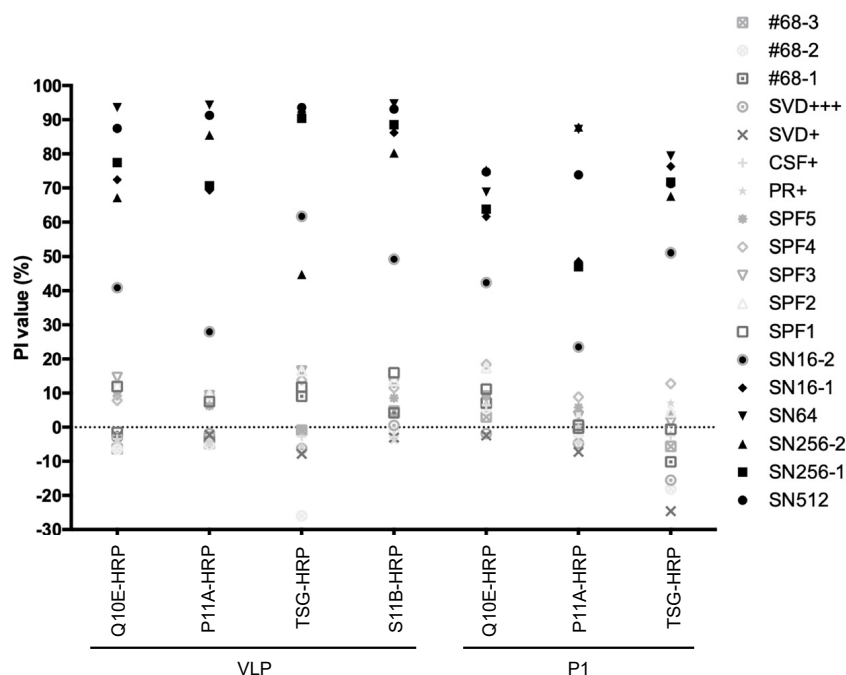


Figure 2. Specificity of VLP- and P1-based blocking ELISA paired with four MAb. Samples included strongly positive anti-FMDV serum (SN512, SN256-1, SN256-2, and SN64), weakly positive serum (SN16-1 and SN16-2), SPF serum (SPF1, SPF2, SPF3, SPF4, and SPF5), anti-pseudorabies virus serum (PR+), anti-classic swine fever virus serum (CSF+), anti-swine vesicular disease virus serum (SVD+ and SVD+++), and FMDV-free samples (#68-1, #68-2, and #68-3). Each test was performed in triplicate.

2.3. Evaluation of VLP- and GST-P1-Based bELISA

To select a suitable pair for bELISA that was positively correlated with the SN titers, we applied 63 samples, including 10 SPF sera (Table S1). According to the OIE manual, samples with SN titers below 16 are considered negative. For positive anti-FMDV sera, the titer should exceed 16, with SN titers of 16–32 indicating a weak positive [4]. Therefore,

we used strongly positive sera from vaccinated pigs ($n = 23$), weakly negative sera ($n = 14$), and negative sera ($n = 26$). The means of triplicate samples were calculated and are demonstrated in Figure 3 and Supplementary Table S2. The PI values for all pairs demonstrated a statistically significant correlation with those of the SN test ($p < 0.0001$); however, the VLP paired with S11B-HRP appeared to be the best combination ($R^2 = 0.8071$), better than the P1 and Q10E-HRP pairing ($R^2 = 0.7680$). The optimal cut-off value for each blocking ELISA was analyzed and determined using ROC analysis (the weak, doubtful positive samples were excluded) (Figure S2). The sensitivity and specificity values were 95.65 and 96.15%, respectively, for the VLP paired with S11B-HRP, indicating very high agreement ($\kappa = 0.92$) (Table 2). Although the P1 and Q10E-HRP pair exhibited relatively low sensitivity (78.26%), the SN titers of five false-negative samples ranged from 64- to 128-fold, while the PI values ranged from 36 to 47%, near the cut-off value of 47.45 for this pair (Table S1).

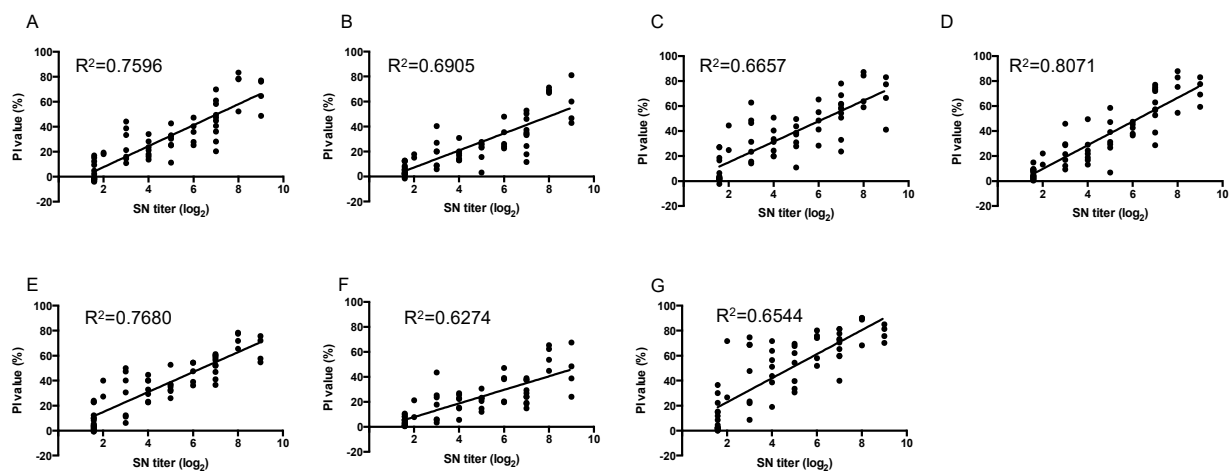


Figure 3. Scatter plots and calculated regression lines for SN titers and PI values as measured with solid-phase blocking ELISA based on VLPs (A–D) or GST-P1 (E–G). Results of VLP-based bELISA with tracers: (A) Q10EHRP, (B) P11A-HRP, (C) TSG-HRP, and (D) S11B-HRP. Results of P1-based bELISA with tracers: (E) Q10E-HRP, (F) P11A-HRP, and (G) TSG-HRP. Each test was performed in triplicate.

Table 2. Comparison of the performance of bELISA with different tracers and antigens.

Antigen		VLP								GST-P1					
Tracer		Q10E		P11A		TSG		S11B		Q10E		P11A		TSG	
SN	Number	+	–	+	–	+	–	+	–	+	–	+	–	+	–
<16	26	1	25	1	25	1	25	1	25	1	25	1	25	1	25
16–32	14	1	13	1	13	2	12	4	10	1	13	2	12	0	14
>32	23	17	6	17	6	17	6	22	1	18	5	15	8	14	9
Cut-off value		39.55		30.06		49.65		33.06		47.45		26.13		72.15	
Sensitivity *		73.91		73.91		73.91		95.65		78.26		65.22		60.87	
Specificity *		96.15		96.15		96.15		96.15		96.15		96.15		96.15	
Kappa value		0.71		0.71		0.71		0.92		0.75		0.63		0.58	

* Samples for SN16–32 were excluded from calculations of sensitivity and specificity.

2.4. Steric Effect between Q10E, P11A, S11B, and the Non-Neutralizing Antibody TSG

Despite the distinct binding epitopes of the four MAbs, we discovered that they interfered with each other within the same antigens (Figure 4A). To verify this, non-conjugates were applied in serial two-fold dilutions (25–200 ng/well) to block the VLPs, followed by the indicated tracers (Figure 4B). The highest PI values in each group were

observed for the pairs with identical MAbs, such as Q10E blocking Q10E-HRP (Figure 4A). However, Q10E-HRP was also blocked by P11A and S11B, which were individually directed to site 2 and site 3, respectively. In contrast, the degree of blocking for P11A-HRP by Q10E was not evident. This trend agreed with the results of the P1-based bELISA (Figure S3A). The PI values in the TSG-HRP group, ranked from high to low, were those of the pairs with TSG, P11A, S11B, and Q10E. S11B-HRP was also blocked by S11B, Q10E, and P11A (Figure 4B).

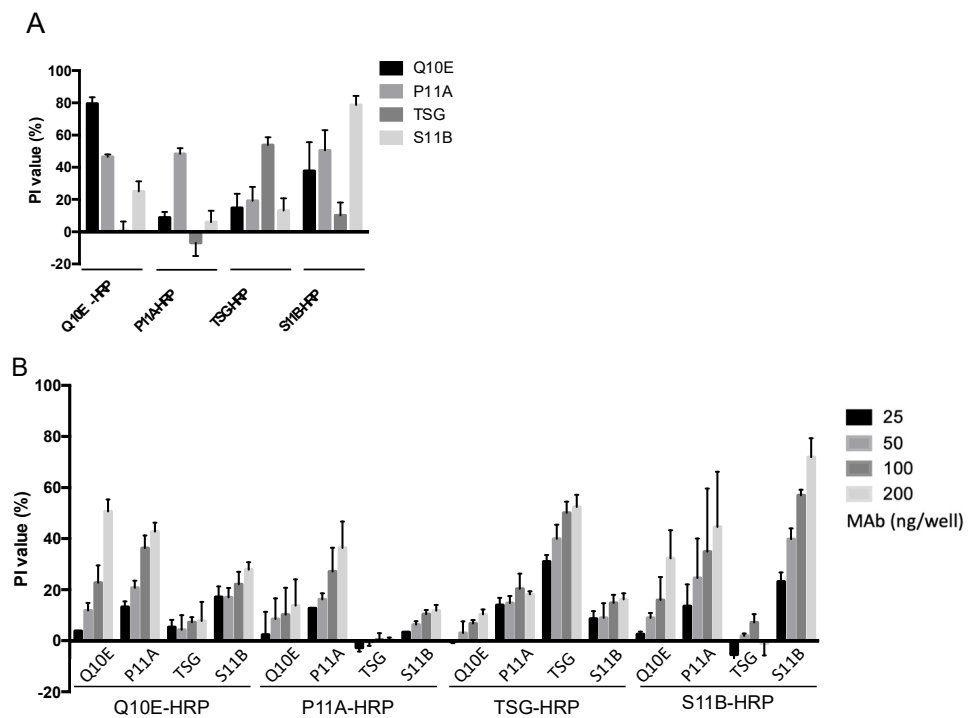


Figure 4. Steric effects between the four monoclonal antibodies (Q10E, P11A, TSG, and S11B). (A) The coated VLPs were blocked with non-conjugated monoclonal antibodies, including Q10E, P11A, TSG, and S11B at 400 ng per well, followed by 100 ng of the indicated conjugate. (B) The VLPs were blocked with different non-conjugated antibodies (25–200 ng per well), followed by 100 ng of conjugates. Each test was performed in triplicate.

To exclude the possibility that the tracers replaced the blocking antibodies, we labeled the blocking antibodies by reversing the order of addition of non-conjugates and conjugates. The extremely low PI values indicated that the conjugates could still bind to the VLP, even after the addition of 400 ng of non-conjugates (Figure S3B). Therefore, in Figures 4B and S3A, the TSG bound to the VLP and P1 was not replaced by P11A-HRP, implying that P11A-HRP and TSG coexisted on the antigens. However, TSG-HRP was blocked by P11A on the VLP and P1 (Figures 4B and S3A). We presumed that the affinity of the tracers (added later) determined the ability to coexist on an antigen with blocking antibodies. Therefore, the PI values reflect not only the binding sites but also the affinity of the indicated tracers when testing the same subjects (blocking antibodies).

3. Discussion

Scientists are currently attempting to reform the format of blocking ELISA to detect protective antibodies against FMDV [16–19,23,24]. However, to our knowledge, no comparative studies of different tracers and different antigens using VLPs and P1 have been reported. Our study identified S11B as the site 3 MAb based on our established platform. The other MAbs, Q10E, P11A, and TSG, were chosen as tracers to represent site 1, site 2, and non-neutralizing antibodies, respectively. Excluding the S11B and P1 pair, the performance

of the seven pairs was compared with 63 swine sera, of which 53 samples were collected from vaccinated pigs and 10 from SPF pigs. VLP:S11B-HRP and P1:Q10E-HRP indicated high performance in detecting protective antibodies and were positively correlated with SN titers ($R^2 = 0.8071$ and 0.7680 , respectively).

Given the highly folded nature of FMDV capsids and their dense packing to form virions, antigenicity should be given serious consideration in vaccines and ELISA detection systems. In the case of serotype O, for example, apart from linear site 1, the other four neutralizing sites are conformational epitopes, which cannot be represented by single subunit proteins [9,25]. For example, S11B, a site 3 MAb, could not recognize VP1 (data not provided) or the unprocessed P1 protomer [15], indicating that site 3 was formed only after the processing and assembly of P1. Similarly, Dong et al. highlighted the subtle differences in the structures of a pentamer and a virion using cryo-EM, indicating that the virion package caused a structural shift in the BC and EF loops of VP2 [26]. Moreover, Wang et al. found that the native site 1 of the serotype Asia 1 may be conformational in structure [27]. Conversely, all site 2 MAbs in our laboratory failed to recognize recombinant VP2 [15].

Although we obtained different R^2 values from the seven pairs for bELISA, the PI values did not represent the amounts of the tested neutralizing antibodies when the indicated site MAb was used as a tracer. Due to the bulk of antibodies being compared to a pentameric unit and the repeating units of VLPs, different MAbs could compete for association with the VLPs, despite their binding to distinct epitopes. To prove this, we chose non-conjugated MAbs to represent the indicated site antibodies in sera. Site 1 was positioned close to site 2; therefore, P11A significantly blocked Q10E-HRP. Additionally, Q10E-HRP was also blocked by S11B, a site 3 MAb. TSG-HRP was blocked by P11A and S11B, implying that portions of the site 2 and site 3 antibodies were detected when the non-neutralizing TSG MAb was used as a tracer. Furthermore, we discovered that the blocking effects were not reciprocal. For instance, P11A blocked TSG-HRP, but TSG did not block P11A-HRP. We also discovered that the blocking antibodies stayed on the antigen, predominantly based on the fact that the exchange of non-conjugates and conjugates led to a PI value near zero. The predominance of the order of addition excluded the possibility that P11A-HRP replaced TSG MAb, which was already bound to the VLP or P1. We presume that the affinity of the tracer may explain why the blocking effects were not reciprocal, as described in more detail below. Given that the viruses were mixed with samples prior to contacting the host receptors during the SN test procedure, we decided solid-phase blocking ELISA, which is step-by-step, would be more reasonable than competitive ELISA, in which tracers and serum antibodies compete for the epitope at the same time.

Based on the results demonstrated in Figure 4, we defined the region of steric effect into “core” and “marginal” regions. The core region was the exact binding site. If the core regions of antibodies overlapped, the antibodies could not coexist on the same protomeric unit. Conversely, the marginal region was blocked by the Fc portion or the other hanging Fab of the blocking antibodies. A high tracer affinity may have been resistant to the steric effect in the marginal regions, resulting in low PI values. The opposite would result in high PI values, such as those observed for TSG-HRP with P11A. Despite the effect of tracer affinity, it has been reported that some neutralizing antibodies not only block viruses but also mimic receptors, resulting in viral uncoating [26]. When two Fabs of antibodies simultaneously bind to adjacent protomers, they mask a large area of the virion [10]. These two types of antibodies within samples could lead to the misinterpretation of PI values. Theoretically, soluble viral receptors [28] might be ideal tracers for bELISA. Nonetheless, there are at least three FMD viral receptors: integrins, heparan sulfate, and JMJD6. Considering their application and our results, purified MAbs were suitable for the role of tracer, as they reflected the SN titer. Moreover, non-neutralizing TSG when used as a tracer was able to detect site 2-directed antibodies.

Empty capsids, albeit with native antigenicity, are unstable and prone to dissociation [29]. There is no guarantee that VLPs will not dissociate after sucrose gradient

purification, which would complicate any application. The small size and simple structure of P1 without the marginal region that VLPs carry do not induce the steric effect, which interferes with the correlation between the SN titer and data generated by bELISA. Although P1 demonstrates a slightly different virion antigenicity, it can at least present the near-native structures of site 1 and site 2 [15], both of which are immunodominant for vaccinated animals [30]. Therefore, unprocessed P1 protomers, given the promising diagnostics, are worth trying. Our results indicated no significant difference between P1 and VLPs. Although antigenicity is important for FMDV vaccines and detection systems, P1 is still a potential target for future applications due to its low production costs.

In conclusion, we established bELISA systems with VLPs and P1 and paired them with different MAbs as tracers. The systems were positively correlated with SN titers and obtained a high sensitivity and specificity (excluding weakly positive sera). Most importantly, two bELISA pairs, VLP:S11B-HRP and P1:Q10E-HRP, showed the highest performance among the seven and could be applied to large-scale serological testing and simultaneously compared with the SN test to further validate their efficacy in identifying neutralizing antibodies in swine sera samples. Additionally, sera samples from different FMD-susceptible species, such as bovines and ovines, are needed for future testing to expand and evaluate the potential for application in FMD disease surveillance.

4. Materials and Methods

4.1. Viruses and Cells

Human TK⁻ 143 (HTK⁻) cells for the recombinant vaccinia virus expression system were cultured in Dulbecco's modified Eagle medium (DMEM, Thermo Scientific, Carlsbad, CA, USA) containing 10% Hyclone fetal calf serum (FBS). The recombinant vaccinia virus used in this study, vTF7-3, was amplified in the human TK⁻ 143 (HTK⁻) cells. The BHK-21 cells used for serum neutralization tests were maintained in DMEM containing 5% FBS.

4.2. Swine Sera

Swine vesicular disease virus anti-serum (SVD+ and SVD+++ (PrioCHECK SVDV Ab ELISA, 7610211 and 7610212) and FMDV-free samples after import testing (#68-1, #68-2, and #68-3) were supplied by the Animal Health Research Institute. Other FMDV-negative serum samples were supplied by the Agricultural Technology Research Institute, including sera against pseudorabies serum (PR+) (IDEXX PR-gp1 Antibody Test Kit) and classic swine fever serum (CSF+) (IDEXX Classical Swine Fever Virus Antibody Test Kit) and sera from specific pathogen-free (SPF) pigs ($n = 15$). Sera from vaccinated pigs ($n = 49$) were collected from farms in the Hog Cholera and FMD Eradication Program of the Council of Agriculture, Taiwan, and supplied by the Agricultural Technology Research Institute. Serum neutralization tests for all samples were carried out using a standard SN test at the Animal Health Research Institute, Taiwan.

4.3. Plasmid Constructions

Point-mutated pcDNA-P1(O97) plasmids were generated using GeneArt site-direct mutagenesis (Invitrogen, Carlsbad, CA, USA, A13282) as described in a previous study [15]; the primers used are listed in Table S2. The P1 gene was further subcloned to pET-42a to generate pET-GST-P1(O97) plasmids using *Bam*HI and *Xho*I.

4.4. Purification and Conjugation of MAbs

MAbs from ascetic fluid were purified with protein G (Cytiva, Marlborough, MA, USA, GE17-0618-01) and conjugated with horseradish peroxidase (HRP) (Novus Biologicals, Centennial, CO, USA, 701-0000).

4.5. Expression of VLPs and mVLPs for ELISA

The antigens, including VLPs and mVLPs, were produced with a recombinant vaccinia virus vTF7-3 expression system as described in previous studies [15,31]. The HTK⁻ cells

were seeded in 6-well plates and infected by vTF7-3 for 1 h. The indicated plasmids containing the T7 promoter were transfected into the cells using Turbofect as per the manufacturer's instructions (Thermo Scientific, Carlsbad, CA, USA). The molar ratio of P1 (or mutated P1) to 3C plasmids (pcDNA-3C) was 40:1 to minimize the excessive production of 3C^{Pro}, which is highly cytotoxic. At 20 h post transfection, the cells were harvested in 500 µL of PBS per well, followed by three freeze–thaw cycles. Cell debris was removed by centrifugation at 10,000 × g for 20 min.

4.6. Sandwich ELISA

ELISA plates were coated with 400 ng/well purified TSG MAb in carbonate–bicarbonate buffer (pH 9.6) (Sigma, St. Louis, MO, USA, C3041) and held at 37 °C for 1 h. TSG was used to capture VLPs (or mutated VLPs) for antibody characterization because its binding epitope was excluded from the neutralizing sites. The plates were washed three times with PBST (PBS with 0.05% Tween-20, pH 7.3) followed by blocking with 0.5% skim milk (Sigma, 70166) in PBS for 30 min. After the removal of the blocking buffer, 1 µL of cell lysates containing VLPs (or mutated VLPs) was added at a dilution of 1:100 and incubated at 37 °C for 1 h. After washing three times, the conjugates (100 ng/well) were incubated for 1 h. After the final washing, freshly prepared TMB substrate (BD biosciences, Franklin Lakes, NJ, USA, 555214) was added and allowed to stand for 15 min. The reaction was stopped with 1 N HCl and measured at 450 nm with a SunriseTM Absorbance Reader (TECAN, Männedorf, Switzerland). Each test was performed in triplicate.

4.7. Expression and Purification of GST-P1

The pET-GST-P1(O97) plasmid was transferred to *Escherichia coli* (BL21) to express the recombinant GST-P1. The recombinant GST-P1 was purified from the total lysate of transformed *Escherichia coli* (BL21) by nickel-charged affinity resin (Ni Sepharose High Performance, Cytiva, Marlborough, MA, USA). The impurities were removed using phosphate-based buffer with 30 mM imidazole (Sigma-Aldrich, St. Louis, MO, USA). The recombinant GST-P1 was eluted using phosphate-based buffer with 250 mM imidazole. The imidazole was removed with a PD-10 desalting column (Cytiva, Marlborough, MA, USA).

4.8. Serum Neutralization Test (SNT)

The SNT was performed according to the OIE manual [32]. A two-fold serial dilution of sample (from 4 × –512 ×) was mixed with 100 TCID₅₀ of O/TAW/97 and held for 1 h at 37 °C. The suspended BHK-21 was added for infection and incubated for two days. After examination under a microscope for cytoplasmic effects, the highest antibody dilution that could still neutralize the virus at the 50% endpoint was regarded as the serum neutralization titer.

4.9. VLP-Based bELISA

ELISA plates were coated with 400 ng/well Q10E (or S11B) MAb and held for 1 h at 37 °C, followed by the addition of blocking buffer for 30 min. Q10E was used in standard bELISA, and S11B was used for the steric effect experiments. As a protocol for sandwich ELISA, 1 µL of VLP cell lysates were added and the mixture was held for 1 h at 37 °C. Ten-fold dilutions of each serum test sample (or dilutions of non-conjugated MAbs) in blocking buffer were added to the plates for 1 h. After washing, tracer (100 ng/well) was added and incubated for 1 h at 37 °C. After the final washing, the reaction was started using TMB substrate (BD OptEIATM, San Diego, CA, USA) and stopped with 1 N HCl. The OD value at 450 nm was measured using a SunriseTM Absorbance Reader (TECAN, Switzerland). Groups with blank blocking buffer without serum samples or antibodies were used as negative controls. The percentage of inhibition (PI) for each test sample was calculated with the following formula. Each test was performed in triplicate.

$$PI (\%) = \left(\frac{OD. \text{negative group} - OD. \text{test sample}}{OD. \text{negative group}} \right) \times 100$$

4.10. P1-Based bELISA

ELISA plates were coated with anti-GST antibodies (Sigma, G7781) and held for 1 h at 37 °C, followed by the addition of blocking buffer for 30 min. Purified GST-P1 (400 ng/well) was incubated for 1 h at 37 °C. The subsequent procedures were performed as described above.

Supplementary Materials: The supporting information can be downloaded at: <https://www.mdpi.com/article/10.3390/ijms23158542/s1>.

Author Contributions: I.-C.C. conceived the project. C.-Y.Y., M.-C.L. and S.-P.C. collected sera samples. Experiments were designed and performed by H.-W.L., except the SN test and P1 expression, which were performed by the Animal Health Research Institute and the Excelsior Bio-System Incorporation, respectively. H.-W.L. wrote the manuscript; H.-W.C., I.-C.C. and S.-P.C. revised the manuscript. All authors have read and agreed to the published version of the manuscript.

Funding: This research was funded by the Council of Agriculture, Taiwan (104AS-10.1.2-BQ-B2 and 105AS-10.4.1-BQ-B1).

Institutional Review Board Statement: The study was conducted in accordance with the ARRIVE (Animal Research: Reporting of In Vivo Experiments) guidelines, and approved by the Institutional Animal Care and Use Committee at National Taiwan University (approval number: NTU107-EL-00203, 2019) for studies involving animals.

Informed Consent Statement: Not applicable.

Data Availability Statement: The data presented in this study are available on request from the corresponding author.

Acknowledgments: We are grateful for the support from the Excelsior Bio-System Incorporation (Taipei, Taiwan, ROC), the Agricultural Technology Research Institute (ATRI), and the Animal Health Research Institute (AHRI). The authors are also indebted to Ming-Chung Deng, Chu-Hsiang Pan, Ling-Chu Hung, Tsu-Han Chen, and Seiu-Yu Lai for collecting samples and facilitating the experiments.

Conflicts of Interest: The authors declare no conflict of interest.

References

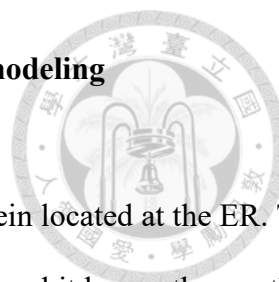
- Jamal, S.M.; Belsham, G.J. Foot-and-mouth disease: Past, present and future. *Vet. Res.* **2013**, *44*, 116. [[CrossRef](#)] [[PubMed](#)]
- Mason, P.W.; Grubman, M.J.; Baxt, B. Molecular basis of pathogenesis of FMDV. *Virus Res.* **2003**, *91*, 9–32. [[CrossRef](#)]
- Dunn, C.S.; Donaldson, A.I. Natural adaptation to pigs of a Taiwanese isolate of foot-and-mouth disease virus. *Vet. Rec.* **1997**, *141*, 174–175. [[CrossRef](#)] [[PubMed](#)]
- OIE. Foot and mouth disease. In *OIE Terrestrial Manual*; OIE: Paris, France, 2021.
- Knowles, N.J.; Samuel, A.R.; Davies, P.R.; Midgley, R.J.; Valarcher, J.F. Pandemic strain of foot-and-mouth disease virus serotype O. *Emerg. Infect. Dis.* **2005**, *11*, 1887–1893. [[CrossRef](#)] [[PubMed](#)]
- Mason, P.W.; Pacheco, J.M.; Zhao, Q.Z.; Knowles, N.J. Comparisons of the complete genomes of Asian, African and European isolates of a recent foot-and-mouth disease virus type O pandemic strain (PanAsia). *J. Gen. Virol.* **2003**, *84 Pt 6*, 1583–1593. [[CrossRef](#)]
- Wang, G.; Wang, Y.; Shang, Y.; Zhang, Z.; Liu, X. How foot-and-mouth disease virus receptor mediates foot-and-mouth disease virus infection. *Virol. J.* **2015**, *12*, 9. [[CrossRef](#)] [[PubMed](#)]
- Lawrence, P.; Rai, D.; Conderino, J.S.; Uddowla, S.; Rieder, E. Role of Jumonji C-domain containing protein 6 (JMJD6) in infectivity of foot-and-mouth disease virus. *Virology* **2016**, *492*, 38–52. [[CrossRef](#)]
- Asfor, A.S.; Upadhyaya, S.; Knowles, N.J.; King, D.P.; Paton, D.J.; Mahapatra, M. Novel antibody binding determinants on the capsid surface of serotype O foot-and-mouth disease virus. *J. Gen. Virol.* **2014**, *95 Pt 5*, 1104–1116. [[CrossRef](#)] [[PubMed](#)]
- Barnett, P.V.; Samuel, A.R.; Pullen, L.; Ansell, D.; Butcher, R.N.; Parkhouse, R.M. Monoclonal antibodies, against O1 serotype foot-and-mouth disease virus, from a natural bovine host, recognize similar antigenic features to those defined by the mouse. *J. Gen. Virol.* **1998**, *79 Pt 7*, 1687–1697. [[CrossRef](#)] [[PubMed](#)]
- Crowther, J.R.; Farias, S.; Carpenter, W.C.; Samuel, A.R. Identification of a fifth neutralizable site on type O foot-and-mouth disease virus following characterization of single and quintuple monoclonal antibody escape mutants. *J. Gen. Virol.* **1993**, *74 Pt 8*, 1547–1553. [[CrossRef](#)]
- Kitson, J.D.; McCahon, D.; Belsham, G.J. Sequence analysis of monoclonal antibody resistant mutants of type O foot and mouth disease virus: Evidence for the involvement of the three surface exposed capsid proteins in four antigenic sites. *Virology* **1990**, *179*, 26–34. [[CrossRef](#)]

13. McCahon, D.; Crowther, J.R.; Belsham, G.J.; Kitson, J.D.; Duchesne, M.; Have, P.; Melen, R.H.; Morgan, D.O.; De Simone, F. Evidence for at least four antigenic sites on type O foot-and-mouth disease virus involved in neutralization; identification by single and multiple site monoclonal antibody-resistant mutants. *J. Gen. Virol.* **1989**, *70 Pt 3*, 639–645. [[CrossRef](#)] [[PubMed](#)]
14. Grazioli, S.; Fallacara, F.; Brocchi, E. Mapping of neutralising sites on FMD virus type Asia 1 and relationships with sites described in other serotypes. In *Report of the Session of the Research Group of the Standing Committee of the European Commission of Foot and Mouth Disease*; Chania: Crete, Greece, 2004; p. 44.
15. Lee, H.W.; Deng, M.C.; Pan, C.H.; Chang, H.W.; Cheng, I.C. Neutralizing monoclonal antibodies against porcineophilic foot-and-mouth disease virus mapped to antigenic site 2 by utilizing novel mutagenic virus-like particles to detect the antigenic change. *Vet. Microbiol.* **2018**, *222*, 124–131. [[CrossRef](#)] [[PubMed](#)]
16. Ma, L.N.; Zhang, J.; Chen, H.T.; Zhou, J.H.; Ding, Y.Z.; Liu, Y.S. An overview on ELISA techniques for FMD. *Virol. J.* **2011**, *8*, 419. [[CrossRef](#)]
17. Mackay, D.K.; Bulut, A.N.; Rendle, T.; Davidson, F.; Ferris, N.P. A solid-phase competition ELISA for measuring antibody to foot-and-mouth disease virus. *J. Virol. Methods* **2001**, *97*, 33–48. [[CrossRef](#)]
18. Chenard, G.; Miedema, K.; Moonen, P.; Schrijver, R.S.; Dekker, A. A solid-phase blocking ELISA for detection of type O foot-and-mouth disease virus antibodies suitable for mass serology. *J. Virol. Methods* **2003**, *107*, 89–98. [[CrossRef](#)]
19. Ran, X.; Yang, Z.; Bai, M.; Zhang, Y.; Wen, X.; Guo, H.; Sun, S. Development and validation of a competitive ELISA based on bacterium-original virus-like particles of serotype O foot-and-mouth disease virus for detecting serum antibodies. *Appl. Microbiol. Biotechnol.* **2019**, *103*, 3015–3024. [[CrossRef](#)]
20. Salem, R.; El-Kholy, A.A.; Omar, O.A.; Abu El-Naga, M.N.; Ibrahim, M.; Osman, G. Construction, Expression and Evaluation of Recombinant VP2 Protein for serotype-independent Detection of FMDV Seropositive Animals in Egypt. *Sci. Rep.* **2019**, *9*, 10135. [[CrossRef](#)]
21. Biswal, J.K.; Bisht, P.; Mohapatra, J.K.; Ranjan, R.; Sanyal, A.; Pattnaik, B. Application of a recombinant capsid polyprotein (P1) expressed in a prokaryotic system to detect antibodies against foot-and-mouth disease virus serotype O. *J. Virol. Methods* **2015**, *215–216*, 45–51. [[CrossRef](#)]
22. Cheng, I.C.; Liang, S.M.; Tu, W.J.; Chen, C.M.; Lai, S.Y.; Cheng, Y.C.; Lee, F.; Huang, T.S.; Jong, M.H. Study on the porcineophilic foot-and-mouth disease virus I. production and characterization of monoclonal antibodies against VP1. *J. Vet. Med. Sci.* **2006**, *68*, 859–864. [[CrossRef](#)]
23. Basagoudanavar, S.H.; Hosamani, M.; Tamil Selvan, R.P.; Sreenivasa, B.P.; Saravanan, P.; Chandrasekhar Sagar, B.K.; Venkataraman, R. Development of a liquid-phase blocking ELISA based on foot-and-mouth disease virus empty capsid antigen for seromonitoring vaccinated animals. *Arch. Virol.* **2013**, *158*, 993–1001. [[CrossRef](#)] [[PubMed](#)]
24. Zhang, J.; Su, G.; Wu, Q.; Liu, J.; Tian, Y.; Liu, X.; Zhou, J.; Gao, J.; Chen, W.; Chen, D.; et al. Rab11-mediated recycling endosome role in nervous system development and neurodegenerative diseases. *Int. J. Neurosci.* **2021**, *131*, 1012–1018. [[CrossRef](#)] [[PubMed](#)]
25. Yang, M.; Xu, W.; Goolia, M.; Zhang, Z. Characterization of monoclonal antibodies against foot-and-mouth disease virus serotype O and application in identification of antigenic variation in relation to vaccine strain selection. *Virol. J.* **2014**, *11*, 136. [[CrossRef](#)]
26. Dong, H.; Liu, P.; Bai, M.; Wang, K.; Feng, R.; Zhu, D.; Sun, Y.; Mu, S.; Li, H.; Harmsen, M.; et al. Structural and molecular basis for foot-and-mouth disease virus neutralization by two potent protective antibodies. *Protein Cell* **2021**, *13*, 446–453. [[CrossRef](#)] [[PubMed](#)]
27. Wang, H.; Zhao, L.; Li, W.; Zhou, G.; Yu, L. Identification of a conformational epitope on the VP1 G-H Loop of type Asia1 foot-and-mouth disease virus defined by a protective monoclonal antibody. *Vet. Microbiol.* **2011**, *148*, 189–199. [[CrossRef](#)] [[PubMed](#)]
28. Lawrence, P.; LaRocco, M.; Baxt, B.; Rieder, E. Examination of soluble integrin resistant mutants of foot-and-mouth disease virus. *Virol. J.* **2013**, *10*, 2. [[CrossRef](#)]
29. Brown, F.; Cartwright, B. Dissociation of foot-and-mouth disease virus into its nucleic acid and protein components. *Nature* **1961**, *192*, 1163–1164. [[CrossRef](#)]
30. Mahapatra, M.; Hamblin, P.; Paton, D.J. Foot-and-mouth disease virus epitope dominance in the antibody response of vaccinated animals. *J. Gen. Virol.* **2012**, *93 Pt 3*, 488–493. [[CrossRef](#)]
31. Fuerst, T.R.; Niles, E.G.; Studier, F.W.; Moss, B. Eukaryotic transient-expression system based on recombinant vaccinia virus that synthesizes bacteriophage T7 RNA polymerase. *Proc. Natl. Acad. Sci. USA* **1986**, *83*, 8122–8126. [[CrossRef](#)]
32. Donaldson, A.I.; JKitching, R.P.; Barnett, P.V. Foot and mouth disease. In *OIE Standards Commission, Manual of Standards for Diagnostic Tests and Vaccines*; Office International des Epizooties: Paris, France, 1996; Chapter 2.1.1.

Chapter VI

Discussion





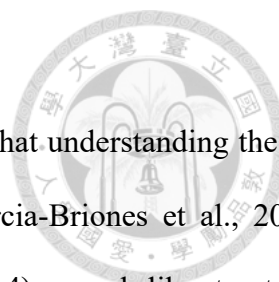
6.1 Mechanism of Foot-and-Mouth Disease Virus 3A Induced-ER Remodeling

6.1.1 Summary

In this study, we prove that FMDV 3A is a peripheral membrane protein located at the ER. The character has been revealed (Gonzalez-Magaldi et al., 2014), while we proved it by another method and tool, self-produced anti-3A monoclonal antibodies and digitonin. The distinctive patterns between full-length 3A and C-terminal truncated 3A (NHR) enforce our presumption that 3A locates at the ER and modifies it into vesicles. Without N- or C-terminus, mGFP-NHR and HRC-eGFP_{2A} appear as a web-like structure similar to the ER structure. In contrast, numerous puncta are generated by full-length of 3A and mGFP-N2HRC1. The puncta are neither COPII vesicles nor autophagosomes. Also, they are not aggregates but vesicles shown by electron tomography.

Next, we found that FMDV 3A could interact with COPII factors, Sar1 and Sec12. Knockdown of Sar1 or Sec12 would inhibit 3A puncta formation. Sar1 can interact with all portions of 3A, especially with N1 (aa 1-41) and HR (aa 59-76) regions. Because D198A mutation on Sar1 would inhibit the interaction of both N2 (aa 42-58) and C1 (aa 77-92) regions, there is a scenario where a single 3A protein connects to the same place of two Sar1. Different from Sar1, the binding sites for Sec12 focus on the C2 (aa 93-153) region of 3A. The formation of 3A puncta would be inhibited by mutated Sar1, including D198A, T39N, or QTTG mutation. However, more 3A puncta would be induced by constitutive Sar1-GTP, H79G mutation.

We hypothesize that FMDV 3A binds inactive Sar1 and Sec12 on the ER, enhancing Sar1 activation. Two active Sar1 bind 3A to curve ER membrane into vesicles. This hypothesis seems reasonable based on our data but requires more supporting evidence, especially by the experiment *de novo*. For example, giant unilateral vesicles (GUVs) (Long et al., 2010) should be modified into small vesicles by purified Sar1 and 3A. In cell-free vesicle budding reaction (Melville et al., 2019; Yuan et al., 2018), 3A and Sar1 should generate 3A-vesicles from donor ER membranes.



6.1.2 The model of 3A expressing cells

To understand the mechanism of FMDV RO formation, we believe that understanding the 3A protein should be the key. The 3A patterns from FMDV-infected (Garcia-Briones et al., 2006; O'Donnell et al., 2001) or 3A-expressing cells (Gonzalez-Magaldi et al., 2014) are web-like structures with puncta. Some describe it as a diffuse reticular structure (Moffat et al., 2005), while, according to the pictures, it is just a different description. Some show a clear reticular pattern in infected cells (Midgley et al., 2013). In our experience, parts of the puncta would be disrupted after cell fixation. Because of these, we prefer to examine mGFP-3A in live cells without fixation. Similarly, in electron tomography, structures shown by APEX2-NHR are much easier to observe and identify than those by APEX2-3A. The modified 3A-vesicles are vulnerable, which should be the same for FMDV RO.

The ER was dramatically dilated by poliovirus (PV) 3A expression (Doedens et al., 1997), showing no vesicles or tubules similar to PV RO. It was co-expression of PV 3A and 2BC that would induce vesicles resembling PV RO (Suhy et al., 2000). However, the precursor, 3AB protein, instead of 3A, is dominant in PV-infected cells; studying PV 3AB protein might be more suitable for PV 3A. In addition, FMDV 3A is longer than that of other picornaviruses. This fact might imply that FMDV undergoes a different mechanism for RO formation. In our study, FMDV 2B and 2C colocalized with ER marker did not induce ER disruption. We cannot exclude the contribution from 2B and 2C for FMDV RO, although they should not be a primary cause.

6.1.3 Secretory pathway not blocked by FMDV 3A

An anonymous objector disagreed with our supposition and argued that if FMDV 3A disrupts the COPII pathway, why 3A does not inhibit protein trafficking? That FMDV 3A would not block the secretory pathway stemmed from the study using the tsO45 VSV-G trafficking model (Moffat et al., 2005). First, I agree with the view that this trafficking model cannot monitor the COPII pathway in some conditions (see 1.2.2). Besides, our hypothesis includes enhancement of Sar1 activation by

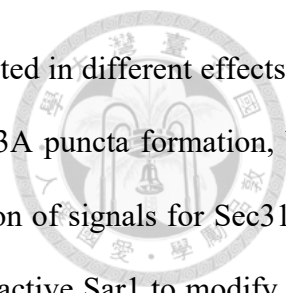
3A. In other words, 3A hijacks Sar1 and enhances its activation, which cannot be described as a "simple" inhibition or activation of the COPII pathway. Based on Sec31 dispersion and downregulation by 3A expression, the evidence is strong enough to claim that 3A disrupts COPII machinery.

6.1.4 Lack evidence of viral infection

Viral protein expression cannot simulate the actual situation in viral infection. However, studying the effect of viral protein should be acceptable and reasonable for understanding the virus. After all, the virus life cycle includes viral entry, translation, host organelles modification, viral RNA duplication, counter-attacking anti-viral activity, and viral release. When each part of the event is blocked, it all results in decreased virus replication (decreased virus titer). For example, knockdown of Sar1 would inhibit FMDV (Midgley et al., 2013). However, it cannot illustrate why FMDV requires Sar1, even though the ER remains intact in Sar1 knockdown cells after exposure to the virus. No viral replication also indicates no detectable viral protein synthesis. On the contrary, 3A expression in Sar1 knockdown cells can be more convincing for proving that 3A utilizes Sar1 for ER remodeling.

The replication-independent expression system should be a theoretical solution to the problem (Melia et al., 2017). In this system, no RNA amplification occurs because of defective 5'NTR. All viral proteins are translated from mRNA. However, the problem would be biosafety. Even though it should be safe, performing in a negative pressure lab is still inappropriate in Taiwan. Furthermore, the technique and platform need much time and effort.

Although our study lacks supporting evidence of a viral infection, the experiments conducted by Midgley and colleagues can fit our model (Midgley et al., 2013). 1) Knockdown of Sar1 inhibited FMDV infection. In my study, Sar1 knockdown would inhibit 3A puncta formation. 2) FMDV was inhibited by constitutive Sar1-GDP but not constitutive Sar1-GTP. In theory, both constitutive Sar1-



GDP and Sar1-GTP should inhibit COPII vesicle formation, but they resulted in different effects on FMDV replication. In my experiments, constitutive Sar1-GDP inhibited 3A puncta formation, but Sar1-GTP enhanced. 3) FMDV infection causes the dispersal and reduction of signals for Sec31 in IFA (Midgley et al., 2013). In our model, FMDV 3A utilizes and hijacks active Sar1 to modify the ER, affecting the normal function for Sec31. Of course, 3A expression causes dispersal and downregulation of Sec31.

6.1.5 The role of dimerization of 3A

3A dimerization is essential for FMDV replication. The dimerization depends on alpha helix 1 and 2 (Gonzalez-Magaldi et al., 2014), mostly located in the N1 region (1-41). Several picornaviral 3A would dimerize, which is essential for viruses (Jackson and Belsham, 2021; Strauss et al., 2003). However, biological meaning has not been revealed. When the N1 region was removed, truncated 3A can still induce ER disruption and dynamic vesicles. Therefore, ER remodeling is independent of 3A dimerization. In our studies, we cannot find any clues as to why 3A dimerization is essential for viral replication.

6.1.6 3A-induced autophagy

FMDV infection would induce autophagy in favor of the virus. Some suggest autophagy improves viral replication, like enterovirus (O'Donnell et al., 2011). Some point out that autophagy facilitates infection during viral entry (Berryman et al., 2012); others claim that autophagy suppresses antiviral interferon response, then promotes the viruses (Ranjitha et al., 2020). Several viral proteins would trigger autophagy. FMDV 2B protein disturbs cellular Ca^{2+} homeostasis, thereby inducing autophagy (Han et al., 2016). Viral VP2 expression triggers ER stress through EIFS1, inhibiting mTOR and activating autophagy. EIFS1 is a subunit of eIF2 α , which would be phosphorylated by PERK (Sun et al., 2018). Viral 3A protein was reported to trigger autophagy. However, the study

examined the cell lines constitutively expressing 3A (H et al., 2021), which might be an ideal approach to studying autophagy.

Sar1 is required for autophagosome formation because COPII vesicles (or ERGIC) provide lipid bilayers for PAS (Phagophore association site) (Bento et al., 2013; Zoppino et al., 2010). Therefore, when the COPII pathway is blocked, activation of autophagy would be inhibited by association. According to our findings, 3A hijacks Sar1 for ER remodeling, disrupting the COPII pathway, but enhances Sar1 activation. Whether 3A induces autophagy should be examined thoroughly. At least, we cannot detect significant autophagy activation or inhibition by 3A.

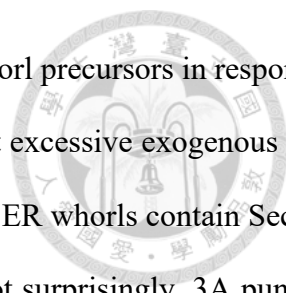
6.1.7 Examples for co-interacting with Sar1 and Sec12

Our study shows two novel interactions, 3A-Sar1 and 3A-Sec12. The binding sites range from different regions on 3A. We speculate that these seemingly "redundant" interactions, called by the objectors, aim to enhance Sar1 activation.

Two publications claim a protein can interact with Sar1 and Sec12. One is for studying Wntless (WLS), a Wnt receptor integrating into the ER membrane (Sun et al., 2017). They proved that both interacting abilities toward Sar1 and Sec12 were essential for packaging Wnts into COPII vesicles (Sun et al., 2017). The other is Fatty-acid binding protein 5 (FABP5) (Melville et al., 2019). Based on cell-free vesicle budding reaction, Melville and colleagues claimed that FABP5 could enhance GTP loading for Sar1 by binding to Sar1 and Sec12 (Melville et al., 2019).

To prove the enhancement of Sar1 activation, we performed an active Sar1 pulldown assay (NewEast Biosciences, 81801) but failed, which means no active Sar1 was pulled down even in positive control, adding abundant GTP into the cell lysates. Therefore, it is reasonable speculation required to be proved in the future.

6.1.7 Speculation of 3A vesicles as ER whorl precursors

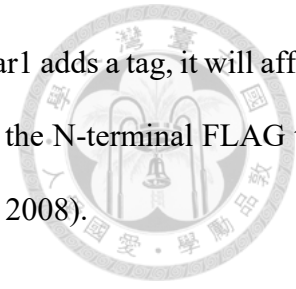


An anonymous rejector disputed that 3A-vesicles were merely ER whorl precursors in response to ER stress (Xu et al., 2021). In other words, it is a worthless finding that excessive exogenous 3A proteins, of course, trigger ER stress for protein translation inhibition. The ER whorls contain Sec61 and PERK, excluding calreticulin, Sec13, and Sec31 (Xu et al., 2021); Not surprisingly, 3A puncta showed no colocalization with mCherry-ER, Sec31A, and Sec24A. However, the ER whorl formation requires the normal function of COPII machinery, in which Sar1 and other COPII factors (Sec13 and Sec24) must be functional (Xu et al., 2021). Constitutive Sar1-GTP (mutated Sar1-H79G) would significantly inhibit ER whorl precursors (Sec61 as a marker) in an *in vitro* COPII budding assay (Xu et al., 2021). By contrast, according to our experiments, Sar1-H79G expression promoted 3A puncta formation. Though, Xu and colleagues did not show many fluorescent images for ER whorl “precursors”. None of the patterns for Sec61 was similar to that for mGFP-3A or mGFP-N2HRC1. Honestly, the pattern similar to ER whorl was occasionally detected, especially in Sar1 (or Sec12) knockdown assays. However, disruption of the ER was found prior to the presence of the whorl, not to mention that only a minor population of 3A expressing cells showed the whorls. According to the reference, the ER is intact when the ER whorl pathway activates (Xu et al., 2021). Therefore, 3A puncta formation should not be irrelevant to ER whorls. Most importantly, numerous studies show that 3A appears as puncta in FMDV infected cells in IFA, indicating that 3A vesicles were not formed merely because of overexpression in transfected cells. The reviewer even claimed that no such structure similar to 3A vesicles had been observed in FMDV infected cells. I have nothing to say if he (or she) means virologists misinterpret FMDV RO.

6.1.8 The query about N-terminal FLAG tag on Sar1

An anonymous rejector doubted the experimental design that the N-terminal FLAG tag on Sar1 would affect its activation. Actually, Sar1 with C-terminal Myc tag used to be conducted in the co-IP assay due to the concern, but, in that condition, 3A from the elution was undetectable. According to

Sar1-3A intercalating model, it is reasonable that when the C terminus of Sar1 adds a tag, it will affect the binding toward 3A. In addition, several researchers used this strategy, the N-terminal FLAG tag on Sar1, to study the COPII pathway (Long et al., 2010; Yamayoshi et al., 2008).



6.1.9 The query about the importance of our findings and C terminus of 3A

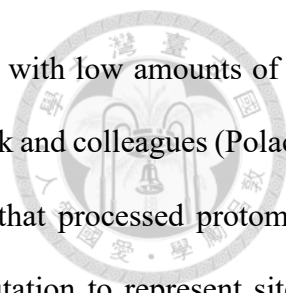
An anonymous rejector questioned that the virus with a large internal deletion in the C terminus of 3A would not affect the porcine infection, meaning the entire C terminus is dispensable for virus replication. First of all, the deletion for O/TW/97 3A and super-deleted artificial strain spans between aa 93-102 and aa 93-144, and the cattle attenuated deletion virus by Pacheco and colleagues was generated by aa 87-106 deletion of 3A (Pacheco et al., 2013; Pacheco et al., 2003). All deletions were not entire C terminus; they preserved the region between aa 77-87 beside the hydrophobic domain (Pacheco et al., 2013). Although the preserved region is slightly shorter than the C1 domain (77-92), it might still preserve the binding activity to Sar1.

Behura and colleagues modified Asia 1 IND 491/1997 strain into Asia 1 IND 491/1997Δ3A81-153 that the entire 3A C terminus, including the 3A-3B₁ cleavage site, was removed (Behura et al., 2016). They claimed the artificial virus grew equally well as the parental virus in BHK-21, LFBK (a pig kidney cell line, they claimed), and IBRS-2 cells. If there are no differences in 3A-patterns and ultrastructures within infected cells by these two strains in IFA and TEM, it should be an undeniable fact against our hypothesis. However, the information about the deletion virus is too few to discuss further.

6.2 Diagnostic Application of Virus-Like Particles

6.2.1 Summary

Our first step is to characterize neutralizing MAbs against O/TAW/97 (O/97) in this study. However, neutralization sites in serotype O, except for site 1, are conformational epitopes requiring



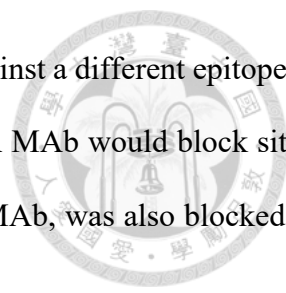
subunits assembly. To present authentic antigenicity, we co-expressed P1 with low amounts of 3C protease for producing virus-like particles (VLPs), as in the study by Polacek and colleagues (Polacek et al., 2013). Sucrose gradient centrifugation followed by TEM proved that processed protomers assembled into VLPs. Among critical residues, we chose VP2-S72N mutation to represent site 2 mutated VLP. After screening out site 2 MAbs by these two VLPs, site 2 MAbs were applied to examine the virus strain, O/Penghu/2012. This strain evolved from O/TAW/97. As a result, all characterized site 2 MAbs cannot recognize O/Penghu/2012, indicating that site 2 has been altered after 15 years of evolution in the field.

Next, we identified S11B MAb recognizes site 3 by the same strategy. We further developed a bELISA with VLP or P1 as the antigen, paired with site 1, site 2, site 3, and non-neutralizing MAb. After testing on 63 samples, two bELISA pairs, VLP:S11B and P1:Q10E, showed the highest performance regarding the correlation with SNT. Excluding weakly positive serum samples (SN = 16–32, n = 14), the sensitivity and specificity were 95.65% and 96.15% (kappa = 0.92) for VLP:S11B.

6.2.2 Escape site 2 mutants in nature

In 1997, O/97 caused a severe outbreak in Taiwan. At that moment, the Taiwan government implemented a mandatory vaccination with inactivated serotype O strains, including O/98, which is homologous to O/97. Within almost 15 years, sporadic events were caused by this series of virus strains, and O/Penghu/2012 was the last isolate from the field. During these years, herd immunity created strong selective pressure for O/97. Five out of eight critical residues of site 2 have been changed in O/Penghu/2012, indicating the importance of site 2 for escaping antibodies' neutralization. In line with this, site 2 had been proved immunodominant in vaccinated animals (Mahapatra et al., 2012).

6.2.3 Diverse steric effects between antibodies



In the simulation in Chimera software, it is evident that antibodies against a different epitope on the FMD virion would inevitably block each other. Therefore, site 2 P11A MAb would block site 1 Q10E MAb and site 3 S11B MAb. Meanwhile, TSG, a non-neutralizing MAb, was also blocked by P11A and S11B. However, TSG barely blocked P11A and S11B.

An anonymous objector argued that not detecting the steric effect should be because MAbs are not saturated on the antigens. However, if unsaturation is a primary cause, all PI values should be the same because all pairs were compared in the same concentration, and the adding order should not affect the results. As the discussion in our publication, we defined the region of steric effect into "core" and "marginal" regions, which indicate "antibody binding sites" and "the region affected by Fc portion or other Fab of antibodies", respectively. When antibodies have bound to VLPs, they would almost not be replaced by another and create a marginal region shielding the following adding antibodies. The following antibodies' affinity should be one factor for staying in the marginal region. For example, P11A can possibly stay at the marginal region shielded by Q10E, while TSG cannot. When discussing the steric effect in bELISA, it is not a Zero-Sum Game.

6.3 Conclusion and Future Works

Although several studies focused on how FMDV invades the cells, few studies have examined virus-induced endomembrane remodeling. In our studies, we raised a hypothesis for 3A-induced ER remodeling, which is distinct from the COPII pathway (Fig. 1). However, it still needs much more convincing evidence. In the future, we can perform a GUVs system with fluorescent lipids. After adding purified constitutive Sar1-GTP, the giant vesicle should turn into a tube bundle, as in the study by Long and colleagues (Long et al., 2010). Next, further adding purified mGFP-3A or 3A, small vesicles with 3A should be formed according to our hypothesis. In a cell-free vesicle budding reaction (Melville et al., 2019; Yuan et al., 2018), 3A vesicles should be generated after the donor ER membrane is mixed with purified 3A and constitutive Sar1-GTP, just like COPII vesicle budding

assay. Besides, Sec23 and Sec31 are not colocalized with 3A puncta, and constitutive Sar1-GTP enhances 3A puncta formation. It is reasonable to claim that 3A vesicle formation differs from the COPII pathway, and COPII coat proteins are dispensable. However, the knockdown of Sec23 or Sec31 should be more intuitive and direct evidence to show that 3A vesicle is independent of the COPII pathway. It could be our future work. Moreover, the enhancement of Sar1 activation by 3A also requires direct evidence.

Compared to enterovirus, studies for FMDV RO are rare. Even RO's morphology shows relatively less information and lacks a three-dimensional model, so we cannot call FMDV ROs single membranous vesicles under the strict definition. If infectious clones were allowed and established, we could try to create an artificial virus with APEX2 on 3A N-terminus, followed by the same procedure in our studies for electron tomography. It would be more convincing for some people that FMDV RO is a natural and functional structure.

In the part of virus-like particles, two critical points should be addressed. First, unprocessed P1 can present site 1 and site 2, while it should be a pentamer that can present site 3 (Fig. 1). It shows the importance of authentic antigenicity. Secondly, antibodies are large and inevitably interfere with other antibodies that bind to different epitopes (Fig. 1). Therefore, detecting specific antibodies based on blocking ELISA with MAbs is almost impossible. However, according to the results, the performance of the pairs for S11B MAb and VLP was outstanding, possibly because it also detects some site 1 and site 2 antibodies in the serum.

We have proved that both Q10E MAb and S11B MAb can recognize O/TAW/99 (data not shown). Considering Cathay topotype virus strains (O/TAW/97 related strains) are not prevalent worldwide, we can directly replace the antigens with those from O/TAW/99 to make this system more practical for widely used.

Besides, monitoring the antigenic shift from O/TAW/97 to O/Penghu/2012 would be an intriguing topic. Now, we only examine the start and the final, O/97 and O/12. According to the

reports from OIE, several strains were isolated, including O/02/02/2009, O/12/02/2010, O/30/10/2011, etcetera. Examining the amino acid sequence and performing IFA by these anti-O/97 MAbs for these strains should show a beautiful process of evolution for O/97. That is, how does O/97 escape antibodies raised by herd immunity?

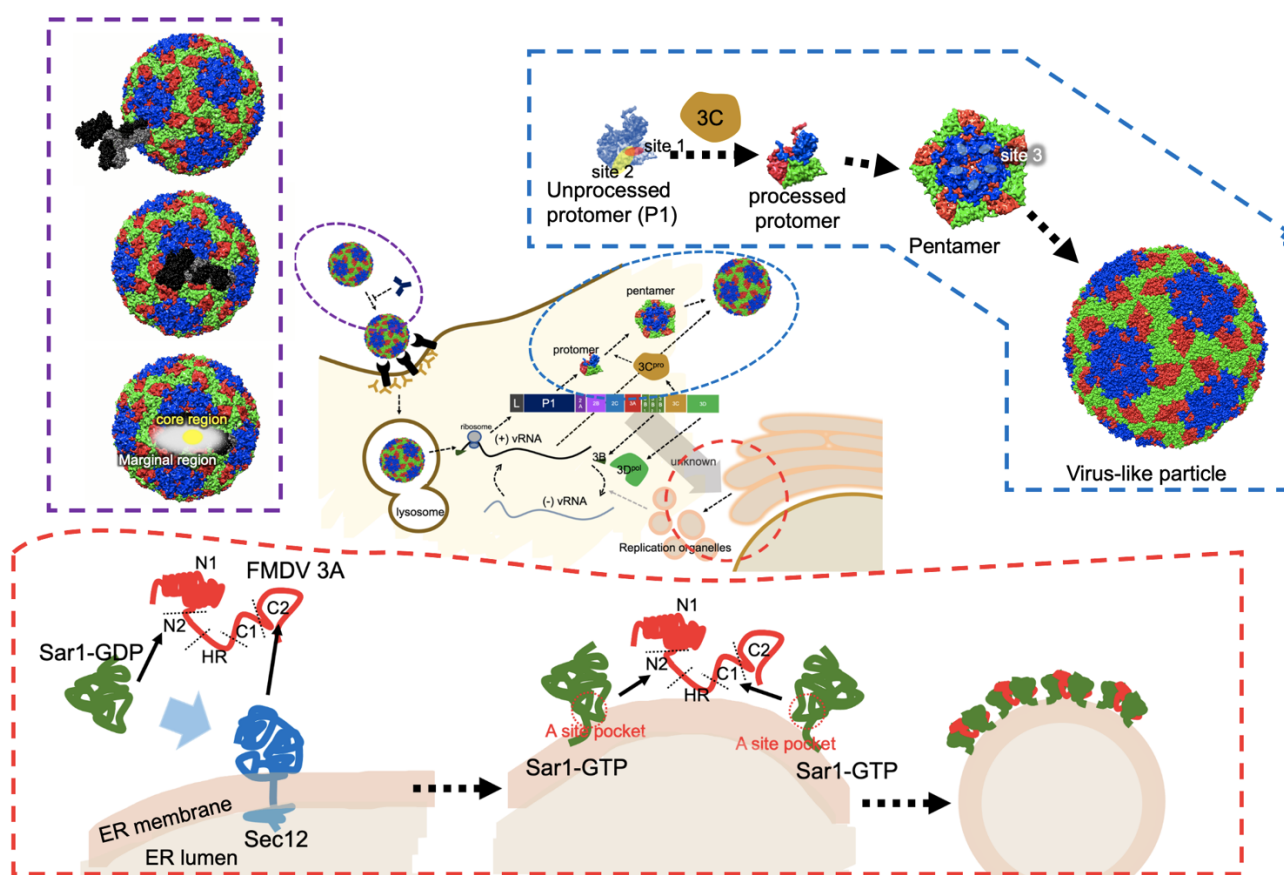
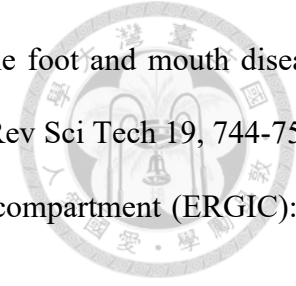


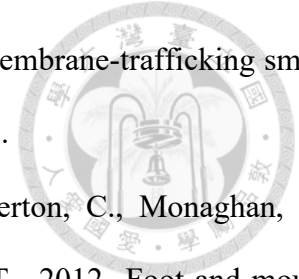
Figure 1. The summary of findings and critical points in the dissertation. The red frame indicates the hypothesis for 3A-induced ER remodeling. The VLP production process and neutralizing site formation were shown in the blue frame. Purple illustrates the dimension of steric effect by an antibody, which can be defined as core and marginal regions.

References

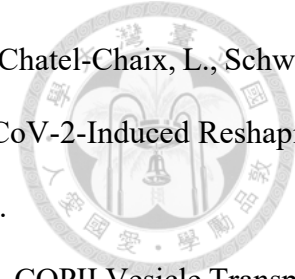
Abrams, C.C., King, A.M., Belsham, G.J., 1995. Assembly of foot-and-mouth disease virus empty capsids synthesized by a vaccinia virus expression system. *J Gen Virol* 76 (Pt 12), 3089-3098.



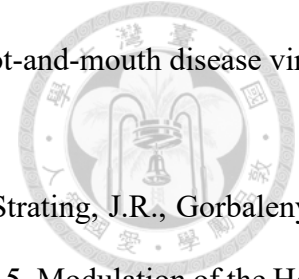
- Aktas, S., Samuel, A.R., 2000. Identification of antigenic epitopes on the foot and mouth disease virus isolate O1/Manisa/Turkey/69 using monoclonal antibodies. *Rev Sci Tech* 19, 744-753.
- Appenzeller-Herzog, C., Hauri, H.P., 2006. The ER-Golgi intermediate compartment (ERGIC): in search of its identity and function. *J Cell Sci* 119, 2173-2183.
- Arita, M., Kojima, H., Nagano, T., Okabe, T., Wakita, T., Shimizu, H., 2013. Oxysterol-binding protein family I is the target of minor enviroxime-like compounds. *J Virol* 87, 4252-4260.
- Asfor, A.S., Upadhyaya, S., Knowles, N.J., King, D.P., Paton, D.J., Mahapatra, M., 2014. Novel antibody binding determinants on the capsid surface of serotype O foot-and-mouth disease virus. *J Gen Virol* 95, 1104-1116.
- Barnett, P.V., Samuel, A.R., Pullen, L., Ansell, D., Butcher, R.N., Parkhouse, R.M., 1998. Monoclonal antibodies, against O1 serotype foot-and-mouth disease virus, from a natural bovine host, recognize similar antigenic features to those defined by the mouse. *J Gen Virol* 79 (Pt 7), 1687-1697.
- Beard, C.W., Mason, P.W., 2000. Genetic determinants of altered virulence of Taiwanese foot-and-mouth disease virus. *J Virol* 74, 987-991.
- Behura, M., Mohapatra, J.K., Pandey, L.K., Das, B., Bhatt, M., Subramaniam, S., Pattnaik, B., 2016. The carboxy-terminal half of nonstructural protein 3A is not essential for foot-and-mouth disease virus replication in cultured cell lines. *Arch Virol* 161, 1295-1305.
- Belov, G.A., Feng, Q., Nikovics, K., Jackson, C.L., Ehrenfeld, E., 2008. A critical role of a cellular membrane traffic protein in poliovirus RNA replication. *PLoS Pathog* 4, e1000216.
- Belov, G.A., Nair, V., Hansen, B.T., Hoyt, F.H., Fischer, E.R., Ehrenfeld, E., 2012. Complex dynamic development of poliovirus membranous replication complexes. *J Virol* 86, 302-312.
- Belsham, G.J., McInerney, G.M., Ross-Smith, N., 2000. Foot-and-mouth disease virus 3C protease induces cleavage of translation initiation factors eIF4A and eIF4G within infected cells. *J Virol* 74, 272-280.



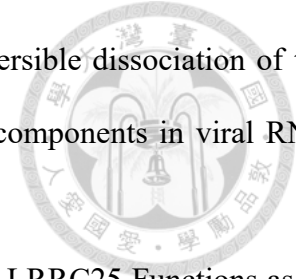
- Bento, C.F., Puri, C., Moreau, K., Rubinsztein, D.C., 2013. The role of membrane-trafficking small GTPases in the regulation of autophagy. *J Cell Sci* 126, 1059-1069.
- Berryman, S., Brooks, E., Burman, A., Hawes, P., Roberts, R., Netherton, C., Monaghan, P., Whelband, M., Cottam, E., Elazar, Z., Jackson, T., Wileman, T., 2012. Foot-and-mouth disease virus induces autophagosomes during cell entry via a class III phosphatidylinositol 3-kinase-independent pathway. *J Virol* 86, 12940-12953.
- Berryman, S., Moffat, K., Harak, C., Lohmann, V., Jackson, T., 2016. Foot-and-mouth disease virus replicates independently of phosphatidylinositol 4-phosphate and type III phosphatidylinositol 4-kinases. *J Gen Virol* 97, 1841-1852.
- Carter, A.P., Diamant, A.G., Urnavicius, L., 2016. How dynein and dynactin transport cargos: a structural perspective. *Curr Opin Struct Biol* 37, 62-70.
- Chatel-Chaix, L., Bartenschlager, R., 2014. Dengue virus- and hepatitis C virus-induced replication and assembly compartments: the enemy inside--caught in the web. *J Virol* 88, 5907-5911.
- Chen, Y.H., Du, W., Hagemeijer, M.C., Takvorian, P.M., Pau, C., Cali, A., Brantner, C.A., Stempinski, E.S., Connelly, P.S., Ma, H.C., Jiang, P., Wimmer, E., Altan-Bonnet, G., Altan-Bonnet, N., 2015. Phosphatidylserine vesicles enable efficient en bloc transmission of enteroviruses. *Cell* 160, 619-630.
- Cheng, I.C., Liang, S.M., Tu, W.J., Chen, C.M., Lai, S.Y., Cheng, Y.C., Lee, F., Huang, T.S., Jong, M.H., 2006. Study on the porcineophilic foot-and-mouth disease virus I. production and characterization of monoclonal antibodies against VP1. *J Vet Med Sci* 68, 859-864.
- Ci, Y., Liu, Z.Y., Zhang, N.N., Niu, Y., Yang, Y., Xu, C., Yang, W., Qin, C.F., Shi, L., 2020. Zika NS1-induced ER remodeling is essential for viral replication. *J Cell Biol* 219.
- Cortese, M., Lee, J.Y., Cerikan, B., Neufeldt, C.J., Oorschot, V.M.J., Kohrer, S., Hennies, J., Schieber, N.L., Ronchi, P., Mizzon, G., Romero-Brey, I., Santarella-Mellwig, R., Schorb, M., Boermel, M., Mocaer, K., Beckwith, M.S., Templin, R.M., Gross, V., Pape, C., Tischer, C., Frankish,



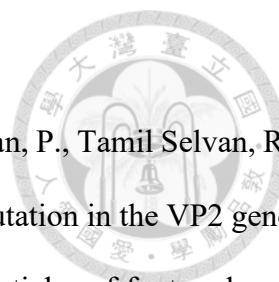
- J., Horvat, N.K., Laketa, V., Stanifer, M., Boulant, S., Ruggieri, A., Chatel-Chaix, L., Schwab, Y., Bartenschlager, R., 2020. Integrative Imaging Reveals SARS-CoV-2-Induced Reshaping of Subcellular Morphologies. *Cell Host Microbe* 28, 853-866 e855.
- Crawford, S.E., Criglar, J.M., Liu, Z., Broughman, J.R., Estes, M.K., 2019. COPII Vesicle Transport Is Required for Rotavirus NSP4 Interaction with the Autophagy Protein LC3 II and Trafficking to Viroplasms. *J Virol* 94.
- Crowther, J.R., Farias, S., Carpenter, W.C., Samuel, A.R., 1993. Identification of a fifth neutralizable site on type O foot-and-mouth disease virus following characterization of single and quintuple monoclonal antibody escape mutants. *J Gen Virol* 74 (Pt 8), 1547-1553.
- Cruz, L., Buchkovich, N.J., 2017. Rerouting the traffic from a virus perspective. *Front Biosci (Landmark Ed)* 22, 1845-1866.
- de Los Santos, T., Diaz-San Segundo, F., Grubman, M.J., 2007. Degradation of nuclear factor kappa B during foot-and-mouth disease virus infection. *J Virol* 81, 12803-12815.
- Deepak, P.R., Saravanan, P., Biswal, J.K., Basagoudanavar, S.H., Dechamma, H.J., Umapathi, V., Sreenivasa, B.P., Tamilselvan, R.P., Krishnaswamy, N., Zaffer, I., Sanyal, A., 2019. Generation of acid resistant virus like particles of vaccine strains of foot-and-mouth disease virus (FMDV). *Biologicals* 60, 28-35.
- Deitz, S.B., Dodd, D.A., Cooper, S., Parham, P., Kirkegaard, K., 2000. MHC I-dependent antigen presentation is inhibited by poliovirus protein 3A. *Proc Natl Acad Sci U S A* 97, 13790-13795.
- den Boon, J.A., Ahlquist, P., 2010. Organelle-like membrane compartmentalization of positive-strand RNA virus replication factories. *Annu Rev Microbiol* 64, 241-256.
- Dodd, D.A., Giddings, T.H., Jr., Kirkegaard, K., 2001. Poliovirus 3A protein limits interleukin-6 (IL-6), IL-8, and beta interferon secretion during viral infection. *J Virol* 75, 8158-8165.
- Dodding, M.P., Way, M., 2011. Coupling viruses to dynein and kinesin-1. *EMBO J* 30, 3527-3539.
- Dong, H., Liu, P., Bai, M., Wang, K., Feng, R., Zhu, D., Sun, Y., Mu, S., Li, H., Harmsen, M., Sun,



- S., Wang, X., Guo, H., 2021. Structural and molecular basis for foot-and-mouth disease virus neutralization by two potent protective antibodies. *Protein Cell*.
- Dorobantu, C.M., Albuлесcu, L., Harak, C., Feng, Q., van Kampen, M., Strating, J.R., Gorbalenya, A.E., Lohmann, V., van der Schaar, H.M., van Kuppeveld, F.J., 2015. Modulation of the Host Lipid Landscape to Promote RNA Virus Replication: The Picornavirus Encephalomyocarditis Virus Converges on the Pathway Used by Hepatitis C Virus. *PLoS Pathog* 11, e1005185.
- Dorobantu, C.M., Albuлесcu, L., Lyoo, H., van Kampen, M., De Francesco, R., Lohmann, V., Harak, C., van der Schaar, H.M., Strating, J.R., Gorbalenya, A.E., van Kuppeveld, F.J., 2016. Mutations in Encephalomyocarditis Virus 3A Protein Uncouple the Dependency of Genome Replication on Host Factors Phosphatidylinositol 4-Kinase IIIalpha and Oxysterol-Binding Protein. *mSphere* 1.
- Dorobantu, C.M., van der Schaar, H.M., Ford, L.A., Strating, J.R., Ulferts, R., Fang, Y., Belov, G., van Kuppeveld, F.J., 2014. Recruitment of PI4KIIIbeta to coxsackievirus B3 replication organelles is independent of ACBD3, GBF1, and Arf1. *J Virol* 88, 2725-2736.
- Du, Y., Bi, J., Liu, J., Liu, X., Wu, X., Jiang, P., Yoo, D., Zhang, Y., Wu, J., Wan, R., Zhao, X., Guo, L., Sun, W., Cong, X., Chen, L., Wang, J., 2014. 3Cpro of foot-and-mouth disease virus antagonizes the interferon signaling pathway by blocking STAT1/STAT2 nuclear translocation. *J Virol* 88, 4908-4920.
- Du, Y., Duan, T., Feng, Y., Liu, Q., Lin, M., Cui, J., Wang, R.F., 2018. LRRC25 inhibits type I IFN signaling by targeting ISG15-associated RIG-I for autophagic degradation. *EMBO J* 37, 351-366.
- Dunn, C.S., and A. I. Donaldson, 1997. Natural adaptation to pigs of a Taiwanese isolate of foot-and-mouth disease virus. *Vet. Rec* 141:174-175.
- Dwivedi, D., Chawla, P., Sharma, M., 2019. Incorporating Motility in the Motor: Role of the Hook Protein Family in Regulating Dynein Motility. *Biochemistry* 58, 1026-1031.




- Egger, D., Pasamontes, L., Bolten, R., Boyko, V., Bienz, K., 1996. Reversible dissociation of the poliovirus replication complex: functions and interactions of its components in viral RNA synthesis. *J Virol* 70, 8675-8683.
- Feng, Y., Duan, T., Du, Y., Jin, S., Wang, M., Cui, J., Wang, R.F., 2017. LRRC25 Functions as an Inhibitor of NF-kappaB Signaling Pathway by Promoting p65/RelA for Autophagic Degradation. *Sci Rep* 7, 13448.
- Flint, S.J., Racaniello, V.R., Rall, G.F., Skalka, A.M., Enquist, L.W., 2015. Principles of virology, 4th edition. Edition. ASM Press, Washington, DC, volumes p.
- Fromme, J.C., Orci, L., Schekman, R., 2008. Coordination of COPII vesicle trafficking by Sec23. *Trends Cell Biol* 18, 330-336.
- Fry, E.E., Newman, J.W.I., Curry, S., Najjam, S., Jackson, T., Blakemore, W., Lea, S.M., Miller, L., Burman, A., King, A.M.Q., Stuart, D.I., 2005. Structure of Foot-and-mouth disease virus serotype A10 61 alone and complexed with oligosaccharide receptor: receptor conservation in the face of antigenic variation. *J Gen Virol* 86, 1909-1920.
- Fu, S.Z., Yang, W.P., Ru, Y., Zhang, K.S., Wang, Y., Liu, X.T., Li, D., Zheng, H.X., 2019. DDX56 cooperates with FMDV 3A to enhance FMDV replication by inhibiting the phosphorylation of IRF3. *Cell Signal* 64, 109393.
- Fuerst, T.R., Niles, E.G., Studier, F.W., Moss, B., 1986. Eukaryotic transient-expression system based on recombinant vaccinia virus that synthesizes bacteriophage T7 RNA polymerase. *Proc Natl Acad Sci U S A* 83, 8122-8126.
- Fujita, K., Krishnakumar, S.S., Franco, D., Paul, A.V., London, E., Wimmer, E., 2007. Membrane topography of the hydrophobic anchor sequence of poliovirus 3A and 3AB proteins and the functional effect of 3A/3AB membrane association upon RNA replication. *Biochemistry* 46, 5185-5199.
- Gamarnik, A.V., Andino, R., 1998. Switch from translation to RNA replication in a positive-stranded

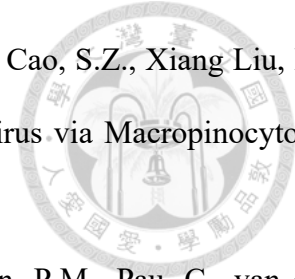


RNA virus. *Genes Dev* 12, 2293-2304.

- Ganji, V.K., Biswal, J.K., Lalzampua, H., Basagoudanavar, S.H., Saravanan, P., Tamil Selvan, R.P., Umaphathi, V., Reddy, G.R., Sanyal, A., Dechamma, H.J., 2018. Mutation in the VP2 gene of P1-2A capsid protein increases the thermostability of virus-like particles of foot-and-mouth disease virus serotype O. *Appl Microbiol Biotechnol* 102, 8883-8893.
- Garcia, M.A., Meurs, E.F., Esteban, M., 2007. The dsRNA protein kinase PKR: virus and cell control. *Biochimie* 89, 799-811.
- Garcia-Briones, M., Rosas, M.F., Gonzalez-Magaldi, M., Martin-Acebes, M.A., Sobrino, F., Armas-Portela, R., 2006. Differential distribution of non-structural proteins of foot-and-mouth disease virus in BHK-21 cells. *Virology* 349, 409-421.
- Gladue, D.P., O'Donnell, V., Baker-Bransetter, R., Pacheco, J.M., Holinka, L.G., Arzt, J., Pauszek, S., Fernandez-Sainz, I., Fletcher, P., Brocchi, E., Lu, Z., Rodriguez, L.L., Borca, M.V., 2014. Interaction of foot-and-mouth disease virus nonstructural protein 3A with host protein DCTN3 is important for viral virulence in cattle. *J Virol* 88, 2737-2747.
- Godi, A., Pertile, P., Meyers, R., Marra, P., Di Tullio, G., Iurisci, C., Luini, A., Corda, D., De Matteis, M.A., 1999. ARF mediates recruitment of PtdIns-4-OH kinase-beta and stimulates synthesis of PtdIns(4,5)P2 on the Golgi complex. *Nat Cell Biol* 1, 280-287.
- Gonzalez-Magaldi, M., Martin-Acebes, M.A., Kremer, L., Sobrino, F., 2014. Membrane topology and cellular dynamics of foot-and-mouth disease virus 3A protein. *PLoS One* 9, e106685.
- Gonzalez-Magaldi, M., Postigo, R., de la Torre, B.G., Vieira, Y.A., Rodriguez-Pulido, M., Lopez-Vinas, E., Gomez-Puertas, P., Andreu, D., Kremer, L., Rosas, M.F., Sobrino, F., 2012. Mutations that hamper dimerization of foot-and-mouth disease virus 3A protein are detrimental for infectivity. *J Virol* 86, 11013-11023.
- Grazioli, S., Fallacara, F., Brocchi, E., 2013. Mapping of antigenic sites of foot-and-mouth disease virus serotype Asia 1 and relationships with sites described in other serotypes. *J Gen Virol* 94,

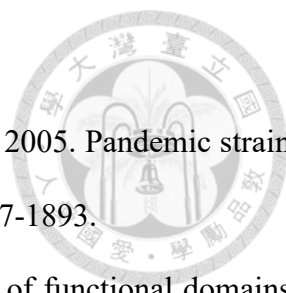
559-569.

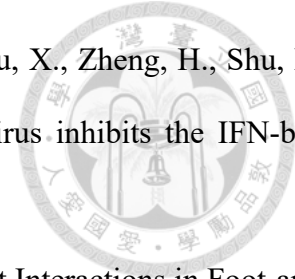
- 
- Greber, U.F., Way, M., 2006. A superhighway to virus infection. *Cell* 124, 741-754.
- Greninger, A.L., 2015. Picornavirus-Host Interactions to Construct Viral Secretory Membranes. *Molecular Basis of Viral Infection* 129, 189-212.
- Greninger, A.L., Knudsen, G.M., Betegon, M., Burlingame, A.L., Derisi, J.L., 2012. The 3A protein from multiple picornaviruses utilizes the golgi adaptor protein ACBD3 to recruit PI4KIIIbeta. *J Virol* 86, 3605-3616.
- Greninger, A.L., Knudsen, G.M., Betegon, M., Burlingame, A.L., DeRisi, J.L., 2013. ACBD3 interaction with TBC1 domain 22 protein is differentially affected by enteroviral and kobuviral 3A protein binding. *mBio* 4, e00098-00013.
- Guan, S.H., Belsham, G.J., 2017. Separation of foot-and-mouth disease virus leader protein activities; identification of mutants that retain efficient self-processing activity but poorly induce eIF4G cleavage. *J Gen Virol* 98, 671-680.
- Gullberg, M., Muszynski, B., Organtini, L.J., Ashley, R.E., Hafenstein, S.L., Belsham, G.J., Polacek, C., 2013. Assembly and characterization of foot-and-mouth disease virus empty capsid particles expressed within mammalian cells. *J Gen Virol* 94, 1769-1779.
- Guo, H.C., Sun, S.Q., Jin, Y., Yang, S.L., Wei, Y.Q., Sun, D.H., Yin, S.H., Ma, J.W., Liu, Z.X., Guo, J.H., Luo, J.X., Yin, H., Liu, X.T., Liu, D.X., 2013. Foot-and-mouth disease virus-like particles produced by a SUMO fusion protein system in *Escherichia coli* induce potent protective immune responses in guinea pigs, swine and cattle. *Vet Res* 44, 48.
- Gurkan, C., Stagg, S.M., Lapointe, P., Balch, W.E., 2006. The COPII cage: unifying principles of vesicle coat assembly. *Nat Rev Mol Cell Biol* 7, 727-738.
- H, L., Kumar Ganji, V., Elango, S., Krishnaswamy, N., V, U., Reddy, G.R., Sanyal, A., Hj, D., 2021. Expression of foot-and-mouth disease virus non-structural protein 3A upregulates the expression of autophagy and immune response genes in vitro. *Virus Res* 292, 198247.



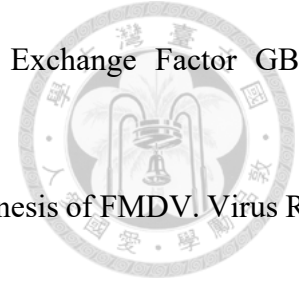
- Han, S.C., Guo, H.C., Sun, S.Q., Jin, Y., Wei, Y.Q., Feng, X., Yao, X.P., Cao, S.Z., Xiang Liu, D., Liu, X.T., 2016. Productive Entry of Foot-and-Mouth Disease Virus via Macropinocytosis Independent of Phosphatidylinositol 3-Kinase. *Sci Rep* 6, 19294.
- Hsu, N.Y., Ilnytska, O., Belov, G., Santiana, M., Chen, Y.H., Takvorian, P.M., Pau, C., van der Schaar, H., Kaushik-Basu, N., Balla, T., Cameron, C.E., Ehrenfeld, E., van Kuppeveld, F.J., Altan-Bonnet, N., 2010. Viral reorganization of the secretory pathway generates distinct organelles for RNA replication. *Cell* 141, 799-811.
- Huang, M., Weissman, J.T., Beraud-Dufour, S., Luan, P., Wang, C., Chen, W., Aridor, M., Wilson, I.A., Balch, W.E., 2001. Crystal structure of Sar1-GDP at 1.7 Å resolution and the role of the NH2 terminus in ER export. *J Cell Biol* 155, 937-948.
- Ilnytska, O., Santiana, M., Hsu, N.Y., Du, W.L., Chen, Y.H., Viktorova, E.G., Belov, G., Brinker, A., Storch, J., Moore, C., Dixon, J.L., Altan-Bonnet, N., 2013. Enteroviruses harness the cellular endocytic machinery to remodel the host cell cholesterol landscape for effective viral replication. *Cell Host Microbe* 14, 281-293.
- Jackson, T., Belsham, G.J., 2021. Picornaviruses: A View from 3A. *Viruses* 13.
- Kirchhausen, T., 2000. Three ways to make a vesicle. *Nat Rev Mol Cell Biol* 1, 187-198.
- Kirchweger, R., Ziegler, E., Lamphear, B.J., Waters, D., Liebig, H.D., Sommergruber, W., Sobrino, F., Hohenadl, C., Blaas, D., Rhoads, R.E., et al., 1994. Foot-and-mouth disease virus leader proteinase: purification of the Lb form and determination of its cleavage site on eIF-4 gamma. *J Virol* 68, 5677-5684.
- Kitson, J.D., McCahon, D., Belsham, G.J., 1990. Sequence analysis of monoclonal antibody resistant mutants of type O foot and mouth disease virus: evidence for the involvement of the three surface exposed capsid proteins in four antigenic sites. *Virology* 179, 26-34.
- Knowles, N.J., Samuel, A.R., Davies, P.R., Kitching, R.P., Donaldson, A.I., 2001. Outbreak of foot-and-mouth disease virus serotype O in the UK caused by a pandemic strain. *Vet Rec* 148, 258-

259.

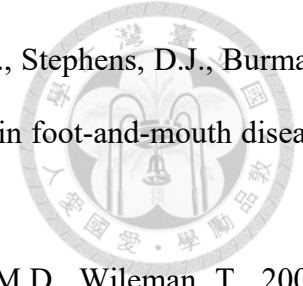
- 
- Knowles, N.J., Samuel, A.R., Davies, P.R., Midgley, R.J., Valarcher, J.F., 2005. Pandemic strain of foot-and-mouth disease virus serotype O. *Emerg Infect Dis* 11, 1887-1893.
- Lamphear, B.J., Kirchweger, R., Skern, T., Rhoads, R.E., 1995. Mapping of functional domains in eukaryotic protein synthesis initiation factor 4G (eIF4G) with picornaviral proteases. Implications for cap-dependent and cap-independent translational initiation. *J Biol Chem* 270, 21975-21983.
- Lanke, K.H., van der Schaar, H.M., Belov, G.A., Feng, Q., Duijsings, D., Jackson, C.L., Ehrenfeld, E., van Kuppeveld, F.J., 2009. GBF1, a guanine nucleotide exchange factor for Arf, is crucial for coxsackievirus B3 RNA replication. *J Virol* 83, 11940-11949.
- Lawrence, P., Rai, D., Conderino, J.S., Uddowla, S., Rieder, E., 2016. Role of Jumonji C-domain containing protein 6 (JMJD6) in infectivity of foot-and-mouth disease virus. *Virology* 492, 38-52.
- Lawrence, P., Rieder, E., 2009. Identification of RNA helicase A as a new host factor in the replication cycle of foot-and-mouth disease virus. *J Virol* 83, 11356-11366.
- Lee, C.D., Yan, Y.P., Liang, S.M., Wang, T.F., 2009. Production of FMDV virus-like particles by a SUMO fusion protein approach in *Escherichia coli*. *J Biomed Sci* 16, 69.
- Lee, H.W., Jiang, Y.F., Chang, H.W., Cheng, I.C., 2022. Foot-and-Mouth Disease Virus 3A Hijacks Sar1 and Sec12 for ER Remodeling in a COPII-Independent Manner. *Viruses* 14.
- Li, C., Zhu, Z., Du, X., Cao, W., Yang, F., Zhang, X., Feng, H., Li, D., Zhang, K., Liu, X., Zheng, H., 2017. Foot-and-mouth disease virus induces lysosomal degradation of host protein kinase PKR by 3C proteinase to facilitate virus replication. *Virology* 509, 222-231.
- Li, D., Lei, C., Xu, Z., Yang, F., Liu, H., Zhu, Z., Li, S., Liu, X., Shu, H., Zheng, H., 2016a. Foot-and-mouth disease virus non-structural protein 3A inhibits the interferon-beta signaling pathway. *Sci Rep* 6, 21888.



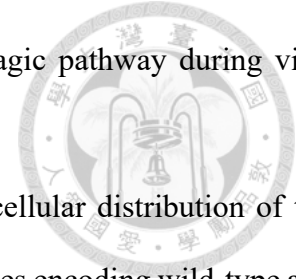
- Li, D., Yang, W., Yang, F., Liu, H., Zhu, Z., Lian, K., Lei, C., Li, S., Liu, X., Zheng, H., Shu, H., 2016b. The VP3 structural protein of foot-and-mouth disease virus inhibits the IFN-beta signaling pathway. *FASEB J* 30, 1757-1766.
- Li, K., Wang, C., Yang, F., Cao, W., Zhu, Z., Zheng, H., 2021. Virus-Host Interactions in Foot-and-Mouth Disease Virus Infection. *Front Immunol* 12, 571509.
- Long, K.R., Yamamoto, Y., Baker, A.L., Watkins, S.C., Coyne, C.B., Conway, J.F., Aridor, M., 2010. Sar1 assembly regulates membrane constriction and ER export. *J Cell Biol* 190, 115-128.
- Longjam, N., Deb, R., Sarmah, A.K., Tayo, T., Awachat, V.B., Saxena, V.K., 2011. A Brief Review on Diagnosis of Foot-and-Mouth Disease of Livestock: Conventional to Molecular Tools. *Vet Med Int* 2011, 905768.
- Loundras, E.A., Herod, M.R., Harris, M., Stonehouse, N.J., 2016. Foot-and-mouth disease virus genome replication is unaffected by inhibition of type III phosphatidylinositol-4-kinases. *J Gen Virol* 97, 2221-2230.
- Ma, L.N., Zhang, J., Chen, H.T., Zhou, J.H., Ding, Y.Z., Liu, Y.S., 2011. An overview on ELISA techniques for FMD. *Virol J* 8, 419.
- Ma, X., Li, P., Bai, X., Sun, P., Bao, H., Lu, Z., Cao, Y., Li, D., Chen, Y., Qiao, Z., Liu, Z., 2014. Sequences outside that of residues 93-102 of 3A protein can contribute to the ability of foot-and-mouth disease virus (FMDV) to replicate in bovine-derived cells. *Virus Res* 191, 161-171.
- Ma, X.X., Ma, L.N., Chang, Q.Y., Ma, P., Li, L.J., Wang, Y.Y., Ma, Z.R., Cao, X., 2018. Type I Interferon Induced and Antagonized by Foot-and-Mouth Disease Virus. *Front Microbiol* 9, 1862.
- Mahapatra, M., Hamblin, P., Paton, D.J., 2012. Foot-and-mouth disease virus epitope dominance in the antibody response of vaccinated animals. *J Gen Virol* 93, 488-493.
- Martinez, J.L., Arnoldi, F., Schraner, E.M., Eichwald, C., Silva-Ayala, D., Lee, E., Sztul, E., Burrone,



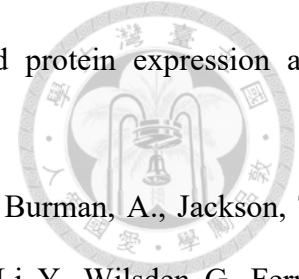
- O.R., Lopez, S., Arias, C.F., 2019. The Guanine Nucleotide Exchange Factor GBF1 Participates in Rotavirus Replication. *J Virol* 93.
- Mason, P.W., Grubman, M.J., Baxt, B., 2003a. Molecular basis of pathogenesis of FMDV. *Virus Res* 91, 9-32.
- Mason, P.W., Pacheco, J.M., Zhao, Q.Z., Knowles, N.J., 2003b. Comparisons of the complete genomes of Asian, African and European isolates of a recent foot-and-mouth disease virus type O pandemic strain (PanAsia). *J Gen Virol* 84, 1583-1593.
- McCahon, D., Crowther, J.R., Belsham, G.J., Kitson, J.D., Duchesne, M., Have, P., Melen, R.H., Morgan, D.O., De Simone, F., 1989. Evidence for at least four antigenic sites on type O foot-and-mouth disease virus involved in neutralization; identification by single and multiple site monoclonal antibody-resistant mutants. *J Gen Virol* 70 (Pt 3), 639-645.
- McKenney, R.J., Huynh, W., Tanenbaum, M.E., Bhabha, G., Vale, R.D., 2014. Activation of cytoplasmic dynein motility by dynactin-cargo adapter complexes. *Science* 345, 337-341.
- McMahon, C., Studer, S.M., Clendinen, C., Dann, G.P., Jeffrey, P.D., Hughson, F.M., 2012. The structure of Sec12 implicates potassium ion coordination in Sar1 activation. *J Biol Chem* 287, 43599-43606.
- Meissner, J.M., Bhatt, J.M., Lee, E., Styers, M.L., Ivanova, A.A., Kahn, R.A., Sztul, E., 2018. The ARF guanine nucleotide exchange factor GBF1 is targeted to Golgi membranes through a PIP-binding domain. *J Cell Sci* 131.
- Melia, C.E., van der Schaar, H.M., Lyoo, H., Limpens, R., Feng, Q., Wahedi, M., Overheul, G.J., van Rij, R.P., Snijder, E.J., Koster, A.J., Barcena, M., van Kuppeveld, F.J.M., 2017. Escaping Host Factor PI4KB Inhibition: Enterovirus Genomic RNA Replication in the Absence of Replication Organelles. *Cell Rep* 21, 587-599.
- Melville, D., Gorur, A., Schekman, R., 2019. Fatty-acid binding protein 5 modulates the SAR1 GTPase cycle and enhances budding of large COPII cargoes. *Mol Biol Cell* 30, 387-399.



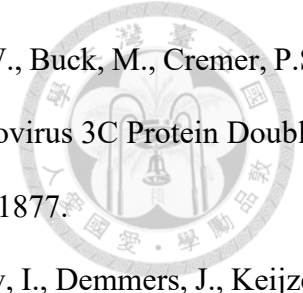
- Midgley, R., Moffat, K., Berryman, S., Hawes, P., Simpson, J., Fullen, D., Stephens, D.J., Burman, A., Jackson, T., 2013. A role for endoplasmic reticulum exit sites in foot-and-mouth disease virus infection. *J Gen Virol* 94, 2636-2646.
- Moffat, K., Howell, G., Knox, C., Belsham, G.J., Monaghan, P., Ryan, M.D., Wileman, T., 2005. Effects of foot-and-mouth disease virus nonstructural proteins on the structure and function of the early secretory pathway: 2BC but not 3A blocks endoplasmic reticulum-to-Golgi transport. *J Virol* 79, 4382-4395.
- Moffat, K., Knox, C., Howell, G., Clark, S.J., Yang, H., Belsham, G.J., Ryan, M., Wileman, T., 2007. Inhibition of the secretory pathway by foot-and-mouth disease virus 2BC protein is reproduced by coexpression of 2B with 2C, and the site of inhibition is determined by the subcellular location of 2C. *J Virol* 81, 1129-1139.
- Moghimi, S., Viktorova, E., Zimina, A., Szul, T., Sztul, E., Belov, G.A., 2020. Enterovirus Infection Induces Massive Recruitment of All Isoforms of Small Cellular Arf GTPases to the Replication Organelles. *J Virol* 95.
- Mohana Subramanian, B., Madhanmohan, M., Sriraman, R., Chandrasekhar Reddy, R.V., Yuvaraj, S., Manikumar, K., Rajalakshmi, S., Nagendrakumar, S.B., Rana, S.K., Srinivasan, V.A., 2012. Development of foot-and-mouth disease virus (FMDV) serotype O virus-like-particles (VLPs) vaccine and evaluation of its potency. *Antiviral Res* 96, 288-295.
- Monaghan, P., Cook, H., Jackson, T., Ryan, M., Wileman, T., 2004. The ultrastructure of the developing replication site in foot-and-mouth disease virus-infected BHK-38 cells. *J Gen Virol* 85, 933-946.
- Moseley, G.W., Roth, D.M., DeJesus, M.A., Leyton, D.L., Filmer, R.P., Pouton, C.W., Jans, D.A., 2007. Dynein light chain association sequences can facilitate nuclear protein import. *Mol Biol Cell* 18, 3204-3213.
- O'Donnell, V., Pacheco, J.M., LaRocco, M., Burrage, T., Jackson, W., Rodriguez, L.L., Borca, M.V.,



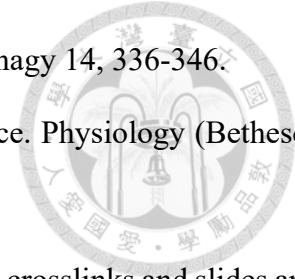
- Baxt, B., 2011. Foot-and-mouth disease virus utilizes an autophagic pathway during viral replication. *Virology* 410, 142-150.
- O'Donnell, V.K., Pacheco, J.M., Henry, T.M., Mason, P.W., 2001. Subcellular distribution of the foot-and-mouth disease virus 3A protein in cells infected with viruses encoding wild-type and bovine-attenuated forms of 3A. *Virology* 287, 151-162.
- OIE. 2021. Foot and mouth disease: Official Disease Status (OIE).
- Pacheco, J.M., Gladue, D.P., Holinka, L.G., Arzt, J., Bishop, E., Smoliga, G., Pauszek, S.J., Bracht, A.J., O'Donnell, V., Fernandez-Sainz, I., Fletcher, P., Piccone, M.E., Rodriguez, L.L., Borca, M.V., 2013. A partial deletion in non-structural protein 3A can attenuate foot-and-mouth disease virus in cattle. *Virology* 446, 260-267.
- Pacheco, J.M., Henry, T.M., O'Donnell, V.K., Gregory, J.B., Mason, P.W., 2003. Role of nonstructural proteins 3A and 3B in host range and pathogenicity of foot-and-mouth disease virus. *J Virol* 77, 13017-13027.
- Pan, L., Zhang, Y., Wang, Y., Wang, B., Wang, W., Fang, Y., Jiang, S., Lv, J., Wang, W., Sun, Y., Xie, Q., 2008. Foliar extracts from transgenic tomato plants expressing the structural polyprotein, P1-2A, and protease, 3C, from foot-and-mouth disease virus elicit a protective response in guinea pigs. *Vet Immunol Immunopathol* 121, 83-90.
- Paul, A.V., Rieder, E., Kim, D.W., van Boom, J.H., Wimmer, E., 2000. Identification of an RNA hairpin in poliovirus RNA that serves as the primary template in the in vitro uridylylation of VPg. *J Virol* 74, 10359-10370.
- Peng, J., Yi, J., Yang, W., Ren, J., Wen, Y., Zheng, H., Li, D., 2020. Advances in Foot-and-Mouth Disease Virus Proteins Regulating Host Innate Immunity. *Front Microbiol* 11, 2046.
- Peotter, J., Kasberg, W., Pustova, I., Audhya, A., 2019. COPII-mediated trafficking at the ER/ERGIC interface. *Traffic* 20, 491-503.
- Polacek, C., Gullberg, M., Li, J., Belsham, G.J., 2013. Low levels of foot-and-mouth disease virus



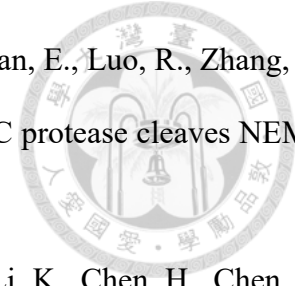
- 3C protease expression are required to achieve optimal capsid protein expression and processing in mammalian cells. *J Gen Virol* 94, 1249-1258.
- Porta, C., Xu, X., Loureiro, S., Paramasivam, S., Ren, J., Al-Khalil, T., Burman, A., Jackson, T., Belsham, G.J., Curry, S., Lomonosoff, G.P., Parida, S., Paton, D., Li, Y., Wilsden, G., Ferris, N., Owens, R., Kotecha, A., Fry, E., Stuart, D.I., Charleston, B., Jones, I.M., 2013. Efficient production of foot-and-mouth disease virus empty capsids in insect cells following down regulation of 3C protease activity. *J Virol Methods* 187, 406-412.
- Puckette, M., Clark, B.A., Smith, J.D., Turecek, T., Martel, E., Gabbert, L., Pisano, M., Hurtle, W., Pacheco, J.M., Barrera, J., Neilan, J.G., Rasmussen, M., 2017. Foot-and-Mouth Disease (FMD) Virus 3C Protease Mutant L127P: Implications for FMD Vaccine Development. *J Virol* 91.
- Quintero, C.A., Giraud, C.G., Villarreal, M., Montich, G., Maccioni, H.J., 2010. Identification of a site in Sar1 involved in the interaction with the cytoplasmic tail of glycolipid glycosyltransferases. *J Biol Chem* 285, 30340-30346.
- Randall, R.E., Goodbourn, S., 2008. Interferons and viruses: an interplay between induction, signalling, antiviral responses and virus countermeasures. *J Gen Virol* 89, 1-47.
- Ranjitha, H.B., Ammanathan, V., Guleria, N., Hosamani, M., Sreenivasa, B.P., Dhanesh, V.V., Santhoshkumar, R., Sagar, B.K.C., Mishra, B.P., Singh, R.K., Sanyal, A., Manjithaya, R., Basagoudanavar, S.H., 2020. Foot-and-mouth disease virus induces PERK-mediated autophagy to suppress the antiviral interferon response. *J Cell Sci* 134.
- Raux, H., Flamand, A., Blondel, D., 2000. Interaction of the rabies virus P protein with the LC8 dynein light chain. *J Virol* 74, 10212-10216.
- Rodriguez Pulido, M., Saiz, M., 2017. Molecular Mechanisms of Foot-and-Mouth Disease Virus Targeting the Host Antiviral Response. *Front Cell Infect Microbiol* 7, 252.
- Schroer, T.A., 2004. Dynactin. *Annu Rev Cell Dev Biol* 20, 759-779.



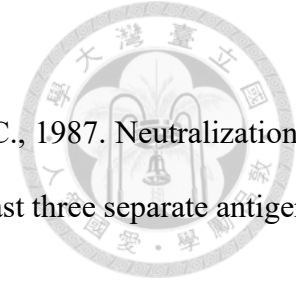
- Shengjuler, D., Chan, Y.M., Sun, S., Moustafa, I.M., Li, Z.L., Gohara, D.W., Buck, M., Cremer, P.S., Boehr, D.D., Cameron, C.E., 2017. The RNA-Binding Site of Poliovirus 3C Protein Doubles as a Phosphoinositide-Binding Domain. *Structure* 25, 1875-1886 e1877.
- Splinter, D., Razafsky, D.S., Schlager, M.A., Serra-Marques, A., Grigoriev, I., Demmers, J., Keijzer, N., Jiang, K., Poser, I., Hyman, A.A., Hoogenraad, C.C., King, S.J., Akhmanova, A., 2012. BICD2, dynactin, and LIS1 cooperate in regulating dynein recruitment to cellular structures. *Mol Biol Cell* 23, 4226-4241.
- Springer, S., Malkus, P., Borchert, B., Wellbrock, U., Duden, R., Schekman, R., 2014. Regulated oligomerization induces uptake of a membrane protein into COPII vesicles independent of its cytosolic tail. *Traffic* 15, 531-545.
- Stenfeldt, C., Arzt, J., Pacheco, J.M., Gladue, D.P., Smoliga, G.R., Silva, E.B., Rodriguez, L.L., Borca, M.V., 2018. A partial deletion within foot-and-mouth disease virus non-structural protein 3A causes clinical attenuation in cattle but does not prevent subclinical infection. *Virology* 516, 115-126.
- Strauss, D.M., Glustrom, L.W., Wuttke, D.S., 2003. Towards an understanding of the poliovirus replication complex: the solution structure of the soluble domain of the poliovirus 3A protein. *J Mol Biol* 330, 225-234.
- Suhy, D.A., Giddings, T.H., Jr., Kirkegaard, K., 2000. Remodeling the endoplasmic reticulum by poliovirus infection and by individual viral proteins: an autophagy-like origin for virus-induced vesicles. *J Virol* 74, 8953-8965.
- Sun, J., Yu, S., Zhang, X., Capac, C., Aligbe, O., Daudelin, T., Bonder, E.M., Gao, N., 2017. A Wntless-SEC12 complex on the ER membrane regulates early Wnt secretory vesicle assembly and mature ligand export. *J Cell Sci* 130, 2159-2171.
- Sun, P., Zhang, S., Qin, X., Chang, X., Cui, X., Li, H., Zhang, S., Gao, H., Wang, P., Zhang, Z., Luo, J., Li, Z., 2018. Foot-and-mouth disease virus capsid protein VP2 activates the cellular



- EIF2S1-ATF4 pathway and induces autophagy via HSPB1. *Autophagy* 14, 336-346.
- Szul, T., Sztul, E., 2011. COPII and COPI traffic at the ER-Golgi interface. *Physiology (Bethesda)* 26, 348-364.
- Tanenbaum, M.E., Vale, R.D., McKenney, R.J., 2013. Cytoplasmic dynein crosslinks and slides anti-parallel microtubules using its two motor domains. *Elife* 2, e00943.
- Toropova, K., Zalyte, R., Mukhopadhyay, A.G., Mladenov, M., Carter, A.P., Roberts, A.J., 2019. Structure of the dynein-2 complex and its assembly with intraflagellar transport trains. *Nat Struct Mol Biol* 26, 823-829.
- Townley, A.K., Feng, Y., Schmidt, K., Carter, D.A., Porter, R., Verkade, P., Stephens, D.J., 2008. Efficient coupling of Sec23-Sec24 to Sec13-Sec31 drives COPII-dependent collagen secretion and is essential for normal craniofacial development. *J Cell Sci* 121, 3025-3034.
- Ujike, M., Taguchi, F., 2015. Incorporation of spike and membrane glycoproteins into coronavirus virions. *Viruses* 7, 1700-1725.
- Urnavicius, L., Zhang, K., Diamant, A.G., Motz, C., Schlager, M.A., Yu, M., Patel, N.A., Robinson, C.V., Carter, A.P., 2015. The structure of the dynactin complex and its interaction with dynein. *Science* 347, 1441-1446.
- van der Schaar, H.M., Dorobantu, C.M., Albuлесcu, L., Strating, J., van Kuppeveld, F.J.M., 2016. Fat(al) attraction: Picornaviruses Usurp Lipid Transfer at Membrane Contact Sites to Create Replication Organelles. *Trends Microbiol* 24, 535-546.
- Viktorova, E.G., Gabaglio, S., Meissner, J.M., Lee, E., Moghimi, S., Sztul, E., Belov, G.A., 2019. A Redundant Mechanism of Recruitment Underlies the Remarkable Plasticity of the Requirement of Poliovirus Replication for the Cellular ArfGEF GBF1. *J Virol* 93.
- Visser, L.J., Medina, G.N., Rabouw, H.H., de Groot, R.J., Langereis, M.A., de Los Santos, T., van Kuppeveld, F.J.M., 2019. Foot-and-Mouth Disease Virus Leader Protease Cleaves G3BP1 and G3BP2 and Inhibits Stress Granule Formation. *J Virol* 93.

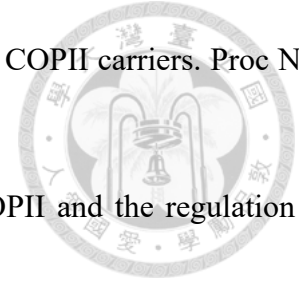


- Wang, D., Fang, L., Li, K., Zhong, H., Fan, J., Ouyang, C., Zhang, H., Duan, E., Luo, R., Zhang, Z., Liu, X., Chen, H., Xiao, S., 2012. Foot-and-mouth disease virus 3C protease cleaves NEMO to impair innate immune signaling. *J Virol* 86, 9311-9322.
- Wang, D., Fang, L., Li, P., Sun, L., Fan, J., Zhang, Q., Luo, R., Liu, X., Li, K., Chen, H., Chen, Z., Xiao, S., 2011a. The leader proteinase of foot-and-mouth disease virus negatively regulates the type I interferon pathway by acting as a viral deubiquitinase. *J Virol* 85, 3758-3766.
- Wang, G., Wang, Y., Shang, Y., Zhang, Z., Liu, X., 2015. How foot-and-mouth disease virus receptor mediates foot-and-mouth disease virus infection. *Virology* 12, 9.
- Wang, H., Zhao, L., Li, W., Zhou, G., Yu, L., 2011b. Identification of a conformational epitope on the VP1 G-H Loop of type Asia1 foot-and-mouth disease virus defined by a protective monoclonal antibody. *Vet Microbiol* 148, 189-199.
- Wang, J., Du, J., Jin, Q., 2014. Class I ADP-ribosylation factors are involved in enterovirus 71 replication. *PLoS One* 9, e99768.
- Wessels, E., Duijsings, D., Lanke, K.H., van Dooren, S.H., Jackson, C.L., Melchers, W.J., van Kuppeveld, F.J., 2006a. Effects of picornavirus 3A Proteins on Protein Transport and GBF1-dependent COP-I recruitment. *J Virol* 80, 11852-11860.
- Wessels, E., Duijsings, D., Niu, T.K., Neumann, S., Oorschot, V.M., de Lange, F., Lanke, K.H., Klumperman, J., Henke, A., Jackson, C.L., Melchers, W.J., van Kuppeveld, F.J., 2006b. A viral protein that blocks Arf1-mediated COP-I assembly by inhibiting the guanine nucleotide exchange factor GBF1. *Dev Cell* 11, 191-201.
- Wolff, G., Limpens, R., Zevenhoven-Dobbe, J.C., Laugks, U., Zheng, S., de Jong, A.W.M., Koning, R.I., Agard, D.A., Grunewald, K., Koster, A.J., Snijder, E.J., Barcena, M., 2020. A molecular pore spans the double membrane of the coronavirus replication organelle. *Science* 369, 1395-1398.
- Wolk, B., Buchele, B., Moradpour, D., Rice, C.M., 2008. A dynamic view of hepatitis C virus



replication complexes. *J Virol* 82, 10519-10531.

- Xie, Q.C., McCahon, D., Crowther, J.R., Belsham, G.J., McCullough, K.C., 1987. Neutralization of foot-and-mouth disease virus can be mediated through any of at least three separate antigenic sites. *J Gen Virol* 68 (Pt 6), 1637-1647.
- Xu, F., Du, W., Zou, Q., Wang, Y., Zhang, X., Xing, X., Li, Y., Zhang, D., Wang, H., Zhang, W., Hu, X., Liu, X., Liu, X., Zhang, S., Yu, J., Fang, J., Li, F., Zhou, Y., Yue, T., Mi, N., Deng, H., Zou, P., Chen, X., Yang, X., Yu, L., 2021. COPII mitigates ER stress by promoting formation of ER whorls. *Cell Res* 31, 141-156.
- Yamayoshi, S., Noda, T., Ebihara, H., Goto, H., Morikawa, Y., Lukashevich, I.S., Neumann, G., Feldmann, H., Kawaoka, Y., 2008. Ebola virus matrix protein VP40 uses the COPII transport system for its intracellular transport. *Cell Host Microbe* 3, 168-177.
- Yang, M., Xu, W., Goolia, M., Zhang, Z., 2014. Characterization of monoclonal antibodies against foot-and-mouth disease virus serotype O and application in identification of antigenic variation in relation to vaccine strain selection. *Virol J* 11, 136.
- Yang, W., Li, D., Ru, Y., Bai, J., Ren, J., Zhang, J., Li, L., Liu, X., Zheng, H., 2020. Foot-and-Mouth Disease Virus 3A Protein Causes Upregulation of Autophagy-Related Protein LRRC25 To Inhibit the G3BP1-Mediated RIG-Like Helicase-Signaling Pathway. *J Virol* 94.
- Ye, X., Pan, T., Wang, D., Fang, L., Ma, J., Zhu, X., Shi, Y., Zhang, K., Zheng, H., Chen, H., Li, K., Xiao, S., 2018. Foot-and-Mouth Disease Virus Counteracts on Internal Ribosome Entry Site Suppression by G3BP1 and Inhibits G3BP1-Mediated Stress Granule Assembly via Post-Translational Mechanisms. *Front Immunol* 9, 1142.
- Ypma-Wong, M.F., Dewalt, P.G., Johnson, V.H., Lamb, J.G., Semler, B.L., 1988. Protein 3CD is the major poliovirus proteinase responsible for cleavage of the P1 capsid precursor. *Virology* 166, 265-270.
- Yuan, L., Kenny, S.J., Hemmati, J., Xu, K., Schekman, R., 2018. TANGO1 and SEC12 are



copackaged with procollagen I to facilitate the generation of large COPII carriers. *Proc Natl Acad Sci U S A* 115, E12255-E12264.

Zanetti, G., Pahuja, K.B., Studer, S., Shim, S., Schekman, R., 2011. COPII and the regulation of protein sorting in mammals. *Nat Cell Biol* 14, 20-28.

Zhang, K., Xu, S., Shi, X., Xu, G., Shen, C., Liu, X., Zheng, H., 2019. Exosomes-mediated transmission of foot-and-mouth disease virus in vivo and in vitro. *Vet Microbiol* 233, 164-173.

Zheng, Q., Zhu, R., Xu, L., He, M., Yan, X., Liu, D., Yin, Z., Wu, Y., Li, Y., Yang, L., Hou, W., Li, S., Li, Z., Chen, Z., Li, Z., Yu, H., Gu, Y., Zhang, J., Baker, T.S., Zhou, Z.H., Graham, B.S., Cheng, T., Li, S., Xia, N., 2019. Atomic structures of enterovirus D68 in complex with two monoclonal antibodies define distinct mechanisms of viral neutralization. *Nat Microbiol* 4, 124-133.

Zhu, R., Antoku, S., Gundersen, G.G., 2017. Centrifugal Displacement of Nuclei Reveals Multiple LINC Complex Mechanisms for Homeostatic Nuclear Positioning. *Curr Biol* 27, 3097-3110 e3095.

Zhu, Z., Yang, F., Cao, W., Liu, H., Zhang, K., Tian, H., Dang, W., He, J., Guo, J., Liu, X., Zheng, H., 2019. The Pseudoknot Region of the 5' Untranslated Region Is a Determinant of Viral Tropism and Virulence of Foot-and-Mouth Disease Virus. *J Virol* 93.

Zoppino, F.C., Militello, R.D., Slavin, I., Alvarez, C., Colombo, M.I., 2010. Autophagosome formation depends on the small GTPase Rab1 and functional ER exit sites. *Traffic* 11, 1246-1261.